UNIVERSITY OF CALIFORNIA SAN DIEGO

The phenomenology of neutrino oscillations in cosmology and core-collapse supernovae

A dissertation submitted in partial satisfaction of the
requirements for the degree
Doctor of Philosophy

in

Physics

by

Lucas Johns

Committee in charge:

Professor George Fuller, Chair
Professor Daniel Arovas
Professor Bruce Driver
Professor Brian Keating
Professor Jean-Bernard Minster

2020

The dissertation of Lucas Johns is approved, and it is acceptable in quality and form for publication on microfilm and electronically:

_____

_____

_____

_____

_____

Chair

University of California San Diego

2020

DEDICATION

To three women, of three generations,

who have been generous with their wisdom:

JoWynn, Anne, and Kaslin

TABLE OF CONTENTS

LIST OF FIGURES

ACKNOWLEDGEMENTS

As I reflect on my time as a grad student, I'm struck by how fortunate I am to have had this opportunity. I believe that we are all transformed by the work we do. It shapes and reveals our passions and priorities, or at the very least our aversions, and gives us material to work with as we carve out our place in the world. I recognize it as a true privilege that my main task during this period has been to breathe in the inspirations of scientific inquiry.

I'm grateful, too, for the people I've encountered. My advisor, George Fuller, has been a role model and friend, and his words and actions have been a constant source of guidance for me—not just in navigating a career in science, but in navigating life. There's a great deal I could say about the influence he's had on me, but I think the greatest tribute may be this: At times of doubt—times when I've questioned whether this path was the right one—a reliable comfort has been the thought that one day I might be the kind of mentor to others that George has been to me. My gratitude to him is deep and heartfelt.

I'd like to single out four other scientists for special thanks. Mark Paris was a co-mentor during the first half of my PhD and continues to be a valued friend and colleague. He introduced me to nuclear theory, made possible my many visits to Los Alamos, and has been unwaveringly supportive. I've learned something from every conversation I've had with Mark, on topics ranging from worker ownership to the TV show *Deadwood*.

Vincenzo Cirigliano has been a role model of mine since I first began work on my dissertation. He's exemplified for me a rare combination of razor-sharp insight and genuine humility. I fondly recall our many discussions at the lab in Los Alamos, the Gordon Research Conference in Hong Kong, and the INT summer school in Seattle.

Pat Diamond has been a towering presence during my time at UCSD, beginning with his mechanics course in my very first quarter. Much of my understanding of transport, turbulence, and complexity—to say nothing of academic politics—traces back to conversations with him. Some of the advice I prize most has come out of chance encounters with Pat on the 4th floor of

SERF.

Adam Burrows has become one of my most important teachers since I turned my attention to supernovae. The depth of his insight and the breadth of his knowledge are inspirations. I knew Adam and I would get along well when, in our first in-person meeting, he began quizzing me on obscure words and their etymologies.

I'm grateful to the many other physicists who have helped me to learn and grow. Among them, I'd especially like to thank Eve Armstrong, Dan Arovas, Baha Balantekin, Daniel Blaschke, Michael Cervia, JJ Cherry, Lauren Gilbert, Evan Grohs, Wick Haxton, Raul Herrera, Patrick Jaffke, Brian Keating, Chad Kishimoto, Jung-Tsung Li, Diego Lonardoni, Kelsey Lund, Mattia Mina, Bernard Minster, Wendell Misch, Hiroki Nagakura, Amol Patwardhan, Ermal Rrapaj, Manibrata Sen, Shashank Shalgar, Sebastien Tawa, Alexey Vlasenko, and my TASI and TALENT friends. I'd also like to thank my friends and fellow grad students who were constantly by my side during the formative first years of grad school, especially Chelsey Dorow, and all of my colleagues in CASS who have made it such a welcoming environment.

And finally, I'm grateful beyond measure for my dear roommates Anna, Elena, Jasmine, and Tucker, all of whom have become like family; my beloved friends Ben, Charlotte, Eleni, Justin, Kaslin, Marina, and Tristan; and of course Anne, JoWynn, Karin, Michelle, Noah, Norma, Pete, Skip, and all the rest of my wonderful family.

Chapter 2 is a reprint of L. Johns, M. Mina, V. Cirigliano, M. W. Paris, and G. M. Fuller, Phys. Rev. D 94, 083505 (2016). Chapter 3 is a reprint of L. Johns and G. M. Fuller, Phys. Rev. D 97, 023020 (2018). Chapter 4 is a reprint of L. Johns and G. M. Fuller, Phys. Rev. D 95, 043003 (2017). Chapter 5 is a reprint of L. Johns, H. Nagakura, G. M. Fuller, and A. Burrows, Phys. Rev. D 101, 043009 (2020). Chapter 6 is a reprint of L. Johns, Phys. Rev. D 100, 083536 (2019). Chapter 7 is a reprint of L. Johns and G. M. Fuller, Phys. Rev. D 100, 023533 (2019). I was the primary investigator and author of these publications.

VITA

2013	B. A. in Physics, Reed College
2015	M. S. in Physics, University of California San Diego
2020	Ph. D. in Physics, University of California San Diego

PUBLICATIONS

L. Johns, H. Nagakura, G. M. Fuller, and A. Burrows, "Neutrino oscillations in supernovae: angular moments and fast instabilities," Phys. Rev. D 101, 043009 (2020).

L. Johns, "Derivation of the sterile neutrino Boltzmann equation from quantum kinetics," Phys. Rev. D 100, 083536 (2019).

L. Johns, "Neutrino oscillations in a trapping potential," Int. J. Mod. Phys. A 34, 1950160 (2019).

L. Johns and G. M. Fuller, "Self-interacting sterile neutrino dark matter: the heavy-mediator case," Phys. Rev. D 100, 023533 (2019).

L. Johns and G. M. Fuller, "Strange mechanics of the neutrino flavor pendulum," Phys. Rev. D 97, 023020 (2018).

E. Armstrong, A. V. Patwardhan, L. Johns, C. T. Kishimoto, G. M. Fuller, and H. D. I. Abarbanel, "An optimization-based approach to neutrino flavor evolution," Phys. Rev. D 96, 083008 (2017).

L. Johns and G. M. Fuller, "Geometric phases in neutrino oscillations with nonlinear refraction," Phys. Rev. D 95, 043003 (2017).

L. Johns, M. Mina, V. Cirigliano, M. W. Paris, and G. M. Fuller, "Neutrino flavor transformation in the lepton-asymmetric universe," Phys. Rev. D 94, 083505 (2016).

B. L. Davis, J. C. Berrier, L. Johns, D. W. Shields, M. T. Hartley, D. Kennefick, J. Kennefick, and C. H. S. Lacy, "The black hole mass function derived from local spiral galaxies," Astrophys. J. 789, 124 (2014).

ABSTRACT OF THE DISSERTATION

The phenomenology of neutrino oscillations in cosmology and core-collapse supernovae

by

Lucas Johns

Doctor of Philosophy in Physics

University of California San Diego, 2020

Professor George Fuller, Chair

Neutrinos have shaped cosmic history in important ways. In early epochs, they left their mark on the expansion of the universe and the genesis of primordial nuclei. In more recent eras, their signature has been repeatedly etched into the explosive dynamics of massive stars and the chemical enrichment of the cosmos. In the guise of sterile neutrinos, they may even constitute the dark matter.

None of these roles is, as of yet, fully understood. Aside from the observational challenges, there are significant theoretical ones. Neutrinos are known to come in at least three different flavors, each of which interacts differently with other particles. They are also known to oscillate: due to quantum mechanics, a neutrino's flavor changes in the course of its propagation. The

phenomenology that emerges in dense neutrino systems as a result of flavor oscillations is a frontier topic of precision cosmology and high-energy astrophysics. It is the focal point of this dissertation.

The central theme is nonlinearity. When a system is dense in neutrinos, kinetic behaviors can arise that differ dramatically from those in systems dense only in "ordinary" matter like electrons and nucleons. The key piece of microphysics in this regard is the forward scattering of neutrinos on one another, which causes the flavor evolution of any given neutrino to depend on the flavor states of all neutrinos that it crosses paths with. The chapters here explore some of the macroscopic consequences of this subtle quantum phenomenon, with applications to the lepton-asymmetric early universe, core-collapse supernovae, and sterile neutrino dark matter.

Chapter 1

Introduction

1.1 Overview

Neutrino physics is an active and sprawling area of research. Many practitioners, myself included, are drawn to it because it transcends the usual disciplinary partitions of physics. It's not uncommon, at least these days, for physicists to write papers on particle physics, astrophysics, and nuclear physics, and yet to think of themselves primarily as *neutrino* physicists. An outsider might reasonably wonder: Why so much emphasis on this one particle?

The neutrino has no less than three unusual properties. (1) The neutrino is very light, but not quite massless; (2) it communicates with other particles predominantly through the weak interaction; and (3) it exhibits flavor oscillations that are observable and practically important. Taken together, these attributes make the neutrino appealing to physicists of a wide variety of backgrounds and motivations.

This dissertation is on cosmology and core-collapse supernovae, so in one respect the motivation here is to better understand these environments. But as it happens, the path from the neutrinos' fundamental properties to its macroscopic effects is in many cases a difficult one, passing through terrain—the phenomenology of dense neutrino systems—that is intellectually

deep in its own right. While the applications give this subject real-world heft, I have often found myself most excited by the ways in which the kinetic theory itself speaks to certain general issues. How is it that quantum fields come to resemble collections of particles? How does quantum decoherence ("the collapse of the wave function") play out when the system includes all the contents of the universe? How does a system relax to equilibrium without the randomizing effects of collisions? Questions like these are somewhat more philosophically hued than the chapters to come, which by and large focus on solving definite astrophysical problems, but they hover in the background all the same.

In the particular problems I've focused on, the origin of the conceptual richness lies mainly in property (3). Neutrinos are known to come in at least three flavors—ν_e, ν_μ, and ν_τ—and the term *oscillation* refers to the experimentally confirmed fact that a ν_e, for example, can transform into a ν_μ or a ν_τ as it propagates. The result is that neutrinos transport an *evolving* quantum degree of freedom (flavor) in addition to the usual package of energy, momentum, and spin. As neutrinos move about, traversing vast distances at nearly the speed of light, a microphysical quantum phenomenon is painted across a macroscopic canvas.

The same property is at the origin of the major practical challenges. The *way* that neutrinos oscillate is affected by the medium they travel in, be it the early universe, the Sun, or an exploding massive star. The causal relationship therefore goes both ways: from oscillations to the environment, and from the environment back to oscillations. What's more, neutrinos themselves make up part of the environment, a feature that injects nonlinear dynamics into an astrophysical or cosmological problem that already spans a wide range of scales.

Each of the subsequent chapters is a publication I've worked on over the course of my PhD. The big-picture contexts are the search for new physics using cosmic neutrinos (Chapters 2 and 3), the ongoing effort to understand how massive stars explode (Chapter 5), and the quest to identify dark matter (Chapters 6 and 7). (Chapter 4, on the connection between neutrino oscillations and geometric phases, is not specific to any one application.) If at times the contents

seem somewhat removed from these overarching goals, it's because my more immediate aim has been to gain a deeper understanding of the neutrino phenomenology itself. This view might be a bit unorthodox in the present-day physics climate, but if given the choice between knowing what makes up the dark matter and having revealed to me the most penetrating insights into the complex dynamics of neutrinos, I'd probably pick the latter. That this dynamical theory is of cosmic significance, and may even bear on the dark matter problem, is a nice bonus.

Still, the applications do matter, and the rest of this chapter will try to establish why someone with no interest in neutrino quantum kinetics per se might still believe this work was worth doing. The next section will summarize the status of neutrinos as a subject within particle physics, and the section after will do the same from the viewpoint of astrophysics and cosmology (though we'll quickly see that the two perspectives are not totally separable). Along the way, I'll put my own work into more specific context. The tone will continue to be relatively informal, leaving technical treatments to the later chapters. References for the background provided here can be found in the individual chapter introductions.

1.2 The particle physics of neutrinos

Let's start with the basic facts. Six different types of neutrinos have been observed. The first pair is made up of the electron neutrino ν_e and its antiparticle $\bar{\nu}_e$. These two can be thought of as the neutral partners of the electron e^- and the positron e^+. The second pair is the muon neutrino ν_μ and its antiparticle $\bar{\nu}_\mu$, partners of the muon and antimuon. The third is the tau pair, ν_τ and $\bar{\nu}_\tau$. The evocative term *flavor* is used to label each of these pairs: ν_e and $\bar{\nu}_e$ both carry electron flavor, and so on.

The fact that neutrinos don't carry electric charge causes them to behave very differently from electrons, muons, and taus. We don't, for instance, find atoms with neutrinos in orbit about protons, nor do engineers build generators that pump "neutricity" into people's homes. In fact,

neutrinos play virtually no role at all in the fields of chemistry, biology, or engineering.

It takes the transfiguration of nuclei, or something equally out of the ordinary, just to get neutrinos to make an appearance. When a neutron decays into a proton, it balances electric charge by emitting an electron. In the present day, we know that this isn't enough: The flavor of the electron must in turn be balanced by the emission of a $\bar{\nu}_e$. In 1930, long before the necessary apparatus existed to detect the antineutrino, the unobserved particle only showed up in the form of missing energy and momentum. That sufficed for Wolfgang Pauli, one of the architects of quantum mechanics, to propose the existence of what we now call the neutrino. Conjecturing a new particle on the basis of kinematics is today a routine and guiding principle, but back then, when the only known particles were the proton and the electron, it was an audacious move.

Because of the particle's neutrality, it took until 1956 for the hypothesized $\bar{\nu}_e$ from nuclear decay to be confirmed, and several more years for the muon flavor to be detected despite the fact that the muon itself had been discovered back in the 1930s. (Although ν_μ couples to the electron and tau as well, it couples more strongly to the muon. This is the sense in which they form a pair.) When the tau was discovered in 1975, it was naturally—and correctly—anticipated that a ν_τ was in the offing.

The couplings that neutrinos have to each other and to other particles are mediated by the weak interaction and gravity. The feebleness of their couplings turns out to be a strength in some contexts. They're hard to detect because they interact weakly, but if you *can* detect them, you can use them to see through matter that's opaque to photons. Historically, this logic was first applied to the Sun, to the mutual and half-unexpected benefit of both solar and particle physics.

Nuclear fusion in the Sun radiates neutrinos, which easily escape from the core and pass through the outer solar layers on their way out to space. The vast majority of neutrinos directed towards Earth make it here, and around 1970 they were detected, for the first time, by the Homestake Experiment stationed deep in a South Dakota mine. It soon became apparent, however, that the flux of neutrinos being detected did not match the flux that was predicted. It

was too low. Physicists began to wonder whether the standard theoretical model of the Sun was in need of serious revision.

Another line of thinking was gaining traction at the same time. Up to that point, the default assumption was that neutrinos were massless. There'd been no evidence otherwise. But it had also been realized that if they were massive, a freely traveling neutrino would, for quantum-mechanical reasons, change flavor in transit. Since Homestake only observed electron flavor, it was conceivable that the full expected flux *was* generated in the Sun's core, but that much of it was disappearing into the other flavors due to neutrino oscillations en route.

This suggestion would prove to be the correct one, vindicating the standard solar model. The discovery of neutrino oscillations—and, by implication, neutrino mass—was also momentous for particle physics, because any mechanism that gives mass to the neutrino requires new particles to be posited, if not something even less conventional. To this day, neutrino mass is one of the most straightforward pieces of evidence we have that the standard models of cosmology and particle physics are not the full story.

The theoretical importance of neutrino mass has motivated an array of more recent experimental efforts. Massive neutrinos are now, by convention, considered part of the Standard Model of particle physics, even though the origin of their mass must lie beyond it, and many of the experiments target the standard parameters introduced by neutrino mass. Some of these are well measured (the mass-squared splittings and mixing angles), some are only somewhat constrained (the Dirac phase, the ordering of the masses, and the absolute mass scale), and still others are not known at all (the Majorana phase and, relatedly, whether the neutrino is its own antiparticle). The best-measured parameters are the ones that show up in oscillation experiments, because they dictate the oscillation patterns. For the same reason, they're the ones that are most relevant for this dissertation.

There are whole classes of other neutrino experiments that aren't especially (or even at all) focused on standard neutrino oscillations. Notable here are the programs that search for additional

types of neutrinos beyond the six standard ones. The common name for these particles is *sterile neutrinos*; they meet the definition of being neutrinos because they mix with the other ones through oscillations, but they're required to be neutral under the non-gravitational Standard Model interactions, including the weak interaction. They need not be inert under *all* non-gravitational interactions, however, and in the last two chapters we'll consider hypothetical sterile neutrinos that have beyond-Standard-Model couplings.

The connection between astrophysics and fundamental neutrino properties that began with the solar neutrino puzzle has only grown stronger in the years since. But while the Homestake Experiment is rightfully celebrated, solar neutrinos don't really do anything *to* the Sun because the solar medium is transparent to them. Passivity isn't always the way of neutrinos, though. In more extreme astrophysical environments—ones with higher densities, fluxes, and temperatures—neutrinos can become active participants. Those environments, and the roles played in them by neutrinos, have been the central focus of my research thus far.

1.3 The cosmology and astrophysics of neutrinos

One of the epochal events in the history of neutrino astronomy took place in 1987, when neutrinos were detected from a core-collapse supernova located in the Large Magellanic Cloud, a satellite of our Galaxy. The source of those particles, SN 1987A, was the first (and still the only) supernova observed in neutrinos.

At that time, the nonzero mass of neutrinos hadn't yet been firmly established, but the proposal had already been made that neutrino oscillations could resolve the solar neutrino problem. The question arose: If neutrino mass did account for the solar flux deficit, what did it imply for the newly detected supernova flux?

To answer that question, one must understand how neutrinos change flavor on their way out from the inner regions of the supernova. In some respects the relevant physics had already

been studied in the context of the Sun. A neutrino traveling in a dense medium is "slowed down" by its interactions with the background particles: It acquires an effective mass that differs from its mass in vacuum. Because the different flavors interact differently, this in-medium-mass effect depends on the flavor state of the neutrino. And because neutrino oscillations depend on mass *differences*, the presence of the medium changes the way that neutrinos oscillate.

Although this is as true of the Sun as it is of SN 1987A, the vastly greater fluxes of neutrinos in supernovae make the in-medium effects in these environments qualitatively distinct. The solar medium, for all practical purposes, just consists of electrons and ions. In contrast, a core-collapse supernova emits neutrinos so intensely that their contribution to their own background can't be ignored. The result is that the effective masses of supernova neutrinos are nonlinear: As a ν_e oscillates into a ν_μ or ν_τ, the number densities of the flavors are altered, and as the number densities change, oscillations are altered. Theoretical insights in the 1990s sharpened the distinction even further. It's not just that the effective masses depend on the number densities. They depend on the neutrinos' own *quantum states*.

The phenomenology that results from this quantum-level nonlinearity is still being pieced together in supernovae and other high-neutrino-density settings such as neutron-star mergers. These environments are also ones in which nucleosynthesis and general relativity are important. (George Fuller, my PhD advisor, has referred to this as the evil cabal of neutrinos, nuclei, and gravitation.) The quantum-kinetic theory of neutrinos has thus grown to become one of the frontiers in the current era of multi-messenger astronomy.

Supernovae and mergers are very complex, however, even without oscillations. Back in the 90s, at the same time that interest in the nonlinear flavor dynamics in supernovae was picking up, it was realized that similar physics might have been important in the much simpler environment of the early universe. The realization actually happened twice, once in connection to oscillations among the Standard Model neutrinos and again in connection to oscillations between a sterile species and the Standard Model ones. Because of the relative simplicity of the medium,

in particular the fact that the early universe was very nearly homogenous and isotropic, the flavor evolution of cosmic neutrinos is phenomenologically rather different from that of supernova neutrinos, and easier to get a handle on.

This dissertation collects my work on oscillations among active (*i.e.*, Standard Model) neutrinos in core-collapse supernovae, among active neutrinos in the early universe, and between active and sterile neutrinos in the early universe. To bring this chapter up to the present, I'll now give a very brief, big-picture overview of each of these topics.

1.3.1 Neutrinos in the early universe

According to the standard cosmology, the universe in the seconds after the Big Bang was a nearly uniform plasma. It was hot and dense, but it was also expanding. As it expanded, it cooled, and after a few minutes the temperature had dropped low enough for nuclei to assemble in a process known as Big Bang nucleosynthesis (BBN). After a few hundred thousand years, atoms formed. With almost all of the once-free charged particles locked away in neutral atoms, photons decoupled from the matter in the universe. Dark matter was increasingly clumping together due to gravity, and atoms began to do so as well. The stage was set for the first galaxies and stars to form, and for the universe to begin looking something like it does now.

The decoupled photons can still be found today, streaming freely throughout the universe in the form of the cosmic microwave background (CMB). They, along with the relic nuclei from BBN, are direct traces of the universe in its earliest epochs, and have become cornerstones of precision observational cosmology. The atoms, now mostly reionized, have also been observed, while dark matter has thus far only been inferred gravitationally.

What of the neutrinos in all this? The early universe was teeming with them as well. Being almost massless, their history in some ways resembles that of photons. They decoupled around the BBN epoch, beginning a phase of free streaming that's expected to be ongoing still, and the existence today of a cosmic *neutrino* background (CνB) is a clear prediction of the

standard cosmology. But because neutrinos are weakly interacting, the CνB is yet to be detected. Information about cosmic neutrinos is instead deduced indirectly from the CMB, primordial nuclei, and other cosmological observables.

Neutrinos affect cosmology primarily through their energy density and, at later times, their mass. The exception to this—the period in the standard cosmology when the details of their interactions matter—is during their decoupling from the plasma. Nonequilibrium dynamics, including oscillations, become important at this time, leaving imprints on both CMB and BBN data.

The effects are heightened in some nonstandard cosmologies with large asymmetries in the densities of neutrino and antineutrino species. Cosmologies of this sort are only weakly constrained by observations and have theoretical links to the cosmic baryon asymmetry (a parameter that's known to be nonzero) and certain models of dark matter. Neutrino-asymmetric scenarios, and the collective flavor phenomena that characterize them, are the subject of Chapters 2 and 3. Chapter 4 then follows with an analysis of how the quantum phenomenon of geometric phases manifests in collective neutrino oscillations. Though the calculations in Chapter 4 employ highly simplified models in order to illustrate general principles, the physics is relevant to flavor evolution in both the early universe and supernovae.

1.3.2 Neutrinos in core-collapse supernovae

Ordinary stars are propped up against gravity by the energy released in nuclear fusion. The Sun, for example, shines because it's currently fusing hydrogen into helium and emitting photons in the process. After its nuclear fuel runs out, the Sun will eventually settle into a white dwarf supported by electron degeneracy pressure (in other words, the Pauli exclusion principle).

A star about eight times the mass of the Sun, or heavier, follows a different track. It undergoes core collapse, meaning that electron degeneracy is insufficient to counteract gravity. In some cases it may be destined to become a neutron star, if repulsive nuclear interactions can supply

enough pressure to halt collapse. (With the failure of electron degeneracy, electrons are effectively pushed inside nuclei, whereupon they are captured by protons. The neutrons that are left behind must likewise obey the Pauli exclusion principle, but the pressure from neutron degeneracy is subdominant to that from repulsive interactions.) In some cases even nuclear interactions and neutron degeneracy aren't enough. Unless some speculative mechanism intervenes, the star's fate as a black hole is then all but sealed. The only other way out—possibly available to stars a couple hundred times the mass of the Sun—is for the star to explode itself entirely, leaving behind no compact remnant at all.

It's estimated that a few core-collapse supernovae occur in the Milky Way each century. Expectations for these events are progenitor-dependent and, even for a known progenitor, uncertain at least in the details. From a theoretical perspective, the question is how an *imploding* star becomes an *exploding* one. Six decades after this problem was first taken up, it's still a forefront issue in astrophysics. For how easy the question is to pose, the physics involved turns out to be remarkably deep and varied.

The consensus view is that most explosions are due to the delayed neutrino-heating mechanism, which at a basic level consists of three stages. First, as collapse proceeds, protons capture electrons and turn into neutrons, the density rises, and the pressure from repulsive nuclear interactions becomes sufficient to prevent the core, at least temporarily, from collapsing further. The core thus stiffens and rebounds in a process known as core bounce.

Second, as the core bounces, a shock wave is blasted outward from the core into the infalling stellar mantle. The shock plows through this material, pushing it outward, but is slowed down by the emission of neutrinos and the dissociation of nuclei. In most cases, after a hundred milliseconds or so, the enervated shock stalls. The initial energy imparted by core bounce was not enough to unbind the mantle. Without another power source, the material pushed out by the shock will fall back onto the core, and explosion will have failed.

Finally, the additional power source takes over: An intense flux of neutrinos emitted from

the hot, central regions of the core deposits energy into the material behind the shock. The heated fluid bubbles and roils, and the shock is revived. The supernova explodes.

The pivotal role of neutrinos is clear. After explosion, moreover, the remnant protoneutron star (if one exists) continues to radiate neutrinos, driving a wind in which supernova nucleosynthesis takes place. Core-collapse supernovae thereby spray their surroundings with chemical elements, which in time become critical in the formation of new stars and the evolution of the host galaxy.

This brief description glosses over many important details of the collapse, explosion, and aftermath. One of them is the subject of Chapter 5: oscillations in the neutrino flux responsible for reviving the shock. Up until recently, it was commonly thought that neutrino oscillations likely have no significant impact on the dynamics of explosion. A new class of collective flavor instabilities has since been discovered, however, calling this conclusion into question. Chapter 5 addresses this oscillation physics, with an eye toward ultimately assessing the effects on explosion.

1.3.3 Sterile neutrino dark matter

In the early 90s, it was pointed out that sterile neutrinos could account for the observed density of dark matter. In contrast to many other models, here the dark matter never comes into thermal equilibrium with the Standard Model sector of the universe. Early on, at high temperatures, there's only a negligible abundance of sterile neutrinos; the active neutrinos, which *are* in equilibrium, are prevented from oscillating into sterile ones by the in-medium alterations of the effective masses. Later, at low temperatures, oscillations are unsuppressed but the scattering rate is too small for the sterile population to be progressively built up by active-to-sterile conversion. (A new and streamlined derivation of the equation describing this physics is given in Chapter 6.) In between these limits, however, there's a window in which the sterile sector can become appreciably populated. If the right parameters are chosen, the abundance ends up matching that of dark matter.

One of the appeals of the Dodelson–Widrow mechanism, as this scenario is often called, was that it predicted *warm* dark matter over much of its originally viable parameter space. That is, because sterile neutrino dark matter is relatively light, it tends to be faster-moving than the classic *cold* dark matter particles. With their higher velocities, sterile neutrinos are able to escape gravitational potential wells that slower particles would be trapped by. As a result, cosmic structure—dark matter halos and galaxies—may bear the imprint of dark matter's hypothetical warmth.

Observations of structure have been used, alongside searches for sterile neutrino decay in dark matter halos, to constrain the Dodelson–Widrow mechanism. It is now strongly disfavored as a way to produce all of the dark matter. This sequence of developments—the proposal of a new particle and production mechanism, the identification of observable predictions, and finally the scenario's ruling-out—exemplifies, perhaps, the closest one can get to progress in the search for dark matter short of actually making a detection.

Nonetheless, sterile neutrinos remain an interesting dark matter candidate. The Dodelson–Widrow mechanism is now seen as only the most minimal entry in a whole class of scenarios. Other models in this class invoke more new physics, besides the sterile neutrino itself. One example is found in Chapter 7, which makes the observation that if sterile neutrinos interact with one another, experimental constraints might be avoided. The trick is that self-interacting sterile neutrinos can nonlinearly enhance their own production. In the parameter space studied in Chapter 7, the mechanism is in fact discovered to be *too* effective; this set of self-interacting models is essentially ruled out by its own dynamics.

Chapter 2

Neutrino flavor transformation in the lepton-asymmetric universe

2.1 Abstract

We investigate neutrino flavor transformation in the early universe in the presence of a lepton asymmetry, focusing on a two-flavor system with $1-3$ mixing parameters. We identify five distinct regimes that emerge in an approximate treatment neglecting collisions as the initial lepton asymmetry at high temperature is varied from values comparable to current constraints on the lepton number down to values at which the neutrino–neutrino forward-scattering potential is negligible. The characteristic phenomena occurring in these regimes are (1) large synchronized oscillations, (2) minimal flavor transformation, (3) asymmetric (ν- or $\bar{\nu}$-only) MSW, (4) partial MSW, and (5) symmetric MSW. We examine our numerical results in the framework of adiabaticity, and we illustrate how they are modified by collisional damping. Finally, we point out the existence of matter–neutrino resonances in the early universe and show that they suffer from non-adiabaticity.

2.2 Introduction

In this paper we examine how cosmological lepton asymmetries spawned at high temperature affect the ensuing evolution of neutrino flavor. Despite the particle's humble stature, the consequences of neutrino physics for the early universe are profound. As the universe cools to a temperature of a few MeV, the weak-interaction rates that have safeguarded thermal equilibrium in the neutrino sector begin to falter in their competition with Hubble expansion. At roughly the same time, electrons and positrons are annihilating and dumping entropy into the plasma. Some neutrinos share in this heating, but not all — leaving their once-equilibrium spectra deformed and cool compared to those of photons, which remain in equilibrium by dint of their swift electromagnetic interactions. (See, for example, Ref. [1] for a recent discussion of the Boltzmann transport of neutrino energy and entropy through weak decoupling and Big Bang nucleosynthesis (BBN).)

During this period neutrinos are all the while undergoing capture on free nucleons and contributing to blocking factors in electron/positron capture and neutron decay. Through their role in these processes, neutrinos shape the neutron-to-proton (n/p) ratio that will be available when the nucleus-building begins in full force at $T \sim 70$ keV. The primordial byproducts of BBN — most promisingly, from an observational perspective, the elements D and ^{4}He — depend on the n/p ratio, and the protracted freeze-out of weak interactions means that there is ample time for the evolving, non-equilibrium neutrino spectra to leave their mark on the nuclide abundances [2].

Even after neutrinos have decoupled from the plasma, they are no mere spectators, as their energy density helps to set the expansion rate of the universe. In the era following $e^{\pm}$ annihilation, neutrinos are relativistic and therefore contribute, along with photons (and possibly other particles beyond the Standard Model), to the radiation energy density $\rho_{\rm rad}$. The energy density of these species is commonly parameterized in terms of the quantity $N_{\rm eff}$, defined by the relation

$$\rho_{\rm rad} = 2\left[1 + \frac{7}{8}\left(\frac{4}{11}\right)^{4/3} N_{\rm eff}\right]\frac{\pi^2}{30}T^4. \tag{2.1}$$

This parameter is sensitive not just to the number of flavors of neutrinos but also to their post-decoupling spectra, which, as noted above, inevitably sustain non-thermal distortions. Determining the precise form of these distortions and their impact on BBN and $N_{\rm eff}$ is a rich and persistent problem in cosmology [1–11].

Of particular importance in this regard is the lepton number

$$L_\nu = \frac{n_\nu - n_{\bar{\nu}}}{n_\gamma}, \tag{2.2}$$

defined in terms of the number densities of neutrinos (n_ν), antineutrinos ($n_{\bar{\nu}}$), and photons (n_γ). In thermal equilibrium a finite lepton number is tantamount to one or more nonzero chemical potentials in the neutrino sector, with clear ramifications for $N_{\rm eff}$. Away from equilibrium the chemical potentials are no longer well-defined, but the implications of nonzero L_ν for the radiation energy density still stand. A cosmological lepton number also exerts an influence through the special role, indicated previously, that the electron flavor plays in mediating the reactions

$$\begin{aligned} \nu_e + n &\rightleftharpoons p + e^- \\ \bar{\nu}_e + p &\rightleftharpoons n + e^+. \end{aligned} \tag{2.3}$$

The unique leverage on the primordial ^{4}He abundance that ν_e and $\bar{\nu}_e$ are afforded by virtue of these reactions [12] has driven interest in the possibility that L_ν is not only nonzero but is (or once was) distributed unevenly across the individual flavors. The evolution of an initial lepton asymmetry — a difference between L_{ν_e} and L_{ν_x} in the effective two-flavor scenario that we will investigate — depends on the interplay between collisions and medium-enhanced oscillations, both of which are capable of shuttling lepton number between flavors. In a lepton-asymmetric universe especially, precise predictions of $N_{\rm eff}$ and Y_P (the mass fraction of ^{4}He) therefore demand a careful treatment of neutrino flavor transformation.

Due to the influence of sphalerons, the lepton number is expected in many baryogenesis

models to be comparable to the baryon asymmetry (or baryon-to-photon ratio) $\eta = n_B/n_\gamma \approx 6 \times 10^{-10}$ [13–16]. But the fact remains that the lepton number is only modestly constrained by measurements: Even the most stringent bounds currently permit asymmetries of $\sim 5 \times 10^{-2}$ [17–22], a full eight orders of magnitude above η. Moreover, the past several decades have brought forth a number of models [23–33] that can generate a large lepton number without contravening the impressive agreement on η between cosmic microwave background (CMB) and BBN data. A measurement of the lepton number of the universe, whatever its value turns out to be, will serve as a probe of physics at and above the scale of electroweak symmetry breaking and will put to the test theories of baryogenesis.

As of recently, a careful treatment is now motivated from yet another direction. The detections [34, 35] of a mysterious X-ray line in a number of galaxies and galaxy clusters at ~ 3.55 keV have ignited speculation that the line may be attributable to dark matter decay. One scenario consistent with this interpretation — indeed, a scenario that may be said to have predicted the appearance of a keV decay line [36] — is the resonant production of sterile neutrino dark matter in the presence of a nonzero lepton number [37–39]. (For reviews of the dark-matter candidacy of sterile neutrinos, see Refs. [40, 41].) Given the energy and flux of the alleged decay line, resonant production singles out a range of pre-resonance lepton numbers on the order of $L_\nu \sim 5 \times 10^{-4}$ as being in best agreement with the X-ray observations [42]. Since the production mechanism is agnostic to the details of how L_ν is distributed, it leaves the door open to lepton asymmetries and any signatures that they may have left behind.

Investigation into the evolution of the individual lepton numbers dates back at least to the work of Savage, Malaney, and Fuller [43], who considered the role of resonant neutrino oscillations — a topic that will be a major theme of the present work. But the current orthodoxy on the subject originated a decade later with the watershed numerical study by Dolgov et al. [17] and the papers by Abazajian et al. [44] and Wong [45] that followed shortly thereafter. (See also Ref. [46].) The authors of Ref. [17] concluded that equilibration of the lepton number across

the flavors — the shorthand for which is simply *flavor equilibration* — is achieved prior to the onset of BBN for a lepton asymmetry on the order of the L_ν constraint. Subsequent papers on the topic [20, 21, 44, 45, 47–49] have refined this original treatment of the problem, examining the connections to $N_{\rm eff}$, Y_P, and the D abundance [D/H].

The literature in this area has largely been inspired by the quest to establish rigorous limits on the neutrino degeneracy parameters $\eta_{\nu_\alpha} = \mu_\alpha/T$, where μ_α is the chemical potential of neutrino flavor α. In the event that a lepton number completely equilibrates, the BBN-derived limits that constrain η_{ν_e} likewise apply to the other flavors. Conversely, if no equilibration occurs, then the constraints on η_{ν_μ} and η_{ν_τ} are considerably weaker than those on η_{ν_e}, as they are bounded solely by their contribution to the radiation energy density. The objective of this paper is not to revisit the question of constraints on neutrino degeneracy, but rather to explore more fully the panoply of flavor evolution that may have occurred in the early universe. While smaller values of L_ν push into the realm of effects that are thought to be currently undetectable, we demonstrate — with an eye to forthcoming observational improvements — that varying the initial lepton number leads to dramatically different behaviors.

To this end we identify five regimes of coherent flavor evolution that may be found for lepton numbers at or below observational constraints (Fig. 2.1). We label these regimes by their principal characteristics, which are, in order of decreasing lepton asymmetry,

I. large synchronized oscillations,

II. minimal flavor transformation,

III. asymmetric (ν- or $\bar{\nu}$-only) MSW conversion,

IV. partial MSW conversion, and

V. symmetric MSW conversion.

We elucidate the physics behind these behaviors with frequent recourse to the framework of (non-)

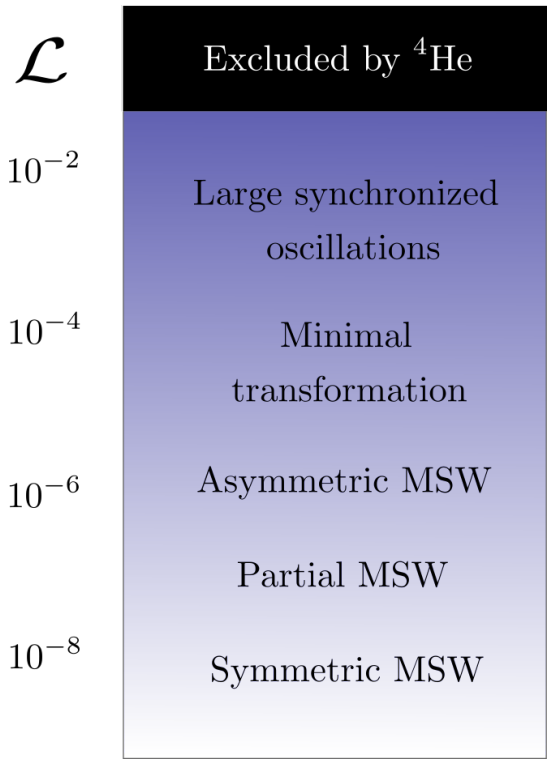

Figure 2.1: Schematic illustration of the landscape of coherent flavor evolution in the inverted hierarchy as a function of lepton asymmetry $\mathcal{L} = L_{\nu_e} - L_{\nu_x}$. The black swath at the top of the figure indicates the realm of lepton asymmetries that are currently excluded by ^{4}He measurements. The five regimes at sub-constraint values of $\mathcal{L}$ are labeled by their most prominent characteristics.

adiabatic level-crossings. We also discuss how the inclusion of collisions, in the approximate form of scattering-induced quantum damping, differently affects these regimes. Coarse features of the coherent oscillation physics are found to persist in the presence of damping. We argue that this finding motivates further exploration of the lepton-asymmetric terrain with a treatment that goes beyond the approximations of the present study.

The equations of motion relevant to the evolution of a lepton asymmetry in the early universe are set out in Sec. 2.3. The regimes of coherent evolution are presented in Sec. 2.4, followed by discussions of adiabaticity, the matter–neutrino resonance, and the importance of collisions. A conclusion is given in Sec. 2.5. Throughout this paper we use natural units in which $c = \hbar = k_B = 1$.

2.3 Neutrino kinetics in the early universe

For reasons made clear below, the active period for neutrino flavor transformation begins around $10 - 20$ MeV and continues down to — or, depending on the lepton asymmetry, through — the epoch of neutrino decoupling at ~ 1 MeV. Over these temperatures the three flavors of active neutrinos are immersed in a hot, dense bath of electrons, positrons, and free nucleons; the $\mu^{\pm}$ and $\tau^{\pm}$ that abounded at higher temperatures have all but disappeared, while $e^{\pm}$ remain relativistic through to the very bottom of this temperature range. Protons and neutrons, in contrast, have long since become nonrelativistic, and their densities are minuscule in comparison on account of the high entropy of the plasma. Within this medium neutrinos experience oscillations enhanced by forward (coherent) scattering with matter particles ($e^{\pm}$) and other neutrinos. They also undergo momentum-changing (incoherent) scattering with both populations.

In Sec. 2.3.1 we explain how the problem of neutrino flavor evolution under these conditions can be reduced to an effective two-flavor scenario. We then go on to describe in Sec. 2.3.2 the potentials that drive the coherent mixing between the two flavors and the incoherent scat-

tering that competes against it. We provide in Sec. 2.3.3 the relevant background on resonant flavor transformation and collective oscillations. Lastly, in Sec. 2.3.4 we briefly summarize the numerical approach adopted in this study.

2.3.1 Two-flavor system

Under the condition that $L_{\nu_\mu} = L_{\nu_\tau}$, the paucity of muons and tauons in the plasma — and, correspondingly, of charged-current interactions involving ν_μ and ν_τ— entails that neutrinos are well modeled by an effective two-flavor system consisting of ν_e and ν_x, where ν_x is a superposition of ν_μ and ν_τ. We present here a derivation of the effective mixing parameters relevant to this two-flavor system. A similar view on the reduction to two flavors can be found in Ref. [50].

An effective mixing angle θ parameterizes vacuum mixing in the two-flavor system, with the orthogonal transformation between the mass and flavor states given by

$$\begin{aligned} \nu_e &= \nu_1 \cos\theta + \nu_2 \sin\theta \\ \nu_x &= -\nu_1 \sin\theta + \nu_2 \cos\theta, \end{aligned} \tag{2.4}$$

where $\nu_{1,2}$ are mass eigenstates with masses $m_{1,2}$. (Strictly speaking, as Eq. 2.6 below will make clear, ν_1 is only an eigenstate in the limit that two of the three physical neutrino masses are degenerate. This is exactly the limit that we will take.) The electron neutrino ν_e in the two-flavor system is identical to its three-flavor counterpart ν'_e, which after transforming to the appropriate mass bases yields the constraint

$$\begin{aligned} \nu_1 \cos\theta + \nu_2 \sin\theta = {} & \nu'_1 \cos\theta'_{12} \cos\theta'_{13} \\ & + \nu'_2 \sin\theta'_{12} \cos\theta'_{13} e^{-i\varphi_1} \\ & + \nu'_3 \sin\theta'_{13} e^{-i\delta} e^{-i\varphi_2}, \end{aligned} \tag{2.5}$$

using primes to denote three-flavor mixing parameters and δ and φ_i to denote the Dirac and Majorana CP-violating phases. We identify $\theta = \theta'_{13}$, so that the two-flavor mass eigenstates are related to the three-flavor ones by the relations

$$\begin{aligned}
\nu_1 &= \nu'_1 \cos\theta'_{12} + \nu'_2 \sin\theta'_{12} e^{-i\varphi_1} \\
\nu_2 &= \nu'_3 e^{-i\delta} e^{-i\varphi_2}.
\end{aligned} \tag{2.6}$$

The phases δ and φ_2 amount to an overall rephasing of ν_2 and exert no influence on our calculations; similarly for the other Majorana phase. We point out that this conclusion regarding δ is consistent with the study of CP violation in the neutrino-degenerate early universe in Ref. [48], which showed that effects of CP violation from the Dirac phase appear only when $L_{\nu_\mu} \neq L_{\nu_\tau}$.

A third mass eigenstate, orthogonal to ν_1 and ν_2 and having mass m_3, may also be defined in order to complete the transformation between the primed and unprimed bases:

$$\nu_3 = -\nu'_1 \sin\theta'_{12} + \nu'_2 \cos\theta'_{12} e^{-i\varphi_1}. \tag{2.7}$$

This state decouples from the other two and is identical to the third flavor eigenstate in the unprimed basis: $\nu_3 = \nu_y$. Written in terms of the physical flavor states,

$$\begin{aligned}
\nu_e &= \nu'_e \\
\nu_x &= \nu'_\mu \sin\theta'_{23} e^{-i\delta} + \nu'_\tau \cos\theta'_{23} e^{-i\delta} \\
\nu_y &= \nu'_\mu \cos\theta'_{23} - \nu'_\tau \sin\theta'_{23}.
\end{aligned} \tag{2.8}$$

From Eqs. (2.6) and (2.7) it follows that

$$\begin{aligned} m_1^2 &= m_1'^2 \cos^2\theta_{12}' + m_2'^2 \sin^2\theta_{12}' \\ m_2^2 &= m_3'^2 \\ m_3^2 &= m_1'^2 \sin^2\theta_{12}' + m_2'^2 \cos^2\theta_{12}'. \end{aligned} \tag{2.9}$$

Since we are concerned primarily with qualitative behavior in this paper, we will be content to take $m_1'^2 \approx m_2'^2$, which leads to

$$\delta m^2 \equiv m_2^2 - m_1^2 \approx m_2^2 - m_3^2 \approx \delta m_{31}'^2. \tag{2.10}$$

To this level of approximation the ν_i ($i = 1, 2, 3$) states are genuine mass eigenstates and, moreover, ν_3 is degenerate with ν_1 and decouples from the $\nu_e - \nu_x$ mixing channel. With the proviso that the lepton numbers L_{ν_μ} and L_{ν_τ} are the same (but not necessarily equal to L_{ν_e}), the flavor transformation that occurs in the temperature range we investigate here is therefore adequately captured by $\nu_e - \nu_x$ oscillations with $1-3$ mixing parameters.

This effective two-flavor system distills many of the important aspects of the full three-flavor problem, and the flavor-transformation phenomena we describe below carry over to mixing in other channels. The locations and sizes of features shift with changing parameters — $\delta m_\odot^2$, for instance, gives rise to resonance behavior at lower temperatures than does $\delta m_{\rm atm}^2$ — but the physics behind these features is resilient. Nonetheless, it should be kept in mind that transformation among three flavors will lead to an even richer landscape of flavor evolution than in the two-flavor scenario, especially in the event that L_{ν_e}, L_{ν_μ}, and L_{ν_τ} are all unequal.

2.3.2 The kinetic equations

Tracking the flavor content of an ensemble of neutrinos and antineutrinos is accomplished by following the evolution of the density matrices ϱ and $\bar{\varrho}$, which for each comoving energy $\varepsilon = E/T \approx p/T$ have the 2×2 structures

$$\varrho(\varepsilon,t) = \begin{pmatrix} \varrho_{ee} & \varrho_{ex} \\ \varrho_{ex}^* & \varrho_{xx} \end{pmatrix}, \; \bar{\varrho}(\varepsilon,t) = \begin{pmatrix} \bar{\varrho}_{ee} & \bar{\varrho}_{ex} \\ \bar{\varrho}_{ex}^* & \bar{\varrho}_{xx} \end{pmatrix}, \tag{2.11}$$

where the individual matrix elements tacitly depend on ε and t. (Throughout this paper we denote the analogous objects for antineutrinos using the prescription $\nu_\alpha \to \bar{\nu}_\alpha$. The antineutrino analogues will always be denoted with an overbar.)

We choose a normalization such that at high temperature ϱ assumes the form

$$\varrho(\varepsilon) \;\cong\; \begin{pmatrix} f(\varepsilon,\eta_{\nu_e}) & 0 \\ 0 & f(\varepsilon,\eta_{\nu_x}) \end{pmatrix}, \tag{2.12}$$

where the diagonal entries are Fermi–Dirac equilibrium distribution functions

$$f(\varepsilon,\eta_{\nu_\alpha}) = \frac{1}{e^{\varepsilon-\eta_{\nu_\alpha}}+1}. \tag{2.13}$$

In general, whether at high temperature or not, the diagonal entries of ϱ encode the number densities of ν_e and ν_x and the off-diagonal entries measure quantum coherence between the two flavors.

The initial conditions given in Eq. (2.12) are justified by the quasi-equilibrium that obtains at the starting temperatures used for our calculations. At these temperatures the neutrinos exchange energy with the plasma on timescales short compared to the Hubble time, ensuring that the neutrino spectra retain their thermal Fermi–Dirac shape on the latter timescale, even while the

chemical potentials are evolving. (To be precise, it is the number densities in *energy* eigenstates that are proportional to Fermi–Dirac functions; the validity of using them in the *flavor*-basis density matrix lies in the fact that at high T the flavor and energy bases are nearly coincident.) As the temperature drops, oscillations grow in importance relative to incoherent scattering, and the ability of scattering to preserve equilibrium spectra diminishes. But in the scattering-dominated limit, in which our initial temperatures safely fall, neutrinos have distribution functions as in Eq. (2.12), and coherence between the flavors is efficiently stamped out by the high scattering rate.

For each mode ε the neutrino and antineutrino density matrices obey the equations of motion

$$\begin{aligned} i\left(\partial_t - Hp\partial_p\right)\rho\left(\varepsilon,t\right) &= \left[\mathcal{H}\left(\varepsilon,t\right),\rho\left(\varepsilon,t\right)\right] + \mathcal{C} \\ i\left(\partial_t - Hp\partial_p\right)\bar{\rho}\left(\varepsilon,t\right) &= \left[\bar{\mathcal{H}}\left(\varepsilon,t\right),\bar{\rho}\left(\varepsilon,t\right)\right] + \bar{\mathcal{C}}, \end{aligned} \tag{2.14}$$

where H is the Hubble parameter, $\mathcal{H}$ is the Hamiltonian, and $\mathcal{C}$ is the collision term encapsulating incoherent scattering [51]. The collision term depends on the neutrino density matrices and the background-particle distribution functions across all energies.

The Hamiltonian consists of three ingredients: a vacuum potential $\mathcal{H}_{\rm vac}$, which is driven by the mass-squared splitting δm^2 and the vacuum mixing angle θ; a thermal potential $\mathcal{H}_e$, which is due to forward scattering of neutrinos with the $e^\pm$ jostling about in the plasma; and a self-coupling potential $\mathcal{H}_\nu$, which arises from neutrino–neutrino scattering. Written out,

$$\begin{aligned} \mathcal{H} &= \mathcal{H}_{\rm vac} + \mathcal{H}_e + \mathcal{H}_\nu \\ &= \frac{\delta m^2}{2E}\mathrm{B} - \frac{8\sqrt{2}G_F E\rho_{e^\pm}}{3m_W^2}\mathrm{L} \\ &\quad + \frac{\sqrt{2}G_F}{2\pi^2}\int dE' E'^2\left[\rho\left(E'\right) - \bar{\rho}^*\left(E'\right)\right], \end{aligned} \tag{2.15}$$

where in the flavor basis $\mathrm{B} = \mathrm{U}\,(\mathrm{diag}\,[-1/2, 1/2])\,\mathrm{U}^\dagger$ with Pontecorvo–Maki–Nakagawa–Sakata (PMNS) matrix U, $\mathrm{L} = \mathrm{diag}\,[1, 0]$, $\rho_{e^\pm}$ denotes the energy density of $e^\pm$, G_F is the Fermi constant, and m_W is the W boson mass. The time-dependence of E, $\rho_{e^\pm}$, ρ, and $\bar{\rho}$ is implicit. Antineutrinos, meanwhile, evolve under the Hamiltonian $\bar{\mathcal{H}} = \mathcal{H}_{\rm vac} + \mathcal{H}_e - \mathcal{H}_\nu^*$.

Strictly speaking, the Hamiltonian relevant to neutrino propagation in a medium contains more terms than those shown in Eq. (2.15) [52]. In addition to the finite-temperature charged-lepton potential ($\sim \rho_{e^\pm}$) and the finite-density neutrino potential ($\sim (n_{\nu_e} - n_{\nu_x})$ for the diagonal portion), neutrinos also experience a finite-temperature neutrino potential ($\sim (\rho_{\nu_e} - \rho_{\nu_x})$, again for the diagonal portion) and a finite-density charged-lepton potential ($\sim (n_{e^-} - n_{e^+})$). By the charge neutrality of the universe, however, the $e^\pm$ asymmetry must balance the baryon asymmetry, making this contribution to the potential very small. The thermal neutrino potential, meanwhile, is $O(G_F^2)$ and is further suppressed by a factor comparable to the lepton asymmetry. Lastly, we leave out the $\mu^\pm$ contribution to $\mathcal{H}_e$, as in the scenarios we are concerned with, their population has dwindled close to zero by the time flavor transformation begins.

The collision term $\mathcal{C}$ in Eq. (2.14) represents inelastic scattering of neutrinos and is proportional to G_F^2. A fully realistic treatment would involve computing quantum Boltzmann collision integrals [53, 54], a task that has only recently been accomplished for the first time [55]. Whereas in Ref. [55] de Salas and Pastor executed a high-precision calculation of $N_{\rm eff}$ in the standard (i.e., lepton-symmetric) scenario, our aim here is to point out that an initial lepton asymmetry at high temperature shapes the subsequent neutrino flavor evolution in diverse and complicated ways. For this study we instead set $\mathcal{C}$ to be a quantum damping term that is proportional to ρ but has vanishing diagonal entries [56–62]. Using such a term for $\mathcal{C}$ amounts to the ansatz that the chief effect of collisions is to eliminate coherence between the flavors.

The paradigm typically associated with quantum damping holds that a collision acts as a measurement of the scattered neutrino, thereby collapsing it into a definite flavor state. Although this picture is only a heuristic and has its limitations, it correctly suggests that a system of

(anti)neutrinos immersed in a thermal bath ultimately approaches a mixed state with equal ν_e ($\bar{\nu}_e$) and ν_x ($\bar{\nu}_x$) probabilities. One of the fundamental issues at stake with a lepton asymmetry is the timescale over which this descent to a maximum-entropy state (and the concomitant flavor equilibration) transpires. Conceptual aid notwithstanding, damping does not in fact capture all of the microphysics of scattering, and in Sec. 2.4.4 we will address the deficiencies of this approximation at length.

Rather than solving for the flavor evolution directly as a function of t, we work in terms of a parameter $x = Ma$, where M is an arbitrary energy scale and a is the scale factor; doing so transfigures the equations of motion into ordinary differential equations. Furthermore, for a two-flavor system the density matrix ρ can be projected onto the Pauli matrices according to

$$\rho = \frac{1}{2}\left(P_0 + \vec{P}\cdot\vec{\sigma}\right). \tag{2.16}$$

Given that $\mathcal{C}$ has vanishing diagonal entries, the trace of ρ is preserved by the equations of motion and has value

$$\mathrm{Tr}\rho = P_0 = f\left(\eta^i_{\nu_e}\right) + f\left(\eta^i_{\nu_x}\right), \tag{2.17}$$

where $f\left(\eta^i_{\nu_\alpha}\right)$ is the initial distribution function of ν_α, prior to any significant flavor transformation. The polarization vector $\vec{P}$, meanwhile, does evolve: If similar projections are performed for $\mathcal{H}$ and $\mathcal{C}$, Eq. (2.14) can be recast as

$$Hx\frac{d\vec{P}}{dx} = \vec{\mathcal{H}}\times\vec{P} - \mathcal{D}\vec{P}_T. \tag{2.18}$$

Along the same lines, we will make use of the notation

$$\mathcal{H} = \begin{pmatrix} \mathcal{H}_z & \mathcal{H}_T \\ \mathcal{H}_T^* & -\mathcal{H}_z \end{pmatrix},\ \mathcal{V} = \begin{pmatrix} \mathcal{V}_z & \mathcal{V}_T \\ \mathcal{V}_T^* & -\mathcal{V}_z \end{pmatrix}, \tag{2.19}$$

where $\mathcal{V} = \mathcal{H}_e + \mathcal{H}_\nu$ denotes the weak-interaction potential arising from coherent forward scattering and where, for example, $\mathcal{H}_T = \mathcal{H}_x - i\mathcal{H}_y$ encodes the component of the Hamiltonian vector $\vec{\mathcal{H}}$ that is transverse to the flavor (z-) axis. The damping parameter $\mathcal{D}$ that appears in Eq. (2.18) is related to the scattering amplitudes of the neutrino flavor states. To illustrate: If the medium were such that the two flavors had equal scattering amplitudes, interactions would be unable to differentiate between the two flavors and there would be no damping ($\mathcal{D} = 0$). At the other extreme, if one of the flavors were non-interacting (for instance, in active–sterile mixing), then the damping parameter would be half the total interaction rate Γ_α of the other flavor ($\mathcal{D} = \Gamma_\alpha/2$).

In the plasma of the early universe, ν_e and ν_x scatter with different (but nonzero) cross sections, and a detailed derivation of $\mathcal{D}$ would add up the contributions from all the individual weak-interaction processes relevant to this environment. We opt for a coarser treatment here, taking

$$\mathcal{D} \approx \frac{1}{2}\left(\Gamma_e - \Gamma_x\right) \approx \frac{1}{2} d_{ex} G_F^2 p T^4 \tag{2.20}$$

with $d_{ex} \approx 0.35$ [62]. The approximation in Eq. (2.20) is sufficiently accurate for the objectives of this study. Indeed, for most of the paper we focus on the coherent regime, in which $\mathcal{D} = 0$; it is only in Sec. 2.4.4 that we let $\mathcal{D}$ assume the approximate form given above. To be sure, the flavor evolution we are tracking occurs over a range of temperatures in which collisions are important. But as we discuss in detail in Sec. 2.4.4, broad characteristics of the coherent regime survive the inclusion of damping, and a close analysis of the coherent transformation sheds light on the physics underlying the behavior in the presence of both oscillations and collisions.

Translating the density matrix ρ into the polarization vector $\vec{P}$ affords a geometric interpretation to the flavor evolution of the system (more detailed expositions of which may be found in Refs. [58, 63]). At high temperatures $\vec{P}$ lies along the z-axis because of the peremptory destruction of coherence by collisions. As the temperature (and by extension the scattering rate) drops, $\vec{P}$ is able to travel away from the z-axis: The path it follows is determined by a competition between its desire to precess around the Hamiltonian vector $\vec{H}$ and the constant push exerted by

collisions back toward the flavor axis. Meanwhile $\vec{H}$ itself migrates in response to the falling temperature and the movement of the individual polarization vectors. $\vec{P}$ tries to track $\vec{H}$ as the latter drifts, but its success in doing so is moderated by the constant buffeting of collisions and the degree of non-adiabaticity. We address the latter criterion in Sec. 2.4.2.

At any time the relative number density of ν_e and ν_x of a given mode ε (taken to have finite width $d\varepsilon$) can be read off by projecting that mode's polarization vector onto the flavor axis and providing the appropriate thermodynamic prefactor:

$$\begin{aligned} & P_{z,\varepsilon} = \rho_{ee,\varepsilon} - \rho_{xx,\varepsilon} \\ \implies & dn_{\nu_e,\varepsilon} - dn_{\nu_x,\varepsilon} = \frac{T^3}{2\pi^2}\, d\varepsilon\, \varepsilon^2 P_{z,\varepsilon}. \end{aligned} \tag{2.21}$$

We have written the number density of ν_α in mode ε as $dn_{\nu_\alpha,\varepsilon}$ in preparation for integrating over all modes. Performing the sum over ε and dividing by T^3 (to get a redshift-invariant quantity) yields the z-component of the *integrated* polarization vector:

$$P_{z,\mathrm{int}} \equiv \frac{1}{2\pi^2} \sum_\varepsilon d\varepsilon\, \varepsilon^2 P_{z,\varepsilon} = \frac{n_{\nu_e} - n_{\nu_x}}{T^3}, \tag{2.22}$$

where n_{ν_e} and n_{ν_x} are the total number densities across all energies. The quantities $\bar{P}_z$ and $\bar{P}_{z,\mathrm{int}}$, appropriate to antineutrinos, are defined analogously. We will present many of our numerical results as plots of $P_{z,\mathrm{int}}$ and $\bar{P}_{z,\mathrm{int}}$, as they convey the "average" flavor evolution of the system; where illuminating, we will zoom in on the individual modes. Note that with these definitions $P_z > 0$ ($\bar{P}_z > 0$) reflects a predominance of electron neutrinos (antineutrinos).

2.3.3 Resonant flavor mixing and collective oscillations

One of the linchpins of neutrino flavor phenomenology in the early universe and other astrophysical environments is the Mikheyev–Smirnov–Wolfenstein (MSW) mechanism by which

coherent scattering with a matter background causes neutrinos to acquire effective masses and mixing angles [64, 65]. Letting $\Delta \equiv \delta m^2/2E$, the in-medium mass-squared splitting δm^2_M is defined by

$$\Delta^2_M \equiv \left(\frac{\delta m^2_M}{2E}\right)^2 \equiv \Delta^2 \sin^2 2\theta + (\Delta \cos 2\theta - \mathcal{V}_z)^2 \tag{2.23}$$

and the in-medium mixing angle θ_M by

$$\sin^2 2\theta_M \equiv \frac{\Delta^2 \sin^2 2\theta}{\Delta^2_M}. \tag{2.24}$$

(For the purposes of introducing the traditional MSW mechanism, we are neglecting neutrino–neutrino scattering in Eqs. (2.23) and (2.24), but we will return to these definitions later on in order to incorporate self-coupling.) Resonance occurs when $\mathcal{V}_z = \Delta \cos 2\theta$: The effective mixing angle is at its maximum (to wit, $\theta_M = \pi/4$) and the effective mass-squared splitting at its minimum. Since the thermal potential $\mathcal{H}_e$ (Eq. (2.15)) depends only on the energy density of $e^\pm$ in the plasma, the matter background modifies the oscillations of neutrinos and antineutrinos in precisely the same way.

Neutrino–neutrino coherent scattering gives rise to "index-of-refraction" effects in much the same fashion as a matter background, but with an added layer of complexity. As seen in Eq. (2.15), the evolution of $\rho(\varepsilon)$ for a particular mode ε depends, through the self-coupling potential $\mathcal{H}_\nu$, on the density matrices for all other modes ε', meaning that the problem of flavor evolution in a dense neutrino system is a nonlinear one. A fascinating range of collective behaviors has been shown to result. (See Ref. [66] for a review, or Refs. [67–72] for a selection of recent work in this active area.) The role of nonlinear coupling in the early universe is perhaps best epitomized by the phenomenon of synchronized oscillations that emerges when the self-coupling is strong enough to "glue" all of the individual modes together and prevent them from kinematically decohering [73–78].

Synchronized oscillations are seen in our results to be one of the hallmarks of coherent

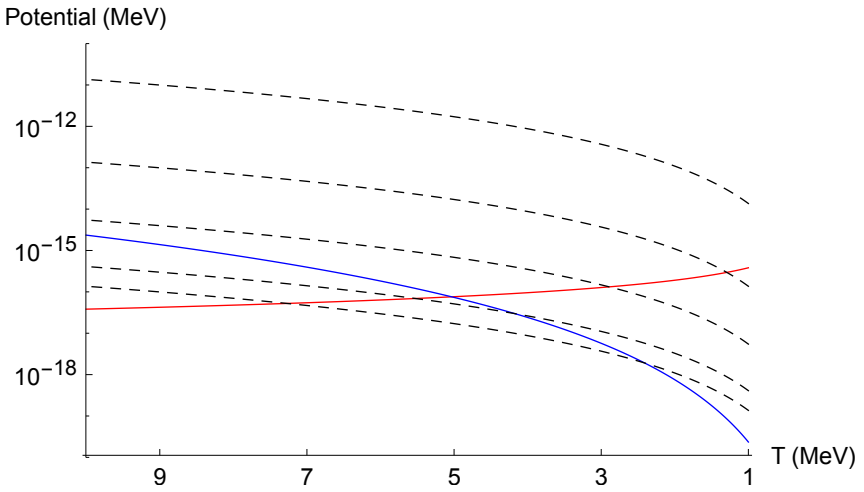

Figure 2.2: Magnitudes of the individual diagonal potentials for $\varepsilon = 3$: $|\mathcal{H}_{\mathrm{vac,\,z}}|$ (red, upper solid curve at $T = 1$ MeV), $|\mathcal{H}_{e,z}|$ (blue, other solid curve), and $|\mathcal{H}_{\nu,z}|$ (black, dashed). The last of these was computed assuming no flavor transformation. From top to bottom the dashed curves correspond to degeneracy parameters $\eta_{\nu_e} = 5\times10^{-3}$, 5×10^{-5}, 2×10^{-6}, 1.5×10^{-7}, and 5×10^{-8} (Eq. (2.25)); chemical potentials in ν_μ were taken to be zero.

flavor evolution in a universe with a lepton asymmetry within a couple orders of magnitude of the current constraint on L_ν. At the other end of the spectrum, with a lepton asymmetry on the order of the baryon asymmetry η, self-coupling is unimportant and the MSW mechanism reigns supreme. In the following section we discuss these two regimes and several others that emerge at intermediate lepton asymmetries.

The type of behavior exhibited depends fundamentally on the relative sizes of the individual contributions to the Hamiltonian. We depict in Fig. 2.2 the magnitudes of the diagonal potentials as functions of temperature, with four different curves for $\mathcal{H}_{\nu,z}$ corresponding to different initial lepton asymmetries. As we describe below, one of the basic determinants of the flavor evolution is the magnitude of $\mathcal{H}_{\nu,z}$ where the vacuum- and thermal-potential curves intersect, which is to say at MSW resonance. We will also see the limitations of this picture, which fails to account for the off-diagonal components of the Hamiltonian.

2.3.4 Numerical details

We have employed two independent programs for solving the equations of motion (Eq. (2.18)), one based on a fourth-order explicit Runge–Kutta solver and the other on a Magnus-method solver. The Magnus method, which is tailor-made for tracking unitary evolution, has been used previously in work on neutrino flavor transformation in supernovae; for a thorough description, see Ref. [79]. We have achieved consistent results with the two codes, and we have confirmed that in the coherent limit each one individually conserves $|\vec{P}|$ and $\mathrm{Tr}\rho = P_0$ to high precision.

As shown below, certain flavor-evolution regimes host rapid, highly aperiodic oscillations, and in such regimes the behavior of individual modes depends sensitively on the physical and computational parameters of the calculation. The very fine features displayed in these scenarios are without (and may simply defy) a detailed physical explanation and, moreover, are beyond the level of precision aimed at in this study. Rather, our focus is on the major qualitative features, which we have found to be robust.

2.4 Results and Discussion

In this section we present our results through the example of five different initial lepton asymmetries that typify the major regimes of coherent flavor evolution in the inverted hierarchy (IH). We then apply the concept of adiabaticity to gain insight into the behaviors manifested in these prototypical cases. Following a discussion of the coherent regimes, we introduce collisions in the form of quantum damping. As a rule of thumb, the impact of damping is (in a non-quantitative sense) proportional to the amount of flavor transformation that would occur in the *absence* of damping: That is to say, for damping to gain leverage on the evolution of $\vec{P}$, a significant $\vec{P}_T$ must develop, and for this to be the case there must be substantial transformation of $\vec{P}$ away from the initial flavor eigenstate. To understand the results with damping, it is therefore

necessary to understand the results without.

In what follows we focus most of our attention on the IH because it, unlike the normal hierarchy (NH), plays host to an MSW resonance and, by implication, to generally more substantial flavor transformation. We will briefly discuss the NH when we turn to damping.

2.4.1 Regimes of coherent evolution

Before any flavor transformation has occurred neutrinos of flavor α are described by a Fermi–Dirac equilibrium spectrum with neutrino degeneracy parameter η_{ν_α} (Eq. (2.13)). For the purposes of this study we assume that at high temperatures the lepton number is positive and entirely contained in ν_e, so that $\eta_{\nu_x} = 0$ and η_{ν_e} can be deduced from the lepton number via

$$L_\nu \approx \frac{1}{12\zeta(3)}\left(\pi^2\eta_{\nu_e} + \eta_{\nu_e}^3\right) \approx 0.68\eta_{\nu_e}, \tag{2.25}$$

where the second approximation applies for the small degeneracy parameters we are considering. We would find similar results, but with the roles of neutrinos and antineutrinos swapped, if instead we were to take a negative η_{ν_e} or were to put the lepton number entirely in ν_x. Furthermore, the choice of setting $\eta_{\nu_x} = 0$ at high temperature is inessential for our results, as it is the lepton *asymmetry* which dictates the role of the self-coupling potential.

Note that we take no stance on what mechanism actually produces the initial lepton numbers. The question of how to generate an asymmetry that survives washout from scattering processes is an important one and has been examined in Ref. [80]. This question is, however, outside the purview of the present study.

The five regimes of coherent flavor evolution that we have identified in our numerical results are depicted schematically in Fig. 2.1. In our sweep of the lepton-number terrain, the values of η_{ν_e} that we have found best embody the features associated with these regimes are as follows: 5×10^{-8}, 1.5×10^{-7}, 2×10^{-6}, 5×10^{-5}, and 5×10^{-3}.

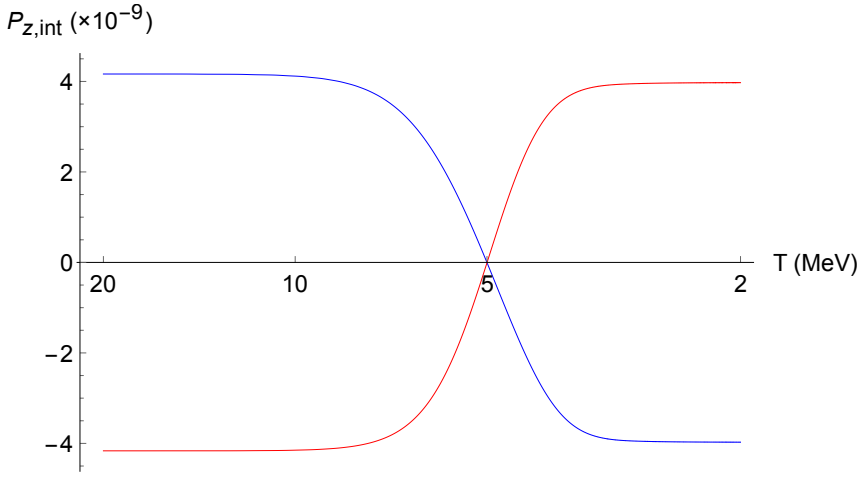

Figure 2.3: Symmetric MSW: $P_{z,\mathrm{int}}$ (blue, upper curve at $T = 20$ MeV) and $\bar{P}_{z,\mathrm{int}}$ (red) in the IH with initial degeneracy parameters $\eta_{\nu_e} = 5 \times 10^{-8}$, $\eta_{\nu_x} = 0$.

$\eta_{\nu_e} = 5 \times 10^{-8}$: Symmetric MSW

Generally speaking, the dominant feature in the flavor-transformation landscape is the equality of $|\mathcal{H}_{\mathrm{vac},z}|$ and $|\mathcal{H}_{e,z}|$, which for $1-3$ mixing occurs in the region of $T \sim 5$ MeV. For $\eta_{\nu_e} \lesssim 5 \times 10^{-8}$ this is the *only* feature (Fig. 2.3), as the self-coupling is so weak as to leave transformation through the resonance essentially untouched. At these small lepton numbers — as would be expected if neutrino–neutrino scattering were simply omitted — neutrinos and antineutrinos of all modes undergo complete MSW conversion. We emphasize that, unlike in a supernova environment, *both* neutrinos and antineutrinos resonantly transform due to $\mathcal{H}_e$ being CP-symmetric: At high temperatures ν_e and $\bar{\nu}_e$ are at energies lower than ν_x and $\bar{\nu}_x$, respectively, thanks to the thermal potential, but at low temperatures (in vacuum) are at higher energies, thanks to the IH.

Evidently, if the neutrino chemical potential is entirely in ν_e and if it is of the same order as the baryon asymmetry η, then neutrino–neutrino scattering has an ignorable impact on flavor evolution. This conclusion is unsurprising given Fig. 2.2, which shows that $|\mathcal{H}_{\nu,z}|$ for $\eta_{\nu_e} = 5 \times 10^{-8}$ is always about an order of magnitude or more below either $|\mathcal{H}_{\mathrm{vac},z}|$ or $|\mathcal{H}_{e,z}|$. It is worth pointing out that at such small lepton numbers the $e^{\pm}$ finite-density potential

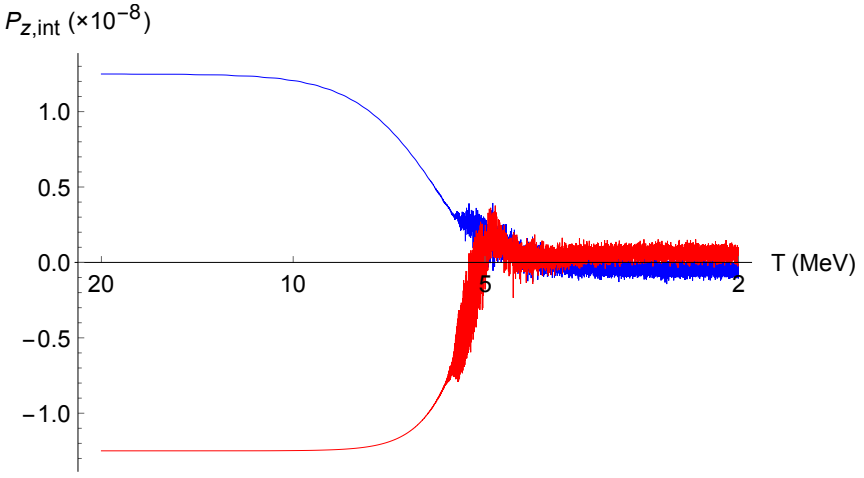

Figure 2.4: Partial MSW: $P_{z,\mathrm{int}}$ (blue, upper curve at $T = 20$ MeV) and $\bar{P}_{z,\mathrm{int}}$ (red) in the IH with initial degeneracy parameters $\eta_{\nu_e} = 1.5 \times 10^{-7}$, $\eta_{\nu_x} = 0$.

$\mathcal{H}_e^{(\mathrm{FD})} = \sqrt{2} G_F \left(n_{e^-} - n_{e^+}\right) \mathrm{L}$ should be included in the equations of motion for consistency, but this term likewise makes an inconsequential contribution to the total Hamiltonian. The effect of the thermal potential from the neutrino background is yet more feeble.

$\eta_{\nu_e} = 1.5 \times 10^{-7}$: Partial MSW

As η_{ν_e} is scaled up, MSW transformation becomes overall less effective for both neutrinos and antineutrinos (Fig. 2.4). The incompleteness of the conversion of $P_{z,\mathrm{int}}$ and $\bar{P}_{z,\mathrm{int}}$ is attributable to the differing outcomes of individual modes: The lowest-energy modes go through MSW unfettered while higher-energy modes exhibit large, aperiodic oscillations of high frequency (Fig. 2.5).

The higher-energy modes transform inefficiently due to a loss of adiabaticity, as indicated in Fig. 2.6. Prior to resonance the off-diagonal potential $\mathcal{H}_T$ fluctuates rapidly and achieves (nearly) vanishing magnitude at various points. Since $|\mathcal{H}_T|$ mediates the transition probability between states, this behavior allows neutrinos to depart from their initial energy-eigenstate track at the level-crossing. In Sec. 2.4.2 we introduce the quantitative measure of adiabaticity traditionally used in studies of resonant neutrino conversion, and we explore further the role it plays in our

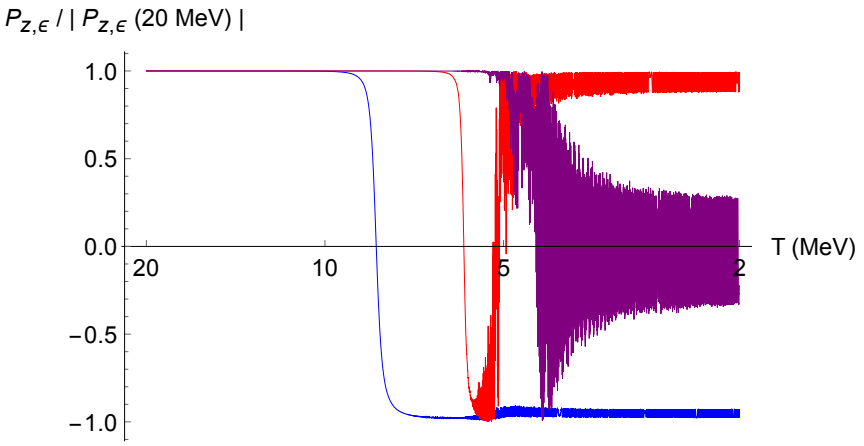

Figure 2.5: Partial MSW: $P_{z,\varepsilon}$ for $\varepsilon = 1.15$ (blue, bottommost curve at $T = 2$ MeV), 2.36 (red, topmost curve at $T = 2$ MeV), and 4.78 (purple), with the same parameters as in Fig. 2.4. Note that here and in subsequent plots $P_{z,\varepsilon}$ has been normalized to an initial value of unity for each ε; this choice puts all modes on equal footing for the purpose of comparing flavor evolution.

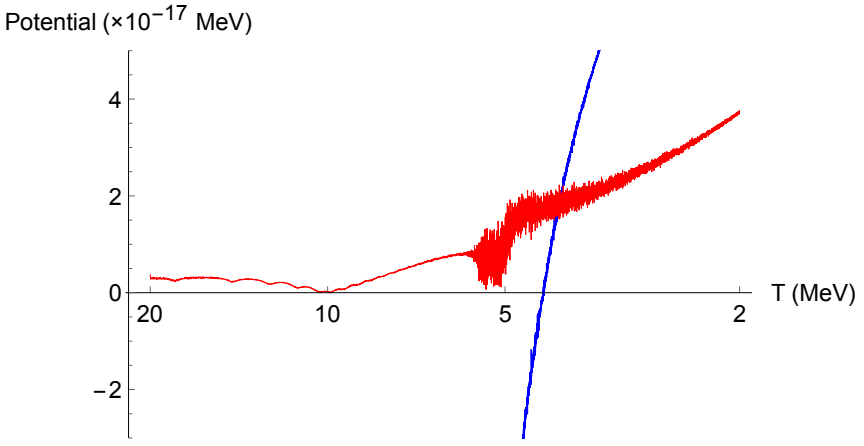

Figure 2.6: Partial MSW: $\mathcal{H}_z$ (blue, nearly vertical curve) and $|\mathcal{H}_T|$ (red) as functions of T for the $\varepsilon = 4.78$ mode shown in Fig. 2.5.

results. For now, suffice it to say that in this regime self-coupling suppresses adiabaticity because it is strong enough to influence $\mathcal{H}$ but not strong enough to force the individual modes to pass through resonance collectively. Such behavior is connected to the fact that for most modes the three contributions to the Hamiltonian are of comparable magnitude in the MSW region.

$\eta_{\nu_e} = 2 \times 10^{-6}$: Asymmetric ($\nu$- or $\bar{\nu}$-only) MSW

Moving to greater values of η_{ν_e}, the partial conversion of neutrinos becomes even more stunted while the conversion of antineutrinos actually grows more *effective* (Fig. 2.7).

The cancellation of $\mathcal{H}_{\mathrm{vac},z}$ and $\mathcal{H}_{e,z}$ in the MSW region precipitates some degree of transformation in both neutrinos and antineutrinos. However, since $\mathcal{H}_{\nu,z}$ exceeds the other two by a factor of ~ 10 in magnitude, MSW conversion is stillborn (in the case of neutrinos) or delayed until the vacuum potential overtakes the self-coupling soon thereafter (in the case of antineutrinos). Starting at the MSW region and continuing down to $T \sim 3$ MeV, antineutrinos gradually cross over from predominantly $\bar{\nu}_x$ to predominantly $\bar{\nu}_e$; by the bottom of this temperature range they have almost completely transformed.

Neutrinos undergo only marginal conversion because the large self-coupling potential, which enhances the effective mass of ν_e relative to ν_x, props up ν_e into the higher energy eigenstate over most of this temperature range, thus wiping out what would otherwise be an MSW resonance. (A level-crossing does occur at higher temperature where the thermal and self-coupling potentials cancel, but this resonance appears well before the MSW region and, as we will discuss in Sec. 2.4.3, is neutralized by non-adiabaticity.) Conversely, the initial population of $\bar{\nu}_x$ is effectively immersed in a bath of ν_e, which serves to elevate the energy of $\bar{\nu}_x$ over that of $\bar{\nu}_e$ until $\mathcal{H}_{\mathrm{vac}}$ becomes dominant. Hence self-coupling does not eliminate the antineutrino level-crossing in the MSW region, though it does significantly alter evolution through it.

A notable characteristic of this regime is that the location of $|\mathcal{H}_{\nu,z}| \sim |\mathcal{H}_{\mathrm{vac},z}|$ has been pulled away from that of $|\mathcal{H}_{e,z}| \sim |\mathcal{H}_{\mathrm{vac},z}|$ — compare to the partial MSW regime, where they

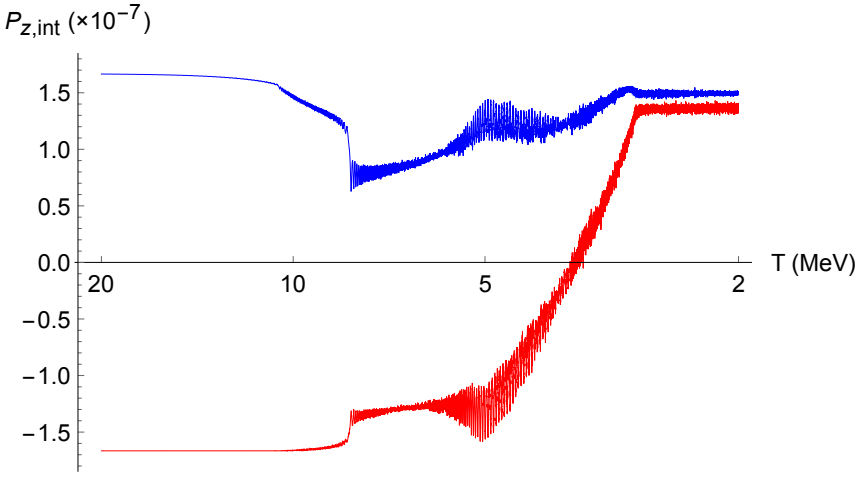

Figure 2.7: Asymmetric MSW: $P_{z,\mathrm{int}}$ (blue, upper curve at $T = 20$ MeV) and $\bar{P}_{z,\mathrm{int}}$ (red) in the IH with initial degeneracy parameters $\eta_{\nu_e} = 2 \times 10^{-6}$, $\eta_{\nu_x} = 0$.

coincide — but the regions are still close enough together that the flavor transformation instigated by the traditional MSW mechanism can be capitalized on to enact a flavor swap by the later $|\mathcal{H}_{\nu,z}| \sim |\mathcal{H}_{\mathrm{vac},z}|$ cancellation. As we observe in the next regime, increasing further the separation between the two locations leads to MSW manqué — but here the separation actually salvages efficient conversion of antineutrinos.

$\eta_{\nu_e} = 5 \times 10^{-5}$: Minimal transformation

With $\eta_{\nu_e} = 5 \times 10^{-5}$ the locations of $|\mathcal{H}_{\nu,z}| \sim |\mathcal{H}_{\mathrm{vac},z}|$ and $|\mathcal{H}_{e,z}| \sim |\mathcal{H}_{\mathrm{vac},z}|$ are well removed from one another. As a result the MSW level-crossing is now thwarted entirely, and virtually no flavor conversion takes place (Fig. 2.8). What transformation does occur commences near $T \sim 5$ MeV, as usual, but fails to get very far due to the strong "inertial" effect exerted by $\mathcal{H}_\nu$. The self-coupling keeps ν_e and $\bar{\nu}_x$ in the heavier eigenstates throughout MSW, preventing $\mathcal{H}_z$ from ever crossing into negative territory (or $\bar{\mathcal{H}}_z$ into positive).

Since coherence between the flavors only marginally develops at these lepton numbers, there is meager fuel for decoherence to consume, and the minimal-transformation regime is consequently the best preserver of its initial lepton asymmetry when damping is turned on. It

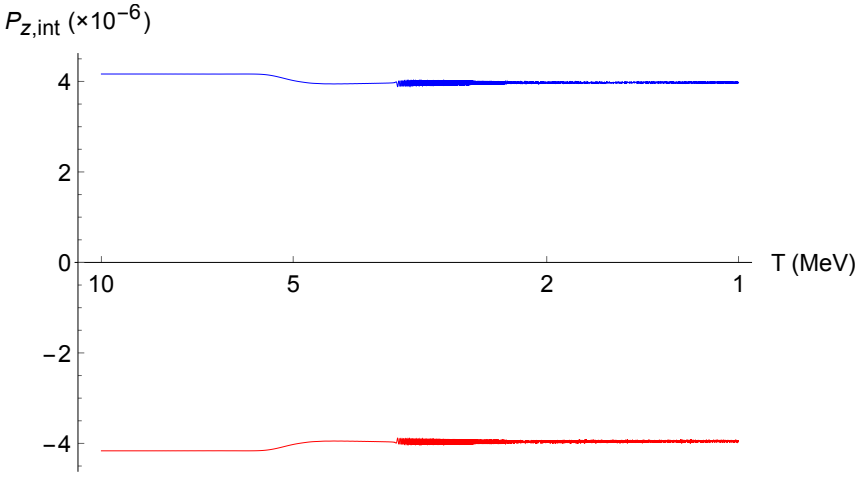

Figure 2.8: Minimal transformation: $P_{z,\mathrm{int}}$ (blue, upper curve at $T = 10$ MeV) and $\bar{P}_{z,\mathrm{int}}$ (red) in the IH with initial degeneracy parameters $\eta_{\nu_e} = 5 \times 10^{-5}$, $\eta_{\nu_x} = 0$.

is a tantalizing coincidence that this regime also encompasses the range of lepton numbers suggested by resonant production of sterile neutrino dark matter, which favors the neighborhood of $L_\nu \sim 5 \times 10^{-4}$ [42] when the ~ 3.55 keV X-ray line of Refs. [34, 35] is attributed to the decay of sterile neutrinos. These lepton numbers occupy the top end of the minimal-transformation regime, where synchronized oscillations are beginning to grow in amplitude but are still unable to realize a large net conversion of flavor.

A phenomenon notably absent from this regime and the foregoing ones is the spectral swap, in which nearly all antineutrinos below a certain energy threshold change flavor and nearly all antineutrinos above the threshold do not (or similarly for neutrinos) [81, 82]. For $\eta_{\nu_e} \lesssim 10^{-7}$ spectral swaps are ruled out by virtue of the fact that the self-coupling potential never dominates. But for $\eta_{\nu_e} = 5 \times 10^{-5}$, for instance, $\mathcal{H}_\nu$ remains dominant sufficiently far below temperatures at which $|\mathcal{H}_{\mathrm{vac},z}| \sim |\mathcal{H}_{e,z}|$ that the requisite conditions for a spectral swap might be thought to prevail as $\mathcal{H}_{\mathrm{vac},z}$ finally does overtake $\mathcal{H}_{\nu,z}$. In actuality the spectral swap is preempted by the MSW region, which in the minimal-transformation regime deposits neutrinos and antineutrinos essentially into the nearest mass eigenstates. With all well-populated modes already in mass eigenstates before $\mathcal{H}_{\mathrm{vac}}$ takes over, no spectral swap can occur. The synchronized-oscillation

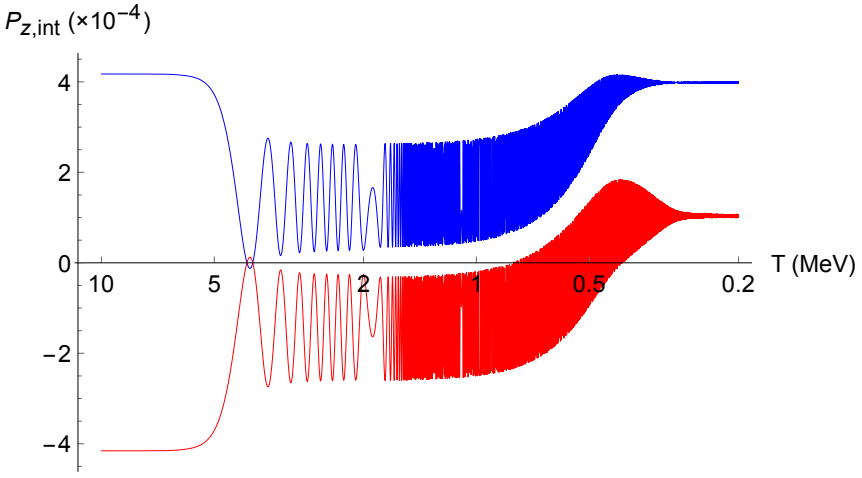

Figure 2.9: Large synchronized oscillations: $P_{z,\mathrm{int}}$ (blue, upper curve at $T = 10$ MeV) and $\bar{P}_{z,\mathrm{int}}$ (red) in the IH with initial degeneracy parameters $\eta_{\nu_e} = 5 \times 10^{-3}$, $\eta_{\nu_x} = 0$.

regime proves to be the exception to this trend, as we discuss below.

$\eta_{\nu_e} = 5 \times 10^{-3}$: Large synchronized oscillations

In this regime the lepton asymmetry is large enough that neutrino–neutrino scattering shifts towards promoting rather than resisting transformation. Once the expansion rate and the $e^{\pm}$ density have dropped sufficiently, large synchronized oscillations ensue, with all of the modes locked together by self-coupling (Fig. 2.9).

Although on the face of it this regime hosts perhaps the most active flavor evolution, in some ways the behavior is just that of the minimal-transformation regime writ large. In both regimes modes undergo synchronized oscillations after first gesturing towards MSW conversion, and then move into mass eigenstates as $\mathcal{H}_\nu$ becomes unimportant. But for larger η_{ν_e} the gesture towards MSW is stronger, the synchronized oscillations last longer and have larger amplitudes, and the movement into mass eigenstates entails more significant transformation at late time. The minimal-transformation scenario of $\eta_{\nu_e} = 5 \times 10^{-5}$ is an extreme example of the shrinking of these features, down to a size indiscernible at the scale of Fig. 2.8.

The qualitatively novel feature that distinguishes the synchronized-oscillation regime from

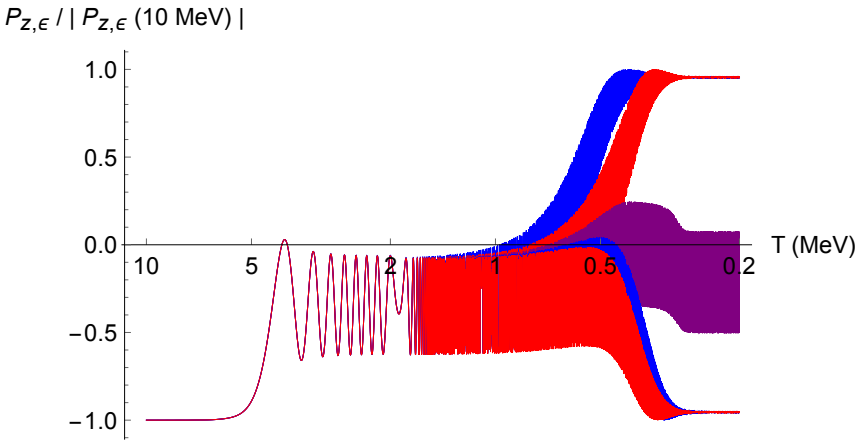

Figure 2.10: Large synchronized oscillations: $\bar{P}_{z,\varepsilon}$ for $\varepsilon = 1.15$ (upper blue curve at $T = 0.2$ MeV), 2.36 (upper red curve at $T = 0.2$ MeV), 3.57 (purple), 4.78 (lower blue curve at $T = 0.2$ MeV), and 5.99 (lower red curve at $T = 0.2$ MeV), computed with the same parameters as in Fig. 2.9. A spectral swap — wherein modes below the threshold $\varepsilon_{\rm th} \approx 3.5$ change flavor and those above do not — is evident.

the minimal-transformation regime is that (for $\eta_{\nu_e} > 0$) antineutrinos do not return en masse to the lighter mass eigenstate; instead many modes move to the heavier one, more closely associated with $\bar{\nu}_e$. Conversion of antineutrinos in this manner is more dramatic for larger initial η_{ν_e}, even causing $\bar{P}_{z,\rm int}$ to change sign for $\eta_{\nu_e} \gtrsim 5 \times 10^{-3}$. The upward drifting of $P_{z,\rm int}$ at low temperatures reflects the spectral swap that occurs as $\mathcal{H}_{\rm vac}$ comes to dominate (Fig. 2.10). The threshold energy, below which $\bar{\nu}$ swap, moves up to higher ε as the lepton asymmetry is increased; it is for this reason that the spectral swap has no discernible impact on the minimal-transformation regime.

Large-amplitude synchronized oscillations are associated with a solution of the equations of motion in which the off-diagonal elements of $\mathcal{H}_\nu$ steer the evolution of the system into self-sustained maximal mixing for both neutrinos and antineutrinos [83]. What our results highlight is the fact that this solution is not easily accessed in the early universe: As shown in Fig. 2.9, even an asymmetry of $\sim 10^{-3}$ does not foster maximal mixing, even though the mixing angle is still significantly enhanced over its value in vacuum. In the minimal-transformation regime, where the mixing angle is *suppressed*, the failure to enter this off-diagonal-driven mode is at its most spectacular.

In a sense the very largest allowable lepton asymmetries — those about an order of magnitude greater even than the exemplar asymmetry portrayed in Fig. 2.9 — actually overshoot this mode of self-sustained maximal mixing, displaying instead synchronized MSW transformation at $T \sim 5$ MeV followed by synchronized oscillations of non-maximal amplitude (Fig. 2.11). The phenomenon of synchronized MSW, where all modes undergo efficient MSW conversion in unison, can be understood from the following perspective. Decomposing the Hamiltonian into its constituents and taking the coherent limit, Eq. (2.18) becomes

$$Hx\frac{d\vec{P}}{dx} = \left(\vec{\mathcal{H}}_{\rm vac} + \vec{\mathcal{H}}_e + \vec{\mathcal{H}}_\nu\right) \times \vec{P}. \tag{2.26}$$

At high temperature all of the individual modes point along the z-axis, and in the limit $|\vec{\mathcal{H}}_\nu| \gg |\vec{\mathcal{H}}_{\rm vac}|, |\vec{\mathcal{H}}_e|$ they remain locked together even as the temperature cools and they depart from that axis. Their alignment implies that, for any given mode, $\vec{P}$ (very nearly) points along $\vec{\mathcal{H}}_\nu$ and so Eq. (2.26) can be approximated as

$$Hx\frac{d\vec{P}}{dx} \approx \left(\vec{\mathcal{H}}_{\rm vac} + \vec{\mathcal{H}}_e\right) \times \vec{P}. \tag{2.27}$$

The upshot is that all modes follow the track that the average energy mode $\varepsilon \approx 3.15$ would undergo if there were *no* self-coupling. (Further details on synchronized MSW conversion are provided in, for example, Ref. [44].)

Lepton asymmetries at the top end of the synchronized-oscillation regime are converging on this limit, but as shown in Fig. 2.11 — for an initial degeneracy parameter $\eta_{\nu_e} = 5 \times 10^{-2}$ — the resonant conversion is incomplete, as the approximation that all $\vec{P}(\varepsilon)$ are aligned is an imperfect one. Since $|\vec{\mathcal{H}}_\nu| \gg |\vec{\mathcal{H}}_{\rm vac}|$ for the entire temperature range depicted in Fig. 2.11, synchronized oscillations then take over at $T \lesssim 5$ MeV, once $|\vec{\mathcal{H}}_e|$ has fallen off. As the lepton asymmetry is dialed up further, the efficiency of conversion through the synchronized MSW mechanism increases and the amplitude of post-MSW synchronized oscillations decreases. In a somewhat

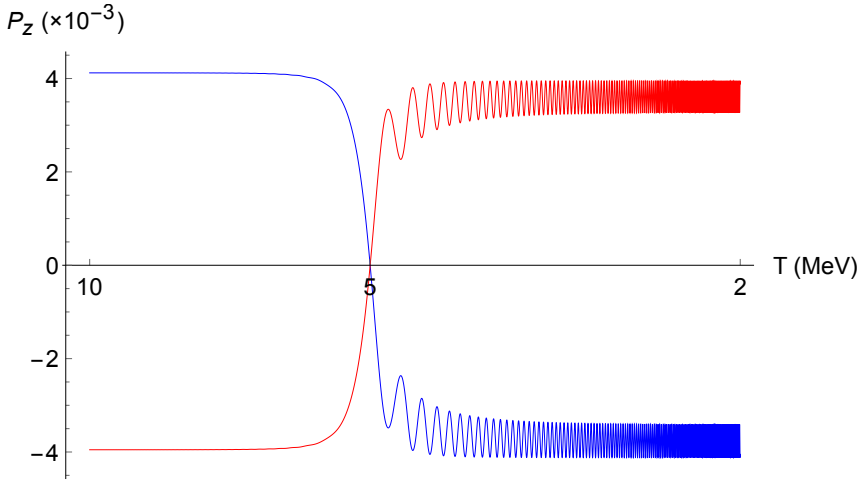

Figure 2.11: Top end of the synchronized-oscillation regime: $P_{z,\mathrm{int}}$ (blue, upper curve at $T = 10$ MeV) and $\bar{P}_{z,\mathrm{int}}$ (red) in the IH with initial degeneracy parameters $\eta_{\nu_e} = 5 \times 10^{-2}$, $\eta_{\nu_x} = 0$.

poetic turn, the evolution of $P_{z,\mathrm{int}}$ and $\bar{P}_{z,\mathrm{int}}$ at infinite lepton asymmetry is identical (up to scale) to that at zero lepton asymmetry.

We wish to underscore the point that despite the dominance by several orders of magnitude of $\mathcal{H}_\nu$ all the way through the MSW region, this regime strongly bears the fingerprints of the matter background. If it were not for the cancellation between $\mathcal{H}_{\mathrm{vac},z}$ and $\mathcal{H}_{e,z}$, the amplitude of the oscillations would be diminished down to the scale set by the vacuum mixing angle (as indeed it is in the NH), and the spectral swaps at these lepton asymmetries would be erased. The synchronized-oscillation regime thus highlights the insistent influence that can be exerted even by a *would-be* MSW resonance.

2.4.2 Adiabaticity

In our discussion of the five regimes just laid out, we have stressed the decisive role of level-crossings in determining flavor transformation. But the presence or absence of level-crossings is not the whole story. An important tool for understanding the behavior of neutrinos as they pass through resonance is the adiabaticity parameter γ, which quantifies the efficiency of

flavor conversion [84–87]. The parameter is defined as

$$\gamma \equiv 2\pi \frac{\delta t}{l_M^{\rm res}} \approx \Delta_M^{\rm res} \left| \frac{d\mathcal{H}_z}{dt} \right|_{\rm res}^{-1} \delta\mathcal{H}_z, \tag{2.28}$$

with $l_M^{\rm res} \equiv 2\pi/\Delta_M^{\rm res}$ the in-medium oscillation length at resonance and δt the resonance width, which is to say the time required for $\sin^2 2\theta_M$ to fall to half its resonant value. The approximation above comes from the definition of $l_M^{\rm res}$ and a recasting of δt in terms of $\delta\mathcal{H}_z$. Since the self-coupling and thermal potentials are varying much more rapidly than the vacuum potential, we can make the further approximation that, for the purposes of computing adiabaticity, $\mathcal{H}_{{\rm vac},z}$ is constant. We then obtain an expression for γ equivalent to that in Ref. [38].

An adiabaticity parameter $\gamma \gg 1$ corresponds to a resonance width broad enough to contain many oscillation lengths, indicating that the potentials change sufficiently slowly that neutrinos are able to track the Hamiltonian through the level-crossing. A small value of γ, conversely, corresponds to a large probability of neutrinos jumping from one energy eigenstate to the other: The Landau–Zener probability for such a transition is $P \approx e^{-\pi\gamma/2}$ [88, 89]. The early universe is ripe for adiabaticity, as γ is ultimately a comparison of the fast-fluttering dynamical timescale set by oscillations to the molasses-like Hubble timescale set by gravity. We will see, however, that under certain circumstances self-coupling can compromise this propensity.

Resonance occurs whenever the vacuum potential cancels with the weak-interaction potential, producing degenerate instantaneous energy eigenstates:

$$\mathcal{V}_z = \frac{\delta m^2 \cos 2\theta}{2\varepsilon_{\rm res} T}. \tag{2.29}$$

The left-hand side implicitly depends on $\varepsilon_{\rm res}$. (Recall the definition of $\mathcal{V}$ in and below Eq. (2.19).)

Solving for the resonant comoving energy yields

$$\varepsilon_{\rm res} = \frac{\mathcal{H}_{\nu,z}}{2\tilde{\mathcal{H}}_{e,z}} \left(1 \pm \sqrt{1 - \frac{2\delta m^2 \cos 2\theta}{T} \frac{\tilde{\mathcal{H}}_{e,z}}{(\mathcal{H}_{\nu,z})^2}} \right), \tag{2.30}$$

with $\tilde{\mathcal{H}}_{e,z} = |\mathcal{H}_{e,z}|/\varepsilon$. While this expression is always valid, its predictive power, in the sense of allowing one to identify where resonance will occur without solving the equations of motion, is questionable due to the nonlinearity inherent in neutrino evolution. Broadly, Eq. (2.30) can be used to predict the locations of level-crossings only so long as no significant flavor transformation has yet occurred. But once the polarization vectors have departed appreciably from their initial alignment along the z-axis, $\mathcal{H}_\nu$ has therefore also departed appreciably from its initial value, and so all bets are off as far as Eq. (2.30) goes. These comments are especially germane to the entire minimal-transformation regime and to much of the synchronized-oscillation regime, wherein resonance is never achieved despite the appearance that Eq. (2.30) would countenance the existence of one.

Our numerical results demonstrate that tuning the lepton asymmetry does not considerably shift the location of the MSW resonance, provided that the self-coupling is not large enough to eliminate the resonance altogether. This finding suggests that an analysis of the adiabaticity neglecting $\mathcal{H}_\nu$ may prove enlightening as to how the lepton asymmetry "perturbs" the matter-only MSW scenario. Ignoring the contribution from self-coupling, the resonant weak-interaction potential is

$$\mathcal{V}_z = \mathcal{H}_{e,z}^{\rm res} = \left(\frac{7\sqrt{2}\pi^2 G_F}{45 m_W^2} \left| \delta m^2 \right| \cos 2\theta \right)^{1/2} T^2, \tag{2.31}$$

introducing the notation $\mathcal{H}_{e,z}^{\rm res}$ to denote the thermal potential of the mode instantaneously at resonance. While for any particular mode ε the thermal potential $\mathcal{H}_{e,z}$ is dropping precipitously as T^5, the resonant thermal potential $\mathcal{H}_{e,z}^{\rm res}$ drops only as T^2. It turns out that the relatively sluggish descent of $\mathcal{H}_{e,z}^{\rm res}$ ensures that MSW is always adiabatic in the early universe, so long as

electrons and positrons are relativistic and the neutrino self-coupling can be neglected. Under these circumstances the adiabaticity parameter is

$$\gamma \approx \frac{1}{2^{3/4}} \frac{1}{5} \sqrt{\frac{7}{\pi}} \frac{m_{Pl}}{m_W} \sqrt{\frac{G_F}{g_*} |\delta m^2| \cos 2\theta \tan^4 2\theta}, \tag{2.32}$$

where m_{Pl} is the Planck mass, m_W is the W boson mass, and g_* is the number of relativistic degrees of freedom. Both m_{Pl} and g_* enter through the derivative of the thermal potential, which is dictated by Hubble expansion: In the radiation-dominated epoch the Hubble constant is

$$H = \sqrt{\frac{8\pi^3 g_*}{90}} \frac{T^2}{m_{Pl}}. \tag{2.33}$$

We have taken g_* to be constant over the span of temperatures relevant to this study, thus ignoring the small decrease that occurs as the last remaining $\mu^\pm$ disappear near the top of this temperature range and the later decrease that occurs as the $e^\pm$ population starts to become non-relativistic near the bottom.

Looking at Eq. (2.32), the adiabaticity parameter is evidently independent of temperature when $\mathcal{H}_\nu = 0$ and is, moreover, very large: $\gamma \approx 130$ for $1-3$ mixing, guaranteeing that all modes undergo efficient MSW conversion, regardless of the temperature at which their respective resonances occur. This fortuitous behavior, which is peculiar to the thermal potential, occurs because the resonance width and the in-medium oscillation length are growing with the same dependence on T. The growth of the resonance width can be traced directly to the slowing-down of the Hubble rate $H \propto T^2$.

Even as the resonance width is broadening, the rate at which the resonance sweeps upward through the energy modes is accelerating as a function of temperature: $\varepsilon_{\rm res} \propto 1/T^3$. Fig. 2.12 shows $\varepsilon_{\rm res}(T)$ for $\mathcal{H}_\nu$ set to zero. Reassuringly, $\varepsilon_{\rm avg} \approx 3.15$ becomes resonant right near 5 MeV.

The preceding discussion gives credence to the notion that the resonant flavor transformation seen at $T \sim 5$ MeV across a range of lepton asymmetries is adiabatic by default — that is,

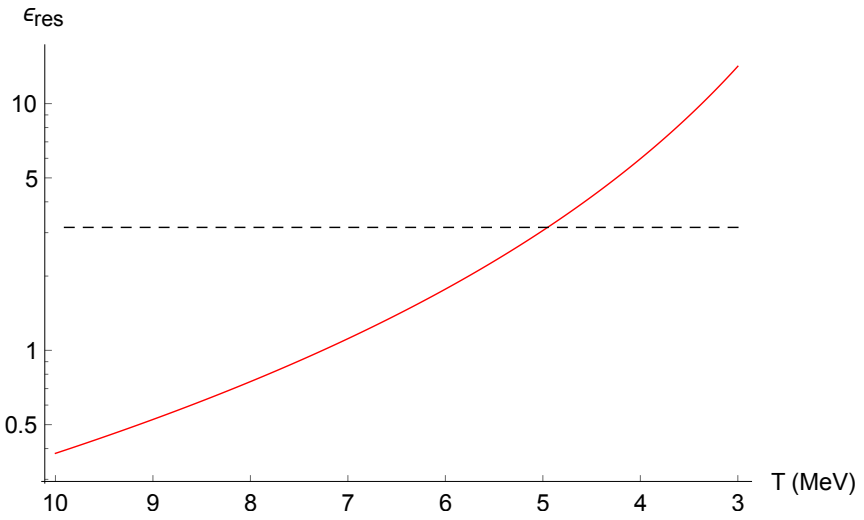

Figure 2.12: Resonant comoving energy $\varepsilon_{\rm res}$ (red, solid) as a function of T, with $\mathcal{H}_\nu = 0$. Also plotted is the Fermi–Dirac average-energy mode $\varepsilon_{\rm avg} \approx 3.15$ (black, dashed).

when only $\mathcal{H}_{\rm vac}$ and $\mathcal{H}_{\rm e}$ are considered. But as our numerical results have revealed, self-coupling can obstruct the efficiency of resonant conversion in non-trivial ways.

One can glean some general insights into the effects of neutrino–neutrino scattering by re-deriving the in-medium mixing angle and mass-squared splitting, allowing in particular for the off-diagonal elements of $\mathcal{H}_\nu$. In general these elements consist of nonzero real and imaginary parts, which (in keeping with our notation in Eq. (2.19)) we write as $\mathcal{V}_x$ and $\mathcal{V}_y$, respectively. A complex potential, however, spoils the reformulation in terms of effective in-medium oscillation parameters, so we rotate to a flavor-space coordinate system in which the off-diagonal part of the entire Hamiltonian $\mathcal{H}$ is real. Effective mixing parameters can be defined in this new coordinate system and then translated back in terms of $\mathcal{V}_x$ and $\mathcal{V}_y$ from the original, with the results

$$\begin{aligned} \Delta_M^2 &= (\mathcal{V}_z - \Delta\cos 2\theta)^2 + (\Delta\sin 2\theta + \mathcal{V}_x)^2 + \mathcal{V}_y^2 \\ \sin^2 2\theta_M &= \frac{(\Delta\sin 2\theta + \mathcal{V}_x)^2 + \mathcal{V}_y^2}{(\Delta\sin 2\theta + \mathcal{V}_x)^2 + \mathcal{V}_y^2 + (\mathcal{V}_z - \Delta\cos 2\theta)^2}. \end{aligned} \tag{2.34}$$

It is important to note that these are only *instantaneous* mixing parameters, as the coordinate

system required to make the off-diagonal elements of $\mathcal{H}$ real is constantly changing. The validity of employing such a technique in an analysis of adiabaticity is made plausible by noting that rotations about the flavor axis do not mix $\mathcal{H}_z$ and $\mathcal{H}_T$.

Working from Eq. (2.34), the resonance width expressed as a weak-interaction potential is

$$\delta\mathcal{V}_z = \sqrt{(\Delta\sin 2\theta + \mathcal{V}_x)^2 + \mathcal{V}_y^2}, \tag{2.35}$$

and, just as in the $\mathcal{H}_\nu = 0$ case, $\Delta_M^{\rm res} = \delta\mathcal{V}_z$. The definition of γ (Eq. (2.28)) then leads to

$$\begin{aligned}\gamma &\approx \frac{(\Delta\sin 2\theta + \mathcal{V}_x)^2 + \mathcal{V}_y^2}{\left|5H\mathcal{H}_{e,z} + 3H\mathcal{H}_{\nu,z} - \frac{\dot{L}_{\nu_e} - \dot{L}_{\nu_x}}{L_{\nu_e} - L_{\nu_x}}\mathcal{H}_{\nu,z}\right|_{\rm res}} \\ &\approx \left|\frac{\left|\mathcal{H}_T\right|^2}{\dot{\mathcal{H}}_z}\right|_{\rm res},\end{aligned} \tag{2.36}$$

where in the last expression we emphasize an alternative interpretation of the adiabaticity parameter as the ratio of the off-diagonal part of $\mathcal{H}$ (squared) to the rate of change of its diagonal part. In evaluating the derivative we have again taken g_* to be constant.

While the term proportional to $\mathcal{H}_{e,z}$ in the denominator of Eq. (2.36) is always negative, the two terms proportional to $\mathcal{H}_{\nu,z}$ are of the same sign leading into resonance. When $\mathcal{H}_{\nu,z}$ dominates over $\mathcal{H}_{e,z}$, the final term in the denominator therefore makes γ smaller. On the other hand, when $\mathcal{H}_{e,z}$ dominates, the term can either make γ smaller (if $\eta_{\nu_e} < 0$ initially) or make it larger (if $\eta_{\nu_e} > 0$ initially). That adiabaticity plummets as flavor conversion proceeds in the moderate-to-large-L regime is well known from studies of resonant production of sterile neutrinos. It reflects the fact that as the potential sweeps through resonance more rapidly, the resonance width contracts and conversion becomes less efficient. What is less familiar is that flavor conversion can evidently feed back *positively* on the adiabaticity of the resonance when the lepton number is small but nonzero.

Eq. (2.36) is comparable to expressions in Refs. [38, 39, 90, 91], all of which consider

resonant transformation between an active and a sterile state. In that context the derivative of the lepton number drags down the adiabaticity with such resolve that the depletion of the lepton number ultimately halts the conversion process. As suggested in the preceding paragraph, in our context as well the possibly adverse effect of $\dot{L}_{\nu_e}$ on γ implies that adiabaticity may fail for some initial lepton asymmetries. It deserves emphasis, however, that there is a crucial difference between the resonant production of sterile neutrino dark matter and the resonant conversion between active flavors: Because the sterile flavor eigenstate is uncharged under weak interactions, the forward-scattering neutrino–neutrino potential in an active–sterile system does not have off-diagonal elements. In the polarization-vector picture for active–sterile mixing, the self-coupling potential consequently points along the z-axis, whereas for active–active mixing it tracks the polarization vectors away from the flavor axis. This distinction corresponds in Eq. (2.36) to $\mathcal{V}_x$ and $\mathcal{V}_y$ being nonzero; it adds, as a result, another lever controlling adiabaticity. In cases where cancellation occurs in the term $(\Delta \sin 2\theta + \mathcal{V}_x)^2$, the off-diagonal weak-interaction potential can in fact enfeeble γ, producing non-adiabaticity so long as $\mathcal{V}_y$ is not too large. In other cases, though, off-diagonal self-coupling bolsters γ by enlarging the resonance width and the in-medium mass-squared splitting.

Adiabaticity accounts for the general behavior seen in our numerical results wherever a level-crossing is present. Despite these successes, as an analytical tool it has two shortcomings: One, it is too coarse an instrument to explain the precise evolution of *individual* modes through resonance, which often display radically different behavior from one another even when nearby in energy. (The partial-MSW regime exemplifies this point, as flavor evolution in this case exhibits highly non-trivial dependence on neutrino energy.) And two, adiabaticity offers no insights into those regimes where the nonlinearity of self-coupling causes the system to avert resonance altogether.

2.4.3 Matter–neutrino resonances in the early universe

In this paper we have presented scenarios in which flavor evolution prior to $T \sim 10$ MeV is quite restrained: The large potentials at high temperatures ensure that θ_M is minuscule, thereby preventing significant transformation away from the initial flavor eigenstates. In truth it is not obvious *a priori* that this statement always holds, as lepton asymmetries for which self-coupling dominates at ~ 10 MeV will have some higher temperature at which $\mathcal{H}_{e,z}$ surpasses $\mathcal{H}_{\nu,z}$ in magnitude. If the two potentials are of opposite sign, then there will be a level-crossing at this higher, pre-MSW temperature. Such a level-crossing has been dubbed a matter–neutrino resonance (MNR) and in recent years has been shown to be a possible conduit for significant flavor transformation in merger and accretion-disk environments [92–97]. (Related, albeit distinct, analyses have also been performed for supernovae [98, 99].) No explorations of MNR in the early universe have yet been conducted.

We have searched the regimes discussed above for signs of flavor transformation associated with the MNR mechanism. Our numerical results have confirmed that level-crossings do indeed occur, but in the scenarios we have examined the transformation associated with these resonances is in most cases negligible. The explanation appears to lie in the fact that the resonances are generally traversed non-adiabatically. Referring again to Eq. (2.36), γ may be diminished either by a small off-diagonal potential $\mathcal{H}_T$ or by a large sweep rate in the diagonal potential $\mathcal{H}_z$. We speculate that both factors are at play in preventing efficient conversion through the MNR. At the high temperatures at which these resonances occur the overall magnitude of $\mathcal{H}_z$ leading into the level-crossing is larger than it is for the lower-temperature MSW resonance. Moreover, the Hubble constant, which sets the resonance sweep rate, is larger as well. At the same time, whereas the off-diagonal weak-interaction potentials are expected to be small leading into either an MSW resonance or an MNR because neutrinos have yet to leave their initial flavor states to any appreciable extent, the off-diagonal vacuum potential is *smaller* at high temperatures.

As one would anticipate based on this argument, the most visible impact of MNR is found

when the level-crossing occurs at relatively low temperatures. In particular, $\eta_{\nu_e} \sim 10^{-6}$ seems to be most clearly affected by the presence of the MNR, which induces non-negligible flavor transformation starting at temperatures near 10 MeV. Hints of MNR conversion can be seen in our asymmetric-MSW exemplar (Fig. 2.7), where it appears that neutrinos are on their way through resonance before abruptly halting their conversion at $T \sim 8$ MeV. Ultimately the overall amount of conversion is limited here too by non-adiabaticity, and the intermingling of the MSW transition with the MNR largely reverses the conversion that does occur. (Interestingly, for $\eta_{\nu_e} \sim 10^{-6}$ the MNR begets some degree of flavor transformation in the NH as well, in defiance of the general trend for this hierarchy. The flavor evolution, as it happens, is very similar to that in the IH but with the behavior of neutrinos and antineutrinos exchanged.)

We conclude that conversion through MNR is limited given the parameters adopted in our study. However, we do not rule out the possibility that a more thorough investigation of the MNR phenomenon in the early universe may reveal sizable effects under appropriate circumstances. We reiterate that such resonances can exist in the early universe, but that the obstacle to significant transformation is non-adiabaticity.

2.4.4 Flavor evolution with quantum damping

Up to this point the discussion has been couched in the coherent limit. In reality collisions — which we model as quantum damping — will modify these results. The generic effect of damping is to battle against the development of coherence between the flavors. It is the combination of oscillations and coherence-erasing damping that leads to depolarization (P_z, $\bar{P}_z \to 0$) and therefore flavor equilibration.

Indeed, equilibration is generally most effective when flavor transformation is, in the absence of damping, most appreciable. An immediate consequence is that equilibration is relatively ineffective for most lepton numbers in the NH, which typically fosters only minimal coherent flavor transformation due to the lack of a level-crossing in the MSW region. While

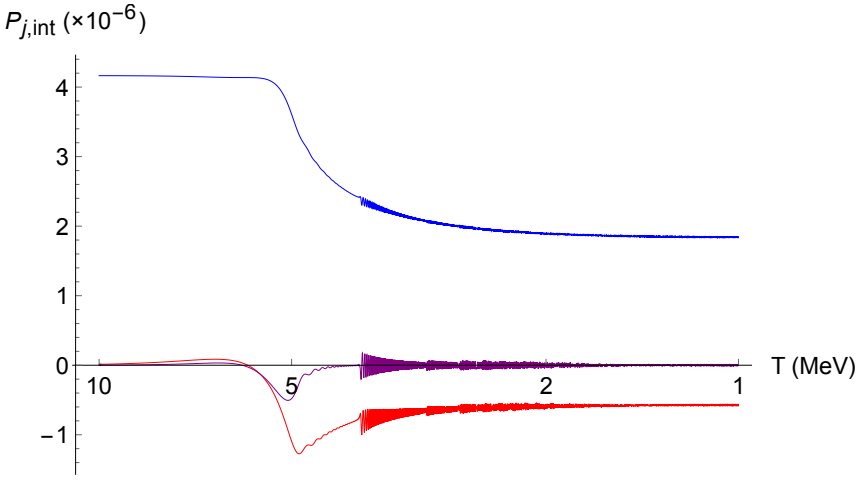

Figure 2.13: Minimal transformation (damped): $P_{j,\mathrm{int}}$ for $j = z$ (blue, topmost curve at $T = 1$ MeV), $j = x$ (red, bottommost curve at $T = 1$ MeV), and $j = y$ (purple), with the parameters of the minimal-transformation scenario in Fig. 2.8 (initial degeneracy parameters $\eta_{\nu_e} = 5 \times 10^{-5}$, $\eta_{\nu_x} = 0$), in the presence of collisional damping. Antineutrinos undergo qualitatively similar evolution.

the effects of damping are not entirely insubstantial in the NH, they are usually confined to the relatively placid period during which neutrinos and antineutrinos migrate from their initial flavor eigenstates to the nearby mass eigenstates.

Damping is a more potent force in the IH. The synchronized-oscillation regime, for example, evinces much more efficient depolarization than is witnessed in the NH for the same lepton asymmetries. At the other end, in the symmetric-MSW regime, depolarization is nearly complete. But the general trend of efficient depolarization in the IH is not without exception: The development of coherence in the minimal-transformation regime is so limited — self-coupling is too overpowering for an MSW resonance to occur but too weak to elicit large-amplitude synchronized oscillations — that damping leaves intact a sizable fraction of the initial asymmetry between the flavors (Fig. 2.13). Previous authors have noted that MSW transitions and synchronized oscillations are vehicles for flavor equilibration, but the existence of a region where neither phenomenon is very compelling, and therefore damping is relatively muted, has not been pointed out before.

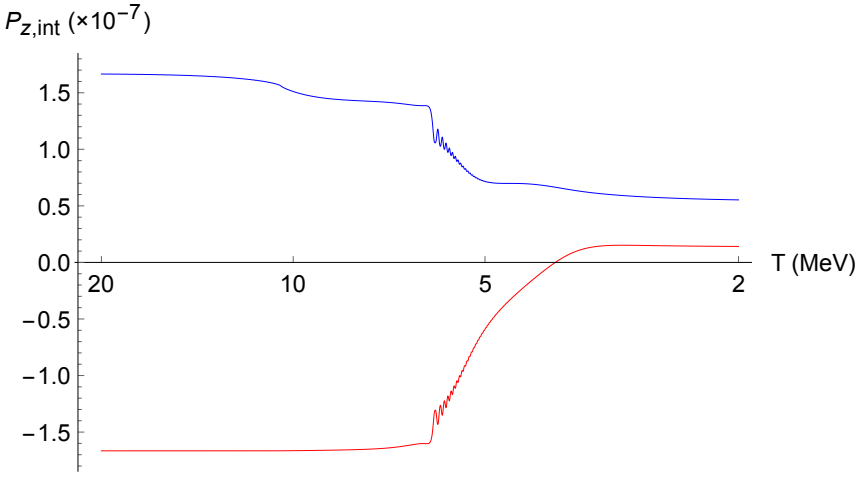

Figure 2.14: Asymmetric MSW (damped): $P_{z,\mathrm{int}}$ for neutrinos (blue, upper curve at $T = 20$ MeV) and $\bar{P}_{z,\mathrm{int}}$ (red), with the parameters of the asymmetric-MSW scenario in Fig. 2.7 (initial degeneracy parameters $\eta_{\nu_e} = 2 \times 10^{-6}$, $\eta_{\nu_x} = 0$), in the presence of collisional damping.

In comparing Fig. 2.13 (damped) with Fig. 2.8 (coherent), it may come as a surprise that equilibration is not *less* substantial in the damped case than what is shown in Fig. 2.13. The reason is that the flavor evolution plays out in a hierarchy of scales in which the oscillation length is smaller than the mean free path, which in turn is smaller than the MSW resonance width that would obtain for $\mathcal{H}_\nu = 0$. The picture is this: In the MSW region neutrinos and antineutrinos partially convert flavor, much as they do in the absence of damping. The polarization vectors accordingly swing away from the flavor axis, and as they do so damping shrinks $\vec{P}_T$. But due to the high oscillation frequency relative to the scattering rate, the change in $|\vec{P}_T|$ is quickly redistributed over all of the components of $\vec{P}$, so that rather than being flattened against the flavor axis, the polarization vectors are able to evolve in a manner reminiscent of the coherent case, albeit with shrinking magnitude. In spite of collisions the modes remain largely synchronized, so that $\vec{P} \sim \vec{\mathcal{H}}_\nu \sim \vec{\mathcal{H}}$ (where $\sim$ indicates that the vectors are roughly parallel) as long as self-coupling dominates. At low temperatures $\vec{\mathcal{H}}_{\mathrm{vac}}$ takes over and all modes move adiabatically into the upper mass eigenstate, just as they do in the coherent limit. As a matter of fact, the evolution of $P_{z,\mathrm{int}}/|\vec{P}|$ is very similar for the damped and coherent cases; the visual differences between Figs. 2.13 and 2.8 are primarily a result of the long timescale over which the MSW region extends.

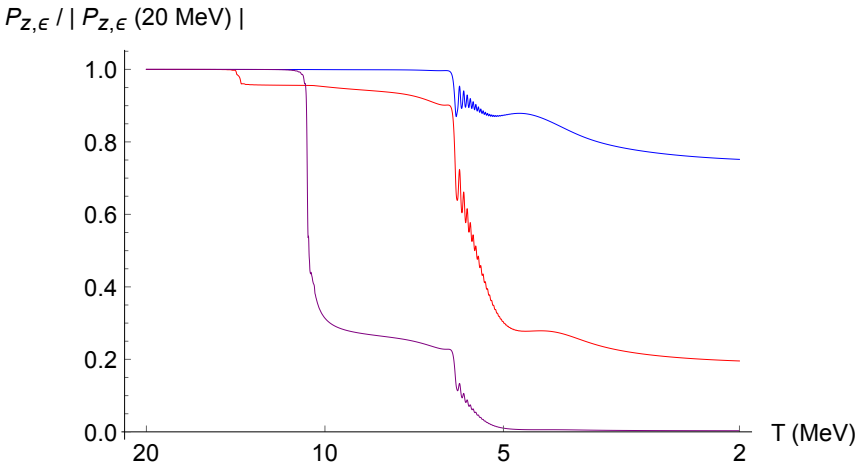

Figure 2.15: Asymmetric MSW (damped): $P_{z,\varepsilon}$ in the collisionally damped scenario depicted in Fig. 2.14, for $\varepsilon = 1.15$ (blue, topmost curve at $T = 2$ MeV), $\varepsilon = 3.57$ (red), and $\varepsilon = 5.99$ (purple, bottommost curve at $T = 2$ MeV).

Fig. 2.14 further illustrates the principle that the degree of depolarization is related to the degree of flavor transformation that takes place in the coherent limit. For $\eta_{\nu_e} = 2 \times 10^{-6}$, $P_{z,\text{int}}$ at weak-decoupling temperatures is $\sim 1/3$ of its initial value at $T \gtrsim 20$ MeV, whereas $\bar{P}_{z,\text{int}}$ only retains $\sim 1/12$ of its initial magnitude and manages to change its sign. The damping of antineutrinos takes place almost entirely during the $\mathcal{H}_\nu$-mediated MSW resonance, of which the small residual $\bar{P}_{z,\text{int}}$ is a consequence. The damping of neutrinos, on the other hand, is more complicated (Fig. 2.15). Low- and medium-energy modes damp through the MSW region, with greater depolarization associated with greater ε, but the high-energy modes undergo damping both through the MSW region and the MNR that occurs at $T \sim 10$ MeV. Since the scattering rate increases rapidly with temperature, the effectiveness of damping is amplified at the MNR.

Although collisional damping has traditionally been employed in studies of lepton asymmetries, it is nonetheless wanting in realism. As some authors have noted [47, 49], modeling incoherent scattering strictly through this traditional off-diagonal damping term is dubious inasmuch as thermal equilibration requires scattering processes that shuffle neutrinos between energy bins, which such a term cannot provide. More specifically, if collisions are taken simply to impose damping ($\mathcal{C} \to -\mathcal{D}\vec{P}_T$ in the polarization-vector language), then one can show that depolarization

is inconsistent with the preservation of Fermi–Dirac spectra.

To see that this is so, suppose that at some initial temperature T_1 the neutrino gas is in thermal equilibrium with the plasma. Then, according to our normalization of ρ, P_0 is the sum of the Fermi–Dirac equilibrium spectra that obtain at this temperature: $P_0(\varepsilon, T_1) = f\left(\varepsilon, \eta^i_{\nu_e}\right) + f\left(\varepsilon, \eta^i_{\nu_x}\right)$. Suppose also that at some lower temperature T_2 damping has achieved complete depolarization: $P_z(\varepsilon, T_2) \approx 0$ for all ε. Using the fact that coherent evolution and quantum damping both preserve $\mathrm{Tr}\rho = P_0$, it follows that

$$\begin{aligned} \rho_{ee}(\varepsilon, T_2) &= \frac{P_z(\varepsilon, T_2) + P_0(\varepsilon, T_2)}{2} \\ &= \frac{f\left(\varepsilon, \eta^i_{\nu_e}\right) + f\left(\varepsilon, \eta^i_{\nu_x}\right)}{2}. \end{aligned} \tag{2.37}$$

Since the average of two Fermi–Dirac spectra is not in general another Fermi–Dirac spectrum, this result implies that the ν_e distribution function ρ_{ee} picks up distortions from Fermi–Dirac as the polarization vectors shrink to zero — a troubling conclusion if P_z goes to 0 at high enough temperature that neutrinos must still be in thermal equilibrium.

The consequences of Eq. (2.37) are borne out numerically: Because the damping term is proportional to neutrino momentum, it engenders a spectral feature wherein higher-energy modes undergo greater depolarization than their lower-energy counterparts. This feature would be smoothed out somewhat by a more rigorous treatment of incoherent scattering, but it is also indicative of the non-trivial evolution of a system of neutrinos toward equilibrium. Spectral distortions associated with the flavor-equilibration process may compound those known to be generated thermally through the overlapping epochs of $e^{\pm}$ annihilation and weak decoupling.

The crucial missing ingredient that enforces thermal equilibrium is momentum-changing scattering, which is disallowed when collisions are modeled strictly as quantum damping. In this vein, the need for a detailed treatment of incoherent scattering was emphasized by Wong [45], who cautioned that the extent of flavor equilibration depends on how collisions are implemented.

To date, the most sophisticated analyses of flavor evolution with a lepton asymmetry are those performed by the authors of Refs. [20, 21, 47, 49], who have combined an off-diagonal damping term with classical Boltzmann collision integrals along the diagonals of $\mathcal{C}$. By revealing a wider range of possible coherent phenomena than has hitherto been recognized, our results buttress the need for continued progress in this direction.

As the findings of Ref. [1] have demonstrated, BBN calculations that self-consistently couple neutrino transport to the thermodynamics of the plasma yield changes in the predicted primordial abundance of D — relative to the case of instantaneous neutrino decoupling — that are an order of magnitude larger than they would be if the non-linear feedback between the neutrinos, plasma, and nuclides were omitted. The calculations of Ref. [1], however, were performed with zero lepton number in the classical Boltzmann limit. Ref. [55], meanwhile, tackled the full problem of oscillations and quantum collision integrals but was predicated on the assumption of zero lepton asymmetry. A similar approach to the complete quantum kinetic equations [53, 100–103], including fully realistic quantum collision integrals [54] *and* a nonzero lepton asymmetry, may divulge signatures of flavor evolution in the early universe that are currently believed to be unobservable.

2.5 Conclusion

In this paper we have numerically solved the coherent equations of motion governing neutrino flavor transformation in the early universe with a range of initial lepton asymmetries. In so doing we have discovered that beneath the current constraints on the lepton number there lurks a menagerie of possible coherent flavor phenomena, which we have sectioned off into five distinct regimes. Starting from a lepton asymmetry comparable to the present bound and moving down to the realm of negligible self-coupling, these regimes are as follows: (1) Large synchronized oscillations, (2) minimal transformation, (3) asymmetric MSW, (4) partial

MSW, and (5) symmetric MSW. The existence of these regimes is a testament to the richness of the nonlinear problem of flavor evolution in a dense, expanding environment. And as we have demonstrated, this richness is not entirely erased by collisional damping — a finding that points to the merits of further study of this problem with quantum kinetics that go beyond the approximations employed here.

To explain the phenomena observed in our numerical results we have employed the conceptual apparatus of (non-)adiabatic level-crossings and the well-established understanding of synchronized evolution as a collective mode that emerges when the self-coupling potential is dominant. Yet we also contend that in fact the minimal-transformation regime, which occurs for lepton asymmetries on the order of $\sim 5 \times 10^{-5}$, points to the limitations of these concepts. The distinctive absence of flavor conversion in this regime is due to it encompassing lepton asymmetries that are strong enough to eliminate level-crossings in the MSW region but not strong enough for $\mathcal{H}_\nu$ to develop the dominant off-diagonal components needed for large-amplitude synchronized oscillations, much less for $\mathcal{H}_\nu$ to bind the individual modes sufficiently for a synchronized MSW transition to take place. As far as we are aware, a convincing analytical understanding of this regime does not currently exist. We note again that it is an intriguing coincidence that the range of lepton numbers most consistent with an interpretation of the unidentified X-ray line reported in Refs. [34, 35] falls within this regime, which is the one most resistant to damping-induced flavor equilibration.

We have also reported for the first time the existence of an MNR in the early universe. The influence of the resonance on coherent flavor evolution is very modest except for a small range of lepton asymmetries for which the level-crossing occurs shortly before the MSW region. Its presence is accentuated by damping, which capitalizes on the coherence developed through the resonance. We have found that adiabaticity restricts the amount of flavor conversion through the MNR, but mixing through the $\delta m^2_\odot$ channel, which has MSW resonances at lower temperatures than those studied here, may permit more adiabatic circumstances.

The sub-constraint lepton asymmetries we have investigated are, by definition, thought to lie presently out of reach of observation. Nonetheless, the diversity of flavor phenomena revealed in this study may have unrecognized implications for BBN. The current era is one of precision cosmology, with 30-meter-class telescopes [104–106], forthcoming spectroscopic galaxy surveys [107–109], and a Stage-IV CMB experiment [108, 110] at the vanguard — to name just a few. Impressive advances in determinations of $N_{\rm eff}$, Y_P, $[{\rm D}/{\rm H}]$, and other cosmological observables are on the horizon. These measurements promise to provide new insights, but exploiting them thoroughly will require a scrupulous treatment of neutrino evolution. It remains to be seen whether a solution of the full quantum kinetic equations coupled to BBN will unearth traces of the physics presented in this study.

2.6 Acknowledgements

We thank Brad Keister, Chad Kishimoto, and Amol Patwardhan for helpful conversations. This work was supported by NSF Grant No. PHY-1307372 at UC San Diego; by the Los Alamos National Laboratory Institute for Geophysics, Space Sciences and Signatures Subcontract No. 257842; by the Los Alamos National Laboratory Institutional Computing Program, under U.S. Department of Energy National Nuclear Security Administration Contract No. DE-AC52-06NA25396; by the Los Alamos National Laboratory LDRD Program; and by the U.S. Department of Energy Office of Science Graduate Student Research (SCGSR) Program.

This chapter is a reprint of L. Johns, M. Mina, V. Cirigliano, M. W. Paris, and G. M. Fuller, Phys. Rev. D 94, 083505 (2016). I was the primary investigator and author of this publication.

Bibliography

[1] E. Grohs, G. M. Fuller, C. T. Kishimoto, M. W. Paris, and A. Vlasenko, Phys. Rev. D **93**, 083522 (2016).

[2] E. Grohs and G. M. Fuller, Nucl. Phys. **B8**, 034 (2016).

[3] S. Dodelson and M. S. Turner, Phys. Rev. D **46**, 3372 (1992).

[4] A. D. Dolgov and M. Fukugita, Phys. Rev. D **46**, 5378 (1992).

[5] A. D. Dolgov, S. H. Hansen, and D. V. Semikoz, Nucl. Phys. **B503**, 426 (1997).

[6] A. D. Dolgov, S. H. Hansen, and D. V. Semikoz, Nucl. Phys. **B543**, 269 (1999).

[7] N. Y. Gnedin and O. Y. Gnedin, Astrophys. J. **509**, 11 (1998).

[8] R. E. Lopez and M. S. Turner, Phys. Rev. D **59**, 103502 (1999).

[9] S. Esposito, G. Miele, S. Pastor, M. Peloso, and O. Pisanti, Nucl. Phys. **B590**, 539 (2000).

[10] G. Mangano, G. Miele, S. Pastor, and M. Peloso, Phys. Lett. B **534**, 8 (2002).

[11] G. Mangano, G. Miele, S. Pastor, T. Pinto, O. Pisanti, and P. D. Serpico, Nucl. Phys. **B729**, 221 (2005).

[12] J. P. Kneller and G. Steigman, New J. Phys. **6**, 117 (2004).

[13] V. A. Kuzmin, V. A. Rubakov, and M. E. Shaposhnikov, Phys. Lett. B **155**, 36 (1985).

[14] P. Arnold and L. McLerran, Phys. Rev. D **36**, 581 (1987).

[15] P. Arnold and L. McLerran, Phys. Rev. D **37**, 1020 (1988).

[16] J. A. Harvey and M. S. Turner, Phys. Rev. D **42**, 3344 (1990).

[17] A. D. Dolgov, S. H. Hansen, S. Pastor, S. T. Petcov, G. G. Raffelt, and D. V. Semikoz, Nucl. Phys. **B632**, 363 (2002).

[18] P. D. Serpico and G. G. Raffelt, Phys. Rev. D **71**, 127301 (2005).

[19] V. Simha and G. Steigman, J. Cosmol. Astropart. Phys. **2008**, 011 (2008).

[20] G. Mangano, G. Miele, S. Pastor, O. Pisanti, and S. Sarikas, Phys. Lett. B **708**, 1 (2012).

[21] E. Castorina, U. Franca, M. Lattanzi, J. Lesgourgues, G. Mangano, A. Melchiorri, and S. Pastor, Phys. Rev. D **86**, 023517 (2012).

[22] G. Steigman, Adv. High Energy Phys. **2012**, 268321 (2012).

[23] J. A. Harvey and E. W. Kolb, Phys. Rev. D **24**, 2090 (1981).

[24] A. D. Dolgov and D. P. Kirilova, J. Mosc. Phys. Soc. **1**, 217 (1991).

[25] R. Foot, M. J. Thomson, and R. R. Volkas, Phys. Rev. D **53**, R5349 (1996).

[26] X. Shi, Phys. Rev. D **54**, 2753 (1996).

[27] A. Casas, W. Y. Cheng, and G. Gelmini, Nucl. Phys. **B538**, 297 (1999).

[28] J. March-Russell, A. Riotto, and H. Murayama, J. High Energy Phys. **1999**, 015 (1999).

[29] J. McDonald, Phys. Rev. Lett. **84**, 4798 (2000).

[30] M. Kawasaki, F. Takahashi, and M. Yamaguchi, Phys. Rev. D **66**, 043516 (2002).

[31] M. Yamaguchi, Phys. Rev. D **68**, 063507 (2003).

[32] M. Shaposhnikov, J. High Energy Phys. **2008**, 008 (2008).

[33] P.-H. Gu, Phys. Rev. D **82**, 093009 (2010).

[34] E. Bulbul, M. Markevitch, A. Foster, R. K. Smith, M. Loewenstein, and S. W. Randall, Astrophys. J. **789**, 13 (2014).

[35] A. Boyarsky, O. Ruchayskiy, D. Iakubovskyi, and J. Franse, Phys. Rev. Lett. **113**, 251301 (2014).

[36] K. Abazajian, G. M. Fuller, and W. H. Tucker, Astrophys. J. **562**, 593 (2001).

[37] X. Shi and G. M. Fuller, Phys. Rev. Lett. **82**, 2832 (1999).

[38] K. Abazajian, G. M. Fuller, and M. Patel, Phys. Rev. D **64**, 023501 (2001).

[39] C. T. Kishimoto and G. M. Fuller, Phys. Rev. D **78**, 023524 (2008).

[40] A. Kusenko, Phys. Rept. **481**, 1 (2009).

[41] R. Adhikari, M. Agostini, N. A. Ky, T. Araki, M. Archidiacono, M. Bahr, J. Baur, J. Behrens, F. Bezrukov, P. B. Dev, D. Borah, A. Boyarsky, A. de Gouvea, C. de S. Pires, H. de Vega, A. Dias, P. D. Bari, Z. Djurcic, K. Dolde, H. Dorrer, M. Durero, O. Dragoun, M. Drewes, G. Drexlin, C. DÃŒllmann, K. Eberhardt, S. Eliseev, C. Enss, N. Evans, A. Faessler, P. Filianin, V. Fischer, A. Fleischmann, J. Formaggio, J. Franse, F. Fraenkle, C. Frenk, G. Fuller, L. Gastaldo, A. Garzilli, C. Giunti, F. GlÃŒck, M. Goodman, M. Gonzalez-Garcia, D. Gorbunov, J. Hamann, V. Hannen, S. Hannestad, S. Hansen, C. Hassel, J. Heeck, F. Hofmann, T. Houdy, A. Huber, D. Iakubovskyi, A. Ianni, A. Ibarra, R. Jacobsson, T. Jeltema, J. Jochum, S. Kempf, T. Kieck, M. Korzeczek, V. Kornoukhov, T. Lachenmaier, M. Laine, P. Langacker, T. Lasserre, J. Lesgourgues, D. Lhuillier, Y. Li, W. Liao, A. Long, M. Maltoni, G. Mangano, N. Mavromatos, N. Menci, A. Merle, S. Mertens, A. Mirizzi, B. Monreal, A. Nozik, A. Neronov, V. Niro, Y. Novikov, L. Oberauer, E. Otten, N. Palanque-Delabrouille, M. Pallavicini, V. Pantuev, E. Papastergis, S. Parke, S. Pascoli, S. Pastor, A. Patwardhan, A. Pilaftsis, D. Radford, P.-O. Ranitzsch, O. Rest, D. Robinson, P. R. da Silva, O. Ruchayskiy, N. Sanchez, M. Sasaki, N. Saviano, A. Schneider, F. Schneider, T. Schwetz, S. SchÃnert, S. Scholl, F. Shankar, R. Shrock,

N. Steinbrink, L. Strigari, F. Suekane, B. Suerfu, R. Takahashi, N. T. H. Van, I. Tkachev, M. Totzauer, Y. Tsai, C. Tully, K. Valerius, J. Valle, D. Venos, M. Viel, M. Vivier, M. Wang, C. Weinheimer, K. Wendt, L. Winslow, J. Wolf, M. Wurm, Z. Xing, S. Zhou, and K. Zuber, J. Cosmol. Astropart. Phys. **2017**, 025 (2017).

[42] K. N. Abazajian, Phys. Rev. Lett. **112**, 161303 (2014).

[43] M. J. Savage, R. A. Malaney, and G. M. Fuller, Astrophys. J. **368**, 1 (1991).

[44] K. N. Abazajian, J. F. Beacom, and N. F. Bell, Phys. Rev. D **66**, 013008 (2002).

[45] Y. Y. Y. Wong, Phys. Rev. D **66**, 025015 (2002).

[46] C. Lunardini and A. Y. Smirnov, Phys. Rev. D **64**, 073006 (2001).

[47] S. Pastor, T. Pinto, and G. G. Raffelt, Phys. Rev. Lett. **102**, 241302 (2009).

[48] J. Gava and C. Volpe, Nucl. Phys. **B837**, 50 (2010).

[49] G. Mangano, G. Miele, S. Pastor, O. Pisanti, and S. Sarikas, J. Cosmol. Astropart. Phys. **2011**, 035 (2011).

[50] A. B. Balantekin and G. M. Fuller, Phys. Lett. B **471**, 195 (1999).

[51] G. Sigl and G. Raffelt, Nucl. Phys. **B406**, 423 (1993).

[52] D. Nötzold and G. Raffelt, Nucl. Phys. **B307**, 924 (1988).

[53] A. Vlasenko, G. M. Fuller, and V. Cirigliano, Phys. Rev. D **89**, 105004 (2014).

[54] D. N. Blaschke and V. Cirigliano, Phys. Rev. D **94**, 033009 (2016).

[55] P. F. de Salas and S. Pastor, J. Cosmol. Astropart. Phys. **2016**, 051 (2016).

[56] R. A. Harris and L. Stodolsky, J. Chem. Phys. **74**, 2145 (1981).

[57] R. A. Harris and L. Stodolsky, Phys. Lett. B **116**, 464 (1982).

[58] L. Stodolsky, Phys. Rev. D **36**, 2273 (1987).

[59] M. J. Thomson, Phys. Rev. A **45**, 2243 (1992).

[60] G. Raffelt, G. Sigl, and L. Stodolsky, Phys. Rev. Lett. **70**, 2363 (1993).

[61] B. H. J. McKellar and M. J. Thomson, Phys. Rev. D **49**, 2710 (1994).

[62] N. F. Bell, R. R. Volkas, and Y. Y. Y. Wong, Phys. Rev. D **59**, 113001 (1999).

[63] C. W. Kim, J. Kim, and W.-K. Sze, Phys. Rev. D **37**, 1072 (1988).

[64] L. Wolfenstein, Phys. Rev. D **17**, 2369 (1978).

[65] S. P. Mikheyev and A. Y. Smirnov, Sov. J. Nucl. Phys. **42**, 913 (1985).

[66] H. Duan, G. M. Fuller, and Y.-Z. Qian, Ann. Rev. Nucl. Part. Sci. **60**, 569 (2010).

[67] J. F. Cherry, J. Carlson, A. Friedland, G. M. Fuller, and A. Vlasenko, Phys. Rev. Lett. **108**, 261104 (2012).

[68] G. Raffelt, S. Sarikas, and D. S. Seixas, Phys. Rev. Lett. **111**, 091101 (2013).

[69] A. Mirizzi, Phys. Rev. D **88**, 073004 (2013).

[70] A. Vlasenko, G. M. Fuller, and V. Cirigliano, arXiv:1406.6724 .

[71] B. D. Keister, Phys. Scripta **90**, 088008 (2015).

[72] S. Abbar, H. Duan, and S. Shalgar, Phys. Rev. D **92**, 065019 (2015).

[73] S. Samuel, Phys. Rev. D **48**, 1462 (1993).

[74] V. A. Kostelecký, J. Pantaleone, and S. Samuel, Phys. Lett. B **315**, 46 (1993).

[75] V. A. Kostelecký and S. Samuel, Phys. Lett. B **318**, 127 (1993).

[76] V. A. Kostelecký and S. Samuel, Phys. Rev. D **49**, 1740 (1994).

[77] V. A. Kostelecký and S. Samuel, Phys. Rev. D **52**, 621 (1995).

[78] S. Pastor, G. Raffelt, and D. V. Semikoz, Phys. Rev. D **65**, 053011 (2002).

[79] H. Duan, G. M. Fuller, and J. Carlson, Comput. Sci. Disc. **1**, 015007 (2008).

[80] J. Ghiglieri and M. Laine, J. Cosmol. Astropart. Phys. **2016**, 015 (2016).

[81] H. Duan, G. M. Fuller, J. Carlson, and Y.-Z. Qian, Phys. Rev. D **74**, 105014 (2006).

[82] G. G. Raffelt and A. Y. Smirnov, Phys. Rev. D **76**, 081301 (2007).

[83] G. M. Fuller and Y.-Z. Qian, Phys. Rev. D **73**, 023004 (2006).

[84] H. A. Bethe, Phys. Rev. Lett. **56**, 1305 (1986).

[85] W. C. Haxton, Phys. Rev. Lett. **57**, 1271 (1986).

[86] S. J. Parke, Phys. Rev. Lett. **57**, 1275 (1986).

[87] C. W. Kim, W.-K. Sze, and S. Nussinov, Phys. Rev. D **35**, 4014 (1987).

[88] L. D. Landau, Phys. Zs. Sowjet. **2**, 46 (1932).

[89] C. Zener, Proc. R. Soc. A **137**, 696 (1932).

[90] K. Abazajian, N. F. Bell, G. M. Fuller, and Y. Y. Y. Wong, Phys. Rev. D **72**, 063004 (2005).

[91] C. T. Kishimoto, G. M. Fuller, and C. J. Smith, Phys. Rev. Lett. **97**, 141301 (2006).

[92] A. Malkus, J. P. Kneller, G. C. McLaughlin, and R. Surman, Phys. Rev. D **86**, 085015 (2012).

[93] A. Malkus, A. Friedland, and G. C. McLaughlin, arXiv:1403.5797 (2014).

[94] A. Malkus, G. C. McLaughlin, and R. Surman, Phys. Rev. D **93**, 045021 (2016).

[95] D. Väänänen and G. C. McLaughlin, Phys. Rev. D **93**, 105044 (2016).

[96] M.-R. Wu, H. Duan, and Y.-Z. Qian, Phys. Lett. B **752**, 89 (2016).

[97] Y.-L. Zhu, A. Perego, and G. C. McLaughlin, arXiv:1607.04671 (2016).

[98] Y.-Z. Qian and G. M. Fuller, Phys. Rev. D **51**, 1479 (1995).

[99] Y.-Z. Qian and G. M. Fuller, Phys. Rev. D **52**, 656 (1995).

[100] C. Volpe, D. Väänänen, and C. Espinoza, Phys. Rev. D **87**, 113010 (2013).

[101] Y. Zhang and A. Burrows, Phys. Rev. D **88**, 105009 (2013).

[102] J. Serreau and C. Volpe, Phys. Rev. D **90**, 125040 (2014).

[103] A. Kartavtsev, G. Raffelt, and H. Vogel, Phys. Rev. D **91**, 125020 (2015).

[104] J. Spyromilio, F. Comerón, S. D'Odorico, M. Kissler-Patig, and R. Gilmozzi, Messenger **133**, 2 (2008).

[105] G. H. Sanders, J. Astrophys. Astron. **34**, 81 (2013).

[106] R. A. Bernstein, P. J. McCarthy, K. Raybould, B. C. Bigelow, A. H. Bouchez, J. M. Filgueira, G. Jacoby, M. Johns, D. Sawyer, S. Shectman, and M. Sheehan, Proc. SPIE **9145**, 91451C (2014).

[107] A. Font-Ribera, P. McDonald, N. Mostek, B. A. Reid, H.-J. Seo, and A. Slosar, J. Cosmol. Astropart. Phys. **2014**, 023 (2014).

[108] K. Abazajian, K. Arnold, J. Austermann, B. Benson, C. Bischoff, J. Bock, J. Bond, J. Borrill, E. Calabrese, J. Carlstrom, C. Carvalho, C. Chang, H. Chiang, S. Church, A. Cooray, T. Crawford, K. Dawson, S. Das, M. Devlin, M. Dobbs, S. Dodelson, O. DorÃ©, J. Dunkley, J. Errard, A. Fraisse, J. Gallicchio, N. Halverson, S. Hanany, S. Hildebrandt, A. Hincks, R. Hlozek, G. Holder, W. Holzapfel, K. Honscheid, W. Hu, J. Hubmayr, K. Irwin, W. Jones, M. Kamionkowski, B. Keating, R. Keisler, L. Knox, E. Komatsu, J. Kovac, C.-L. Kuo,

C. Lawrence, A. Lee, E. Leitch, E. Linder, P. Lubin, J. McMahon, A. Miller, L. Newburgh, M. Niemack, H. Nguyen, H. Nguyen, L. Page, C. Pryke, C. Reichardt, J. Ruhl, N. Sehgal, U. Seljak, J. Sievers, E. Silverstein, A. Slosar, K. Smith, D. Spergel, S. Staggs, A. Stark, R. Stompor, A. Vieregg, G. Wang, S. Watson, E. Wollack, W. Wu, K. Yoon, and O. Zahn, Astropart. Phys. **63**, 66 (2015).

[109] A. Kim, N. Padmanabhan, G. Aldering, S. Allen, C. Baltay, R. Cahn, C. D'Andrea, N. Dalal, K. Dawson, K. Denney, D. Eisenstein, D. Finley, W. Freedman, S. Ho, D. Holz, D. Kasen, S. Kent, R. Kessler, S. Kuhlmann, E. Linder, P. Martini, P. Nugent, S. Perlmutter, B. Peterson, A. Riess, D. Rubin, M. Sako, N. Suntzeff, N. Suzuki, R. Thomas, W. Wood-Vasey, and S. Woosley, Astropart. Phys. **63**, 2 (2015), Dark Energy and CMB.

[110] W. L. K. Wu, J. Errard, C. Dvorkin, C. L. Kuo, A. T. Lee, P. McDonald, A. Slosar, and O. Zahn, Astrophys. J. **788**, 138 (2014).

Chapter 3

Strange mechanics of the neutrino flavor pendulum

3.1 Abstract

We identify in the flavor transformation of astrophysical neutrinos a new class of phenomena, a common outcome of which is the suppression of flavor conversion. Appealing to the equivalence between a bipolar neutrino system and a gyroscopic pendulum, we find that these phenomena have rather striking interpretations in the mechanical picture: in one instance, the gyroscopic pendulum initially precesses in one direction, then comes to a halt and begins to precess in the opposite direction—a counterintuitive behavior that we analogize to the motion of a toy known as a rattleback. We analyze these behaviors in the early universe, wherein a chance connection to sterile neutrino dark matter emerges, and we briefly suggest how they might manifest in compact-object environments.

3.2 Main

Neutrino flavor transformation in dense astrophysical environments has incited considerable fervor in recent years, owing to its importance in properly appraising the role of the neutrino sector in such disparate arenas as dark matter [1–9], baryogenesis [10–15], weak decoupling and Big Bang nucleosynthesis [16–23], and dynamics and nucleosynthesis in supernovae and compact-object mergers [24–39]. Moreover, the flavor structure of a Galactic core-collapse supernova neutrino burst is of interest for terrestrial detectors aimed at understanding not only the physics of the source but also the fundamental properties of neutrinos themselves [40–42]. Far from providing neat resolution, the prolonged siege on this topic has instead continued to reveal facets of the problem that may solicit new conceptual and computational paradigms altogether [43–61].

In what follows, we revisit the surprising equivalence that exists between an astrophysical neutrino system, treated in a certain limit, and the mechanical system of a gyroscopic pendulum (*i.e.*, a spinning top whose axis of rotation can swing freely under gravity) [62, 63]. In this mapping between systems, the pendulum can swing, spin, and precess—and each of these motions corresponds to a change in the flavor content of the neutrino population. We show here that under appropriate circumstances the neutrino system also exhibits some previously unidentified behaviors with rather startling mechanical analogues. In one case, the spin of the top reverses, leading to a flip in the handedness of precession (Fig. 3.1). In another, the precession frequency of the top falls precipitously until reaching a critical threshold, after which it hastily speeds up again. Beyond being counterintuitive, these phenomena may in fact be significant in such environments as the early universe or core-collapse supernovae.

The fact that background particles can dramatically alter neutrino flavor transformation is well known, having played a pivotal part in the solution to the solar neutrino puzzle. But whereas the Mikheyev–Smirnov–Wolfenstein (MSW) mechanism [64, 65] in the Sun is driven

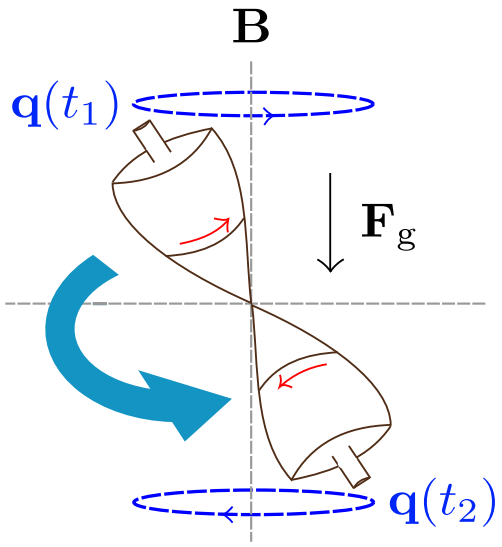

Figure 3.1: One of the strange behaviors exhibited by certain bipolar neutrino systems. In going from an early time t_1 to a late time t_2, the flavor pendulum $\mathbf{q}$ falls from its upright position and reverses its spin, hence also the handedness of its precession.

by the forward scattering of neutrinos on electrons, flavor conversion in the inner region of a core-collapse supernova (which has a neutrino number density ~ 25 *orders of magnitude* greater than that found in the solar interior) is a nonlinear dynamical problem in which the quantum flavor states of all neutrinos on intersecting trajectories are coupled together by virtue of neutrino–neutrino forward scattering. This yoking-together of neutrinos gives rise to a host of flavor-transformation phenomena, many radically different from the classic MSW effect, which are grouped together under the epithet *collective oscillations* [53, 66].

In the two-flavor approximation, the flavor content of neutrinos (antineutrinos) of a given energy is customarily written as a polarization vector $\mathbf{P}$ ($\bar{\mathbf{P}}$), where the projection onto the z-axis gives the difference in number densities of the two flavors. One striking example of collective oscillations is the phenomenon of bipolar flavor transformation, in which the evolution of the system is captured by two interacting blocks of polarization vectors, one representing neutrinos of all energies, the other antineutrinos of all energies [67, 68]. In the absence of a matter background

(*e.g.*, charged leptons), the equations of motion in the bipolar regime are

$$\begin{aligned}\dot{\mathbf{P}} &= \left(+\omega\mathbf{B} - \mu\bar{\mathbf{P}}\right) \times \mathbf{P}, \\ \dot{\bar{\mathbf{P}}} &= \left(-\omega\mathbf{B} + \mu\mathbf{P}\right) \times \bar{\mathbf{P}},\end{aligned} \tag{3.1}$$

where the dot denotes a time derivative and $\mathbf{B} = \pm\left(\sin 2\theta, 0, -\cos 2\theta\right)$, with θ the vacuum mixing angle. The choice of plus (minus) corresponds to the normal (inverted) neutrino mass hierarchy. The oscillation frequency ω is an average of the oscillation frequencies ω_i of the individual neutrinos (labelled by index i), which in vacuum are $\omega_i = |\delta m^2|/4E_i$, where E_i designates the neutrino energy. Lastly, μ is the potential generated by neutrino–neutrino forward scattering. In the early-universe calculations that follow we use a normalization such that $\mu = \sqrt{2}G_F T^3$, with G_F the Fermi coupling constant and T the temperature. For the time being, we postpone discussion of the matter background. Throughout this study we neglect non-forward scattering (*i.e.*, collisions); see the Appendices for justification.

To see the equivalence of this system to a gyroscopic pendulum, we introduce the vectors $\mathbf{D} = \mathbf{P} - \bar{\mathbf{P}}$ and $\mathbf{Q} = \mathbf{P} + \bar{\mathbf{P}} - (\omega/\mu)\,\mathbf{B} = \mathbf{S} - (\omega/\mu)\,\mathbf{B}$. (We are adhering to the notation employed, for instance, in Ref. [62].) One can readily show that if ω, μ, and $\mathbf{B}$ are all constant, then Eqs. (3.1) lead to

$$\begin{aligned}\dot{\mathbf{D}} &= \omega\mathbf{B} \times \mathbf{Q}, \\ \dot{\mathbf{Q}} &= \mu\mathbf{D} \times \mathbf{Q}.\end{aligned} \tag{3.2}$$

It is clear that $\mathbf{D}\cdot\mathbf{Q}$ and $Q = |\mathbf{Q}|$ are both constants of motion. Defining $\mathbf{q} = \mathbf{Q}/Q$ and $\sigma = \mathbf{D}\cdot\mathbf{Q}/Q$, Eqs. (3.2) can be used to obtain

$$\frac{\mathbf{q} \times \ddot{\mathbf{q}}}{\mu} = \omega Q \mathbf{B} \times \mathbf{q} - \sigma\dot{\mathbf{q}}. \tag{3.3}$$

This equation describes a gyroscopic pendulum with total angular momentum

$$\mathbf{D} = \frac{\mathbf{q} \times \dot{\mathbf{q}}}{\mu} + \sigma \mathbf{q}, \tag{3.4}$$

where the first term corresponds to the orbital angular momentum, the second term to the spin. Moreover, the total energy is found to be

$$E = \omega Q \mathbf{B} \cdot \mathbf{q} + \frac{\mu}{2} \mathbf{D}^2. \tag{3.5}$$

Interpreting the first half of the right-hand side as the potential energy, the following picture emerges: the bipolar neutrino system is equivalent to a gyroscopic pendulum, with position vector $\mathbf{Q}$, moment of inertia μ^{-1}, and spin σ, swinging under the influence of a gravitational force $-\omega\mathbf{B}$ [62].

Bipolar oscillations are thought to occur in the neutrino emission from a core-collapse supernova, during, for instance, the late-time, neutrino-driven-wind phase, when the luminosities of the individual species are comparable but there exists a stark energy hierarchy due to the differing opacities of these species in the outflowing material: $\langle E_{\nu_e} \rangle < \langle E_{\bar{\nu}_e} \rangle < \langle E_{\nu_\beta} \rangle \approx \langle E_{\bar{\nu}_\beta} \rangle$, $\beta = \mu, \tau$. This scenario, in fact, has been the standard one in studies of the gyroscopic pendulum

The above hierarchy, however, is not universally applicable, and we find, by considering other arrangements, that the gyroscopic pendulum can exhibit rather bizarre precession behavior. As an illustration, we consider neutrino flavor transformation in the early universe in the presence of a nonzero lepton number. Lepton asymmetries are not only weakly constrained by present data [21, 69–71] but, in the case of lepton asymmetries much larger than the baryon asymmetry, are motivated by leptogenesis models [14, 72] and are integral to a viable production mechanism for sterile neutrino dark matter [1, 2, 5].

Prior to any significant flavor conversion, neutrinos are described by Fermi–Dirac equilibrium distribution functions, with the number density of flavor β given by $n_{\nu_\beta} = \left(T^3/2\pi^2\right) F_2\left(\eta_\beta\right)$,

where $\eta_\beta = \mu_\beta/T$ is the degeneracy parameter, defined in terms of the chemical potential μ_β, and $F_2\left(\eta_\beta\right) = \int_0^\infty dx \frac{x^2}{e^{x-\eta_\beta}+1}$ is the relativistic Fermi integral. We work with two-flavor mixing between ν_e and a state ν_x representing some particular superposition of ν_μ and ν_τ. Since chemical equilibrium obtains at high temperature, antineutrinos of flavor β have degeneracy $-\eta_\beta$.

In the bipolar regime, absent a matter background, the flavor evolution of the system is dictated by Eqs. (3.1), with the asymmetry between $|\mathbf{P}|$ and $|\bar{\mathbf{P}}|$ parameterized by

$$\alpha = \frac{\bar{P}_z(T_i)}{P_z(T_i)} = \frac{F_2(-\eta_e) - F_2(-\eta_x)}{F_2(+\eta_e) - F_2(+\eta_x)}, \tag{3.6}$$

where the system is taken to be comprised of flavor eigenstates at initial temperature T_i. To first order in the degeneracy parameters, $\alpha \approx -1 + \left(12/\pi^2\right)\log 2\,(\eta_e + \eta_x)$, indicating that $\mathbf{P}$ and $\bar{\mathbf{P}}$ are *antialigned* at high temperature, in contrast to the initial alignment of the polarization vectors that is typical of supernova neutrino fluxes. Moreover, by taking the $T \longrightarrow \infty$ limit and dropping prefactors roughly of order unity, the position and angular-momentum vectors are found to have magnitudes $Q \sim |\eta_e^2 - \eta_x^2|$ and $D = |\mathbf{D}| \sim |\eta_e - \eta_x|$ (see Appendices): the angular momentum is parametrically enhanced relative to the length of the pendulum. The significance of this point will appear shortly.

In the early universe Eqs. (3.2) are slightly modified: while the equation of motion for $\mathbf{D}$ is unchanged, the second line becomes $\dot{\mathbf{Q}} = \mu\mathbf{D} \times \mathbf{Q} - 4H\,(\omega/\mu)\,\mathbf{B}$, where H is the Hubble constant. In principle the expansion of the universe, which induces time-dependence in ω and μ, causes the behavior of the system to be quite complicated, but analytical insights may be gained by making a few observations. Firstly, there are two quantities that are strictly conserved in spite of the redshift:

$$\mathbf{B} \cdot \mathbf{D} = \text{constant}, \tag{3.7}$$

which can be interpreted as the magnitude (up to sign) of the angular momentum along the

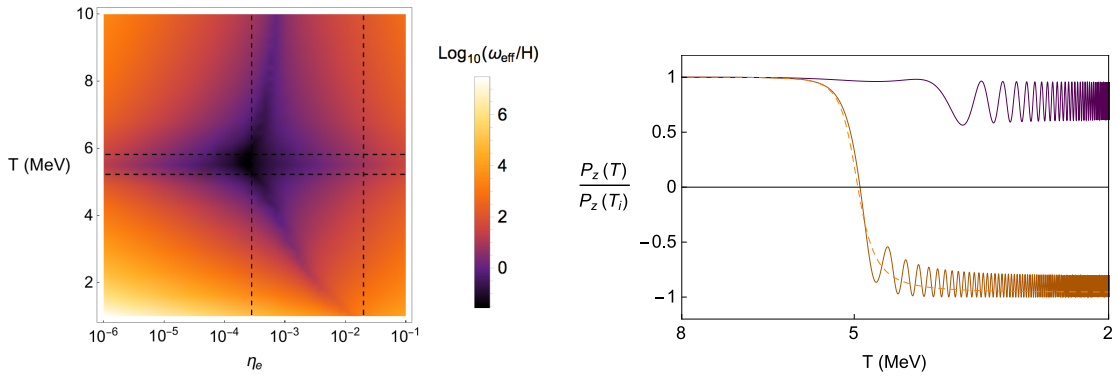

Figure 3.2: (Left) Ratio of ω_{eff} to the Hubble rate H as a function of temperature T and chemical potential η_e, calculated using pre-oscillation flavor states and the appropriate modification of Eq. (3.10) needed to accommodate a matter background (as detailed in the Appendices). The dashed horizontal lines bracket the matter-only MSW resonance width; the vertical lines correspond to the two solid curves in the plot to the right. (Right) $P_z(T)/P_z(T_i) = [n_{\nu_e}(T) - n_{\nu_x}(T)]\,/\,[n_{\nu_e}(T_i) - n_{\nu_x}(T_i)]$, for $\eta_x = 0$ and $\eta_e = 10^{-8}$ (dashed orange), 2.8×10^{-4} (solid purple), and 2×10^{-2} (solid burnt orange). The first of these is indistinguishable from matter-only MSW conversion, due to the small asymmetry.

gravitational field, and

$$\mathbf{D} \cdot \mathbf{Q} + \frac{\omega}{\mu} \mathbf{B} \cdot \mathbf{D} = \text{constant}, \tag{3.8}$$

which ultimately encodes unitarity in the flavor evolution. Furthermore, although the "total energy" in Eq. (3.5) is not truly conserved, the gyroscopic-pendulum picture is still valid over time scales shorter than a Hubble time. In particular, the pendulum in the early universe may be regarded as being dominated by kinetic energy, in the sense that the second term in Eq. (3.5) is much larger than the first one all the way down to very low temperature, when the neutrino number density finally becomes sufficiently dilute. This claim follows from the observation that, by the estimates above, Q is roughly of the same order as $\mathbf{D}^2$ and therefore the ratio of potential to kinetic energy is $\sim \omega/\mu$. The pendulum can only transfer a limited fraction of its total energy to potential energy (*i.e.*, by standing straight up against gravity). Since the kinetic energy vastly exceeds this maximum potential energy, the system is prevented from significantly draining its kinetic energy. As a consequence, D is roughly constant.

Since both D and $\mathbf{B} \cdot \mathbf{D}$ are (approximately) constant, the angular momentum is well

described by

$$\dot{\mathbf{D}} \cong \omega_{\text{eff}} \mathbf{B} \times \mathbf{D}, \tag{3.9}$$

where ω_{eff} is the frequency that emerges because $\mathbf{D}$ is effectively constrained to precess about $\mathbf{B}$. Since the first line of Eq. (3.2) must still be satisfied, this frequency is deduced to be

$$\omega_{\text{eff}} = \omega \frac{Q\sigma - (\mathbf{B}\cdot\mathbf{Q})(\mathbf{B}\cdot\mathbf{D})}{\mathbf{D}^2 - (\mathbf{B}\cdot\mathbf{D})^2}, \tag{3.10}$$

using $\mathbf{D}\cdot\mathbf{Q} = Q\sigma$. Employing Eqs. (3.7) and (3.8) and $D \sim$ constant, one finds that the only impediment to calculating ω_{eff} "by hand" is the presence of the factor $\mathbf{B}\cdot\mathbf{Q}$.

Even with this a priori unknown factor we can draw important qualitative conclusions from Eqs. (3.9) and (3.10). It can be shown that, in the normal mass hierarchy, the spin σ *at high temperature* has the same sign as $\mathbf{B}\cdot\mathbf{D}$ *at low temperature* if and only if $\eta_e^2 < \eta_x^2$; in the inverted hierarchy, the condition is $\eta_e^2 > \eta_x^2$. If the signs match, then Eq. (3.8) requires σ to reverse its sign at some point as the universe cools. Put another way, the blueshifting of ω/μ causes the spin of the gyroscope to slow down to a stop and then to spin up in the opposite direction.

In the course of σ changing sign, ω_{eff} itself goes through zero. When this occurs, $\mathbf{B}\times\mathbf{Q} \cong 0$: the gyroscopic pendulum momentarily stands upright against gravity. But recalling the definition $\mathbf{Q} = \mathbf{S} - (\omega/\mu)\mathbf{B}$, one discerns that the pendulum must subsequently fall to a lower height as the growing factor ω/μ progressively weighs it down. In falling from an inverted to a normal pendulum, the gyroscope continues its precession—but now with the opposite handedness. This qualitative analysis has been verified numerically and is visualized in Fig. 3.1.

More significant from the perspective of flavor transformation is the behavior of the angular-momentum vector during this period. As ω_{eff} passes through zero, $\mathbf{D}$ comes nearly to a dead stop and then begins, like $\mathbf{Q}$, to precess with the opposite handedness. The importance of this is that $\mathbf{D}(t) \approx 2\mathbf{P}(t) \approx -2\bar{\mathbf{P}}(t)$, on account of the initial condition $\bar{\mathbf{P}}(t_i) \approx -\mathbf{P}(t_i)$ and the nature of Eqs. (3.1). The evolution of $\mathbf{D}$ therefore reflects the transformation of flavor: when the

precession of **D** comes to a halt and then reverses, so too do the oscillations of **P** and $\bar{\mathbf{P}}$.

Amusingly, this mechanism can be analogized, with some poetic license, to the behavior of a real-life, canoe-shaped toy known as a rattleback. When spun in one direction, a rattleback rattles to a halt and then spins back in the opposite direction. The rattling is caused by the growth of a rotational instability due to the misalignment of the principal axes of the toy and the symmetry axis of its bottom surface [73]. The gyroscopic pendulum does not rattle, but it too has a sort of instability that causes a reversal: in this case it is the misalignment of the neutrino mass and flavor axes that facilitates the growth of the instability.

Up to this point we have ignored the electrons and positrons in the background, but the lessons from the foregoing analysis carry over straightforwardly, for the following reasons. At some temperature, which we will denote by $T_{\rm MSW}$, the refractive contribution from the $e^{\pm}$ background transitions from dominant ($T \gtrsim T_{\rm MSW}$) to subdominant ($T \lesssim T_{\rm MSW}$) relative to the contribution from neutrino mass. At $T \gtrsim T_{\rm MSW}$, the principal effect of $e^{\pm}$ is to suppress flavor mixing, while at $T \lesssim T_{\rm MSW}$ the effects are negligible. The interesting behavior is thus confined to the MSW region, $T \sim T_{\rm MSW}$, where maximal mixing is expected to occur in the IH, at least in the absence of nonlinear neutrino–neutrino coupling.

How does the gyroscopic pendulum evolve through the MSW region? If the frequency $\omega_{\rm eff}$ is fast relative to the Hubble expansion rate, then significant flavor conversion occurs as expected. If, however, $\omega_{\rm eff}$ happens to be close to zero at $T \sim T_{\rm MSW}$, then conversion is stifled. There is an intuitive visual explanation for this behavior: Imagine a rapidly precessing pendulum. Now imagine—and this is easier said than done—rotating the orientation of gravity. If the pendulum precesses rapidly enough, it will track the gravitational field as it rotates. But if the precession is slow on the scale of the gravity-rotation time scale, then the pendulum will be left behind.

These considerations suggest that the precession-reversal mechanism, should it occur close to the MSW resonance, may impede flavor conversion. It turns out, in fact, that the reversal is associated with a more general phenomenon that impairs adiabaticity even when the conditions are

not met for σ to change sign. Inspection of Eq. (3.10) reveals that, prior to flavor transformation, the dependence of $\omega_{\rm eff}$ on the chemical potentials factors out as Q/D. Having noted earlier that $D \sim$ constant, we now note that Q is dominated, except over a small temperature range, either by the contribution from $\mathbf{S}$ or from the part proportional to $\mathbf{B}$. Using $\mu = \sqrt{2} G_F T^3$, $\omega = |\delta m^2|/4\varepsilon$ for comoving energy ε, and the dependence of $\mathbf{S}$ and $\mathbf{D}$ on the chemical potentials (see Appendices), the frequency scaling in these two limits is found to be $\omega_{\rm eff} \propto \omega |\mathbf{S}|/D \propto T^{-1} |\eta_e + \eta_x|$ when $\mathbf{S}$-dominated and $\omega_{\rm eff} \propto \omega^2/\mu D \propto T^{-5} |\eta_e - \eta_x|^{-1}$ when $\mathbf{B}$-dominated.

The frequency at resonance is thus minimized by the smallest $|\eta_e + \eta_x|$ such that T^{-5} scaling is pushed below the MSW region, or, in other words, such that the transition temperature $T_{\rm trans}$, at which $|\mathbf{S}| \sim |-(\omega/\mu)\mathbf{B}|$, is smaller than $T_{\rm MSW}$. These temperatures compare as

$$\frac{T_{\rm trans}}{T_{\rm MSW}} \sim 1.913 \left(\frac{\delta m^2 \, \varepsilon}{G_F m_W^4 |\eta_e^2 - \eta_x^2|^3 \cos^2 2\theta} \right)^{1/12}, \tag{3.11}$$

where m_W is the W boson mass. For $1-3$ mixing parameters, this becomes $T_{\rm trans}/T_{\rm MSW} \sim \sqrt{5.87 \times 10^{-4}/\sqrt{|\eta_e^2 - \eta_x^2|}}$. Incidentally, the coefficient corresponds to a chemical potential not too far below current constraints. Note that the choice of mixing channel is virtually immaterial, owing to the small exponent.

Fig. 3.2 shows, in a manner consistent with Eq. (3.11), the influence of $\omega_{\rm eff}$ on the flavor transformation of a cosmic bipolar neutrino system. It is intriguing that, for neutrino degeneracies that are not very nearly equal in magnitude, the most profound suppression of flavor conversion occurs for lepton asymmetries in the neighborhood relevant for the resonant production of sterile neutrino dark matter [1, 2, 5, 74–76].

The impact of a small $\omega_{\rm eff}$ was actually identified in an earlier study [77], but the mechanism underlying the suppression of flavor conversion was then unknown. Indeed, the estimates of the preceding paragraph seem to be borne out quite well in the numerical results of that paper. Interpreting the results of Ref. [77] in light of the present analysis, it appears that this phenomenon

may be of considerable importance for neutrino flavor evolution in the early universe. Possible connections between the suppression of flavor conversion and production of the light nuclides in Big Bang nucleosynthesis were speculated on in Ref. [77] and still appear viable.

Whether the precession phenomena analyzed in this paper manifest in compact-object environments is an open question. A plausible candidate is the O-Ne-Mg core-collapse supernova, which is expected to occur for some progenitor stars in the mass range $\sim 8-10\,M_{\odot}$. From the viewpoint of neutrino flavor, the intriguing characteristic of this site is the extremely steep density gradient at the surface of the core, which places the MSW resonances inside the region where neutrino number density is still high and therefore collective effects are still influential [78–81]. Sufficiently adiabatic MSW conversion may conceivably manufacture a hierarchy of fluxes such that the foregoing analysis, with proper modifications, is applicable post-resonance. In a similar vein, an environment in which the density of free neutrons or protons is very high outside the neutrino decoupling surface may deplete enough ν_e or $\bar{\nu}_e$ via charged-current capture to alter the initial flux hierarchy, thereby engineering the requisite conditions. Targeted numerical analysis can be used to confirm whether the foregoing speculations are borne out in these environments, where temporal and spatial instabilities and trajectory dependence [82, 83] are also in play.

It is intriguing that the nonlinear problem of neutrino flavor transformation, although extensively explored, may harbor surprising phenomena—such as those pointed out in this paper—that have implications for cosmology and compact-object physics.

3.3 Acknowledgments

This work was supported by NSF Grant Nos. PHY-1307372 and PHY-1614864 at UC San Diego. During the completion of this work, L.J. was supported by an Inamori Fellowship. We thank Brad Keister and Sebastien Tawa for helpful conversations.

This chapter is a reprint of L. Johns and G. M. Fuller, Phys. Rev. D 97, 023020 (2018). I

was the primary investigator and author of this publication.

3.A MSW and the matter background

In the early universe, effective in-medium mixing parameters can be introduced to account for the influence of the matter background on vacuum oscillations. Recalling the definition $\omega = |\delta m^2|/4E$ for neutrinos of energy E, the in-medium oscillation frequency ω_m and in-medium mixing angle θ_m are respectively given by

$$\omega_m = \sqrt{\omega^2 \sin^2 2\theta + (\pm\omega\cos 2\theta + \mathcal{V})^2}, \tag{3.12}$$

and

$$\sin^2 2\theta_m = \frac{\omega^2 \sin^2 2\theta}{\omega_m^2}, \tag{3.13}$$

where the $+$ $(-)$ is for the normal (inverted) neutrino mass hierarchy and $\mathcal{V}$ is the potential from forward scattering of neutrinos on matter particles. This potential is

$$\mathcal{V} = \frac{2\sqrt{2}G_F E \rho_{e^\pm}}{3m_W^2}, \tag{3.14}$$

with Fermi coupling constant G_F, $e^\pm$ energy density $\rho_{e^\pm}$, and W boson mass m_W [84]. Setting aside the impact of the neutrino self-coupling potential, an MSW resonance is expected to occur in the inverted hierarchy where θ_m is maximal. The temperature at which this occurs is denoted $T_{\rm MSW}$.

In a compact-object environment, the dominant contribution to the matter potential is CP-asymmetric and therefore cannot be incorporated into effective mixing parameters describing both neutrinos and antineutrinos simultaneously. However, a co-rotating reference frame can be adopted: the matter term drops out of the Hamiltonian, but at the expense of the vacuum

Hamiltonian vector **B** oscillating. This approach is laid out in Refs. [62, 63, 82, 85].

3.B Nonadiabaticity and precession

Letting T_i denote a temperature above the onset of significant flavor transformation, the initial "sum" and "difference" vectors are

$$\begin{aligned}\mathbf{S}(T_i) &= \mathbf{P}(T_i) + \bar{\mathbf{P}}(T_i) = \frac{1+\alpha}{2\pi^2}\left[F_2(\eta_e) - F_2(\eta_x)\right]\hat{\mathbf{z}},\\ \mathbf{D}(T_i) &= \mathbf{P}(T_i) - \bar{\mathbf{P}}(T_i) = \frac{1-\alpha}{2\pi^2}\left[F_2(\eta_e) - F_2(\eta_x)\right]\hat{\mathbf{z}}.\end{aligned} \tag{3.15}$$

After expanding the relativistic Fermi integrals to first order, evaluating them, and using the approximation for α given in the main text, the vectors become

$$\begin{aligned}\mathbf{S}(T_i) &\approx \frac{\log 2}{\pi^2}\left(\eta_e^2 - \eta_x^2\right)\hat{\mathbf{z}},\\ \mathbf{D}(T_i) &\approx \frac{1}{6}\left(\eta_e - \eta_x\right)\hat{\mathbf{z}}.\end{aligned} \tag{3.16}$$

These expressions then give the scaling of Q/D, and thereby of $\omega_{\rm eff}$, in the (matter-free) limits $\mathbf{Q} \sim \mathbf{S}$ and $\mathbf{Q} \sim -(\omega/\mu)\mathbf{B}$. The transition between these two limits occurs at $T_{\rm trans}$, found by setting $|\mathbf{S}| = |-(\omega/\mu)\mathbf{B}|$, where again the influence of matter is being neglected.

A first approximation at including the influence of matter is to effect the replacements $\omega \longrightarrow \omega_m$ and $\theta \longrightarrow \theta_m$ in the matter-free analysis, making sure to choose the quadrant of θ_m appropriately. For notational convenience, we also replace **B** with $\mathbf{B}_m$, differing only by the use of θ versus θ_m in the definition. Under this prescription, the effective precession frequency of the angular-momentum vector **D** becomes

$$\omega_{\rm eff} = \omega_m \frac{Q\sigma - (\mathbf{B}_m\cdot\mathbf{Q})(\mathbf{B}_m\cdot\mathbf{D})}{\mathbf{D}^2 - (\mathbf{B}_m\cdot\mathbf{D})^2}, \tag{3.17}$$

where now the precession is about the (temperature-dependent) vector $\mathbf{B}_m$. The left panel of Fig. 3.2 of the main text plots this function, using pre-oscillation values of $\mathbf{Q}$ and $\mathbf{D}$. Eq. (3.11) of the main text, and the scaling limits of $\omega_{\rm eff}$ that precede it, were calculated using the same prescription.

Absent the coupling of different neutrino modes, the adiabaticity is set by ω_m/H, where H is the Hubble rate. If the coupling is strong, the adiabaticity is instead set by $\omega_{\rm eff}/H$. In the early universe, resonance is traversed adiabatically by default ($\omega_m/H \gg 1$ due to the slowness of Hubble expansion) but adiabaticity is lost if $\omega_{\rm eff}$ is sufficiently small. As we argue in the main text, $\omega_{\rm eff}$ scales like $T^{-1}|\eta_e+\eta_x|$ in the $\mathbf{Q}\sim\mathbf{S}$ regime ($T \gtrsim T_{\rm trans}$) and like $T^{-5}|\eta_e-\eta_x|^{-1}$ in the $\mathbf{Q}\sim-(\omega/\mu)\mathbf{B}$ regime ($T \lesssim T_{\rm trans}$). The frequency at resonance is therefore minimized if the rapid increase in the latter regime is delayed at least until the resonance temperature $T_{\rm MSW}$ is reached. On the other hand, given the scaling with neutrino degeneracy, minimizing $\omega_{\rm eff}$ also requires minimizing $|\eta_e+\eta_x|$, such that $T_{\rm trans} \lesssim T_{\rm MSW}$ still holds.

3.C Non-forward scattering

The calculations presented in the main text were performed neglecting non-forward scattering (*i.e.*, collisions) [48, 86–89]. In Fig. 3.3 we display the results of repeating the calculations shown in the right panel of Fig. 3.2 of the main text but with collisions now accounted for. The suppression of flavor conversion witnessed in the collisionless analysis translates to a suppression of flavor equilibration ($P_z \to 0$) in the calculation with collisions.

In producing Fig. 3.3 we have employed the damping approximation used in Refs. [16, 90–92] and elsewhere. With this prescription, the equations of motion, given in Eq. (3.1) of the

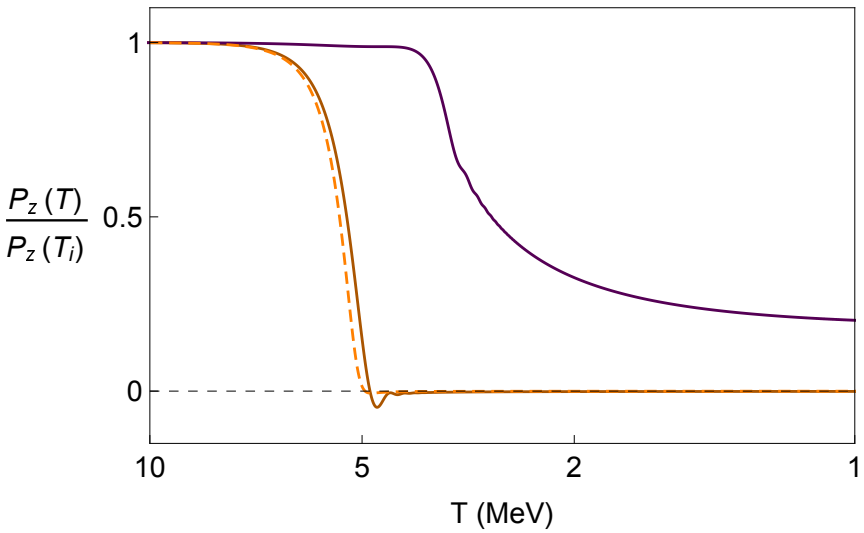

Figure 3.3: Identical to the right panel of Fig. 3.2 of the main text except that the influence of collisions is accounted for here. The curves correspond to lepton asymmetries of $\eta_x = 0$ and $\eta_e = 10^{-8}$ (dashed orange), 2.8×10^{-4} (solid purple), and 2×10^{-2} (solid burnt orange).

main text, become

$$\dot{\mathbf{P}} = \left(+\omega\mathbf{B} - \mu\bar{\mathbf{P}}\right) \times \mathbf{P} - D\mathbf{P}_T,$$
$$\dot{\bar{\mathbf{P}}} = \left(-\omega\mathbf{B} + \mu\mathbf{P}\right) \times \bar{\mathbf{P}} - D\bar{\mathbf{P}}_T, \tag{3.18}$$

where the subscript T denotes the part of the vector transverse to the flavor (z) axis and D is a damping coefficient proportional to the scattering rate. The expression for D and the derivation of this prescription can be found in the references above.

By a plasma temperature of 1 MeV neutrinos have begun to decouple and subsequent effects of collisions are small. The survival of coherent (collisionless) flavor phenomena through to the epochs of neutrino decoupling and Big Bang nucleosynthesis is discussed at greater length in Ref. [77].

Bibliography

[1] X. Shi and G. M. Fuller, Phys. Rev. Lett. **82**, 2832 (1999).

[2] K. Abazajian, G. M. Fuller, and M. Patel, Phys. Rev. D **64**, 023501 (2001).

[3] T. Asaka and M. Shaposhnikov, Phys. Lett. B **620**, 17 (2005).

[4] T. Asaka, S. Blanchet, and M. Shaposhnikov, Phys. Lett. B **631**, 151 (2005).

[5] C. T. Kishimoto and G. M. Fuller, Phys. Rev. D **78**, 023524 (2008).

[6] K. Petraki and A. Kusenko, Phys. Rev. D **77**, 065014 (2008).

[7] F. Bezrukov, A. Kartavtsev, and M. Lindner, J. Phys. G **40**, 095202 (2013).

[8] T. Venumadhav, F.-Y. Cyr-Racine, K. N. Abazajian, and C. M. Hirata, Phys. Rev. D **94**, 043515 (2016).

[9] R. Adhikari, M. Agostini, N. A. Ky, T. Araki, M. Archidiacono, M. Bahr, J. Baur, J. Behrens, F. Bezrukov, P. B. Dev, D. Borah, A. Boyarsky, A. de Gouvea, C. de S. Pires, H. de Vega, A. Dias, P. D. Bari, Z. Djurcic, K. Dolde, H. Dorrer, M. Durero, O. Dragoun, M. Drewes, G. Drexlin, C. DÃŒllmann, K. Eberhardt, S. Eliseev, C. Enss, N. Evans, A. Faessler, P. Filianin, V. Fischer, A. Fleischmann, J. Formaggio, J. Franse, F. Fraenkle, C. Frenk, G. Fuller, L. Gastaldo, A. Garzilli, C. Giunti, F. GlÃŒck, M. Goodman, M. Gonzalez-Garcia, D. Gorbunov, J. Hamann, V. Hannen, S. Hannestad, S. Hansen, C. Hassel, J. Heeck, F. Hofmann, T. Houdy, A. Huber, D. Iakubovskyi, A. Ianni, A. Ibarra, R. Jacobsson, T. Jeltema, J. Jochum, S. Kempf, T. Kieck, M. Korzeczek, V. Kornoukhov, T. Lachenmaier, M. Laine, P. Langacker, T. Lasserre, J. Lesgourgues, D. Lhuillier, Y. Li, W. Liao, A. Long, M. Maltoni, G. Mangano, N. Mavromatos, N. Menci, A. Merle, S. Mertens, A. Mirizzi, B. Monreal, A. Nozik, A. Neronov, V. Niro, Y. Novikov, L. Oberauer, E. Otten, N. Palanque-Delabrouille, M. Pallavicini, V. Pantuev, E. Papastergis, S. Parke, S. Pascoli, S. Pastor, A. Patwardhan, A. Pilaftsis, D. Radford, P.-O. Ranitzsch, O. Rest, D. Robinson, P. R. da Silva, O. Ruchayskiy, N. Sanchez, M. Sasaki, N. Saviano, A. Schneider, F. Schneider, T. Schwetz, S. SchÃnert, S. Scholl, F. Shankar, R. Shrock, N. Steinbrink, L. Strigari, F. Suekane, B. Suerfu, R. Takahashi, N. T. H. Van, I. Tkachev, M. Totzauer, Y. Tsai, C. Tully, K. Valerius, J. Valle, D. Venos, M. Viel, M. Vivier, M. Wang, C. Weinheimer, K. Wendt, L. Winslow, J. Wolf, M. Wurm, Z. Xing, S. Zhou, and K. Zuber, J. Cosmol. Astropart. Phys. **2017**, 025 (2017).

[10] E. K. Akhmedov, V. A. Rubakov, and A. Y. Smirnov, Phys. Rev. Lett. **81**, 1359 (1998).

[11] A. Abada, S. Davidson, F.-X. Josse-Michaux, M. Losada, and A. Riotto, J. Cosmol. Astropart. Phys. **2006**, 004 (2006).

[12] E. Nardi, Y. Nir, E. Roulet, and J. Racker, J. High Energy Phys. **2006**, 164 (2006).

[13] S. Blanchet and P. D. Bari, J. Cosmol. Astropart. Phys. **2007**, 018 (2007).

[14] M. Shaposhnikov, J. High Energy Phys. **2008**, 008 (2008).

[15] L. Canetti, M. Drewes, T. Frossard, and M. Shaposhnikov, Phys. Rev. D **87**, 093006 (2013).

[16] A. D. Dolgov, S. H. Hansen, S. Pastor, S. T. Petcov, G. G. Raffelt, and D. V. Semikoz, Nucl. Phys. **B632**, 363 (2002).

[17] K. N. Abazajian, J. F. Beacom, and N. F. Bell, Phys. Rev. D **66**, 013008 (2002).

[18] Y. Y. Y. Wong, Phys. Rev. D **66**, 025015 (2002).

[19] V. Simha and G. Steigman, J. Cosmol. Astropart. Phys. **2008**, 011 (2008).

[20] G. Mangano, G. Miele, S. Pastor, O. Pisanti, and S. Sarikas, J. Cosmol. Astropart. Phys. **2011**, 035 (2011).

[21] G. Mangano, G. Miele, S. Pastor, O. Pisanti, and S. Sarikas, Phys. Lett. B **708**, 1 (2012).

[22] S. Pastor, T. Pinto, and G. G. Raffelt, Phys. Rev. Lett. **102**, 241302 (2009).

[23] J. Gava and C. Volpe, Nucl. Phys. **B837**, 50 (2010).

[24] G. Fuller, R. Mayle, J. Wilson, and D. Schramm, Astrophys. J. **322**, 795 (1987).

[25] G. M. Fuller, R. Mayle, B. S. Meyer, and J. R. Wilson, Astrophys. J. **389**, 517 (1992).

[26] Y.-Z. Qian and G. M. Fuller, Phys. Rev. D **51**, 1479 (1995).

[27] Y.-Z. Qian and G. M. Fuller, Phys. Rev. D **52**, 656 (1995).

[28] Y.-Z. Qian, W. C. Haxton, K. Langanke, and P. Vogel, Phys. Rev. C **55**, 1532 (1997).

[29] C. J. Horowitz and G. Li, Phys. Rev. Lett. **82**, 5198 (1999).

[30] G. C. McLaughlin, J. M. Fetter, A. B. Balantekin, and G. M. Fuller, Phys. Rev. C **59**, 2873 (1999).

[31] R. C. Schirato and G. M. Fuller, arXiv:0205390 (2002).

[32] S. Pastor, G. Raffelt, and D. V. Semikoz, Phys. Rev. D **65**, 053011 (2002).

[33] S. Pastor and G. Raffelt, Phys. Rev. Lett. **89**, 191101 (2002).

[34] J. Fetter, G. C. McLaughlin, A. B. Balantekin, and G. M. Fuller, Astropart. Phys. **18**, 433 (2003).

[35] H. Duan, G. M. Fuller, J. Carlson, and Y.-Z. Qian, Phys. Rev. Lett. **97**, 241101 (2006).

[36] H. Duan, A. Friedland, G. C. McLaughlin, and R. Surman, J. Phys. G **38**, 035201 (2011).

[37] I. Tamborra, G. G. Raffelt, L. Hüdepohl, and H.-T. Janka, J. Cosmol. Astropart. Phys. **2012**, 013 (2012).

[38] A. Malkus, J. P. Kneller, G. C. McLaughlin, and R. Surman, Phys. Rev. D **86**, 085015 (2012).

[39] M.-R. Wu, Y.-Z. Qian, G. Martínez-Pinedo, T. Fischer, and L. Huther, Phys. Rev. D **91**, 065016 (2015).

[40] A. S. Dighe and A. Y. Smirnov, Phys. Rev. D **62**, 033007 (2000).

[41] K. Abazajian, E. Calabrese, A. Cooray, F. De Bernardis, S. Dodelson, A. Friedland, G. Fuller, S. Hannestad, B. Keating, E. Linder, C. Lunardini, A. Melchiorri, R. Miquel, E. Pierpaoli, J. Pritchard, P. Serra, M. Takada, and Y. Wong, Astropart. Phys. **35**, 177 (2011).

[42] K. Scholberg, arXiv:1707.06384 (2017).

[43] R. F. Sawyer, Phys. Rev. D **72**, 045003 (2005).

[44] J. F. Cherry, J. Carlson, A. Friedland, G. M. Fuller, and A. Vlasenko, Phys. Rev. Lett. **108**, 261104 (2012).

[45] G. Raffelt, S. Sarikas, and D. S. Seixas, Phys. Rev. Lett. **111**, 091101 (2013).

[46] R. S. Hansen and S. Hannestad, Phys. Rev. D **90**, 025009 (2014).

[47] A. Vlasenko, G. M. Fuller, and V. Cirigliano, arXiv:1406.6724 .

[48] J. Serreau and C. Volpe, Phys. Rev. D **90**, 125040 (2014).

[49] S. Abbar, H. Duan, and S. Shalgar, Phys. Rev. D **92**, 065019 (2015).

[50] A. Mirizzi, G. Mangano, and N. Saviano, Phys. Rev. D **92**, 021702 (2015).

[51] B. D. Keister, Phys. Scripta **90**, 088008 (2015).

[52] E. Armstrong, A. V. Patwardhan, L. Johns, C. T. Kishimoto, H. D. I. Abarbanel, and G. M. Fuller, Phys. Rev. D **96**, 083008 (2017).

[53] S. Chakraborty, R. Hansen, I. Izaguirre, and G. Raffelt, Nucl. Phys. **B908**, 366 (2016).

[54] R. F. Sawyer, Phys. Rev. Lett. **116**, 081101 (2016).

[55] C. Volpe, J. Phys. Conf. Ser. **718**, 062068 (2016).

[56] L. Johns and G. M. Fuller, Phys. Rev. D **95**, 043003 (2017).

[57] B. Dasgupta, A. Mirizzi, and M. Sen, J. Cosmol. Astropart. Phys. **2017**, 019 (2017).

[58] J. Y. Tian, A. V. Patwardhan, and G. M. Fuller, Phys. Rev. D **95**, 063004 (2017).

[59] M.-R. Wu and I. Tamborra, Phys. Rev. D **95**, 103007 (2017).

[60] I. Izaguirre, G. Raffelt, and I. Tamborra, Phys. Rev. Lett. **118**, 021101 (2017).

[61] V. Cirigliano, M. W. Paris, and S. Shalgar, Phys. Lett. B **774**, 258 (2017).

[62] S. Hannestad, G. G. Raffelt, G. Sigl, and Y. Y. Y. Wong, Phys. Rev. D **74**, 105010 (2006).

[63] H. Duan, G. M. Fuller, J. Carlson, and Y.-Z. Qian, Phys. Rev. D **75**, 125005 (2007).

[64] L. Wolfenstein, Phys. Rev. D **17**, 2369 (1978).

[65] S. P. Mikheyev and A. Y. Smirnov, Sov. J. Nucl. Phys. **42**, 913 (1985).

[66] H. Duan, G. M. Fuller, and Y.-Z. Qian, Ann. Rev. Nucl. Part. Sci. **60**, 569 (2010).

[67] V. A. Kostelecký and S. Samuel, Phys. Rev. D **52**, 621 (1995).

[68] S. Samuel, Phys. Rev. D **53**, 5382 (1996).

[69] G. Steigman, Adv. High Energy Phys. **2012**, 268321 (2012).

[70] E. Castorina, U. Franca, M. Lattanzi, J. Lesgourgues, G. Mangano, A. Melchiorri, and S. Pastor, Phys. Rev. D **86**, 023517 (2012).

[71] G. Barenboim, W. H. Kinney, and W.-I. Park, Phys. Rev. D **95**, 043506 (2017).

[72] S. Eijima and M. Shaposhnikov, Phys. Lett. B **771**, 288 (2017).

[73] W. Case and S. Jalal, Am. J. Phys. **82**, 654 (2014).

[74] K. N. Abazajian, Phys. Rev. Lett. **112**, 161303 (2014).

[75] B. Bozek, M. Boylan-Kolchin, S. Horiuchi, S. Garrison-Kimmel, K. Abazajian, and J. S. Bullock, Mon. Not. R. Astron. Soc. **459**, 1489 (2016).

[76] S. Horiuchi, B. Bozek, K. N. Abazajian, M. Boylan-Kolchin, J. S. Bullock, S. Garrison-Kimmel, and J. Onorbe, Mon. Not. R. Astron. Soc. **456**, 4346 (2016).

[77] L. Johns, M. Mina, V. Cirigliano, M. W. Paris, and G. M. Fuller, Phys. Rev. D **94**, 083505 (2016).

[78] H. Duan, G. M. Fuller, J. Carlson, and Y.-Z. Qian, Phys. Rev. Lett. **100**, 021101 (2008).

[79] B. Dasgupta, A. Dighe, A. Mirizzi, and G. G. Raffelt, Phys. Rev. D **77**, 113007 (2008).

[80] C. Lunardini, B. Müller, and H.-T. Janka, Phys. Rev. D **78**, 023016 (2008).

[81] J. F. Cherry, G. M. Fuller, J. Carlson, H. Duan, and Y.-Z. Qian, Phys. Rev. D **82**, 085025 (2010).

[82] H. Duan, G. M. Fuller, J. Carlson, and Y.-Z. Qian, Phys. Rev. D **74**, 105014 (2006).

[83] A. Mirizzi and R. Tomàs, Phys. Rev. D **84**, 033013 (2011).

[84] D. Nötzold and G. Raffelt, Nucl. Phys. **B307**, 924 (1988).

[85] H. Duan, G. M. Fuller, and Y.-Z. Qian, Phys. Rev. D **74**, 123004 (2006).

[86] G. Sigl and G. Raffelt, Nucl. Phys. **B406**, 423 (1993).

[87] P. Strack and A. Burrows, Phys. Rev. D **71**, 093004 (2005).

[88] A. Vlasenko, G. M. Fuller, and V. Cirigliano, Phys. Rev. D **89**, 105004 (2014).

[89] D. N. Blaschke and V. Cirigliano, Phys. Rev. D **94**, 033009 (2016).

[90] L. Stodolsky, Phys. Rev. D **36**, 2273 (1987).

[91] M. J. Thomson, Phys. Rev. A **45**, 2243 (1992).

[92] N. F. Bell, R. R. Volkas, and Y. Y. Y. Wong, Phys. Rev. D **59**, 113001 (1999).

Chapter 4

Geometric phases in neutrino oscillations with nonlinear refraction

4.1 Abstract

Neutrinos propagating in dense astrophysical environments sustain nonlinear refractive effects due to neutrino–neutrino forward scattering. We study geometric phases in neutrino oscillations that arise out of cyclic evolution of the potential generated by these forward-scattering processes. We perform several calculations, exact and perturbative, that illustrate the robustness of such phases, and of geometric effects more broadly, in the flavor evolution of neutrinos. The scenarios we consider are highly idealized in order to make them analytically tractable, but they suggest the possible presence of complicated geometric effects in realistic astrophysical settings. We also point out that in the limit of extremely high neutrino densities, the nonlinear potential in three flavors naturally gives rise to non-Abelian geometric phases. This paper is intended to be accessible to neutrino experts and non-specialists alike.

4.2 Introduction

Geometric phases in neutrino propagation have been investigated in various guises [1–14] over the decades since it was recognized that neutrino flavor transformation might provide the solution to the mysterious deficit of solar neutrinos [15, 16]. In the intervening years the understanding of how neutrino oscillations are modified in medium has undergone a sea change. In particular, it is now recognized that in environments with very high neutrino density the flavor evolution of one neutrino is coupled to that of all other neutrinos with which it interacts. The result is a colorful tapestry of flavor-transformation phenomena that extends far beyond the classic resonance mechanism at work in solar neutrinos.

In this paper we conduct the first study of neutrino geometric phases that accounts for the nonlinear coupling of flavor states, a phenomenon known in the neutrino literature as *self-coupling*. The phases that we exhibit in our calculations persist at the probability level and are therefore detectable in principle, though no attempt is made here to extract geometric phases from models of any degree of astrophysical realism. By and large such models would necessitate numerical analysis, which may obscure some of the insights otherwise made transparent by an analytical treatment. Our present aim is to explore the manifestations of geometric phases precisely without the complications that continue to make the modeling of neutrino flavor such a disobliging task. Even so, as we argue here, one gleans a hint that geometric quantum effects of one form or another may be nearly unavoidable in the flavor evolution of neutrinos in such dense environments as core-collapse supernovae or neutron-star mergers.

Broadly, geometric phase refers to the extra, path-dependent quantum phase that a state accumulates in addition to the dynamical phase from the "local" influence of the Hamiltonian. The latter phase is present even for a time-independent Hamiltonian and its importance has been appreciated since the very advent of quantum mechanics; we denote it by δ, and for a state $|\psi\rangle$

and Hamiltonian H it has the usual form

$$\delta = -\int dt\ \langle\psi(t)|H(t)|\psi(t)\rangle. \tag{4.1}$$

The appreciation of geometric phases as a common and observable feature of many quantum systems is much more recent, dating back to the seminal realization by Berry [17] that a state acted on by a cyclic, adiabatically changing Hamiltonian acquires a phase whose value depends on the circuit traced out by the Hamiltonian in the space of its parameters. If $|\psi\rangle$ begins as an instantaneous energy eigenstate $|\eta\rangle$, the adiabatic theorem dictates that it remains so, *i.e.*, $|\psi(t)\rangle = e^{i\phi(t)}|\eta(t)\rangle$, and the total phase has the form $\phi = \delta + \gamma$ with the geometric phase given by γ. After the system, which is described by time-dependent parameters $\vec{R}(t)$, completes a circuit C, the state $|\psi\rangle$ has developed a geometric phase

$$\gamma = i\oint_C \langle\eta(t)|\nabla|\eta(t)\rangle \cdot d\vec{R}, \tag{4.2}$$

where ∇ is the gradient operator in $\vec{R}$-space.

The particular incarnation of the geometric phase defined by this expression is often called the *Berry phase* and is specific to cyclic, adiabatic systems. The notion can be generalized enormously: to entangled states [18]; to mixed states [19]; and to non-adiabatic [1, 20, 21], non-cyclic [22–26], and even open or non-Hamiltonian [27–31] systems. In this paper we use the broad term *geometric phase* but our typical targets are indeed Berry phases of the form in Eq. (4.2). At several points we will make contact with some of these generalizations.

On an intuitive level the existence of geometric phases in quantum systems is perhaps most immediately grasped by analogy to the classical world: A Foucault pendulum, carried around a closed loop on the surface of the Earth in such a way that the plane of oscillation is never rotated, nonetheless returns to its starting point with a rotated plane of oscillation, and the angle by which the plane has rotated (known as the Hannay angle) is, moreover, equal to the solid

angle enclosed by the loop. Quantum geometric phases are rotations of the wavefunction and arise, in much the same way, from parallel transport along a path. For readers seeking a deeper understanding of the phenomenon, we sketch a picture in Sec. 4.3 of geometric phases from the perspective of differential geometry, which permits a rigorous translation of this classical intuition into the quantum realm. The picture is also intimately related to the "polarization vectors" (formally introduced in Sec. 4.4) that are ubiquitous in the literature on neutrino flavor evolution. Put succinctly, this connection is why geometry is relevant to neutrino oscillations.

The observability of geometric phases is today well-established in a variety of settings thanks to such landmark experiments as those in Refs. [32–40] and the vast sweep of investigations carried out in more recent years. The modern understanding of geometric phases has also shed light on instances and variations of the phenomenon that were predicted or observed *before* Berry's original analysis, perhaps the most famous cases being the Aharonov–Bohm effect [41], the Pancharatnam phase [42], and the (retroactively named) molecular Berry phase [43, 44].

Interferometry experiments, which comprise a large share of the corpus of geometric-phase studies, are plainly out of the question when it comes to neutrinos. But neutrino oscillations are themselves fundamentally an interference phenomenon: As mass eigenstates propagate in vacuum they pick up phases at different rates, and the interference between these phases gives rise to flavor oscillation. It is natural, then, to wonder whether the interference intrinsic to neutrino oscillations might function in some way as an "interferometer" sensitive to geometric phases.

Much of the earliest interest in this possibility surrounded the idea that the resolution of the missing-solar-neutrinos puzzle may come from the conversion of neutrinos into antineutrinos via the interaction of their magnetic moments with solar magnetic fields [2, 4, 45, 46]. Although the consensus is that the Mikheyev–Smirnov–Wolfenstein (MSW) mechanism [15, 47] ultimately won the day as far as the solar neutrino problem, neutrino geometric phases continue to be explored in the context of astrophysical magnetic fields [14]. Furthermore, just as magnetic field vectors can trace out closed loops in physical space, the optical potentials generated by

coherent forward scattering of neutrinos with background particles raise the possibility that a similar mechanism might operate in flavor space.

Shortly after the explosion of interest in geometric phases began, Nakagawa [1] acknowledged this possibility but observed that geometric phases cannot appear in two-flavor neutrino oscillations in a matter background, for the simple reason that there is just one parameter in the Hamiltonian that is varying (viz., the density of matter particles) and therefore a cycle of finite area cannot be traced out. Naumov [7, 8] later showed that geometric phases can emerge in three flavors, provided that there is both CP violation and a cyclically varying number density of scatterers. These papers regarded vacuum mixing as the sole contributor to the off-diagonal (in the flavor basis) Hamiltonian matrix elements; Pantaleone's insight [48] that self-coupling can also supply off-diagonal contributions was not yet widely appreciated.

More recently geometric phases were studied by He *et al.* [11] in a paper generalizing Naumov's work to active–sterile mixing and nonstandard interactions. Although the authors noted that the neutrino-background density is an additional parameter varying independently of the matter-background density, they did not consider the contribution of coherent neutrino–neutrino scattering to the off-diagonal Hamiltonian elements. We thus point out for the first time in the literature that geometric phases can arise out of the self-coupling potential and can appear even with just two flavors. We also argue that because of the nonlinear nature of this potential, neutrino self-coupling in flavor space is a particularly rich avatar for geometric phases.

Our approach is to perform calculations on several toy models that reveal various facets of geometric phases in the presence of nonlinear neutrino–neutrino coupling. The calculations that follow shed light on the precise role of adiabaticity, the nonlinear entangling of the geometric phases developed by neutrinos in interaction with one another, the fragile cyclicity of flavor transformation, and the non-Abelian phase structure of a certain three-flavor limit. While we do not attempt to locate geometric phases in realistic astrophysical models, our results are suggestive of the prevalence in sophisticated numerical computations of geometric effects generally, if not

specifically the cyclic, adiabatic phases we investigate.

In Sec. 4.3 we sketch the picture of geometric phases from the viewpoint of differential geometry. In Sec. 4.4 we present the relevant background on medium-enhanced neutrino oscillations. We then turn our attention to the flavor evolution that occurs in a system of two coupled neutrino populations. Working in the two-flavor approximation, we examine three limiting cases: the mixed-potential limit in Sec. 4.5, the pure-self-coupling limit in Sec. 4.6, and the weak-self-coupling limit in Sec. 4.7. After examining these two-flavor scenarios, we return in Sec. 4.8 to the mixed-potential limit, this time in three flavors, and show how it begets non-Abelian geometric phases. We conclude in Sec. 4.9.

4.3 The differential-geometric picture

The Born rule implies that the overall phase of a quantum state $|\psi\rangle$ is inessential for computing or measuring observables at some time t. With a rephasing $|\tilde{\psi}(t)\rangle = e^{i\alpha}|\psi(t)\rangle$ by some arbitrary phase α,

$$\langle\tilde{\psi}(t)|O|\tilde{\psi}(t)\rangle = \langle\psi(t)|O|\psi(t)\rangle \tag{4.3}$$

for any Hermitian operator O. As a result the value of α in $|\tilde{\psi}(t)\rangle$ can be chosen arbitrarily, but as shown by Berry it does not follow that the overall phase can be ignored altogether. At a basic level, geometric phases are in fact amenable to observation because once α is chosen for $|\tilde{\psi}(t)\rangle$, the phase of $|\tilde{\psi}(t')\rangle$ at any other time t' is predetermined by this choice (in conjunction, of course, with the dynamics of the system). In other words, phase *changes* are physically significant.

Granting that geometric phases exist, it is perhaps not so surprising that they are observable—but that they should exist at all is a profound fact about quantum mechanics. Fundamentally the existence of geometric phases is a consequence of Hilbert space having nontrivial geometry, and the values of the phases are governed by that geometry in tandem with the relevant Hamiltonian. Just as the spheroidal shape of the Earth determines the Hannay angle [49] of a Foucault pendu-

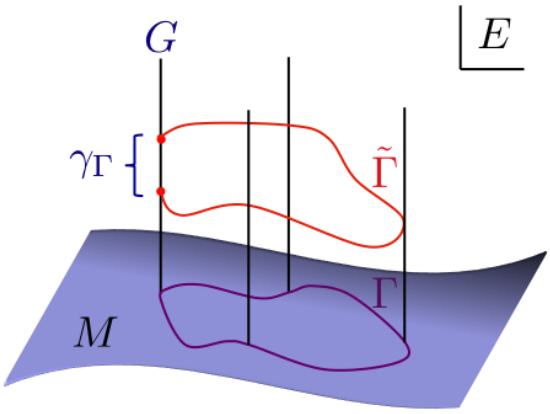

Figure 4.1: A visualization of the differential-geometric structures underpinning the geometric phase. The curve $\tilde{\Gamma}$ in Hilbert space projects down to a curve Γ in projective Hilbert space. $\tilde{\Gamma}$ begins and ends on the same fiber (labeled G, denoting the Lie group) but may not return to the same element in the fiber. The group element at the start of the loop is brought to the element at the end by the holonomy γ_Γ. The holonomy is precisely the geometric phase acquired upon completing the cycle.

lum carried along the planet's surface, in an analogous way does the "shape" of Hilbert space determine how a wavefunction rotates—that is, picks up phase—as it is moved along a path.

These ideas are most naturally expressed in a rigorous manner using the language of principal fiber bundles and their associated structures. The relation between geometric phases and fiber bundles was the powerful insight of Simon [50] and has been elaborated by many subsequent authors. We now try to elucidate this helpful way of understanding geometric phases.

For a Hamiltonian $H[\vec{R}]$ that depends on the time-dependent parameters $\vec{R}(t)$, a given nondegenerate instantaneous eigenstate $|\tilde{\psi}\rangle$ can be specified by the pair $\left(\vec{R}, \exp(i\alpha)\right)$, where α is the arbitrary overall phase referred to previously. We have already established that this pair corresponds to the same physical state regardless of the value of α; in technical terms, the pair projects down to the same ray in projective Hilbert space for all α. Hilbert space can thus be visualized as a manifold with an identical string piercing through every point: A given point on the manifold corresponds to a physical state (or, equivalently, a value of $\vec{R}$) and the string through that point represents the possible choices of phase α for that particular physical state.

A principal fiber bundle describes precisely such an object. It consists of three parts (Fig. 4.1): a total space E, a base manifold M, and a Lie-group fiber G. The translation into bundle language uses the following associations:

$$\begin{aligned} E &\longleftrightarrow \text{States in Hilbert space,} \\ &\qquad \text{identified by } (\vec{R}, \exp(i\alpha)), \\ M &\longleftrightarrow \text{Physical states in projective} \\ &\qquad \text{Hilbert space,} \\ G &\longleftrightarrow \text{Elements } e^{i\alpha} \text{ of the group } U(1). \end{aligned} \tag{4.4}$$

If the eigenstate is part of an n-degenerate subspace, then the fiber G is instead the non-Abelian group $U(n)$. For simplicity we will continue to assume non-degeneracy throughout the remainder of this section, but we will demonstrate the emergence of non-Abelian fibers in the context of neutrino oscillations in Sec. 4.8.

As $\vec{R}(t)$ evolves, a curve $C(t)$ in parameter space, hence also a curve on the base manifold M, is traced out. The curve on M, $\Gamma(t)$, can be visualized as the shadow of a curve $\tilde{\Gamma}(t)$ on E: At every point in M there is a point in E elevated above the base manifold according to its fiber element. The freedom to choose the value of α for $|\tilde{\psi}(t_i)\rangle$ at a specific time t_i is manifested as a freedom to choose the fiber element at $\tilde{\Gamma}(t_i)$, but having made this choice, the fiber elements are non-arbitrary for $t > t_i$ (and, for that matter, for $t < t_i$). For us, the condition of adiabaticity furnishes the principal fiber bundle with a connection, which is to say a way of moving a state from one fiber to the next. The adiabatic connection is equivalent to the condition

$$\left\langle \tilde{\psi}(t) \left| \frac{d}{dt} \right| \tilde{\psi}(t) \right\rangle = 0. \tag{4.5}$$

This constraint describes the parallel transport of the state along the path and captures the intuitive

notion that the state vector moves in such a way that locally it never appears to be rotating, modulo the dynamical phase evolution (Eq. (4.1)).

If $\vec{R}(t_f) = \vec{R}(t_i)$, then Γ forms a closed loop and the state returns at t_f to the same fiber it began on at t_i. It is not guaranteed, however, that the state will return to the same fiber *element*. The difference

$$e^{i\left[\alpha(t_f)-\alpha(t_i)\right]} \equiv e^{i\Delta\alpha} \tag{4.6}$$

is itself an element of the Lie group and is termed the holonomy of the connection on the principal fiber bundle. It is precisely equal to the geometric phase: $\Delta\alpha = \gamma$. The plausibility of a global rotation occurring without any local rotation can be seen from the non-transitivity of phase [42, 51]: $\langle\tilde{\psi}_1|\tilde{\psi}_2\rangle$ and $\langle\tilde{\psi}_2|\tilde{\psi}_3\rangle$ having the same phase does not necessarily imply that $\langle\tilde{\psi}_1|\tilde{\psi}_3\rangle$ has the same phase as well.

The numerical value of the holonomy depends on the curve Γ and the geometry of the manifold M on which Γ lies. To illustrate this point concretely, we consider the evolution of two-flavor neutrinos in flavor space. As with any two-level system, wavefunction normalization and the arbitrariness of $\alpha(t_i)$ relegate a $\mathbb{C}^2$ state vector to the Bloch sphere S^2. In two flavors, therefore, it is the geometry of the Bloch sphere that determines the geometric phase associated with passage along a closed loop $\mathcal{C}$ in parameter space. The principal fiber bundle can be pictured in this case as a ball ($M = S^2$) with spikes ($G = U(1)$) sticking out of it. The three-flavor case with two degenerate eigenstates, which we turn to toward the end of this study, has base manifold $\mathbb{C}P^2 = SU(3)/U(2)$ and is not as easily visualized, but the message is the same: The geometry of Hilbert space leaves its footprint in the flavor conversion of neutrinos.

4.4 Neutrino oscillations in medium

Neutrino oscillations are conveniently studied by tracking the time-evolution of the flavor wavefunction

$$|\psi\rangle = \begin{pmatrix} a_e \\ a_\mu \\ a_\tau \end{pmatrix}, \tag{4.7}$$

where a_α is the amplitude for the neutrino to have α flavor. This same state, expressed above in the flavor basis, can be translated into the mass basis via the Pontecorvo–Maki–Nakagawa–Sakata (PMNS) matrix U_{PMNS}:

$$|\psi\rangle_{\text{f}} = U_{\text{PMNS}}|\psi\rangle_{\text{m}}, \tag{4.8}$$

where the subscript denotes the basis. (The wavefunction in Eq. (4.7) is really $|\psi\rangle_{\text{f}}$, but we will be dropping the subscripts as we proceed, leaving that job to the context.) The mixing matrix is traditionally parameterized as

$$U_{\text{PMNS}} = \begin{pmatrix} c_{12}c_{13} & s_{12}c_{13} & s_{13}e^{-i\delta} \\ -s_{12}c_{23} - c_{12}s_{23}s_{13}e^{i\delta} & c_{12}c_{23} - s_{12}s_{23}s_{13}e^{i\delta} & s_{23}c_{13} \\ s_{12}s_{23} - c_{12}c_{23}s_{13}e^{-i\delta} & -c_{12}s_{23} - s_{12}c_{23}s_{13}e^{i\delta} & c_{23}c_{13} \end{pmatrix}, \tag{4.9}$$

using the notation $c_{ij} \equiv \cos\theta_{ij}$ and $s_{ij} \equiv \sin\theta_{ij}$ in terms of the oscillation angles θ_{12}, θ_{23}, and θ_{13}. The parameter δ is the Dirac CP-violating phase. Measurements of the three mixing angles represent major triumphs of experimental particle physics over the past two decades; the Dirac phase, meanwhile, remains largely unconstrained but with several groups in hot pursuit, including those, for example, at NOνA [52], T2K [53], and DUNE [54]. Two additional phases are present if neutrinos are Majorana particles. As the Majorana phases have no effect on oscillations, we take them to vanish.

The mismatch between the flavor and mass eigenstates is one of the fundamental facts

about neutrinos. It gives rise to oscillations in vacuum and is essential to the rich phenomenology of in-medium flavor evolution that has been discovered since Wolfenstein's pioneering revelation [47] that neutrinos propagating in matter sustain refractive effects in much the same way that photons do. The derivation of neutrino oscillations and detection probabilities from $U_{\rm PMNS}$ can be found in the standard references [55].

Throughout this paper we confine our attention to the coherent limit of neutrino propagation, which is to say that collisions (scattering processes that alter the momentum of the neutrino) are negligible [56–59]. This approximation holds to varying degrees of accuracy in many settings of interest: It is applicable in vacuum, for one, as well as in astrophysical environments such as the Earth, the solar interior, the region far outside a core-collapse supernova or compact-object merger, and the early universe after weak decoupling, but it fails in the extremely dense interior of a supernova or merger remnant or at high enough temperatures in the early universe that neutrinos are thermally equilibrated with the plasma. The coherent and incoherent limits are tied together by a regime in which neither collisions nor the medium-enhanced flavor transformation that occurs between scattering events can be neglected, as is the case during the protracted transition of neutrinos in the early universe from being strongly coupled to the plasma to being fully free-streaming. This worst-of-both-worlds regime is also exemplified by the "neutrino halo" region of core-collapse supernovae [60], which is negligible during the late-time neutrino-driven-wind epoch but may be important during the neutronization burst or shock revival. Environments bridging the coherent and incoherent extremes are a frontier of research in neutrino astrophysics and lie beyond the ambitions of the present paper.

In the coherent limit, which we henceforth adopt, the neutrino flavor state obeys a Schrödinger-like equation

$$i\frac{d|\psi\rangle}{dt} = H|\psi\rangle, \tag{4.10}$$

with Hamiltonian

$$H = H_{\rm vac} + H_{\rm matt} + H_{\nu}, \tag{4.11}$$

where the three contributions to the Hamiltonian are respectively due to neutrino mass, forward scattering off of matter particles (nucleons, charged leptons), and forward scattering off of other neutrinos [61]. We briefly discuss each of these in turn.

The vacuum term $H_{\rm vac}$ is present in all environments and encodes the masses of the individual neutrino eigenstates. In the mass basis it is simply the matrix $(1/2E)\,\mathrm{diag}\left(m_1^2, m_2^2, m_3^2\right)$, where m_i is the mass of eigenstate ν_i and E is the neutrino energy. In the flavor basis it has the form

$$H_{\rm vac} = U_{\rm PMNS}\left(\frac{1}{2E}\mathrm{diag}\left(m_1^2, m_2^2, m_3^2\right)\right)U_{\rm PMNS}^{\dagger}. \tag{4.12}$$

It is evident that $H_{\rm vac}$ has non-zero off-diagonal elements in the flavor basis that cause mixing between the flavor states: This, of course, is the phenomenon of neutrino oscillations in vacuum.

When neutrinos are immersed in a dense bath of matter particles, as they are in many astrophysical settings, the dispersion relations of the individual flavors are modified by forward scattering off of the background. The most common scenario is one in which electrons (and possibly positrons) are abundant but muons and tauons are all but absent; a thermal environment requires quite a high temperature for the heavier charged leptons to be plentiful. Under these circumstances, all flavors feel a forward-scattering potential generated by the neutral-current weak interaction with $e^{\pm}$, but only ν_e feels the additional potential from the charged-current interaction. This effect is encoded in $H_{\rm matt}$. In this paper we are not concerned with the precise form of the matter Hamiltonian (for reasons that will become evident momentarily), so to illustrate its structure we write down the matrix in the scenario where the matter background consists entirely of e^- with number density n_e. In the flavor basis,

$$H_{\rm matt} = \sqrt{2}G_F n_e \mathrm{diag}\left(1,0,0\right), \tag{4.13}$$

where G_F is the Fermi constant. Since $H_{\rm matt}$ is diagonal in the flavor basis and $H_{\rm vac}$ is diagonal in the mass basis, the energy eigenstates in medium differ from both the mass and the flavor

eigenstates. Under the right conditions, the adiabatic decrease in n_e from very high down to vanishing density induces efficient conversion through the MSW mechanism.

The final constituent of the Hamiltonian stems from forward scattering with other neutrinos. The physics introduced by this term is rich, as it generalizes the effect of H_{matt} to a nonlinear, matrix-structured index of refraction. The matrix structure enters because the neutrino–neutrino forward-scattering amplitude depends not just on the density of the background neutrinos but on their quantum states. The potential generated by these processes is therefore proportional to a sum over the density matrices $\rho = |\psi\rangle\langle\psi|$ of each background neutrino. Explicitly,

$$\rho = \begin{pmatrix} \rho_{ee} & \rho_{e\mu} & \rho_{e\tau} \\ \rho^*_{e\mu} & \rho_{\mu\mu} & \rho_{\mu\tau} \\ \rho^*_{e\tau} & \rho^*_{\mu\tau} & \rho_{\tau\tau} \end{pmatrix} = \begin{pmatrix} |a_e|^2 & a_e^* a_\mu & a_e^* a_\tau \\ a_\mu^* a_e & |a_\mu|^2 & a_\mu^* a_\tau \\ a_\tau^* a_e & a_\tau^* a_\mu & |a_\tau|^2 \end{pmatrix}. \tag{4.14}$$

The diagonal element $\rho_{\alpha\alpha}$ is proportional to the number density of neutrinos of flavor α and the off-diagonal element $\rho_{\alpha\beta}$ ($\alpha \neq \beta$) measures the quantum coherence between flavors α and β. If neutrinos of momentum $\vec{q}$ have number density $n_{\nu,\vec{q}}$ and flavor state $\rho_{\vec{q}}$, then a neutrino of momentum $\vec{p}$ propagating through this background experiences

$$H_\nu = \sqrt{2} G_F \sum_{\vec{q}} (1 - \hat{p}\cdot\hat{q})\, n_{\nu,\vec{q}} \rho_{\vec{q}}, \tag{4.15}$$

where the sum is over all momentum states but could be expanded to include any additional indices used to label neutrinos in the system. (By writing $\rho = |\psi\rangle\langle\psi|$, we have assumed that each density matrix describes a pure state.) The geometric factor $(1 - \vec{p}\cdot\vec{q})$ originates from the structure of the weak-interaction current. For the sake of brevity, we will later use $\mu_{\vec{q}} \equiv \sqrt{2} G_F\, (1 - \hat{p}\cdot\hat{q})\, n_{\nu,\vec{q}}$. Note that this contribution is nonlinear in the sense that it couples together the different neutrino trajectories in flavor space. (Note also that we are ignoring antineutrinos in this discussion. We will continue to do so in the calculations that follow, as antineutrinos do not change the analysis

in any essential way.)

Throughout much of this paper we will perform calculations in the two-flavor approximation that is appropriate when ν_μ and ν_τ have the same interaction potentials, which holds whenever (1) muons and tauons are scarce and (2) ν_μ and ν_τ have identical spectra. Specifically, we consider mixing between ν_e and a state ν_x, the latter being a particular superposition of ν_μ and ν_τ. In this case $|\psi\rangle$, ρ, and the interaction potentials reduce in an obvious manner from the three-flavor expressions given above. There is now just a single mixing angle θ_v, with no CP-violating phase, and the 2×2 mixing matrix is simply the rotation

$$U = \begin{pmatrix} \cos\theta_v & \sin\theta_v \\ -\sin\theta_v & \cos\theta_v \end{pmatrix}. \tag{4.16}$$

It follows from Eq. (4.12) that the vacuum Hamiltonian is

$$H_{\rm vac} = \frac{\omega}{2} \begin{pmatrix} -\cos 2\theta_v & \sin 2\theta_v \\ \sin 2\theta_v & \cos 2\theta_v \end{pmatrix}, \tag{4.17}$$

with the vacuum oscillation frequency defined in terms of the mass-squared splitting $\delta m^2 \equiv m_2^2 - m_1^2$ by $\omega \equiv \delta m^2/2E$. The mass hierarchy, which remains experimentally ambiguous, is reflected in the sign of the oscillation frequency: $\omega > 0$ for the normal hierarchy (NH), $\omega < 0$ for the inverted hierarchy (IH).

With only two flavors, coherent neutrino evolution is tantamount to a two-level problem and can be mapped onto the Bloch sphere; in this regard it is analogous to the physics of electron spins, nuclear isospins, qubits, and so on. The Bloch vector $\vec{P}$ formed from the su(2)-algebra decomposition of the density matrix ρ is commonly known in the neutrino community as the

polarization vector, in deference to photon polarization:

$$\rho = \frac{1}{2}\left(\mathbb{I} + \vec{P}\cdot\vec{\sigma}\right). \tag{4.18}$$

Noting that Eq. (4.10) can be recast as a Liouville–von Neumann equation

$$i\frac{d\rho}{dt} = [H,\rho], \tag{4.19}$$

a similar decomposition of the Hamiltonian permits the coherent equations of motion to be written as a Bloch-like equation with infinite relaxation time:

$$\frac{d\vec{P}}{dt} = \vec{H}\times\vec{P}. \tag{4.20}$$

$\vec{P}$ can be visualized as a vector pointing from the origin to the surface of the S^2 manifold described at the end of the previous section. In this picture the parallel transport condition in Eq. (4.5) forbids $\vec{P}$ from spinning and thereby moving locally along the fiber, even as $\vec{P}$ precesses about $\vec{H}$. Given our emphasis on the two-flavor limit, it will be helpful to have this polarization-vector picture in mind. Indeed, it is precisely the geometric nature of Eq. (4.20) that underlies the geometric phases exhibited below.

Absent the self-coupling potential H_ν, the Hamiltonian can be rewritten in terms of effective in-medium mixing parameters:

$$H_{\rm vac} + H_{\rm matt} = \frac{\omega_{\rm m}}{2}\begin{pmatrix} -\cos 2\theta_{\rm m} & \sin 2\theta_{\rm m} \\ \sin 2\theta_{\rm m} & \cos 2\theta_{\rm m} \end{pmatrix}, \tag{4.21}$$

with in-medium oscillation frequency (using the analogous form of Eq. (4.13) for two flavors)

$$\omega_{\rm m} \equiv \sqrt{\omega \sin^2 2\theta_{\rm v} + \left(\omega \cos 2\theta_{\rm v} - \frac{\sqrt{2}}{2} G_F n_e\right)^2} \tag{4.22}$$

and in-medium mixing angle given by

$$\sin^2 2\theta_{\rm m} \equiv \frac{\omega^2 \sin^2 2\theta_{\rm v}}{\omega_{\rm m}^2}. \tag{4.23}$$

The upshot is that flavor evolution in a matter background looks like vacuum oscillations with modified frequency and amplitude. For this reason, in the rest of the paper we will ignore $H_{\rm matt}$; it is assumed to have been absorbed into the vacuum mixing parameters.

With H_ν present, the nonlinear communication between flavor states considerably expands the range of flavor-evolution phenomena. These behaviors are grouped under the heading of *collective neutrino oscillations* and have been the subject of intense study in recent years [62–125]. One paradigmatic collective effect is the synchronization of flavor: When H_ν dominates the Hamiltonian, all neutrinos experience roughly the same potential, leading them to undergo nearly identical oscillations at a common effective frequency. Synchronized oscillations are perhaps the cleanest example of cyclic evolution of the Hamiltonian at strong nonlinear coupling, but they are not alone.

Geometrically the crucial feature of neutrino self-coupling is that even in two flavors a complex off-diagonal potential can develop, opening the possibility for cyclic evolution of the Hamiltonian. With the standard matrix representation of the Pauli matrices, the y-component of $\vec{H}$ corresponds to the imaginary parts of these off-diagonal elements. Since H can always be written as a real symmetric matrix in the standard MSW (vacuum+matter) scenario, in a matter background $\vec{H}$ never leaves the xz-plane and closed loops on the Bloch sphere, other than the trivial one formed by following the xz great circle, are precluded. This conclusion no longer holds

in a *neutrino* background. The coherent coupling of neutrino flavor states can thus be framed as a geometric statement.

4.5 Mixed potentials with two flavors

In this and the next two sections we analyze geometric effects that arise in a scenario with two-flavor neutrinos interacting with each other by way of coherent forward scattering. For simplicity we neglect any contributions from a matter background, which as noted previously can be absorbed into the vacuum potential by working in terms of effective in-medium mixing parameters. By dialing the strengths of the vacuum and self-coupling potentials, one finds that the system gives rise to a panoply of flavor-transformation phenomena. We take three different limits of the coupling strengths that illuminate in particular how the flavor transformation enmeshes with geometry.

The equations of motion for two pure populations of neutrinos interacting with one another are

$$\begin{aligned} i\frac{d|\psi_1(t)\rangle}{dt} &= [\omega_1 B + \mu_2 \rho_2(t)]\,|\psi_1(t)\rangle, \\ i\frac{d|\psi_2(t)\rangle}{dt} &= [\omega_2 B + \mu_1 \rho_1(t)]\,|\psi_2(t)\rangle, \end{aligned} \tag{4.24}$$

where mode i has wavefunction $|\psi_i(t)\rangle$, vacuum oscillation frequency ω_i, and density parameter μ_i (defined below Eq. (4.15)). The matrix B is equal to $H_{\rm vac}$ with the energy-dependent part taken out. In the mass basis it is $B = \mathrm{diag}\,(-1/2, 1/2)$ and has vector form $\vec{B} = -(1/2)\,\hat{z}$.

In this section we consider the limit in which the neutrinos of mode 2 are extremely dilute

but those of mode 1 are extremely dense:

$$\begin{aligned} i\frac{d|\psi_1(t)\rangle}{dt} &= \omega_1 B|\psi_1(t)\rangle, \\ i\frac{d|\psi_2(t)\rangle}{dt} &= \mu_1\rho_1(t)|\psi_2(t)\rangle. \end{aligned} \tag{4.25}$$

As a shorthand, we term this arrangement *mixed potentials*.

The first equation of motion describes vacuum oscillations and is easily solved:

$$|\psi_1(t)\rangle = \exp(-i\omega_1 Bt)\,|\psi_1(0)\rangle. \tag{4.26}$$

In the mass basis the matrix exponential is diagonal and, taking as an initial state

$$|\psi_1(0)\rangle = \begin{pmatrix} \cos\frac{\theta_1}{2} \\ e^{i\phi_1}\sin\frac{\theta_1}{2} \end{pmatrix}, \tag{4.27}$$

one finds that $|\psi_1\rangle$ corresponds to a polarization vector $\vec{P}_1$ precessing about the z-axis with fixed frequency ω_1 and at fixed polar angle θ_1:

$$|\psi_1(t)\rangle = \begin{pmatrix} \cos\frac{\theta_1}{2} \\ e^{i(\phi_1-\omega_1 t)}\sin\frac{\theta_1}{2} \end{pmatrix}. \tag{4.28}$$

In the case of the IH, $\omega_1 < 0$ and the direction of precession is reversed. The other mode $|\psi_2\rangle$—a flavor state evolving under a Hamiltonian that sweeps out a circle in flavor space—is mathematically identical to a spin in a magnetic field that sweeps out a circle in *physical* space. Although we are indicating with the notation that $|\psi_1\rangle$ represents a pure state of neutrinos at a chosen energy, it may be that $|\psi_2\rangle$ interacts with an ensemble—pure or mixed—with some spectrum. If the ensemble undergoes synchronized oscillations, then the computation proceeds almost unchanged.

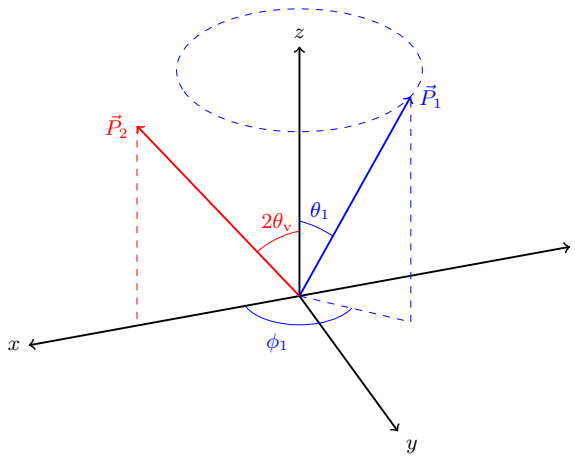

Figure 4.2: Initial ($t = 0$) configuration of polarization vectors in the mixed-potentials scenario. $\vec{P}_1$ undergoes vacuum oscillations (clockwise about $\hat{z} = -\hat{B}$ for the NH, counterclockwise for the IH). Its trajectory is shown by the dashed circle. $\vec{P}_2$ is in an electron-flavor eigenstate and points along $\hat{L}$.

In Sec. 4.5.1 we adopt an adiabatic treatment, thereby reproducing the neutrino version of the classic result for the geometric phase of a spin in a cyclic magnetic field, and we point out that in principle this phase is observable. In Sec. 4.5.2 we find the exact (non-adiabatic) solution and demonstrate the geometric-dynamical phases that appear as perturbative corrections to the traditional purely geometric phase.

4.5.1 Adiabatic treatment

We now set out to determine, under the assumption of adiabatic evolution, the phase acquired by $|\psi_2\rangle$ after $\vec{H}_2(t) = \mu_1 \vec{P}_1(t)$ undergoes one period of cyclic evolution. Based on the foregoing discussion, we know that $\vec{H}_2$ rotates with frequency ω_1 about the mass-eigenstate axis $\hat{B} = -\hat{z}$ ($\Phi_1(t) = \phi_1 - \omega_1 t$), maintaining a constant magnitude $|\vec{H}_2(t)| = \mu_1$ and a constant polar angle $\Theta_1(t) = \theta_1$. The coordinate system is chosen such that the flavor-eigenstate axis $\hat{L}$, which is defined to point along the polarization vector associated with ν_e, is in the xz-plane. This set-up is depicted in Fig. 4.2.

If the test neutrino is initially electron flavor, that is,

$$|\psi_2(0)\rangle = |\nu_e\rangle\,, \tag{4.29}$$

then $\vec{P}_2$ has initial azimuthal angle $\Phi_2(0) = 0$ and initial polar angle $\Theta_2(0) = 2\theta_{\rm v}$, where $\theta_{\rm v}$ is the mixing angle in vacuum. We stress that this problem has four physically relevant vectors. Making the reasonable stipulation that $|\psi_1\rangle$ also decouples into a flavor eigenstate, then at any given time the vectors $\hat{L}$, $\hat{B}$, $\hat{P}_1$, and $\hat{P}_2$ are generally not coincident. One can see quite readily that should any two of these unit vectors be identical at all times, then geometric phases in $|\psi_2\rangle$ are either absent or unobservable:

- If $\hat{B} = \hat{L}$, then oscillations do not occur.
- If $\hat{P}_1(t) = \hat{B}$, then the path of $\vec{H}_2$ does not enclose a finite area in parameter space.
- If $\hat{P}_2(t) = \hat{P}_1(t)$, then in the adiabatic limit $|\psi_2\rangle$ is in an energy eigenstate at all times and its phase will not show up at the probability level.
- If $\hat{P}_1(t) = \hat{L}$, $\hat{P}_2(t) = \hat{L}$, or $\hat{P}_2(t) = \hat{B}$, then $\hat{L}$ must be equal to $\hat{B}$.

It follows immediately that if decoupling occurs into flavor eigenstates, it is a prerequisite for the appearance of an observable adiabatic geometric phase that two parameters be nonzero: the initial relative phase ϕ_1 between the two modes and the vacuum mixing angle $\theta_{\rm v}$. With these considerations in mind, we now proceed to derive the geometric phase.

In the chosen coordinate system the Hamiltonian matrix is

$$H_2 = \frac{\mu_1}{2}\begin{pmatrix} \cos\theta_1 & e^{-i(\phi_1-\omega_1 t)}\sin\theta_1 \\ e^{i(\phi_1-\omega_1 t)}\sin\theta_1 & -\cos\theta_1 \end{pmatrix}, \tag{4.30}$$

which is represented by the vector

$$\vec{H}_2 = \frac{\mu_1}{2}\begin{pmatrix} \sin\theta_1 \cos(\phi_1 - \omega_1 t) \\ \sin\theta_1 \sin(\phi_1 - \omega_1 t) \\ \cos\theta_1 \end{pmatrix}. \tag{4.31}$$

The energy eigenstates of this Hamiltonian correspond to the normalized polarization vectors parallel and antiparallel with $\vec{H}_2$. As kets they are

$$\begin{aligned} |\nu_+(t)\rangle &= \begin{pmatrix} \cos\frac{\theta_1}{2} \\ e^{i(\phi_1-\omega_1 t)}\sin\frac{\theta_1}{2} \end{pmatrix}, \\ |\nu_-(t)\rangle &= \begin{pmatrix} -\sin\frac{\theta_1}{2} \\ e^{i(\phi_1-\omega_1 t)}\cos\frac{\theta_1}{2} \end{pmatrix}, \end{aligned} \tag{4.32}$$

and they have energy eigenvalues $E_\pm = \pm\mu_1/2$.

The geometric phase, defined in Eq. (4.2), can be recast in the form

$$\gamma = \oint_C \vec{A}\cdot d\vec{R}, \quad \vec{A} = i\langle\eta(t)|\nabla|\eta(t)\rangle \tag{4.33}$$

for eigenstate $|\eta(t)\rangle$. The vector $\vec{A}$ is the gauge potential associated with the adiabatic connection. In this case the gauge potentials are given by

$$\begin{aligned} \vec{A}_+ &= i\langle\nu_+|\nabla|\nu_+\rangle = -\frac{\sin^2\frac{\Theta_1}{2}}{\sin\Theta_1}\hat{\Phi}, \\ \vec{A}_- &= i\langle\nu_-|\nabla|\nu_-\rangle = -\frac{\cos^2\frac{\Theta_1}{2}}{\sin\Theta_1}\hat{\Phi}. \end{aligned} \tag{4.34}$$

Integration along the curve swept out by $\vec{H}_2$ then yields the geometric phases acquired by these

energy eigenstates:

$$\begin{aligned}\gamma_+ &= \oint_C \vec{A}_+ \cdot d\vec{R} = \pm\pi(1-\cos\theta_1)\,,\\ \gamma_- &= \oint_C \vec{A}_- \cdot d\vec{R} = \pm\pi(1+\cos\theta_1)\,,\end{aligned} \tag{4.35}$$

where the upper (lower) signs are for the NH (IH). Evidently the geometric phase is sensitive to the mass hierarchy, with the proper sign being fixed by the direction of traversal about the loop. The dynamical phase, meanwhile, is

$$\delta_\pm = -\int_0^T E_\pm dt = \mp\frac{\mu_1}{2}T, \tag{4.36}$$

so that the energy eigenstates after one period T are

$$\begin{aligned}|\nu_+(T)\rangle &= e^{\pm i\pi(1-\cos\theta_1)}e^{-i\frac{\mu_1}{2}T}\,|\nu_+(0)\rangle\,,\\ |\nu_-(T)\rangle &= e^{\pm i\pi(1+\cos\theta_1)}e^{+i\frac{\mu_1}{2}T}\,|\nu_-(0)\rangle\,,\end{aligned} \tag{4.37}$$

where again the upper (lower) signs are for the NH (IH).

The calculation thus far is identical to the standard one for a spin-$1/2$ particle in a rotating magnetic field, and as usual the geometric phase is half the solid angle enclosed in parameter space by the loop traced out by the Hamiltonian vector. But a key point for neutrinos is that their production and detection project onto the flavor axis. It is therefore necessary to convert between the interaction and energy bases. The unitary matrix $\mathcal{U}$ effecting the transformation

$$\begin{pmatrix} |\nu_-\rangle \\ |\nu_+\rangle \end{pmatrix} = \mathcal{U}\begin{pmatrix} |\nu_e\rangle \\ |\nu_x\rangle \end{pmatrix} \tag{4.38}$$

is given by

$$\mathcal{U} = \begin{pmatrix} \mathcal{U}_{11} & \mathcal{U}_{12} \\ \mathcal{U}_{21} & \mathcal{U}_{22} \end{pmatrix} = \begin{pmatrix} e^{i\Phi_1}\sin\theta_v\cos\frac{\theta_1}{2} - \cos\theta_v\sin\frac{\theta_1}{2} & e^{i\Phi_1}\cos\theta_v\cos\frac{\theta_1}{2} + \sin\theta_v\sin\frac{\theta_1}{2} \\ e^{i\Phi_1}\sin\theta_v\sin\frac{\theta_1}{2} + \cos\theta_v\cos\frac{\theta_1}{2} & e^{i\Phi_1}\cos\theta_v\sin\frac{\theta_1}{2} - \sin\theta_v\cos\frac{\theta_1}{2} \end{pmatrix}. \tag{4.39}$$

Note that $\mathcal{U}$ is time-dependent, since $\Phi_1(t) = \phi_1 - \omega_1 t$.

Using the unitarity of $\mathcal{U}$, one can write the initial state—assumed to be ν_e—as

$$|\psi_2(0)\rangle = \mathcal{U}_{11}^* |\nu_-(0)\rangle + \mathcal{U}_{21}^* |\nu_+(0)\rangle . \tag{4.40}$$

After one period has elapsed, the state has evolved to

$$\begin{aligned} |\psi_2(T)\rangle = {} & \mathcal{U}_{11}^* e^{-i\pi(1+\cos\theta_1)} e^{i\frac{\mu_1}{2}T} |\nu_-(0)\rangle \\ & + \mathcal{U}_{21}^* e^{-i\pi(1-\cos\theta_1)} e^{-i\frac{\mu_1}{2}T} |\nu_+(0)\rangle . \end{aligned} \tag{4.41}$$

Projecting $|\psi_2(T)\rangle$ onto the flavor state in which it was produced at $t = 0$ yields

$$|\langle\nu_e|\psi_2(T)\rangle|^2 = 1 - 4\,|\mathcal{U}_{11}|^2\,|\mathcal{U}_{21}|^2 \sin^2\left(\pi\cos\theta_1 - \frac{\mu_1}{2}T\right). \tag{4.42}$$

Letting $x \equiv \cos 2\theta_v \cos\theta_1 + \cos\phi_1 \sin 2\theta_v \sin\theta_1$, we have

$$|\mathcal{U}_{11}|^2 = \frac{1}{2}(1-x), \quad |\mathcal{U}_{21}|^2 = \frac{1}{2}(1+x), \tag{4.43}$$

allowing us to write

$$|\langle\nu_e|\psi_2(T)\rangle|^2 = 1 - \left(1-x^2\right)\sin^2\left(\pi\cos\theta_1 - \frac{\mu_1}{2}T\right). \tag{4.44}$$

Recalling that $\gamma_\pm = -\pi \pm \pi\cos\theta_1$, one has, finally,

$$|\langle \nu_e|\psi_2(T)\rangle|^2 = 1 - \left(1-x^2\right)\sin^2\left(\gamma_\pm + \delta_\pm\right), \tag{4.45}$$

where the choice of $\pm$ is arbitrary. We would have arrived at the same expression if we had instead chosen the neutrino to be initially ν_x.

Moreover, Eq. (4.45) is independent of the choice of hierarchy. But since the overall sign of γ changes upon flipping the hierarchy—whereas the sign of δ goes unchanged—the transition probability turns out to be hierarchy-dependent. This finding has a simple explanation in the polarization-vector picture: The precession direction of $\vec{P}_1$ about $\hat{B}$ is set by the hierarchy, while the precession direction of $\vec{P}_2$ about $\hat{P}_1$ is not.

It may be helpful to note that $|\langle \nu_\pm(0)|\nu_\pm(T)\rangle| = 1$, since the geometric and dynamical phases vanish under the modulus. In other words, the fact that the neutrino is produced and detected in a state other than one of the energy eigenstates is necessary for the phases to appear at the probability level. In fact, if one knows the flavor of the neutrino at $t = 0$, then by measuring the flavor of the neutrino at $t = T$, one is effectively performing an interferometry experiment capable in principle of probing the geometric phase. In this case, that phase is a measure of the flavor-space path traced out by the *other* neutrino, which need not be directly observed.

4.5.2 Exact solution

The formulae applied in the previous section are appropriate to the adiabatic limit, in which the energy eigenvectors track the Hamiltonian vector as it sweeps out a circuit. But it turns out that an exact solution can be found even without this assumption. Let

$$|\psi_2(t)\rangle = a(t)|\nu_+(t)\rangle + b(t)|\nu_-(t)\rangle \tag{4.46}$$

and suppose that $|\psi_2(0)\rangle = |\nu_+(t)\rangle$, so that $a(0) = 1$ and $b(0) = 0$. This initial condition is equivalent to the one in the previous subsection, but here we are not demanding that $|\psi_2\rangle$ remain in the eigenstate $|\nu_+\rangle$.

The Schrödinger equation says that the coefficients of $|\psi_2(t)\rangle$ obey the system of equations

$$\begin{aligned}
\frac{da(t)}{dt} + a(t)\left\langle \nu_+(t)\left|\frac{d}{dt}\right|\nu_+(t)\right\rangle + b(t)\left\langle \nu_+(t)\left|\frac{d}{dt}\right|\nu_-(t)\right\rangle \\
= -i\frac{\mu_1}{2}a(t), \\
\frac{db(t)}{dt} + a(t)\left\langle \nu_-(t)\left|\frac{d}{dt}\right|\nu_+(t)\right\rangle + b(t)\left\langle \nu_-(t)\left|\frac{d}{dt}\right|\nu_-(t)\right\rangle \\
= i\frac{\mu_1}{2}b(t).
\end{aligned} \tag{4.47}$$

Enforcing $b(t) = 0$ amounts to the adiabatic approximation; it can be seen that the deviation from this limit is associated with the "cross terms" that mix the eigenstates. The coupled first-order differential equations can be rewritten as decoupled second-order differential equations. The equation for $a(t)$ is

$$\frac{d^2a}{dt^2} - i\omega_1\frac{da}{dt} + \left[\left(\frac{\mu_1}{2}\right)^2 + \frac{\mu_1}{2}\omega_1\cos\theta_1\right]a = 0. \tag{4.48}$$

This is the equation of a (complex) damped harmonic oscillator with real frequency-squared and imaginary friction and can be solved with the usual ansatz $a(t) \sim \exp\alpha t$. The resulting algebraic equation for α has solutions

$$\alpha_\pm = \frac{i\omega_1}{2} \pm \frac{i\mu_1}{2}\sqrt{1 + 2\frac{\omega_1}{\mu_1}\cos\theta_1 + \left(\frac{\omega_1}{\mu_1}\right)^2}. \tag{4.49}$$

The general solution, of course, can be written as

$$a(t) = c_+e^{\alpha_+ t} + c_-e^{\alpha_- t}, \tag{4.50}$$

and the initial condition $|\nu(0)\rangle = |\nu_+(0)\rangle$ implies that

$$c_+ = \frac{1}{2} - \frac{1}{2\Delta}\left[1 + \frac{\omega_1}{\mu_1}\cos\theta_1\right],$$
$$c_- = \frac{1}{2} + \frac{1}{2\Delta}\left[1 + \frac{\omega_1}{\mu_1}\cos\theta_1\right], \tag{4.51}$$

where Δ is the square root of the discriminant,

$$\Delta \equiv \sqrt{1 + 2\frac{\omega_1}{\mu_1}\cos\theta_1 + \left(\frac{\omega_1}{\mu_1}\right)^2}. \tag{4.52}$$

Observe that $\alpha_\pm$ are purely imaginary regardless of the values of ω_1, μ_1, and θ_1.

An important quantity found throughout the neutrino literature is the adiabaticity parameter Υ (usually denoted γ, but our hands are tied), upon which the transition probability P through a resonance depends exponentially: $P \approx e^{-\pi\Upsilon/2}$ [126]. The parameter can be cast into the form [123]

$$\Upsilon \approx \frac{|H_T|^2}{\left|\dot{H}_z\right|}, \tag{4.53}$$

where $H_T = H_x^2 + H_y^2$ is the transverse part of the Hamiltonian vector and the right-hand side is evaluated at resonance. In circumstances where a flavor-state level crossing occurs, such as in the MSW mechanism, this definition implies that transitions are unlikely to occur if the separation between the energy eigenstates at closest approach is large relative to the speed with which the resonance is traversed. Although the system we are analyzing has no such level crossing, Υ nonetheless coheres with what we mean by adiabaticity. Applying the definition above, one has

$$\Upsilon \approx \frac{\mu_1 |P_{1,T}|^2}{\left|\omega_1 \left(\vec{B} \times \vec{P}_1\right)_z\right|}. \tag{4.54}$$

Dropping factors of order unity, this becomes simply $\Upsilon \approx \mu_1/\omega_1$, so that the adiabatic limit corresponds to $\omega_1/\mu_1 \longrightarrow 0$. Thus the neutrino adiabaticity parameter, even in this non-resonant

scenario, is consistent with the more general intuition that adiabaticity prevails when the change in the Hamiltonian is slow compared to the response of the particle.

To zeroth order in ω_1/μ_1 one has, for $T = 2\pi/\omega_1$,

$$\alpha_\pm T \longrightarrow \pm i\frac{\mu_1}{2}T + i\pi(1 \mp \cos\theta_1). \tag{4.55}$$

The dynamical and geometric phases from the previous section are therefore recovered as the leading-order terms in the perturbation expansion in the adiabaticity parameter.

The probability of $|\psi_2(t)\rangle$ being in the upper eigenstate at any time t is

$$|a(t)|^2 = 1 - 2c_+c_-(1 - \cos\mu_1\Delta t). \tag{4.56}$$

It is interesting to coerce $a(t)$ into the form $r(t)\exp i\phi(t)$. The modulus is simply $r(t) = |a(t)|$ and the phase is

$$\phi(t) = \arctan\left[\frac{c_+\sin\left(\frac{\omega_1 t}{2} + \frac{\mu_1\Delta t}{2}\right) + c_-\sin\left(\frac{\omega_1 t}{2} - \frac{\mu_1\Delta t}{2}\right)}{c_+\cos\left(\frac{\omega_1 t}{2} + \frac{\mu_1\Delta t}{2}\right) + c_-\cos\left(\frac{\omega_1 t}{2} - \frac{\mu_1\Delta t}{2}\right)}\right]. \tag{4.57}$$

Specifying $t = T$ leads to

$$\begin{aligned} r(T) &= \sqrt{1 - 2c_+c_-(1 - \cos\mu_1\Delta T)} \\ \phi(T) &= \arctan\left[(1 - 2c_-)\tan\frac{\mu_1\Delta T}{2}\right], \end{aligned} \tag{4.58}$$

Expanding each to first order in ω_1/μ_1 yields

$$r(T) \approx 1 - \frac{\omega_1}{2\mu_1}\sin^2\theta_1 \sin^2\left(\frac{\mu_1}{2}T + \pi\cos\theta_1\right),$$
$$\phi(T) \approx -\frac{\mu_1}{2}T - \pi\cos\theta_1 - \frac{\omega_1}{\mu_1}\frac{\pi\sin^2\theta_1}{2}. \tag{4.59}$$

These can be combined to give an expression for $a(T)$, with the adiabatic-limit geometric and dynamical phases substituted appropriately:

$$a(T) \approx -\left[1 + \frac{\pi}{2\delta_+}\sin^2\theta_1\sin^2(\delta_+ + \gamma_+)\right] \times \exp\left\{i\left[\delta_+ + \gamma_+ + \frac{\pi^2\sin^2\theta_1}{2\delta_+}\right]\right\}. \tag{4.60}$$

As expected, in the zeroth-order expansion one obtains

$$a(T) = -\exp\left[i(\delta_+ + \gamma_+)\right]. \tag{4.61}$$

This is identical to our result from the previous subsection, up to an unobservable minus sign. Note also that the corrections to the fully adiabatic result intertwine geometry and dynamics. It is only at lowest order that the two can be neatly separated.

4.6 Pure self-coupling with two flavors

We have seen that if the Hamiltonian for a neutrino sweeps out a circle, then the neutrino acquires a geometric phase after one period that is proportional to the solid angle of this circle on the Bloch sphere. It is well-known from geometric-phase lore that in fact the path could be any closed circuit and in all cases the phase acquired is determined by the enclosed solid angle.

In the neutrino context with strong nonlinear coupling between modes, the possibility

arises that the geometric phase is not *set* by the path but rather that the phase and the path mutually determine one another. The simplest case, which we shall examine in this section, is that of two modes interacting with one another and experiencing negligible vacuum potential. We can picture this scenario as two vectors rotating about each other in some complicated way. If it can be shown that the Hamiltonian generated by one vector $\vec{P}_1$ is cyclic (*i.e.*, if that vector is itself cyclic) and if the other vector $\vec{P}_2$ does not adiabatically track an energy eigenstate, then it is to be expected that geometric phases will appear at the probability level in the second mode, which is to say that the position of $\vec{P}_2$ depends on the geometric phases generated by $\vec{P}_1$. Thus far all of this applies equally to the mixed-potentials scenario, as we just saw. But with two neutrino populations interacting solely through self-coupling, these considerations are mutual, implying that the paths and geometric phases of the vectors are inextricably bound. The scenario of the previous section was analogous to a spin in a rotating magnetic field; the scenario here is more akin to two spins interacting through their magnetic moments.

With these thoughts in mind, we return to the general equations of motion in Eq. (4.24) and set $\omega_1 = \omega_2 = 0$, leaving the self-coupling potentials nonzero. To be explicit, we have

$$\begin{aligned} i\frac{d|\psi_1\rangle}{dt} &= \mu_2\rho_2|\psi_1\rangle, \\ i\frac{d|\psi_2\rangle}{dt} &= \mu_1\rho_1|\psi_2\rangle. \end{aligned} \tag{4.62}$$

Formally the solutions are

$$\begin{aligned} |\psi_1(t)\rangle &= \mathcal{P}\exp\left(-i\mu_2\int_0^t dt'\rho_2(t')\right)|\psi_1(0)\rangle, \\ |\psi_2(t)\rangle &= \mathcal{P}\exp\left(-i\mu_1\int_0^t dt'\rho_1(t')\right)|\psi_2(0)\rangle, \end{aligned} \tag{4.63}$$

where $\mathcal{P}$ denotes the path-ordering operator, but clearly these expressions are of little help since the equations have not been decoupled.

In fact the equations can be decoupled, allowing for exact solutions to be obtained. First note the important fact that

$$i\frac{d}{dt}\langle\psi_2|\psi_1\rangle = (\mu_2-\mu_1)\,\langle\psi_2|\psi_1\rangle, \tag{4.64}$$

hence the solution at time t is given by

$$\langle\psi_2(t)|\psi_1(t)\rangle = \exp\left[-i\,(\mu_2-\mu_1)\,t\right]\langle\psi_2(0)|\psi_1(0)\rangle \tag{4.65}$$

and $|\langle\psi_2(t)|\psi_1(t)\rangle|^2$ is constant. The geometric meaning of these statements is more transparent when Eq. (4.62) is rephrased in terms of polarization vectors:

$$\begin{aligned}\frac{d\vec{P}_1}{dt} &= \mu_2\vec{P}_2\times\vec{P}_1,\\ \frac{d\vec{P}_2}{dt} &= \mu_1\vec{P}_1\times\vec{P}_2.\end{aligned} \tag{4.66}$$

The magnitudes of the polarization vectors are conserved as usual, as is $\vec{P}_1\cdot\vec{P}_2$, and the conservation of $|\langle\psi_2(t)|\psi_1(t)\rangle|^2$ corresponds to the preservation of the angle between $\vec{P}_1$ and $\vec{P}_2$ even as the vectors drift through flavor space. From a certain viewpoint, these are consequence of the conservation of $\vec{D}\equiv\mu_1\vec{P}_1+\mu_2\vec{P}_2$, which acts as a kind of "center of flavor" in analogy to the center of mass of a mechanical system.

The first equation of motion in Eq. (4.62) can be rearranged to read

$$|\psi_2\rangle = \frac{1}{\mu_2\langle\psi_2|\psi_1\rangle}i\frac{d|\psi_1\rangle}{dt}. \tag{4.67}$$

Differentiating this—while keeping in mind Eq. (4.65)—and using the second equation of motion yields

$$\frac{d^2|\psi_1\rangle}{dt^2} + i\,(\mu_2-\mu_1)\,\frac{d|\psi_1\rangle}{dt} + \mu_1\mu_2|\langle\psi_2|\psi_1\rangle|^2|\psi_1\rangle = 0. \tag{4.68}$$

$|\psi_1\rangle$ obeys the complex conjugate of this equation. As with the decoupled equations of motions in the mixed-potentials limit, the friction coefficient is imaginary and the frequency-squared is real.

Both flavor amplitudes must individually satisfy Eq. (4.68), which has solutions that are superpositions of $e^{\lambda_+ t}$ and $e^{\lambda_- t}$ with

$$\lambda_\pm = i\frac{\mu_1-\mu_2}{2}\left[1 \pm \sqrt{1+4\frac{\mu_1\mu_2}{(\mu_1-\mu_2)^2}|\langle\psi_2(0)|\psi_1(0)\rangle|^2}\right]. \tag{4.69}$$

Note that the signs of the eigenvalues depend on whether μ_1 or μ_2 is larger. In both cases we are letting λ_+ denote the eigenvalue of greater magnitude. Thus

$$\begin{aligned}\psi_1(t) &= \begin{pmatrix} a_+e^{\lambda_+ t} + a_-e^{\lambda_- t} \\ b_+e^{\lambda_+ t} + b_-e^{\lambda_- t} \end{pmatrix}, \\ \psi_2(t) &= \begin{pmatrix} c_+e^{-\lambda_+ t} + c_-e^{-\lambda_- t} \\ d_+e^{-\lambda_+ t} + d_-e^{-\lambda_- t} \end{pmatrix}. \end{aligned} \tag{4.70}$$

With pure self-coupling, the mass axis is irrelevant and we are free to choose more convenient coordinates than those used in the previous section. We let $\vec{P}_1(0)$ point along the z-axis, and we let $\vec{P}_2(0)$ be at an angle θ (Fig. 4.3). Then $|\langle\psi_1(t)|\psi_2(t)\rangle|^2 = \cos^2\frac{\theta}{2}$ and the coefficients in Eq. (4.70) are fixed by the parameters of the system.

We now pose this question: If H_1 undergoes cyclic evolution, does $|\psi_2\rangle$ acquire a geometric phase? Given the structure of the solutions in Eq. (4.70) it is clear that H_1 and H_2 both cycle after a shared period T. The same question can then be asked of $|\psi_1\rangle$ with respect to cyclic evolution of H_2, and the geometric phases that emerge in this scenario must in some sense be coupled to one another. Based on the solutions found above, $|\psi_1\rangle$ and $|\psi_2\rangle$ each complete a cycle

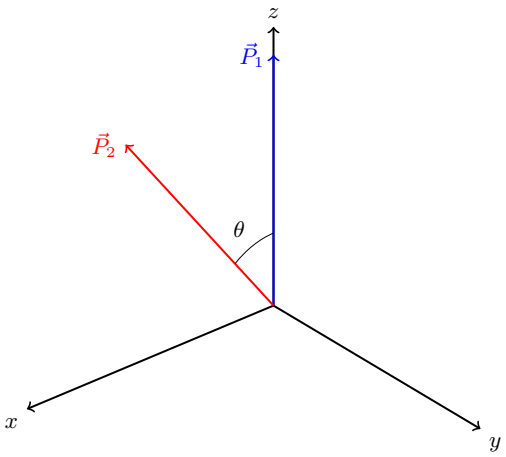

Figure 4.3: Initial ($t = 0$) configuration of polarization vectors in the pure-self-coupling scenario. For convenience the coordinate system is chosen such that $\vec{P}_1$ lies along the z-axis.

after a time

$$T = \frac{2\pi}{|\mu_1 - \mu_2| \sqrt{1 + 4\frac{\mu_1\mu_2}{(\mu_1-\mu_2)^2}\cos^2\frac{\theta}{2}}}, \tag{4.71}$$

at which point the wavefunctions have acquired the phases $e^{i\alpha_1}$ and $e^{i\alpha_2}$, respectively, with $\alpha_2 = -\alpha_1$ and

$$\alpha_1 = \mathrm{sgn}(\mu_1 - \mu_2)\left[\frac{\pi}{\sqrt{1 + 4\frac{\mu_1\mu_2}{(\mu_1-\mu_2)^2}\cos^2\frac{\theta}{2}}} + \pi\right]. \tag{4.72}$$

These are the exact phases acquired by the states after a time T. Their geometric structure is manifest, and they are clearly coupled, as one is the negative of the other regardless of the choice of system parameters. The result is also notable in that the dynamical phase makes no appearance: Since there are neither external parameters tuning the system nor even internal parameters associated with vacuum oscillations, the only timescale available is the intrinsic dynamical one set by the neutrino densities and the initial flavor states.

If $\mu_1 = \mu_2$, then no observable phase results at all. With the neutrino densities equal, the first-derivative term in Eq. (4.68) drops out and the eigenvalues are related by a sign change. The result is that only trivial overall phases can develop over the course of a cycle. It is also straightforward to show that in the extreme limit $\mu_1 \gg \mu_2$, the geometric phase acquired by $|\psi_1\rangle$

reduces to

$$\alpha_1 \longrightarrow -2\pi\frac{\mu_2}{\mu_1}\cos^2\frac{\theta}{2}, \tag{4.73}$$

and still $\alpha_2 = -\alpha_1$. Using Eq. (4.53), an analysis like the one in the previous section shows that the $|\psi_2\rangle$ adiabaticity parameter is $\Upsilon \sim \mu_1/\mu_2$. This limit therefore describes adiabatic evolution of the relatively dilute population of neutrinos.

The same result can be obtained through the usual adiabatic treatment, where the eigensystem is solved for and the gauge potentials are calculated. To demonstrate this, we now assume adiabaticity and compute the eigenvectors of $H_2 = \mu_1\rho_1$. The first eigenvector is simply $|\nu_\mu(t)\rangle = |\psi_1(t)\rangle$, with eigenvalue $\lambda_\mu = \mu_1$. The second eigenvector $|\nu_0(t)\rangle$ has eigenvalue $\lambda_0 = 0$ and satisfies $\langle\nu_0(t)|\psi_1(t)\rangle = 0$. These can be written out as

$$\begin{aligned}
|\nu_\mu\rangle &= \begin{pmatrix} a_+e^{\lambda_+ t} + a_-e^{\lambda_- t} \\ b_+e^{\lambda_+ t} + b_-e^{\lambda_- t} \end{pmatrix}, \\
|\nu_0\rangle &= \begin{pmatrix} -b_+^*e^{\lambda_+^* t} - b_-^*e^{\lambda_-^* t} \\ a_+^*e^{\lambda_+^* t} + a_-^*e^{\lambda_-^* t} \end{pmatrix},
\end{aligned} \tag{4.74}$$

from which the gauge potentials—now written as scalars in order to facilitate the computation—may be evaluated:

$$A_\mu = i\left\langle \nu_\mu \middle| \frac{d}{dt} \middle| \nu_\mu \right\rangle = \mu_2\cos^2\frac{\theta}{2} \tag{4.75}$$

$$A_0 = i\left\langle \nu_0 \middle| \frac{d}{dt} \middle| \nu_0 \right\rangle = -\mu_2\cos^2\frac{\theta}{2}, \tag{4.76}$$

The computation of the first of these is significantly aided by using $i\langle\nu_\mu|\frac{d}{dt}|\nu_\mu\rangle = \langle\psi_1|H_1|\psi_1\rangle$, and the second can then be obtained easily by confirming that $\langle\nu_0|\frac{d}{dt}|\nu_0\rangle = \langle\nu_\mu|\frac{d}{dt}|\nu_\mu\rangle^*$. Thus, to

first order,

$$i\int_0^T dt\left\langle \nu_\mu\left|\frac{d}{dt}\right|\nu_\mu\right\rangle = 2\pi\frac{\mu_2}{\mu_1}\cos^2\frac{\theta}{2}$$
$$i\int_0^T dt\left\langle \nu_0\left|\frac{d}{dt}\right|\nu_0\right\rangle = -2\pi\frac{\mu_2}{\mu_1}\cos^2\frac{\theta}{2}. \tag{4.77}$$

These results yield a geometric phase consistent with the expansion of the exact phase in the $\mu_1 \gg \mu_2$ limit. Here we have exhibited phases that, while not purely geometric, nonetheless arise in addition to the dynamical phase.

It is in fact not immediately apparent that this adiabatic treatment, where the geometric phase is calculated from the gauge potentials, even *should* give the correct result. To see why, consider that the "off-diagonal" matrix elements are

$$\left\langle \nu_0\left|\frac{d}{dt}\right|\nu_\mu\right\rangle = -i\mu_2\cos\frac{\theta}{2}\sin\frac{\theta}{2}e^{i(\mu_2-\mu_1)t} \tag{4.78}$$

and $\langle\nu_\mu|\frac{d}{dt}|\nu_0\rangle = -\langle\nu_0|\frac{d}{dt}|\nu_\mu\rangle^*$, which is to say that they do not vanish any faster in the small-μ_2 limit than the diagonal gauge potentials do. Evidently, however, one gets the correct results if these terms are simply dropped. The reason is that if the state is purely $|\nu_\mu\rangle$ or $|\nu_0\rangle$ at $t = 0$, then the component along the other eigenstate grows slowly by virtue of being driven by μ_2. This small component in turn contributes to the phase evolution of the dominant component with another factor of μ_2. Hence it is appropriate after all to ignore the overlap with the small component.

What we have shown in this section is that even away from the adiabatic limit phases arise that depend on (1) the number densities of the two neutrino populations and (2) the constant angle between the polarization vectors, but *not* explicitly on the time over which the system is evolved. Furthermore, the geometric phases associated with the two states are necessarily related. In contrast to what was found in the previous section, the geometric phases here are living creatures: $|\psi_1\rangle$ and $|\psi_2\rangle$ mutually settle, simultaneously, on their paths in flavor space and on the attendant

phases.

4.7 The $\mu \ll \omega$ limit with two flavors

In Sec. 4.5 we showed that a neutrino acquires a geometric phase when it is strongly coupled to another neutrino undergoing vacuum oscillations; under these circumstances the Hamiltonian acts like an external, time-dependent "flavor-magnetic" field. In Sec. 4.6 we showed that geometric phases can survive when the evolution of the magnetic field is coupled back to the test neutrino. We now ask whether geometric phases persist when vacuum oscillations and self-coupling are accounted for in both population of neutrinos. In particular we consider geometric effects arising in the $\mu \ll \omega$ limit.

We return to Eq. (4.24) and assume that the neutrino–neutrino forward-scattering potentials are small compared to the vacuum potentials. To prepare to use perturbation theory, we write the equations of motion as

$$\begin{aligned} i\frac{d|\psi_1\rangle}{dt} &= [\omega_1 B + \varepsilon\mu_2\rho_2]\,|\psi_1\rangle, \\ i\frac{d|\psi_2\rangle}{dt} &= [\omega_2 B + \varepsilon\mu_1\rho_1]\,|\psi_2\rangle. \end{aligned} \tag{4.79}$$

We expand perturbatively in the small parameter ε:

$$\begin{aligned} |\psi_1\rangle &= |\psi_1^{(0)}\rangle + \varepsilon|\psi_1^{(1)}\rangle + \ldots, \\ |\psi_2\rangle &= |\psi_2^{(0)}\rangle + \varepsilon|\psi_2^{(1)}\rangle + \ldots. \end{aligned} \tag{4.80}$$

To zeroth order the equations of motion are just those for vacuum oscillation:

$$\begin{aligned} i\frac{d|\psi_1^{(0)}\rangle}{dt} &= \omega_1 B|\psi_1^{(0)}\rangle, \\ i\frac{d|\psi_2^{(0)}\rangle}{dt} &= \omega_2 B|\psi_2^{(0)}\rangle, \end{aligned} \tag{4.81}$$

which have solutions

$$\begin{aligned} |\psi_1^{(0)}(t)\rangle &= \exp(-i\omega_1 Bt)\,|\psi_1^{(0)}(0)\rangle, \\ |\psi_2^{(0)}(t)\rangle &= \exp(-i\omega_2 Bt)\,|\psi_2^{(0)}(0)\rangle. \end{aligned} \tag{4.82}$$

The first-order equation for $|\psi_1\rangle$ is

$$i\frac{d|\psi_1^{(1)}\rangle}{dt} = \omega_1 B\psi_1^{(1)} + \mu_2\rho_2^{(0)}|\psi_1^{(0)}\rangle, \tag{4.83}$$

which, after plugging in the zeroth-order solution for $|\psi_2\rangle$, becomes

$$\begin{aligned} \frac{d|\psi_1^{(1)}\rangle}{dt} =& -i\omega_1 B|\psi_1^{(1)}(t)\rangle \\ & - i\mu_2 e^{-i\omega_2 Bt}\rho_2^{(0)}(0)e^{i(\omega_2-\omega_1)Bt}|\psi_1^{(0)}(0)\rangle. \end{aligned} \tag{4.84}$$

This has solution

$$|\psi_1^{(1)}(t)\rangle = e^{-i\omega_1 Bt}\left[|\psi_1^{(1)}(0)\rangle - i\mu_2\int_0^t dt' e^{i\omega_1 Bt'}\rho_2^{(0)}(t')|\psi_1^{(0)}(t')\rangle\right], \tag{4.85}$$

and $|\psi_2^{(1)}(t)\rangle$ has an identical form but with subscripts interchanged.

Cyclicity fails to materialize as naturally here as it did in earlier sections. To find geometric

effects analogous to the ones reported above, we seek values of the period T such that

$$|\psi_2(T)\rangle = e^{i\alpha}|\psi_2(0)\rangle. \tag{4.86}$$

The phase α is to be solved for concomitantly. Since $|\psi_1\rangle$ may not be cyclic with the same period, in general α will not be a phase of the Berry genus.

The phase and period are expanded as

$$\begin{aligned} \alpha &= \alpha^{(0)} + \varepsilon\alpha^{(1)}, \\ T &= T^{(0)} + \varepsilon T^{(1)}. \end{aligned} \tag{4.87}$$

If $\vec{P}_2$ is initially at angles (θ_2, ϕ_2), then the initial conditions for this mode are

$$\begin{aligned} |\psi_2^{(0)}(0)\rangle &= \begin{pmatrix} \cos\frac{\theta_2}{2} \\ e^{i\phi_2}\sin\frac{\theta_2}{2} \end{pmatrix}, \\ |\psi_2^{(1)}(0)\rangle &= \begin{pmatrix} 0 \\ 0 \end{pmatrix}. \end{aligned} \tag{4.88}$$

Demanding that $|\psi_2\rangle$ satisfy Eq. (4.86) then amounts to the following requirements on α and T:

$$\begin{aligned} &|\psi_2^{(0)}(T^{(0)})\rangle = e^{i\alpha^{(0)}}|\psi_2^{(0)}(0)\rangle, \\ &|\psi_2^{(1)}(T^{(0)})\rangle + T^{(1)}\frac{d|\psi_2^{(0)}\rangle}{dt}\bigg|_{T^{(0)}} = i\alpha^{(1)}e^{i\alpha^{(0)}}|\psi_2^{(0)}(0)\rangle. \end{aligned} \tag{4.89}$$

The first equation is satisfied if

$$T^{(0)} = \frac{2\pi n}{\omega_2}, \quad \alpha^{(0)} = n\pi, \tag{4.90}$$

with $n \in \mathbb{Z}$. The second equation then becomes

$$\left|\psi_2^{(1)}\left(\frac{2\pi n}{\omega_2}\right)\right\rangle = \pm i\left(\alpha^{(1)} + \omega_2 T^{(1)} B\right)|\psi_2^{(0)}(0)\rangle, \tag{4.91}$$

where $|\psi_2^{(1)}\rangle$ can be evaluated using Eq. (4.85). The $+$ $(-)$ corresponds to even (odd) n.

In deriving the first-order corrections to the phase and period it is helpful to note a few intermediate results. First, the term in the integrand of Eq. (4.85) that multiplies $|\psi_1^{(0)}(t)\rangle$ is

$$e^{i(\omega_2-\omega_1)Bt}\rho_1^{(0)}(0)e^{-i(\omega_2-\omega_1)Bt} = \begin{pmatrix} \cos^2\frac{\theta_1}{2} & e^{i(\omega_1-\omega_2)t}e^{-i\phi_1}\cos\frac{\theta_1}{2}\sin\frac{\theta_1}{2} \\ e^{-i(\omega_1-\omega_2)t}e^{i\phi_1}\cos\frac{\theta_1}{2}\sin\frac{\theta_1}{2} & \sin^2\frac{\theta_2}{2} \end{pmatrix}. \tag{4.92}$$

The two conditions that can be extracted from the matrix solution for $|\psi_1^{(1)}(t)\rangle$ are then

$$\begin{aligned} 2\pi n\frac{\mu_1}{\omega_2}\cos^2\frac{\theta_1}{2} + \xi^*\tan\frac{\theta_2}{2} &= -\alpha^{(1)} + \frac{\omega_2 T^{(1)}}{2}, \\ 2\pi n\frac{\mu_1}{\omega_2}\sin^2\frac{\theta_1}{2} + \xi\cot\frac{\theta_2}{2} &= -\alpha^{(1)} - \frac{\omega_2 T^{(1)}}{2}, \end{aligned} \tag{4.93}$$

where

$$\xi \equiv i\mu_1\frac{e^{-2\pi n i\left(\frac{\omega_1}{\omega_2}-1\right)}-1}{\omega_1-\omega_2}e^{i(\phi_1-\phi_2)}\cos\frac{\theta_1}{2}\sin\frac{\theta_1}{2}. \tag{4.94}$$

These equations can be solved to yield

$$\begin{aligned} \alpha^{(1)} &= -n\pi\frac{\mu_1}{\omega_2} - \frac{\xi}{2}\cot\frac{\theta_2}{2} - \frac{\xi^*}{2}\tan\frac{\theta_2}{2}, \\ T^{(1)} &= \frac{2\pi n}{\omega_2}\frac{\mu_1}{\omega_2}\cos\theta_1 + \frac{\xi^*}{\omega_2}\tan\frac{\theta_2}{2} - \frac{\xi}{\omega_2}\cot\frac{\theta_2}{2}. \end{aligned} \tag{4.95}$$

Notice that in general ξ is complex. Demanding that the period be real (but without putting contrived restrictions on the angles) requires that ω_1/ω_2 be a rational number of the form m/n,

with $m \in \mathbb{Z}$. Choosing ω_1 to satisfy this constraint, one obtains

$$\begin{aligned} \alpha^{(1)} &= -\pi n \frac{\mu_1}{\omega_2}, \\ T^{(1)} &= 2\pi n \frac{\mu_1}{\omega_2^2} \cos\theta_1, \end{aligned} \tag{4.96}$$

so that to first order we have

$$\begin{aligned} T &= \frac{2\pi n}{\omega_2}\left(1 + \frac{\mu_1}{\omega_1}\cos\theta_1\right), \\ \alpha &= n\pi\left(1 - \frac{\mu_1}{\omega_2}\right). \end{aligned} \tag{4.97}$$

To ensure that $|\psi_2\rangle$ is cyclic, the rationality condition $\omega_1/\omega_2 = m/n$ is necessary—but having so picked the vacuum oscillation frequencies, $|\psi_2\rangle$ oscillates with a geometry-dependent period and acquires a phase sensitive to the density of the other neutrino population.

Analogous results apply if instead we take $|\psi_1\rangle$ to be cyclic and seek out the period and phase consistent with such a requirement. If $\mu_1 = \mu_2$ and $\omega_1 = \omega_2$, then $|\psi_1\rangle$ and $|\psi_2\rangle$ are cyclic with the same period and accrue identical phases. In this particular scenario, where the two neutrino populations consist of particles of the same energy and density, the phases are of the classic Berry type, with each population experiencing adiabatic evolution under a cyclic Hamiltonian. In general the adiabaticity parameter for $|\psi_1\rangle$ is $\Upsilon_1 \sim \omega_1^2/\mu_2|\omega_2|$, and similarly for $|\psi_2\rangle$. Adiabaticity is therefore established automatically by taking the limit $\mu \ll \omega$, so long as the frequencies are of comparable magnitude. This observation also matches intuition: The time-dependent self-coupling potential, which elicits deviations from adiabaticity, is only a small part of the total Hamiltonian.

In the final assessment, cyclicity is typically jeopardized when the nonlinear coupling acts to perturb the neutrinos away from vacuum oscillations. Nonetheless geometry remains relevant to the flavor transformation that occurs in such a system, as evidenced by the noncyclic variants

of the geometric phase already alluded to in Sec. 4.2 (see, *e.g.*, Refs. [10, 13] for applications to neutrinos in vacuum+matter). We do not pursue this direction any further but we do emphasize that the imprints of geometry in flavor transformation transcend the cyclic, adiabatic phase.

4.8 Mixed potentials with three flavors: non-Abelian phase

We now generalize the mixed-potentials scenario of Sec. 4.5 to three flavors. As before, the vacuum oscillations of one neutrino determine the Hamiltonian experienced by the other. That is,

$$\begin{aligned} i\frac{d|\psi_1(t)\rangle}{dt} &= \mu_2\rho_2(t)|\psi_1(t)\rangle, \\ i\frac{d|\psi_2(t)\rangle}{dt} &= H_{\rm vac,2}|\psi_2(t)\rangle, \end{aligned} \tag{4.98}$$

where $|\psi_i\rangle$ is a three-component vector, ρ_i is a 3×3 matrix, and in the mass basis

$$H_{\rm vac,2} = \frac{1}{3}\begin{pmatrix} -\Delta_{21}-\Delta_{31} & 0 & 0 \\ 0 & \Delta_{21}-\Delta_{32} & 0 \\ 0 & 0 & \Delta_{32}+\Delta_{31} \end{pmatrix}, \tag{4.99}$$

using the notation $\Delta_{ij} \equiv \delta m^2_{ij}/2E$. The equations of motion have solutions

$$\begin{aligned} |\psi_1(t)\rangle &= \mathcal{P}\exp\left(-i\mu_1\int_0^t dt'\rho_2(t')\right)|\psi_1(0)\rangle, \\ |\psi_2(t)\rangle &= \exp\left(-iH_{\rm vac,2}t\right)|\psi_2(0)\rangle. \end{aligned} \tag{4.100}$$

The matrix exponential for the second of these is straightforward to compute. The solution, for $|\psi_2(0)\rangle = (a,b,c)^T$, is

$$|\psi_2(t)\rangle = \begin{pmatrix} \exp\left(i\frac{\Delta_{21}+\Delta_{31}}{3}t\right)a \\ \exp\left(i\frac{\Delta_{32}-\Delta_{21}}{3}t\right)b \\ \exp\left(-i\frac{\Delta_{32}+\Delta_{31}}{3}t\right)c \end{pmatrix}. \tag{4.101}$$

It follows that

$$\rho_2(t) = \begin{pmatrix} |a|^2 & \exp(i\Delta_{21}t)\,ab^* & \exp(i\Delta_{31}t)\,ac^* \\ \exp(-i\Delta_{21}t)\,ba^* & |b|^2 & \exp(i\Delta_{32}t)\,bc^* \\ \exp(-i\Delta_{31}t)\,ca^* & \exp(-i\Delta_{32}t)\,cb^* & |c|^2 \end{pmatrix} \tag{4.102}$$

and thus the geometric phases induced by the Hamiltonian $H_1(t) = \mu_2\rho_2(t)$ can be found by solving for the eigensystem. (In carrying out this procedure, one is aided by the Cardano formula.) The eigenvalues are $E_\mu = \mu_2$, $E_0 = 0$, and $E_{0'} = 0$, which correspond respectively to the eigenvectors

$$\begin{aligned} |\nu_\mu\rangle &= \frac{1}{|c|}\begin{pmatrix} \exp(i\Delta_{31}t)\,ac^* \\ \exp(i\Delta_{32}t)\,bc^* \\ |c|^2 \end{pmatrix}, \\ |\nu_0\rangle &= \frac{1}{\sqrt{1+\frac{|c|^2}{|b|^2}}}\begin{pmatrix} \exp(i\Delta_{31}t)\,ac^*\left(1-\frac{1}{|a|^2}\right) \\ \exp(i\Delta_{32}t)\,bc^* \\ |c|^2 \end{pmatrix}, \\ |\nu_{0'}\rangle &= \frac{|a|^2}{|c|^2\sqrt{1-|a|^2}}\begin{pmatrix} 0 \\ -\exp(i\Delta_{32}t)\,\frac{c^*}{b^*} \\ 1 \end{pmatrix}. \end{aligned} \tag{4.103}$$

In this scenario two of the energy eigenstates are always degenerate, indicating that the geometric phases have a non-Abelian gauge structure [127].

In the two-flavor case, where the gauge was Abelian, the geometric phases acquired by the energy eigenstates could be deduced by solving the Schrödinger equation with $|\psi_\pm(t)\rangle = \exp(i\phi_\pm(t))\,|\nu_\pm(t)\rangle$; this is the condition that enforces perfect adiabaticity. But nothing prevents the states within the degenerate subsystem from mixing with each other, regardless of how adiabatic the evolution is. To find the phases in the degenerate subsystem, one must therefore solve the Schrödinger equation with $|\psi_i(t)\rangle = U_{ij}(t)|\nu_j(t)\rangle$, where $|\nu_j(t)\rangle$ is the j^{th} eigenstate and $U(t)$ is the matrix generalizing the Abelian phase from the two-flavor case. If the path over a time t corresponds to a closed loop $\mathcal{C}$, then the matrix is given by the Wilson loop

$$U(\mathcal{C}) = \mathcal{P}\exp\left(i\oint_{\mathcal{C}} \vec{A}\cdot d\vec{R}\right), \tag{4.104}$$

where the gauge potential is now a vector-valued matrix with components

$$\vec{A}_{ij} = i\big\langle \nu_i(t)\big|\nabla\big|\nu_j(t)\big\rangle. \tag{4.105}$$

Eq. (4.104) generalizes Eq. (4.2). We do not write out all of the gauge potentials since they are not particularly enlightening, but we do note that the off-diagonal elements of A are nonzero, allowing for transitions between $|\nu_0\rangle$ and $|\nu_{0'}\rangle$ even in the adiabatic limit. If $|\psi_2(0)\rangle = |\nu_\alpha\rangle$ for $\alpha = e,\mu,\tau$, the transitions occur between orthogonal linear combinations of the other two flavors.

For H_1 to be cyclic, the period must be an integer multiple, all at once, of $2\pi/\Delta_{21}$, $2\pi/\Delta_{31}$, and $2\pi/\Delta_{32}$. This reflects the requirement for a three-flavor neutrino to oscillate back into its original state in finite time, a condition that was guaranteed in the two-flavor case. Supposing that such a T does exist, one can show that indeed the phases arising from the gauge potentials do not depend explicitly on time.

The non-Abelian structure owes its existence to a basic fact about the Hamiltonian for

$|\psi_1\rangle$. It is a fact that appeared previously in our study of the pure-self-coupling scenario in two flavors: When $H \sim \rho = |\psi\rangle\langle\psi|$, one eigenstate is $|\psi\rangle$ itself and all others are orthogonal states with eigenvalue 0. (Note that for the mixed-potential scenario in two flavors, where this trait of the Hamiltonian was also relevant, we pulled out the trace of the self-coupling Hamiltonian and thereby shifted the orthogonal-eigenstate energy down to $-\mu_1/2$.) To put it more starkly, the non-Abelian phase structure is a consequence of the coupling of neutrino flavor quantum states—with off-diagonal coherence included—rather than merely neutrino flavor number densities.

4.9 Conclusion

We have pointed out that the self-coupling potential generated by neutrino–neutrino forward scattering is capable of inducing geometric phases in flavor evolution. The mechanism is most easily understood in the two-flavor approximation, where a neutrino's flavor state and Hamiltonian correspond graphically to vectors ending on the Bloch sphere. In a background consisting strictly of matter particles, the Hamiltonian vector $\vec{H}$ is confined to a plane. But in a medium dense in neutrinos, $\vec{H}$ is liberated from the plane and, should it undergo a closed cycle, may return to its initial point having enclosed a finite solid angle on the sphere. Path-dependent geometric phases in the energy eigenstates are the result—and since flavor transformation at its heart is an interference phenomenon of the neutrino's energy eigenstates, the phases surface in flavor transition probabilities and are observable in principle.

To examine these phases in an analytically tractable setting, we have considered various limits of a very simple toy model devoid of the astrophysical complications that beckon a numerical treatment. Despite the model's simplicity, the calculations presented in this paper illuminate several facets of geometric phases in environments with nonlinear refraction from neutrino self-coupling.

Foremost among these aspects are the roles of adiabaticity and cyclicity. We have seen that

adiabatic evolution is not a necessity, and that geometric effects are apparent in the non-adiabatic corrections, albeit in a way entangled with the dynamics. We have also seen that the complicated interplay between oscillations and self-coupling tends to compromise cyclicity. But cyclicity is also dispensable, and though we have not pursued this direction here, it is expected that geometric effects should prove to be a generic feature of noncyclic evolution as well.

Beyond these, two other interesting phenomena have emerged from the calculations: the entwining of the paths and phases of the two neutrino populations, as exhibited in the pure-self-coupling scenario, and the non-Abelian phase structure of the three-flavor case. These effects hinge on the peculiar nature of the neutrino–neutrino forward-scattering potential, which allows neutrinos to communicate to one another the quantum coherence of their flavor states.

This study was motivated by the possibility for collective flavor-transformation effects in the extreme environments found, for instance, in the torrid plasma of the early universe or the incendiary outflow from a core-collapse supernova. We have made no attempt to locate geometric phases in astrophysically realistic models but have instead strived to make clear, based on calculations in uncluttered toy models, how such phases might emerge. Indeed, we expect that the ideas underlying this study may find a place, in some form, in a variety of applications: in synchronized or bipolar oscillations in the early universe, in a possibly cyclic halo-affected region outside a supernova, in active–sterile oscillations, and elsewhere. To be sure, sophisticated numerical computations already have geometric effects built in implicitly, albeit in far more complicated manifestations than those analyzed here. After all, the provenance of these effects—the shape of Hilbert space and the structure of the Hamiltonian—is encoded in the equations of motion. But the importance of geometry in the results that these equations output is often overlooked.

4.10 Acknowledgements

We thank Amol Patwardhan for helpful conversations. This work was supported by NSF Grant No. PHY-1307372 at UC San Diego. The majority of the project was completed while one of us (L.J.) was stationed at Los Alamos National Laboratory, with support from the U.S. Department of Energy Office of Science Graduate Student Research (SCGSR) Program. This author thanks the Lab for their hospitality.

This chapter is a reprint of L. Johns and G. M. Fuller, Phys. Rev. D 95, 043003 (2017). I was the primary investigator and author of this publication.

Bibliography

[1] N. Nakagawa, Ann. Phys. **179**, 145 (1987).

[2] J. Vidal and J. Wudka, Phys. Lett. B **249**, 473 (1990).

[3] C. Aneziris and J. Schechter, Int. J. Mod. Phys. A **6**, 2375 (1991).

[4] A. Y. Smirnov, Phys. Lett. B **260**, 161 (1991).

[5] E. K. Akhmedov, P. I. Krastev, and A. Y. Smirnov, Z. Phys. C **52**, 701 (1991).

[6] M. M. Guzzo and J. Bellandi, Phys. Lett. B **294**, 243 (1992).

[7] V. A. Naumov, Int. J. Mod. Phys. D **1**, 379 (1992).

[8] V. A. Naumov, Phys. Lett. B **323**, 351 (1994).

[9] M. Blasone, P. A. Henning, and G. Vitiello, Phys. Lett. B **466**, 262 (1999).

[10] X.-B. Wang, L. C. Kwek, Y. Liu, and C. H. Oh, Phys. Rev. D **63**, 053003 (2001).

[11] X.-G. He, X.-Q. Li, B. H. J. McKellar, and Y. Zhang, Phys. Rev. D **72**, 053012 (2005).

[12] M. Blasone, A. Capolupo, E. Celeghini, and G. Vitiello, Phys. Lett. B **674**, 73 (2009).

[13] P. Mehta, Phys. Rev. D **79**, 096013 (2009).

[14] S. Joshi and S. R. Jain, Phys. Lett. B **754**, 135 (2016).

[15] S. P. Mikheyev and A. Y. Smirnov, Sov. J. Nucl. Phys. **42**, 913 (1985).

[16] H. A. Bethe, Phys. Rev. Lett. **56**, 1305 (1986).

[17] M. V. Berry, Proc. R. Soc. A **392**, 45 (1984).

[18] E. Sjöqvist, Phys. Rev. A **62**, 022109 (2000).

[19] E. Sjöqvist, A. K. Pati, A. Ekert, J. S. Anandan, M. Ericsson, D. K. L. Oi, and V. Vedral, Phys. Rev. Lett. **85**, 2845 (2000).

[20] Y. Aharonov and J. Anandan, Phys. Rev. Lett. **58**, 1593 (1987).

[21] J. Anandan, Phys. Lett. A **133**, 171 (1988).

[22] J. Samuel and R. Bhandari, Phys. Rev. Lett. **60**, 2339 (1988).

[23] A. K. Pati, Ann. Phys. **270**, 178 (1998).

[24] G. García de Polavieja, Phys. Rev. Lett. **81**, 1 (1998).

[25] G. García de Polavieja and E. Sjöqvist, Am. J. Phys. **66**, 431 (1998).

[26] A. Mostafazadeh, J. Phys. A **32**, 8157 (1999).

[27] J. Garrison and E. M. Wright, Phys. Lett. A **128**, 177 (1988).

[28] D. Gamliel and J. H. Freed, Phys. Rev. A **39**, 3238 (1989).

[29] G. Dattoli, R. Mignani, and A. Torre, J. Phys. A **23**, 5795 (1990).

[30] C.-P. Sun, Phys. Scripta **48**, 393 (1993).

[31] A. Carollo, I. Fuentes-Guridi, M. F. Santos, and V. Vedral, Phys. Rev. Lett. **90**, 160402 (2003).

[32] A. Tomita and R. Y. Chiao, Phys. Rev. Lett. **57**, 937 (1986).

[33] T. Bitter and D. Dubbers, Phys. Rev. Lett. **59**, 251 (1987).

[34] D. Suter, G. C. Chingas, R. A. Harris, and A. Pines, Molecular Physics **61**, 1327 (1987).

[35] R. Tycko, Phys. Rev. Lett. **58**, 2281 (1987).

[36] R. Bhandari and J. Samuel, Phys. Rev. Lett. **60**, 1211 (1988).

[37] D. M. Bird and A. R. Preston, Phys. Rev. Lett. **61**, 2863 (1988).

[38] T. H. Chyba, R. Simon, L. J. Wang, and L. Mandel, Opt. Lett. **13**, 562 (1988).

[39] D. Suter, K. T. Mueller, and A. Pines, Phys. Rev. Lett. **60**, 1218 (1988).

[40] H. Weinfurter and G. Badurek, Phys. Rev. Lett. **64**, 1318 (1990).

[41] Y. Aharonov and D. Bohm, Phys. Rev. **115**, 485 (1959).

[42] S. Pancharatnam, Proc. Indian Acad. Sci. A **44**, 398 (1956).

[43] G. Herzberg and H. Longuet-Higgins, Disc. Farad. Soc. **35**, 77 (1963).

[44] C. A. Mead and D. G. Truhlar, J. Chem. Phys. **70**, 2284 (1979).

[45] A. Cisneros, Astrophys. Space Sci. **10**, 87 (1971).

[46] M. B. V. L. B. Okun and V. I. Vysotsky, Sov. J. Nucl. Phys. **44**, 440 (1986).

[47] L. Wolfenstein, Phys. Rev. D **17**, 2369 (1978).

[48] J. Pantaleone, Phys. Lett. B **287**, 128 (1992).

[49] J. H. Hannay, J. Phys. A **18**, 221 (1985).

[50] B. Simon, Phys. Rev. Lett. **51**, 2167 (1983).

[51] J. Anandan, Nature **360**, 307 (1992).

[52] NOνA Collaboration, hep-ex/0503053 (2005).

[53] T2K Collaboration, Prog. Theor. Exp. Phys. **2015**, 043C01 (2015).

[54] DUNE Collaboration, arXiv:1512.06148 (2015).

[55] Particle Data Group, Chin. Phys. C **40**, 1000001 (2016).

[56] C. Volpe, D. Väänänen, and C. Espinoza, Phys. Rev. D **87**, 113010 (2013).

[57] A. Vlasenko, G. M. Fuller, and V. Cirigliano, Phys. Rev. D **89**, 105004 (2014).

[58] A. Kartavtsev, G. Raffelt, and H. Vogel, Phys. Rev. D **91**, 125020 (2015).

[59] B. D. Keister, Phys. Scripta **90**, 088008 (2015).

[60] J. F. Cherry, J. Carlson, A. Friedland, G. M. Fuller, and A. Vlasenko, Phys. Rev. Lett. **108**, 261104 (2012).

[61] G. Sigl and G. Raffelt, Nucl. Phys. **B406**, 423 (1993).

[62] V. A. Kostelecký, J. Pantaleone, and S. Samuel, Phys. Lett. B **315**, 46 (1993).

[63] V. A. Kostelecký and S. Samuel, Phys. Lett. B **318**, 127 (1993).

[64] S. Samuel, Phys. Rev. D **48**, 1462 (1993).

[65] V. A. Kostelecký and S. Samuel, Phys. Rev. D **49**, 1740 (1994).

[66] V. A. Kostelecký and S. Samuel, Phys. Rev. D **52**, 621 (1995).

[67] Y.-Z. Qian and G. M. Fuller, Phys. Rev. D **51**, 1479 (1995).

[68] A. B. Balantekin and G. M. Fuller, Phys. Lett. B **471**, 195 (1999).

[69] S. Pastor, G. Raffelt, and D. V. Semikoz, Phys. Rev. D **65**, 053011 (2002).

[70] S. Pastor and G. Raffelt, Phys. Rev. Lett. **89**, 191101 (2002).

[71] N. F. Bell, A. A. Rawlinson, and R. F. Sawyer, Physics Letters B **573**, 86 (2003).

[72] A. B. Balantekin and H. Yüksel, New J. Phys. **7**, 51 (2005).

[73] H. Duan, G. M. Fuller, J. Carlson, and Y.-Z. Qian, Phys. Rev. D **74**, 105014 (2006).

[74] H. Duan, G. M. Fuller, J. Carlson, and Y.-Z. Qian, Phys. Rev. Lett. **97**, 241101 (2006).

[75] H. Duan, G. M. Fuller, and Y.-Z. Qian, Phys. Rev. D **74**, 123004 (2006).

[76] G. M. Fuller and Y.-Z. Qian, Phys. Rev. D **73**, 023004 (2006).

[77] S. Hannestad, G. G. Raffelt, G. Sigl, and Y. Y. Y. Wong, Phys. Rev. D **74**, 105010 (2006).

[78] A. B. Balantekin and Y. Pehlivan, J. Phys. G **34**, 47 (2007).

[79] H. Duan, G. M. Fuller, J. Carlson, and Y.-Z. Qian, Phys. Rev. Lett. **99**, 241802 (2007).

[80] H. Duan, G. M. Fuller, J. Carlson, and Y.-Z. Qian, Phys. Rev. D **75**, 125005 (2007).

[81] H. Duan, G. M. Fuller, and Y.-Z. Qian, Phys. Rev. D **76**, 085013 (2007).

[82] G. Fogli, E. Lisi, A. Marrone, and A. Mirizzi, J. Cosmol. Astropart. Phys. **12**, 010 (2007).

[83] G. G. Raffelt and A. Y. Smirnov, Phys. Rev. D **76**, 081301 (2007).

[84] G. G. Raffelt and G. Sigl, Phys. Rev. D **75**, 083002 (2007).

[85] G. G. Raffelt and A. Y. Smirnov, Phys. Rev. D **76**, 125008 (2007).

[86] M. Blennow, A. Mirizzi, and P. D. Serpico, Phys. Rev. D **78**, 113004 (2008).

[87] S. Chakraborty, S. Choubey, B. Dasgupta, and K. Kar, J. Cosmol. Astropart. Phys. **9**, 013 (2008).

[88] B. Dasgupta and A. Dighe, Phys. Rev. D **77**, 113002 (2008).

[89] B. Dasgupta, A. Dighe, A. Mirizzi, and G. Raffelt, Phys. Rev. D **78**, 033014 (2008).

[90] B. Dasgupta, A. Dighe, A. Mirizzi, and G. G. Raffelt, Phys. Rev. D **77**, 113007 (2008).

[91] H. Duan, G. M. Fuller, and J. Carlson, Comput. Sci. Disc. **1**, 015007 (2008).

[92] H. Duan, G. M. Fuller, J. Carlson, and Y.-Z. Qian, Phys. Rev. Lett. **100**, 021101 (2008).

[93] H. Duan, G. M. Fuller, and Y.-Z. Qian, Phys. Rev. D **77**, 085016 (2008).

[94] A. Esteban-Pretel, A. Mirizzi, S. Pastor, R. Tomàs, G. G. Raffelt, P. D. Serpico, and G. Sigl, Phys. Rev. D **78**, 085012 (2008).

[95] A. Esteban-Pretel, S. Pastor, R. Tomàs, G. G. Raffelt, and G. Sigl, Phys. Rev. D **77**, 065024 (2008).

[96] J. Gava and C. Volpe, Phys. Rev. D **78**, 083007 (2008).

[97] B. Dasgupta, A. Dighe, G. G. Raffelt, and A. Y. Smirnov, Phys. Rev. Lett. **103**, 051105 (2009).

[98] H. Duan, G. M. Fuller, and Y.-Z. Qian, Journal of Physics G Nuclear Physics **36**, 105003 (2009).

[99] H. Duan and J. P. Kneller, J. Phys. G **36**, 113201 (2009).

[100] G. Fogli, E. Lisi, A. Marrone, and I. Tamborra, J. Cosmol. Astropart. Phys. **4**, 030 (2009).

[101] J. Gava, J. Kneller, C. Volpe, and G. C. McLaughlin, Phys. Rev. Lett. **103**, 071101 (2009).

[102] R. F. Sawyer, Phys. Rev. D **79**, 105003 (2009).

[103] A. Friedland, Phys. Rev. Lett. **104**, 191102 (2010).

[104] H. Duan, G. M. Fuller, and Y.-Z. Qian, Ann. Rev. Nucl. Part. Sci. **60**, 569 (2010).

[105] S. Chakraborty, S. Choubey, S. Goswami, and K. Kar, J. Cosmol. Astropart. Phys. **6**, 007 (2010).

[106] B. Dasgupta, A. Mirizzi, I. Tamborra, and R. Tomàs, Phys. Rev. D **81**, 093008 (2010).

[107] A. Banerjee, A. Dighe, and G. Raffelt, Phys. Rev. D **84**, 053013 (2011).

[108] S. Chakraborty, T. Fischer, A. Mirizzi, N. Saviano, and R. Tomàs, Phys. Rev. Lett. **107**, 151101 (2011).

[109] S. Chakraborty, T. Fischer, A. Mirizzi, N. Saviano, and R. Tomàs, Phys. Rev. D **84**, 025002 (2011).

[110] H. Duan, A. Friedland, G. C. McLaughlin, and R. Surman, J. Phys. G **38**, 035201 (2011).

[111] S. Galais and C. Volpe, Phys. Rev. D **84**, 085005 (2011).

[112] Y. Pehlivan, A. B. Balantekin, T. Kajino, and T. Yoshida, Phys. Rev. D **84**, 065008 (2011).

[113] G. G. Raffelt, Phys. Rev. D **83**, 105022 (2011).

[114] B. Dasgupta, E. P. O'Connor, and C. D. Ott, Phys. Rev. D **85**, 065008 (2012).

[115] A. de Gouvêa and S. Shalgar, J. Cosmol. Astropart. Phys. **2012**, 027 (2012).

[116] S. Sarikas, G. G. Raffelt, L. Hüdepohl, and H.-T. Janka, Phys. Rev. Lett. **108**, 061101 (2012).

[117] S. Sarikas, I. Tamborra, G. Raffelt, L. Hüdepohl, and H.-T. Janka, Phys. Rev. D **85**, 113007 (2012).

[118] G. Raffelt, S. Sarikas, and D. S. Seixas, Phys. Rev. Lett. **111**, 091101 (2013).

[119] G. Raffelt and D. S. Seixas, Phys. Rev. D **88**, 045031 (2013).

[120] A. Vlasenko, G. M. Fuller, and V. Cirigliano, arXiv:1406.6724 .

[121] S. Chakraborty, R. Hansen, I. Izaguirre, and G. Raffelt, Nucl. Phys. **B908**, 366 (2016).

[122] A. Malkus, G. C. McLaughlin, and R. Surman, Phys. Rev. D **93**, 045021 (2016).

[123] L. Johns, M. Mina, V. Cirigliano, M. W. Paris, and G. M. Fuller, Phys. Rev. D **94**, 083505 (2016).

[124] J. Y. Tian, A. V. Patwardhan, and G. M. Fuller, arXiv:1610.08586 .

[125] E. Armstrong, A. V. Patwardhan, L. Johns, C. T. Kishimoto, H. D. I. Abarbanel, and G. M. Fuller, Phys. Rev. D **96**, 083008 (2017).

[126] W. C. Haxton, Phys. Rev. Lett. **57**, 1271 (1986).

[127] F. Wilczek and A. Zee, Phys. Rev. Lett. **52**, 2111 (1984).

Chapter 5

Neutrino oscillations in supernovae: angular moments and fast instabilities

5.1 Abstract

Recent theoretical work indicates that the neutrino radiation in core-collapse supernovae may be susceptible to flavor instabilities that set in far behind the shock, grow extremely rapidly, and have the potential to profoundly affect supernova dynamics and composition. Here we analyze the nonlinear collective oscillations that are prefigured by these instabilities. We demonstrate that a zero-crossing in $n_{\nu_e} - n_{\bar{\nu}_e}$ as a function of propagation angle is not sufficient to generate instability. Our analysis accounts for this fact and allows us to formulate complementary criteria. Using FORNAX simulation data, we show that fast collective oscillations qualitatively depend on how forward-peaked the neutrino angular distributions are.

5.2 Main

In this paper we address a key aspect of neutrino physics in core-collapse supernovae. The stakes are high, as supernova explosions are central to our understanding of the origin of elements and the history of galaxies.

Recently it has been realized that the neutrino flavor field in core-collapse supernovae is prone to a host of instabilities [1–11] that were artificially concealed by the symmetries adopted in older studies [12–18]. Of particular urgency is the subclass known as *fast* instabilities, so named because they exhibit growth rates proportional to the self-coupling potential $\mu = \sqrt{2} G_F n_\nu$ and are not suppressed by the typically much smaller vacuum oscillation frequency $\omega = \delta m^2/2E$ [19–34]. They are commonly, if not always, associated with zero-crossings of the electron lepton number carried by neutrinos (νELN) as a function of propagation angle. Global variations in $n_{\bar{\nu}_e}/n_{\nu_e}$—possibly related to LESA (lepton-number emission self-sustained asymmetry) [35–41]—and coherent neutrino–nucleus scattering [42] independently make this condition a live possibility in core-collapse supernovae [42–47]. If fast flavor conversion (FFC) does occur, it could substantially alter our current view of supernova dynamics and nucleosynthesis [48, 49].

The aim of the present study is to gain some degree of understanding of the nonlinear collective effects heralded by fast flavor instabilities. Our basic approach is to study the evolution of the neutrino flavor field in terms of its momentum-space angular moments. Three considerations motivate this choice. The first is realism: Neutrino angular distributions within ~ 100 km are quite unlike the forms they are given in bulb or beam models. In point of fact, they transition—very gradually relative to the μ^{-1} scale—from nearly isotropic to narrowly forward-peaked [50–53]. The second consideration is computational: As it is, many state-of-the-art supernova simulations only track the first few angular moments, and cohesion between hydrodynamic and oscillation calculations is clearly desirable [54–61]. The last is theoretical: In multipole space, the factor $(1 - \hat{\mathbf{p}} \cdot \hat{\mathbf{q}})$ that couples neutrinos of momenta $\mathbf{p}$ and $\mathbf{q}$ becomes a sum of monopole and dipole

couplings [62, 63]. Angular moments are consequently a natural lens through which to examine collective oscillations.

This last observation is especially true of fast modes, which can be isolated by taking $\mu \gg \omega$. Because neutrino energy drops out of the coherent evolution, we can work with polarization vectors that are integrated over the spectrum. Neutrinos propagating in a homogeneous environment at angle $v = \cos\theta$ (axial symmetry is assumed throughout) then obey the hybrid multipole/momentum equation

$$\dot{\mathbf{P}}_v = \mu(\mathbf{D}_0 - v\mathbf{D}_1) \times \mathbf{P}_v. \tag{5.1}$$

Here $\mathbf{D}_0$ and $\mathbf{D}_1$ are the monopole and dipole difference vectors ($\mathbf{D}_l = \mathbf{P}_l - \bar{\mathbf{P}}_l$) and the matter potential $\lambda = \sqrt{2}G_F n_e$ has been rotated out. It is immediately apparent that the only way for the flavor content $P_{v,z}$ to change significantly on a fast time scale is for $\mathbf{D}_0 - v\mathbf{D}_1$ to swing away from the flavor axis.

In terms of the difference vectors and their counterpart sum vectors $\mathbf{S}_l = \mathbf{P}_l + \bar{\mathbf{P}}_l$, the multipole equations of motion are [62]

$$\begin{aligned}
\dot{\mathbf{S}}_l &= \mu\mathbf{D}_0 \times \mathbf{S}_l - \frac{\mu}{2}\mathbf{D}_1 \times (a_l\mathbf{S}_{l-1} + b_l\mathbf{S}_{l+1}), \\
\dot{\mathbf{D}}_l &= \mu\mathbf{D}_0 \times \mathbf{D}_l - \frac{\mu}{2}\mathbf{D}_1 \times (a_l\mathbf{D}_{l-1} + b_l\mathbf{D}_{l+1}),
\end{aligned} \tag{5.2}$$

where $a_l = 2l/(2l+1)$ and $b_l = 2(l+1)/(2l+1)$. $\mathbf{D}_0$ is constant on μ^{-1} time scales, implying that fast collective modes must be driven by $\mathbf{D}_1$. It is helpful at this point to switch to a frame rotating about $\hat{\mathbf{D}}_0$ at frequency μD_0, where $D_0 = |\mathbf{D}_0|$. Using primes to denote vectors in the

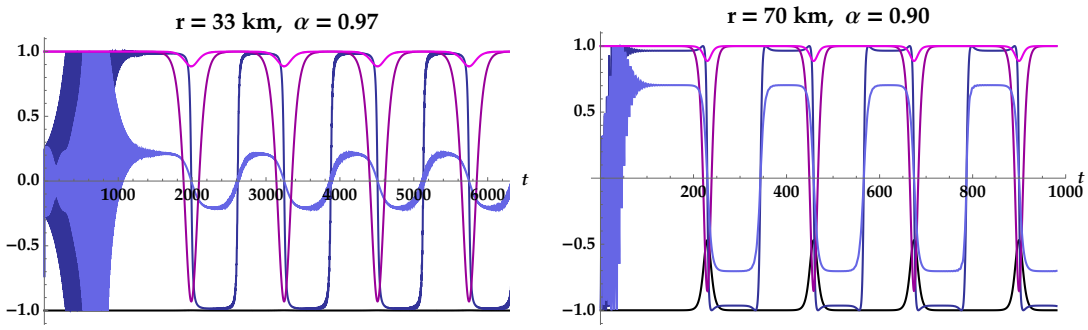

Figure 5.1: Angular coordinates over four periods of fast flavor conversion. Two values of $v = \cos\theta$ are shown in each panel. The one that experiences more significant flavor conversion is distinguished by the use of darker shades: purple for $\cos\theta_v$, blue for $\sin(\phi_v - \phi_1)$. The thick black curve depicts $\cos\theta_1$. Time is in units of $[\sqrt{2}G_F(n_{\nu_e} - n_{\bar{\nu}_e})]^{-1} \sim 14$ ps (154 ps) for the upper (lower) panel. See the text for discussion and Fig. 5.2 for more information on the choice of parameters.

rotating frame and introducing $\mathbf{L}' = (\mathbf{D}'_0 + 2\mathbf{D}'_2)/3$ and $\mathbf{G}' = 2\mathbf{D}'_3/5$, we then have

$$\begin{aligned} \dot{\mathbf{D}}'_1 &= \mu \mathbf{L}' \times \mathbf{D}'_1, \\ \dot{\mathbf{D}}'_2 &= \frac{3}{2}\mu \mathbf{G}' \times \mathbf{D}'_1. \end{aligned} \tag{5.3}$$

Computing $\mathbf{D}'_1 \times \ddot{\mathbf{D}}'_1$ leads to a pendulum equation, which can be written in a form comparable to that of the bipolar pendulum (Eq. 39 of Ref. [13]) by defining $\boldsymbol{\delta}' = \mathbf{D}'_1/D_1$ and $\sigma = \boldsymbol{\delta}' \cdot \mathbf{L}'$. The result is

$$\frac{\boldsymbol{\delta}' \times \ddot{\boldsymbol{\delta}}'}{\mu} + \sigma \dot{\boldsymbol{\delta}}' = \mu D_1 \boldsymbol{G}' \times \boldsymbol{\delta}'. \tag{5.4}$$

One critical distinction with respect to the bipolar pendulum is that in this case "gravity" is not a fixed external potential. In fact, $\mathbf{G}'$ couples directly to $\mathbf{D}'_1$, making this a sort of *nonlinear* gyroscopic pendulum. Nevertheless, the possibility for collective pendulum motion is built into the structure of Eq. (5.2). Numerical realizations of it are shown in Figs. 5.1 and 5.2.

The dynamics of the system is also restricted by a tower of conservation laws, which can be constructed by differentiating $\mathbf{D}'_1 \cdot \mathbf{D}'_l$ and recursively reducing the right-hand side until it is

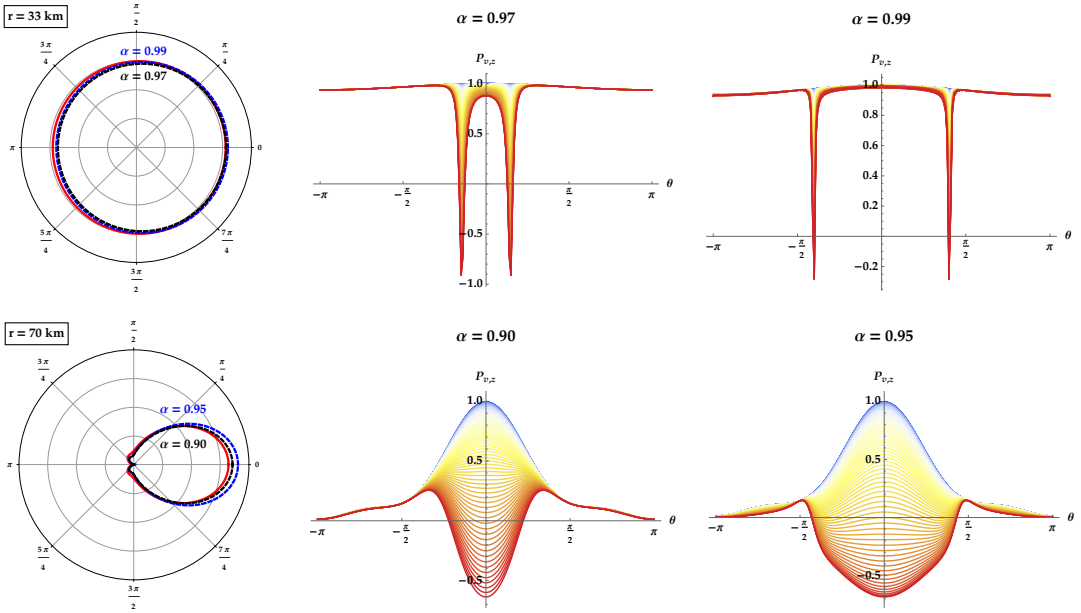

Figure 5.2: *Left*: n_{ν_e} (red) and $n_{\bar{\nu}_e}$ (blue and black) as functions of propagation angle θ, with arbitrary normalization. The angular distributions are drawn at 200 ms post-bounce from a spherically symmetric FORNAX simulation [64, 65] of the 16 $M_\odot$ progenitor from Ref. [66]. M1 closure is used to provide the radiative pressures and radiative heat fluxes [67], and $\alpha = n_{\bar{\nu}_e}/n_{\nu_e}$ is treated as a free parameter in order to trigger instability. *Middle and right*: Snapshots of $P_{v,z}$ color-coded by time (going from blue to red) and spanning the descent phase of a single dip in $D_{1,z}$. The normalization is such that $P_{v=1,z} = 1$. To isolate the fast mode, ω is assigned an artificially small value.

expressed as a total derivative. The first three conserved quantities are D_1, σ, and

$$E_D = \mu \boldsymbol{G}' \cdot \mathbf{D}_1' + \frac{\mu}{2}\mathbf{L}'^2, \tag{5.5}$$

which respectively denote the length of the pendulum, its spin, and its total energy. In a foundational study, Raffelt and Sigl [62] showed that the dipole term is the driving force behind kinematic decoherence. This remains true on short time scales, and it is clear from Eq. (5.1) that $\mathbf{D}_1$ causes dephasing of neutrinos with different values of v. But the constraints on the motion of $\mathbf{D}_1$ mean that the dephasing can give rise to persistent collective oscillations rather than effectively irreversible relaxation, at least until the effects of finite ω become important. The additional fact that some of these constraints involve only the first four angular moments gives us some hope of capturing the important features of FFC without having fine-grained information about the distributions in momentum space. Indeed, the higher conservation laws, which encode the fact that all angular moments are dynamically linked, may have utility for closing the moment hierarchy in a sensible way.

We can be more specific about the connection to kinematic decoherence by recalling that $\mathbf{S}_0$ obeys a pendulum equation as well [13, 62, 68, 69], with energy

$$E_S = \omega \mathbf{B} \cdot \mathbf{S}_0 + \frac{\mu}{2}\left(\mathbf{D}_0^2 - \mathbf{D}_1^2\right). \tag{5.6}$$

Kinematic decoherence arises because $\mathbf{D}_0^2$ and $\mathbf{D}_1^2$ are able to evolve at the cost of $\mathbf{S}_0$ shrinking [62]. But if $\mu \gg \omega$, then the $\mathbf{S}_0$ pendulum generally has very little sway over the $\mathbf{D}_1$ pendulum. The opposite is not true, however: $\mathbf{D}_1$ steers the evolution of $\mathbf{S}_0$. Relaxation occurs through the mutual interaction of the two pendula; the fact that the influence is one-way in the $\omega \to 0$ limit enables sustained collective motion.

It remains for us to understand how the predilection of $\mathbf{D}_1'$ for pendulum motion is expressed through the individual polarization vectors. Ultimately our interest is in the projection

onto the flavor axis:

$$\dot{P}_{v,z} = -\mu v \left(\mathbf{D}_1 \times \mathbf{P}_v\right)_z . \tag{5.7}$$

Writing the vectors in terms of their angular coordinates (θ_v and ϕ_v being the polar and azimuthal angles of $\mathbf{P}_v$, θ_1 and ϕ_1 being the same of $\mathbf{D}_1$), Eq. (5.7) becomes

$$\dot{\theta}_v = \mu v D_1 \sin\theta_1 \sin\left(\phi_v - \phi_1\right). \tag{5.8}$$

Approximating ϕ_v and ϕ_1 as developing under the influence of their *initial* Hamiltonians, the phase difference accumulates at a rate

$$\dot{\phi}_v - \dot{\phi}_1 \simeq -\mu \left(\frac{1}{3} D_{0,z}(0) + v D_{1,z}(0) + \frac{2}{3} D_{2,z}(0)\right). \tag{5.9}$$

Suppose that $\mathbf{P}_v(0) \propto \mathbf{z}$. If the phase difference develops slowly enough that the right-hand side of Eq. (5.8) is positive over many cycles of ϕ_1, then θ_v can grow to a size unsuppressed by the vacuum mixing angle.

As the instability grows, Eq. (5.9) breaks down and is replaced by the collective motion seen in Fig. 5.1. $P_{v,z}$ dips in proportion to $v\sin(\phi_v - \phi_1)$ and is reflected in—and driven by—peaks in $D_{1,z}$ (which are imperceptibly small in the upper panel because the angular distributions are very nearly isotropic). As Fig. 5.2 illustrates, there are two qualitatively different outcomes as a function of v. Setting Eq. (5.9) equal to zero, we find the trajectory which in this approximation has constant phase with respect to $\mathbf{D}_1$:

$$\tilde{v} = -\frac{1}{3R_1} - \frac{2R_2}{3R_1}, \tag{5.10}$$

with $R_l = D_{l,z}(0)/D_{0,z}(0)$. The quantity $\tilde{v}$ serves as a control parameter that shapes the v-dependence of the collective oscillations. When $\tilde{v}$ is comfortably inside the range $[-1,1]$ (as in the test cases at $r = 33$ km), it indicates the presence of narrow resonances. When $\tilde{v} \approx \pm 1$ (as at

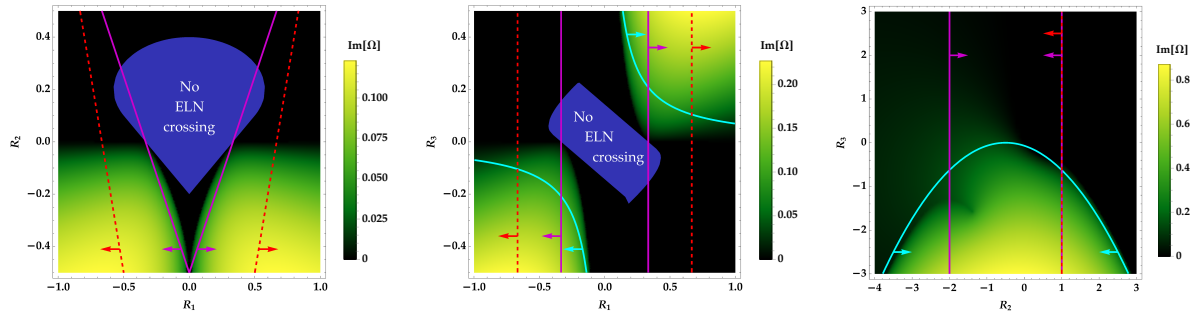

Figure 5.3: Regions of instability. Each point represents a family of angular distributions (Eq. (5.13)). *Left*: The (R_1, R_2) parameter space, with $R_{l\geq 3} = 0$. *Center*: (R_1, R_3), with $R_2 = R_{l\geq 4} = 0$. *Right*: (R_2, R_3), with $R_1 = -1$ and $R_{l\geq 4} = 0$. The color map shows the instability growth rate obtained from the linear analysis [Eq. (5.11)] in units of $\sqrt{2}G_F(n_{\nu_e} - n_{\bar{\nu}_e})$; the blue region indicates parameters for which no zero-crossing occurs in the electron lepton number carried by neutrinos; and the magenta, cyan, and red curves border the unstable regions according to Eqs. (5.10), (5.15), and (5.16), respectively. Arrows point *into* the unstable regions. For reference, the Fig. 5.1 angular distributions at 33 km have $R_1 = -0.35$ (-1.11), $R_2 = -0.02$ (-0.05), and $R_3 = 0$ (0) for $\alpha = 0.97$ (0.99). The angular distributions at 70 km have $R_1 = -0.17$ (-0.87), $R_2 = -0.24$ (-0.71), and $R_3 = -0.12$ (-0.34) for $\alpha = 0.90$ (0.95).

$r = 70$ km), the resonances fuse. Going one step further, we can use this parameter as the basis for a simple stability criterion: If $|\tilde{\nu}| > 1$, FFC cannot occur.

Conducting a linear stability analysis in terms of angular moments is revealing as well. Following the usual procedure [70], we take the flavor coherence to be of the collective form $S_{E,\nu} = Q_{E,\nu}\exp(-i\Omega t)$ and search for growing solutions (Im $\Omega > 0$) to the dispersion relation

$$(1+I_0)(1-I_2)+I_1^2 = 0, \tag{5.11}$$

where

$$\begin{aligned} I_j &= \sqrt{2}G_F\left(n_{\nu_e} - n_{\bar{\nu}_e}\right)\sum_{l=0}^{\infty}\left(l+\frac{1}{2}\right)R_l I_{j,l}, \\ I_{j,l} &= \int_{-1}^{1} dv \frac{v^j L_l(v)}{\Omega - \sqrt{2}G_F\left(n_{\nu_e} - n_{\bar{\nu}_e}\right)(1-R_1 v)}. \end{aligned} \tag{5.12}$$

We continue to set $\lambda = \omega = 0$, and we assume that $n_{\nu_x} = n_{\bar{\nu}_x}$. In these expressions L_l is the l^{th}

Legendre polynomial and R_l is the ratio of the l^{th} Legendre moment of the νELN to the total νELN (*i.e.*, R_l is the same parameter that appears in Eq. (5.10)):

$$R_l = \frac{(n_{\nu_e} - n_{\bar{\nu}_e})_l}{n_{\nu_e} - n_{\bar{\nu}_e}}. \tag{5.13}$$

As the pendulum analysis suggests, it *is* possible to have instability with $n_{\nu_e} = n_{\bar{\nu}_e}$, but for the convenience of working with dimensionless ratios whose meanings are fairly transparent, we assume that the number densities are not extremely close in value. Since $\sqrt{2}G_F(n_{\nu_e} - n_{\bar{\nu}_e})$ only serves to set the time scale, stability is entirely controlled by the parameters $R_{l\geq 1}$.

One virtue of assessing stability in terms of angular moments is that any $I_{j,l}$ (or the equivalent when $\omega \neq 0$) can be evaluated analytically, thereby preserving the singularity structure. The singular feature in this case is a branch cut along the real axis of the complex-Ω plane; it spans the values for which the integrand of $I_{j,l}$ diverges for some $v \in [-1,1]$. By retaining the logarithms in Eq. (5.11), one avoids the unwelcome appearance of spurious instabilities [71]. We suspect that this advantage carries over to nonlinear calculations that directly evolve the angular moments.

As for what the stability analysis reveals, we find that it qualitatively bears out the $\mathbf{D}_1$ pendulum dynamics. The primary features of Fig. 5.3, which presents the regions of instability in three different ways, are all accounted for by Eqs. (5.4) and (5.5). In brief, the main takeaway is that the system is destabilized if the $l = 2$ moment of the νELN has the *opposite* sign to the $l = 0$ moment (because the spin σ is thereby diminished, up to a point) or if the $l = 3$ moment has the *same* sign as the $l = 0$ moment (because then $\mathbf{G}'(0) \cdot \boldsymbol{\delta}'(0) > 0$ and the pendulum is initially inverted). The liminal case $R_2 = 0$ in the leftmost color map is also necessarily stable, because $\mathbf{D}_3$ never becomes nonzero: no gravity, no instability. A related observation can be made about the numerical solution of the nonlinear equations, where we have confirmed that FFC occurs when the system is truncated at $l = 3$ but disappears when the system is truncated at $l = 2$.

While a νELN crossing is commonly believed to be a necessary condition for FFC [21, 23, 24, 28], Fig. 5.3 shows that it is not a sufficient one. An alternative estimate of the unstable region can be obtained by supposing that $\mathbf{D}_3$ is constant. Using conservation of energy and conservation of angular momentum along $\mathbf{D}_3$, we can solve for the southernmost deviation $\theta_{1,\max}$ reached by an initially inverted pendulum [13]:

$$\cos\theta_{1,\max} = \frac{9\sigma^2}{D_1 D_3} - 1. \tag{5.14}$$

Solutions disappear in the stable region of parameter space. In terms of νELN ratios, the system is unstable if

$$R_1 R_3 \geq \frac{5}{72}(1+2R_2)^2. \tag{5.15}$$

In Fig. 5.3 we compare Eq. (5.15) to the exact results from linear stability analysis and to the $|\tilde{v}| \leq 1$ criterion [Eq. (5.10)].

A different stability test was recently proposed in Ref. [25], one which (like $\tilde{v}$) involves only the $l \leq 2$ νELN angular moments. To make contact with that work, we now allow for spatially inhomogeneous collective modes: $S_{E,v} = Q_{E,v}\exp(-i\Omega t + iKr)$. In the linear regime, the only change to the foregoing results is that a term $-Kv$ is added to the denominator of $I_{j,l}$. A central insight of Ref. [25] is that $K = \sqrt{2}G_F(n_{\nu_e} - n_{\bar{\nu}_e})R_1$ cancels the other term proportional to v, turning a transcendental dispersion relation into a quadratic equation. In our notation, they find the instability criterion

$$R_1^2 > \frac{(2+R_2)^2}{9}. \tag{5.16}$$

We plot this result in Fig. 5.3 as well, bearing in mind that it is being compared to the $K = 0$ mode. The comparison should therefore be interpreted with suitable caution. In our view, all of these criteria are complementary, and they are bound to have more or less diagnostic power depending on factors such as the neutrino angular distributions and the spectrum of inhomogeneities.

Continuing in the same vein, we now show that *spatially* growing, steady-state fast modes have pendulum-like behavior built into their equations of motion as well. The replacement for Eq. (5.1) is

$$\dot{\mathbf{P}}_v = \mu \left(\frac{1}{v} \mathbf{D}_0 - \mathbf{D}_1 \right) \times \mathbf{P}_v, \tag{5.17}$$

where $v \neq 0$ and the overdot now denotes a spatial derivative. (Homogeneity along the transverse directions requires that $v = 0$ trajectories exhibit no flavor transformation.) It is again possible to rotate out λ—and we have done so—provided that we work in the nearly homogeneous limit. More precisely, we ignore small-scale fluctuations and assume that the scale heights of λ and μ are much greater than any fast oscillation length, so that the two parameters are approximately constant over the region we consider.

Dividing through by v leads, after taking angular moments, to equations that each contain a derivative of a single l:

$$\dot{\mathbf{P}}_l = -\mu \mathbf{D}_1 \times \mathbf{P}_l + \mu \mathbf{D}_0 \times \sum_{l'=0}^{\infty} \left(l' + \frac{1}{2} \right) c_{ll'} \mathbf{P}_{l'}, \tag{5.18}$$

where

$$c_{ll'} = \int_{-1}^{1} dv \frac{L_l(v) L_{l'}(v)}{v}. \tag{5.19}$$

To make sure the integrals converge, we interpret them as denoting their principal values, or equivalently assert that $\mathbf{P}_v = 0$ at $v = 0$. We presume that the collective modes of the system are not particularly sensitive to the flavor distribution of neutrinos traveling *precisely* transverse to the symmetry axis. From the orthogonality and recursion relations of Legendre polynomials, it follows that

$$c_{ll'} = \begin{cases} \frac{2}{l+1} \prod (-1)^{\frac{l'-2n+1}{l'-2n+2}} & \text{odd } l' > \text{even } l \\ \frac{2}{l} \prod (-1)^{\frac{l'+2n}{l'+2n-1}} & \text{even } l' < \text{odd } l \\ 0 & \text{otherwise.} \end{cases} \tag{5.20}$$

The product in both cases is from $n = 1$ up to $n = (|l - l'| - 1)/2$ and is equal to 1 if $|l - l'| = 1$.

An immediate consequence of Eqs. (5.18) and (5.20) is that $\mathbf{D}_1$ is constant. It is therefore possible to shift to a rotating frame in which the $-\mu\mathbf{D}_1 \times \mathbf{D}_l$ terms drop out. Letting primes denote the new frame, we introduce (or, rather, repurpose) the vectors

$$\begin{aligned} \mathbf{L}' &= -\sum_{l'} \left(l' + \frac{1}{2}\right) c_{0l'} \mathbf{D}'_{l'}, \\ \mathbf{G}' &= \sum_{l',l''} \left(l' + \frac{1}{2}\right)\left(l'' + \frac{1}{2}\right) c_{0l'} c_{l'l''} \mathbf{D}'_{l''}, \\ \boldsymbol{\delta}' &= \frac{\mathbf{D}'_0}{D_0}, \quad \sigma = \boldsymbol{\delta}' \cdot \mathbf{L}', \end{aligned} \tag{5.21}$$

Calculating $\boldsymbol{\delta}' \times \ddot{\boldsymbol{\delta}}'$, we find ourselves back at Eq. (5.4), but with D_1 replaced by D_0. Once again the pendulum's length, spin, and mechanical energy (given by Eq. (5.5) after sending $\mathbf{D}'_1 \to \mathbf{D}'_0$) are all conserved. Besides this replacement, there is another fundamental difference between the temporal and spatial flavor development: Eq. (5.20) tells us that $\mathbf{L}'$ is a superposition of *all* odd moments, whereas $\mathbf{G}'$ is a superposition of *all* even moments. Inhomogeneity brings a host of complications with it, and so we leave for future work the task of exploring numerically how the pendulum-like tendency manifests in spatially evolving collective modes.

The aim of this study has been to extract analytic insights into FFC from the nonlinear equations of motion. The central finding is that the angular-moment equations exhibit a certain pendulum-like structure in the two limits which are most analytically tractable (*viz.*, when the neutrino density is high, the matter background is homogeneous, and the neutrino flavor field is *either homogeneous or stationary*). In general, of course, a flavor field develops both spatially *and* temporally. More work must be done to understand what our finding implies for the full PDE problem.

The analysis presented here opens new paths toward understanding collective oscillations and incorporating their effects into frontline supernova simulations.

5.3 Acknowledgements

We are grateful to David Radice for making the FORNAX data accessible, and to Vincenzo Cirigliano, Pat Diamond, Mark Paris, and David Vartanyan for enlightening discussions. HN acknowledges Taiki Morinaga, Shoichi Yamada and Sherwood Richers for valuable comments and discussions. LJ and GMF acknowledge support from NSF Grant Nos. PHY-1614864 and PHY-1914242, from the Department of Energy Scientific Discovery through Advanced Computing (SciDAC-4) grant register No. SN60152 (award number de-sc0018297), and from the NSF N3AS Hub Grant No. PHY-1630782 and Heising-Simons Foundation Grant No. 2017-22. AB acknowledges support from the U.S. Department of Energy Office of Science and the Office of Advanced Scientific Computing Research via the Scientific Discovery through Advanced Computing (SciDAC4) program and Grant DE-SC0018297 (subaward 00009650). In addition, he acknowledges support from the U.S. NSF under Grants AST-1714267 and PHY-1144374.

This chapter is a reprint of L. Johns, H. Nagakura, G. M. Fuller, and A. Burrows, Phys. Rev. D 101, 043009 (2020). I was the primary investigator and author of this publication.

Bibliography

[1] J. F. Cherry, J. Carlson, A. Friedland, G. M. Fuller, and A. Vlasenko, Phys. Rev. Lett. **108**, 261104 (2012).

[2] G. Raffelt, S. Sarikas, and D. S. Seixas, Phys. Rev. Lett. **111**, 091101 (2013).

[3] S. Chakraborty and A. Mirizzi, Phys. Rev. D **90**, 033004 (2014).

[4] G. Mangano, A. Mirizzi, and N. Saviano, Phys. Rev. D **89**, 073017 (2014).

[5] H. Duan and S. Shalgar, Phys. Lett. B **747**, 139 (2015).

[6] S. Abbar, H. Duan, and S. Shalgar, Phys. Rev. D **92**, 065019 (2015).

[7] S. Abbar and H. Duan, Phys. Lett. B **751**, 43 (2015).

[8] B. Dasgupta and A. Mirizzi, Phys. Rev. D **92**, 125030 (2015).

[9] S. Chakraborty, R. Hansen, I. Izaguirre, and G. Raffelt, Nucl. Phys. **B908**, 366 (2016).

[10] F. Capozzi, B. Dasgupta, E. Lisi, A. Marrone, and A. Mirizzi, Phys. Rev. D **96**, 043016 (2017).

[11] I. Izaguirre, G. Raffelt, and I. Tamborra, Phys. Rev. Lett. **118**, 021101 (2017).

[12] H. Duan, G. M. Fuller, J. Carlson, and Y.-Z. Qian, Phys. Rev. D **74**, 105014 (2006).

[13] S. Hannestad, G. G. Raffelt, G. Sigl, and Y. Y. Y. Wong, Phys. Rev. D **74**, 105010 (2006).

[14] G. Fogli, E. Lisi, A. Marrone, and A. Mirizzi, J. Cosmol. Astropart. Phys. **12**, 010 (2007).

[15] A. Esteban-Pretel, A. Mirizzi, S. Pastor, R. Tomàs, G. G. Raffelt, P. D. Serpico, and G. Sigl, Phys. Rev. D **78**, 085012 (2008).

[16] B. Dasgupta, A. Dighe, G. G. Raffelt, and A. Y. Smirnov, Phys. Rev. Lett. **103**, 051105 (2009).

[17] H. Duan, G. M. Fuller, and Y.-Z. Qian, Ann. Rev. Nucl. Part. Sci. **60**, 569 (2010).

[18] B. Dasgupta, E. P. O'Connor, and C. D. Ott, Phys. Rev. D **85**, 065008 (2012).

[19] R. F. Sawyer, Phys. Rev. D **72**, 045003 (2005).

[20] R. F. Sawyer, Phys. Rev. D **79**, 105003 (2009).

[21] R. F. Sawyer, Phys. Rev. Lett. **116**, 081101 (2016).

[22] S. Chakraborty, R. S. Hansen, I. Izaguirre, and G. Raffelt, J. Cosmol. Astropart. Phys. **2016**, 028 (2016).

[23] S. Chakraborty, R. S. Hansen, I. Izaguirre, and G. Raffelt, J. Cosmol. Astropart. Phys. **2016**, 042 (2016).

[24] B. Dasgupta, A. Mirizzi, and M. Sen, J. Cosmol. Astropart. Phys. **2017**, 019 (2017).

[25] B. Dasgupta, A. Mirizzi, and M. Sen, Phys. Rev. D **98**, 103001 (2018).

[26] B. Dasgupta and M. Sen, Phys. Rev. D **97**, 023017 (2018).

[27] S. Airen, F. Capozzi, S. Chakraborty, B. Dasgupta, G. Raffelt, and T. Stirner, J. Cosmol. Astropart. Phys. **2018**, 019 (2018).

[28] S. Abbar and H. Duan, Phys. Rev. D **98**, 043014 (2018).

[29] S. Abbar and M. C. Volpe, Phys. Lett. B **790**, 545 (2019).

[30] F. Capozzi, B. Dasgupta, A. Mirizzi, M. Sen, and G. Sigl, Phys. Rev. Lett. **122**, 091101 (2019).

[31] F. Capozzi, G. Raffelt, and T. Stirner, J. Cosmol. Astropart. Phys. **2019**, 002 (2019).

[32] C. Yi, L. Ma, J. D. Martin, and H. Duan, Phys. Rev. D **99**, 063005 (2019).

[33] J. D. Martin, C. Yi, and H. Duan, arXiv:1909.05225 (2019).

[34] M. Chakraborty and S. Chakraborty, arXiv:1909.10420 (2019).

[35] I. Tamborra, F. Hanke, H.-T. Janka, B. Müller, G. G. Raffelt, and A. Marek, Astrophys. J. **792**, 96 (2014).

[36] L. Walk, I. Tamborra, H.-T. Janka, and A. Summa, Phys. Rev. D **98**, 123001 (2018).

[37] E. P. O'Connor and S. M. Couch, Astrophys. J. **865**, 81 (2018).

[38] D. Vartanyan, A. Burrows, D. Radice, M. A. Skinner, and J. Dolence, Mon. Not. R. Astron. Soc. **477**, 3091 (2018).

[39] R. Glas, H.-T. Janka, T. Melson, G. Stockinger, and O. Just, Astrophys. J. **881**, 36 (2019).

[40] D. Vartanyan, A. Burrows, and D. Radice, Mon. Not. R. Astron. Soc. **489**, 2227 (2019).

[41] L. Walk, I. Tamborra, H.-T. Janka, and A. Summa, arXiv:1901.06235 (2019).

[42] T. Morinaga, H. Nagakura, C. Kato, and S. Yamada, arXiv:1909.13131 (2019).

[43] I. Tamborra, L. Hüdepohl, G. G. Raffelt, and H.-T. Janka, Astrophys. J. **839**, 132 (2017).

[44] S. Abbar, H. Duan, K. Sumiyoshi, T. Takiwaki, and M. C. Volpe, Phys. Rev. D **100**, 043004 (2019).

[45] M. Delfan Azari, S. Yamada, T. Morinaga, W. Iwakami, H. Okawa, H. Nagakura, and K. Sumiyoshi, Phys. Rev. D **99**, 103011 (2019).

[46] S. Shalgar and I. Tamborra, arXiv:1904.07236 (2019).

[47] H. Nagakura, T. Morinaga, C. Kato, and S. Yamada, arXiv:1910.04288 (2019).

[48] G. Fuller, R. Mayle, J. Wilson, and D. Schramm, Astrophys. J. **322**, 795 (1987).

[49] G. M. Fuller, R. Mayle, B. S. Meyer, and J. R. Wilson, Astrophys. J. **389**, 517 (1992).

[50] T. A. Thompson, A. Burrows, and P. A. Pinto, Astrophys. J. **592**, 434 (2003).

[51] C. D. Ott, A. Burrows, L. Dessart, and E. Livne, Astrophys. J. **685**, 1069 (2008).

[52] H. Nagakura, W. Iwakami, S. Furusawa, H. Okawa, A. Harada, K. Sumiyoshi, S. Yamada, H. Matsufuru, and A. Imakura, Astrophys. J. **854**, 136 (2018).

[53] A. Harada, H. Nagakura, W. Iwakami, H. Okawa, S. Furusawa, H. Matsufuru, K. Sumiyoshi, and S. Yamada, Astrophys. J. **872**, 181 (2019).

[54] P. Strack and A. Burrows, Phys. Rev. D **71**, 093004 (2005).

[55] Y. Zhang and A. Burrows, Phys. Rev. D **88**, 105009 (2013).

[56] D. Nötzold and G. Raffelt, Nucl. Phys. **B307**, 924 (1988).

[57] C. Volpe, D. Väänänen, and C. Espinoza, Phys. Rev. D **87**, 113010 (2013).

[58] A. Vlasenko, G. M. Fuller, and V. Cirigliano, Phys. Rev. D **89**, 105004 (2014).

[59] A. Kartavtsev, G. Raffelt, and H. Vogel, Phys. Rev. D **91**, 125020 (2015).

[60] S. A. Richers, G. C. McLaughlin, J. P. Kneller, and A. Vlasenko, Phys. Rev. D **99**, 123014 (2019).

[61] C. J. Stapleford, C. Fröhlich, and J. P. Kneller, arXiv:1910.04172 (2019).

[62] G. G. Raffelt and G. Sigl, Phys. Rev. D **75**, 083002 (2007).

[63] H. Duan and S. Shalgar, J. Cosmol. Astropart. Phys. **2014**, 084 (2014).

[64] D. Radice, A. Burrows, D. Vartanyan, M. A. Skinner, and J. C. Dolence, Astrophys. J. **850**, 43 (2017).

[65] M. A. Skinner, J. C. Dolence, A. Burrows, D. Radice, and D. Vartanyan, Astrophys. J. Suppl. Ser. **241**, 7 (2019).

[66] T. Sukhbold, T. Ertl, S. E. Woosley, J. M. Brown, and H.-T. Janka, Astrophys. J. **821**, 38 (2016).

[67] N. Vaytet, E. Audit, B. Dubroca, and F. Delahaye, J. Quant. Spectrosc. Radiat. Transfer **112**, 1323 (2011).

[68] H. Duan, G. M. Fuller, J. Carlson, and Y.-Z. Qian, Phys. Rev. D **75**, 125005 (2007).

[69] L. Johns and G. M. Fuller, Phys. Rev. D **97**, 023020 (2018).

[70] A. Banerjee, A. Dighe, and G. Raffelt, Phys. Rev. D **84**, 053013 (2011).

[71] T. Morinaga and S. Yamada, Phys. Rev. D **97**, 023024 (2018).

Chapter 6

Derivation of the sterile neutrino Boltzmann equation from quantum kinetics

6.1 Abstract

An extensive, growing body of work has been penned on cosmologies that include one or more sterile neutrinos. Early entries in the literature formulated a Boltzmann-like equation describing sterile-neutrino production in a way that bypasses the numerical tracking of high-frequency complex phases, and meticulous quantum-kinetic analyses shortly thereafter put the formula on firmer ground. A new and more direct derivation is given here, showing that the equation follows almost immediately from a quantum relaxation-time approximation and an expansion in the mixing angle. Besides reproducing the desired result, the relaxation ansatz captures to a high degree of accuracy the interlaced dynamics of oscillations, decoherence, and plasma repopulation. Successes and limitations of the semiclassical equation are illustrated numerically and are shown to reflect the accuracy of the approximations employed in the derivation. The

inclusion of interactions among the sterile neutrinos is also briefly addressed.

6.2 Introduction

Sterile neutrinos continue to be actively studied as sources of oscillation anomalies, as reconcilers of cosmic tensions, and as candidates for dark matter. In all these cases the cosmological abundance must be calculated, and so the dynamics of active–sterile mixing must be contended with. The essential challenge is that the full quantum-kinetic problem involves disparate time scales and the interplay of coherent ($\propto G_F$) and incoherent ($\propto G_F^2$) effects.

A Boltzmann-like equation is often used to calculate the nonthermal abundance of sterile neutrinos produced from active ones [1–3]:

$$\frac{df_s}{dt} = \frac{\Gamma_a}{4} \frac{\sin^2 2\theta_m}{1 + \left(\frac{\Gamma_a}{2\omega_m}\right)^2} (f_a - f_s) \,, \tag{6.1}$$

where $f_{a(s)}$ is the active (sterile) distribution function, Γ_a is the scattering rate of active neutrinos, and θ_m and ω_m are the in-medium mixing angle and oscillation frequency. (We suppress dependence on momentum here and throughout.) Eq. (6.1) is a semiclassical approximation of the quantum kinetic equation (QKE) [4–12]

$$i\frac{d\rho}{dt} = [H, \rho] + iC \tag{6.2}$$

for the density matrix ρ. Its computational appeal lies in the fact that, by packaging together the effects of the Hamiltonian H and collision term C as a single effective production rate, one can overlook the quantum phases and evolve only the classical densities.

The first derivations of Eq. (6.1) (or variations of it) were based on single-particle arguments that equated the ν_s production rate with the product of the ν_a scattering rate and the probability of a ν_a oscillating into a ν_s [1, 2]. Later analyses hearteningly arrived at similar

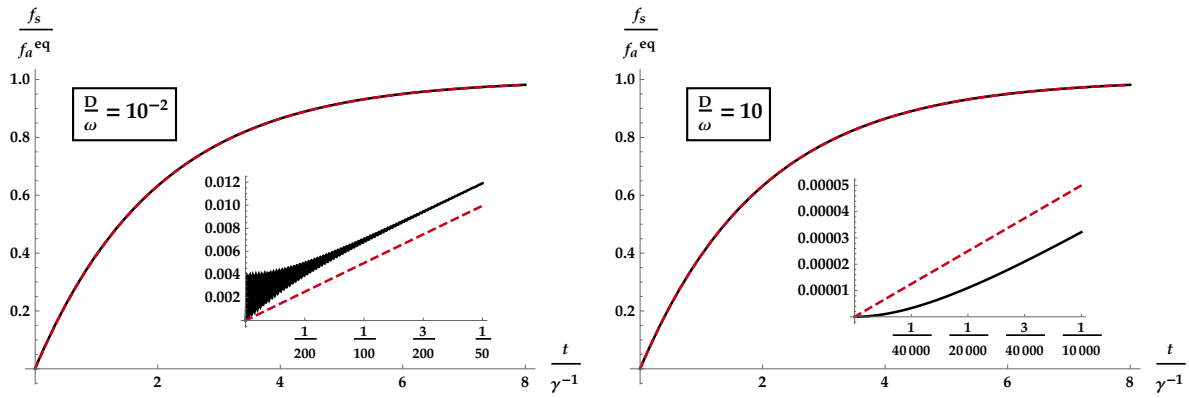

Figure 6.1: Comparison of the Boltzmann [Eq. (6.1); dashed red curve] and QKE [Eqs. (6.8); black] solutions for $f_s(t)$. The latter solution uses the conversion $f_s = P_0(1-P_z)/2$. The mixing angle is small: $\theta = \pi/100$. Insets show the same curves on shorter time scales. On γ^{-1} time scales the curves are indistinguishable by eye.

formulas working from quantum-kinetic descriptions and judiciously applying approximations for the evolution in flavor space [13–20]. Our purpose here is to add another entry to the list, one that is complementary to the references just cited and whose virtue is the insight it gives into the quantum dynamics underlying the semiclassical behavior. Given the ongoing interest in sterile neutrinos, having a robust simplification of the quantum dynamics may prove useful for future applications. The guiding idea, which we support numerically, is that the evolution of ρ at small mixing angle is well described by the exponential decay of its deviations from equilibrium. As we demonstrate below, this simple ansatz leads promptly to Eq. (6.1).

In Sec. 6.3 we go through the derivation and discuss it in the context of other treatments. In Sec. 6.4 we present numerical comparisons of the Boltzmann and QKE solutions, highlighting the accuracy not only of Eq. (6.1) but also of the ansatz on which it is based. In Sec. 6.5 we conclude.

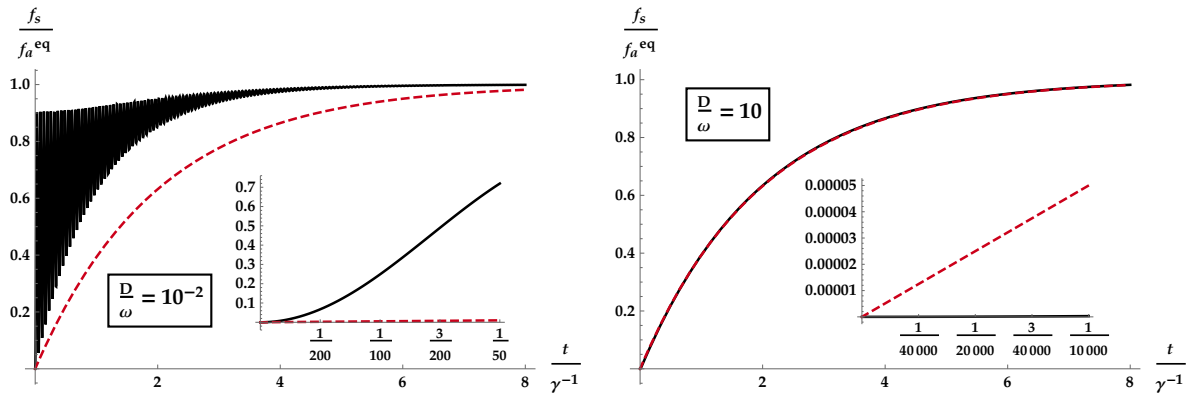

Figure 6.2: Same as Fig. 6.1 but here the mixing angle is *not* small: $\theta = \pi/5$. Unlike in the small-θ case, strong damping is necessary to coerce ρ toward the Boltzmann solution. Early-time discrepancy is magnified compared to Fig. 6.1.

6.3 Derivation

We begin by applying the quantum relaxation-time approximation to the collision term [5, 16, 21, 22]:

$$iC = \left\{ i\Gamma, \rho_C^{\rm eq} - \rho \right\}, \tag{6.3}$$

where $\Gamma = (1/2)\,\mathrm{diag}(\Gamma_a, \Gamma_s)$ and $\rho_C^{\rm eq}$ is the $H = 0$ equilibrium. If the states do not mix, then the *classical* relaxation-time approximation is recovered, and the densities f_a and f_s approach their equilibrium values with time scales Γ_a^{-1} and Γ_s^{-1} respectively. We posit that the same approximation applies to the entire right-hand side of Eq. (6.2), with a single effective relaxation parameter replacing the individual scattering rates and the flavor equilibrium $\rho_F^{\rm eq}$ replacing the classical equilibrium. That is,

$$i\frac{d\rho}{dt} = \left\{ i\Gamma_{\rm eff}, \rho_F^{\rm eq} - \rho \right\}, \tag{6.4}$$

with $\Gamma_{\rm eff} = (\gamma_m/4)\,\mathrm{diag}\,(1,1)$. (The extra factor of $1/2$ is added as a matter of preference.) Hence

$$\frac{d\rho}{dt} = \frac{\gamma_m}{2}\left(\rho_F^{\rm eq} - \rho\right), \tag{6.5}$$

and in particular

$$\frac{df_s}{dt} = \frac{\gamma_m}{2}\left(f_a^{\rm eq} - f_s\right). \tag{6.6}$$

If the mixing angle is small, $f_a^{\rm eq}$ can safely be replaced in this equation by f_a.

Using $\rho = P_0\left(1 + \mathbf{P}\cdot\boldsymbol{\sigma}\right)/2$, it follows from Eq. (6.5) that the polarization vector obeys

$$\begin{aligned}\frac{dP_0}{dt} &= \frac{\gamma_m}{2}\left(2f_a^{\rm eq} - P_0\right),\\ \frac{d\mathbf{P}}{dt} &= -\gamma_m\frac{f_a^{\rm eq}}{P_0}\mathbf{P}.\end{aligned} \tag{6.7}$$

At the same time, using $H = (\omega_m/2)B_m$ and setting $\Gamma_s = 0$, Eqs. (6.2) and (6.3) imply

$$\begin{aligned}\frac{dP_0}{dt} &= 2D\left(f_a^{\rm eq} - P_0\frac{1+P_z}{2}\right)\\ \frac{d\mathbf{P}}{dt} &= \omega_m\mathbf{B}_m\times\mathbf{P} - D\mathbf{P}_T - \frac{\dot{P}_0}{P_0}\mathbf{P} + \frac{\dot{P}_0}{P_0}\mathbf{z},\end{aligned} \tag{6.8}$$

where $D = \Gamma_a/2$ is the decoherence rate and $\mathbf{B}_m = \sin 2\theta_m\mathbf{x} - \cos 2\theta_m\mathbf{z}$. The ansatz tells us that Eqs. (6.7) and Eqs. (6.8) can be set equal to each other at any moment in the evolution. For the sake of extracting γ_m, we choose to equate them prior to significant sterile production, during which time $\mathbf{P}$ nearly equals $\mathbf{z}$ and P_0 and f_a nearly equal $f_a^{\rm eq}$. To first order in the deviations, $\mathbf{P}$ satisfies the eigenvalue equation

$$\omega_m\mathbf{B}_m\times\mathbf{P} - D\mathbf{P}_T = -\gamma_m\mathbf{P}. \tag{6.9}$$

Nontrivial solutions of Eq. (6.9) correspond to roots of the cubic equation

$$\gamma_m^3 - 2D\gamma_m^2 + \left(D^2 + \omega_m^2\right)\gamma_m - D\omega_m^2\sin^2 2\theta_m = 0. \tag{6.10}$$

Applying perturbation theory to zeroth order in $\sin^2 2\theta_m$ uncovers two of the roots, with values

$D \pm i\omega_m$. The third root, which is the purely real one that we seek, appears at first order:

$$\gamma_m = \frac{D\omega_m^2 \sin^2 2\theta_m}{\omega_m^2 + D^2} \tag{6.11}$$

Plugging this into Eq. (6.6), we arrive at Eq. (6.1) as desired.

The analysis applies just as well to antineutrinos (or the right-handed states, if Majorana) as it does to neutrinos (or the left-handed states). If chemical potentials are involved in the dynamics, they are simply incorporated into the equilibrium distribution functions.

Eq. (6.9) was also considered in Ref. [4] (albeit not in the context of sterile neutrinos), Ref. [20] (albeit in a somewhat different form), and Refs. [13, 16, 17]. The last two were part of a series, along with Refs. [14, 15, 18, 19], that provided significant insights into the dynamics of active–sterile oscillations. Vital to the derivation developed in those works is the approximation $dP_0/dt = 0$, which was carefully shown in Ref. [19] to be justified despite its inconsistency with f_a remaining near equilibrium during sterile production. We similarly find that the correct value of γ_m is obtained by dropping the repopulation terms from the equation of motion obeyed by $\mathbf{P}$, even though repopulation is crucial for accurately describing the evolution of the system as a whole. Our findings, based on the quantum relaxation-time approximation, are consistent in this regard with those of Ref. [19], based (in the words of the authors) on the "brute-force" approach.

Besides reproducing Eq. (6.1) with minimal effort, the preceding analysis also has the advantage of pointing to a deeper physical picture: the small-θ_m dynamics is dominated by a flavor-space trajectory in which nonequilibrium deviations $\rho_F^{\text{eq}} - \rho$ decay with (instantaneous) lifetime $2/\gamma_m$. Moreover, as we show in the next section, this approach sacrifices little in the way of accuracy for what it gains in simplicity.

But before moving on to the numerical analysis, let us briefly comment on the generalization to scenarios in which sterile neutrinos remain inert under the Standard Model couplings but

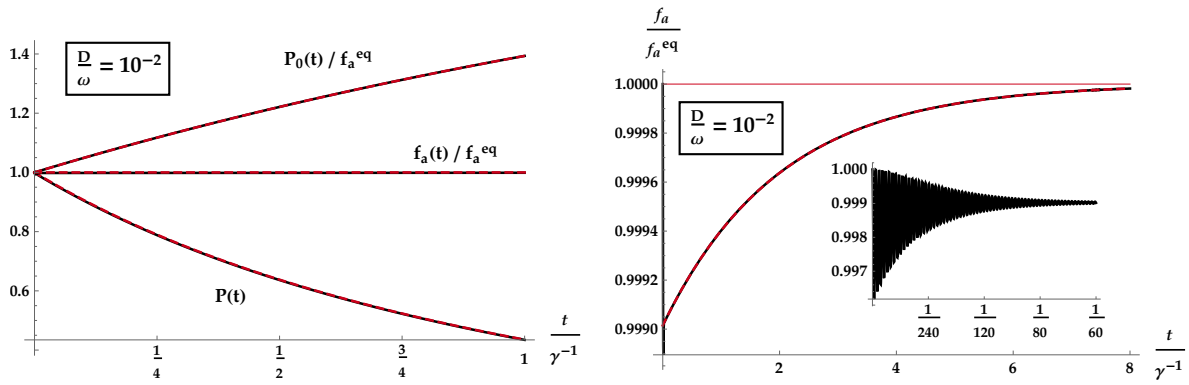

Figure 6.3: Comparison of the relaxation [Eq. (6.5); dashed, red curve] and QKE [Eq. (6.2); black] solutions for $P_0(t)$, $f_a(t)$, and $P(t) = |\mathbf{P}(t)|$. The thin red line in the right panel denotes the equilibrium value. The onset time of the relaxation solution is fit by hand.

interact via new ones. Reinstating $\Gamma_s \neq 0$ in Eq. (6.3) leads to

$$\frac{dP_0}{dt} = 2D_a\left(f_a^{\rm eq} - P_0\frac{1+P_z}{2}\right) + 2D_s\left(f_s^{\rm eq} - P_0\frac{1-P_z}{2}\right)$$
$$\frac{d\mathbf{P}}{dt} = \omega_m\mathbf{B}_m\times\mathbf{P} - (D_a+D_s)\,\mathbf{P}_T - \frac{\dot{P}_0}{P_0}\mathbf{P} + \left[2D_a\left(f_a^{\rm eq} - P_0\frac{1+P_z}{2}\right) - 2D_s\left(f_s^{\rm eq} - P_0\frac{1-P_z}{2}\right)\right]\mathbf{z}, \tag{6.12}$$

where $D_{a,s} = \Gamma_{a,s}/2$ and $f_s^{\rm eq}$ denotes the equilibrium that f_s tends toward if the mixing is turned off. Because repopulation of f_s drives $\mathbf{P}$ toward $-\mathbf{z}$, the net effect of repopulation on $\mathbf{P}$ no longer takes the second-order form $(\dot{P}_0/P_0)(\mathbf{z}-\mathbf{P})$.

However, suppose that Γ_s is much faster than the active–sterile conversion rate. In that case f_s is always very close to $f_s^{\rm eq}$ on the conversion time scale, and the new repopulation terms can once again be dropped from the equations so long as f_s is consistently interpreted as being at the sterile-sector equilibrium value. The same relaxation ansatz can then be used as before, again leading to Eq. (6.9). The only difference now is that the decoherence rate in the expression for γ_m should be interpreted as the sum $D_a + D_s$, in agreement with Refs. [23–25]. Note that the distinction between $\rho_C^{\rm eq}$ and $\rho_F^{\rm eq}$ is generally important to make, but is rendered moot when $\Gamma_s = 0$.

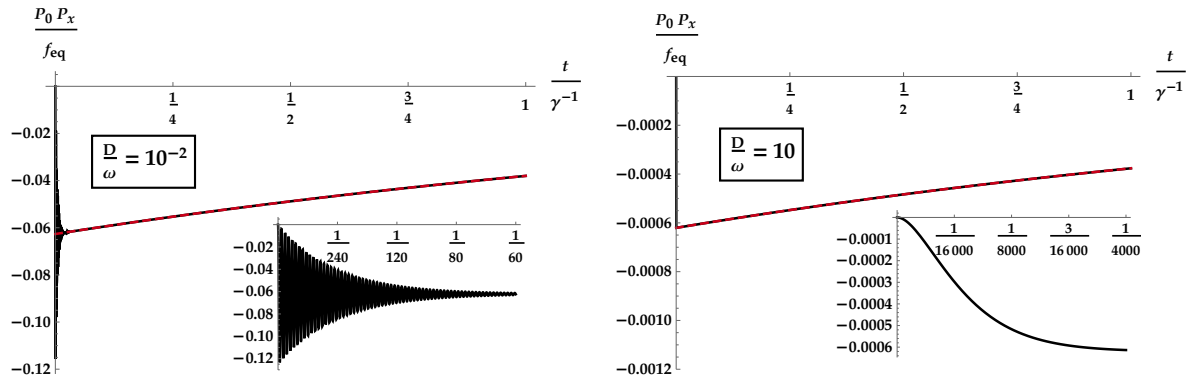

Figure 6.4: Comparison of the relaxation [Eq. (6.5); dashed, red curve] and QKE [Eq. (6.2); black] solutions for $P_0(t)P_x(t) = \rho_{as}(t) + \rho_{sa}(t)$. As in Fig. 6.3, the onset time of the relaxation solution is fit by hand.

6.4 Numerical analysis

In this section we numerically study the validity of the quantum relaxation-time approximation, including the sterile neutrino Boltzmann equation implied by it. For simplicity we begin by assuming time-independent mixing and scattering parameters ω, $\sin^2 2\theta$, and D. We then go on to introduce a time-dependent potential and follow the system through resonance.

Fig. 6.1 compares the solutions of the Boltzmann equation [Eq. (6.1)] and the QKEs [Eqs. (6.8)] for two choices of the ratio D/ω. In both cases the mixing angle is taken to be $\theta = \pi/100$, and in the Boltzmann equation f_a is always set equal to $f_a^{\rm eq}$. The insets show that the solutions are discrepant at very early times before the QKE solution settles into the decay mode [Eq. (6.6)] on which the Boltzmann equation is based. Once it does so, both solutions grow linearly in time, as expected when $f_s \ll f_a^{\rm eq}$. As production proceeds, the early-time discrepancy becomes less important as a fraction of the sterile abundance, and on times longer than γ^{-1} the evolution as a function of $t' = \gamma t$ is virtually independent of the chosen parameters:

$$f_s(t') = f_a^{\rm eq}\left(1 - e^{-\frac{t'}{2}}\right). \tag{6.13}$$

For cosmological applications it is typically undesirable to have the density of sterile

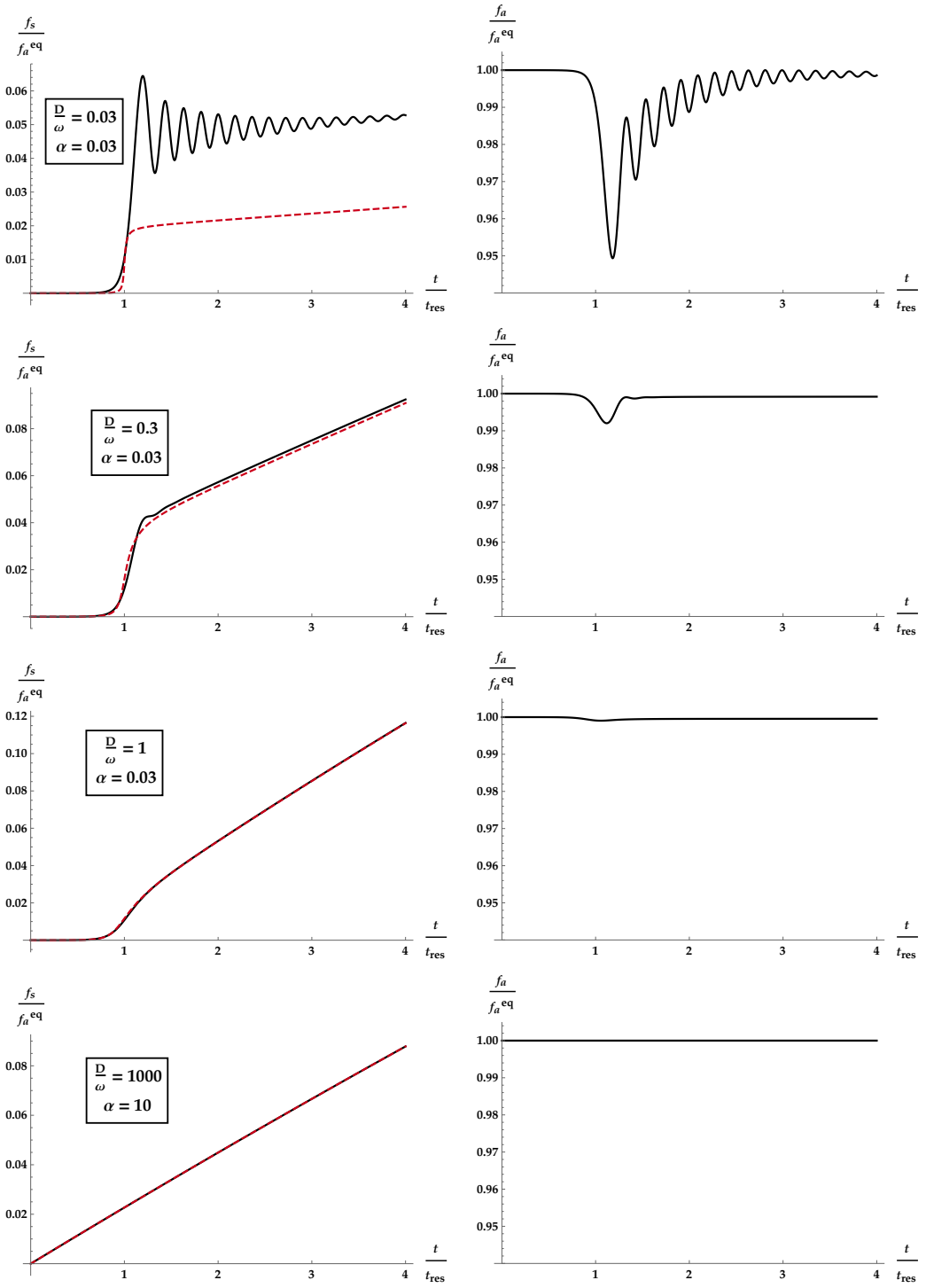

Figure 6.5: Left panels: Comparison of the Boltzmann and QKE solutions for $f_s(t)$ in the presence of a time-dependent potential $V(t) = V_0 e^{-\nu t}$. Right panels: QKE solution for $f_a(t)$; the Boltzmann solution (not shown) is simply $f_a(t) = f_a^{\rm eq}$. Unlike in the previous figures, time is plotted in units of $t_{\rm res}$, defined by $\omega \cos 2\theta = V(t_{\rm res})$. From top to bottom, the coherence parameter κ is 4.4, 0.44, 0.13, and 4.0×10^{-7}.

neutrinos approach the thermal value, and the insets in Fig. 6.1 are therefore the relevant comparison. Achieving agreement on these shorter time scales requires θ to be small. Fig. 6.2 illustrates this point: the same quantities are plotted here as in Fig. 6.1, but now with $\theta = \pi/5$. Early-time discrepancies are greatly exacerbated.

The relaxation ansatz asserts that f_a should decay exponentially toward $f_a^{\rm eq}$. Since a small mixing angle inhibits f_a from ever deviating greatly from the equilibrium value, the ansatz also implies a delicate near-cancellation between the growth of P_0 and the decay of $P = |\mathbf{P}|$. Fig. 6.3 verifies that both of these expectations are indeed borne out in the case $D/\omega = 10^{-2}$. The result is similar for stronger damping.

Interestingly, it was shown in Ref. [26] that the Boltzmann equation can be derived from the assumption that ρ_{as} and ρ_{sa} are both constant. Despite its expedience, that approximation is not an accurate description of how the active-sterile coherence develops, particularly on a γ^{-1} time scale. Fig. 6.4 shows that in fact the real part declines throughout production and is well fit by the relaxation ansatz. The imaginary part is similar.

Cosmological production of sterile neutrinos involves time-dependent parameters of course, and many scenarios of interest involve resonant mixing in particular [25, 27–33]. It is well-known that the Boltzmann equation is inadequate when the system passes adiabatically and coherently through a resonance [28, 30, 34]. To illustrate this claim, and to make a connection with the foregoing analysis, we add a potential $V(t)\mathbf{z}$ to $\omega\mathbf{B}$, with

$$V(t) = V_0 e^{-\nu t}. \tag{6.14}$$

The adiabaticity parameter [34] is defined to be

$$\alpha = \omega\mathcal{H}\sin 2\theta \tan 2\theta, \tag{6.15}$$

where $\mathcal{H}$ is the potential scale height,

$$\mathcal{H} = \left| \frac{1}{V} \frac{dV}{dt} \right|^{-1} = \frac{1}{\nu}. \tag{6.16}$$

We also define $\kappa = D^{-1}/\mathcal{H}$, or in terms of the adiabaticity,

$$\kappa = \frac{\omega}{D} \frac{\sin 2\theta \tan 2\theta}{\alpha} \tag{6.17}$$

While α—proportional to the number of *oscillation lengths* that fit within a resonance width—sets the probability of a neutrino coherently transitioning between energy eigenstates at resonance, the coherence parameter κ—the number of *mean free paths* that fit within a resonance width—indicates the degree to which scattering affects the evolution.

In Fig. 6.5 we compare the Boltzmann and QKE solutions for several choices of D/ω and α. Each panel on the right shows $f_a(t)$ calculated with the same parameters used in the panel to its left. The extent to which f_a dips away from the equilibrium value at resonance indicates the inapplicability of the relaxation ansatz during this period of production. The top three rows show nonadiabatic resonances with increasing rates of decoherence. The bottom row shows an adiabatic resonance with a very large decoherence rate. Regardless of the adiabaticity, production through the resonance is flattened out as D/ω increases, and the accuracy of the Boltzmann solution improves. The key to the Boltzmann equation being a valid approximation is always that κ be small, to ensure that the relaxation ansatz for ρ is not too badly violated at resonance.

6.5 Summary

A few different derivations of the sterile neutrino Boltzmann equation can be found in the literature. Aside from its simplicity, the relaxation-time approach is notable in that it is based on an accurate description of the full quantum dynamics of active–sterile mixing. Replicating

Eq. (6.1) is one implication, but the approximation describes equally well the repopulation of the active species and the decay of coherence.

We have numerically shown that the limitations of Eq. (6.1) reflect the assumptions used here to derive it: the Boltzmann solution works best when θ_m is small, and it comes up short when resonance coherently steers the system away from relaxation. Cosmological sterile-neutrino production is just one scenario of interest that is covered, at least partially, by this range of validity. A similar analysis can be applied to the mixing of active states in the presence of unequal chemical potentials—a circumstance that is realized in supernovae, binary neutron-star mergers, and possibly the early universe. In light of the computational obstacles faced in these environments, there is a clear need for good quantum-kinetic approximations.

6.6 Acknowledgments

The author gratefully acknowledges conversations with Daniel Blaschke, Vincenzo Cirigliano, George Fuller, Evan Grohs, Chad Kishimoto, Mark Paris, and Shashank Shalgar. This work was supported by NSF Grant No. PHY-1614864.

This chapter is a reprint of L. Johns, Phys. Rev. D 100, 083536 (2019). I was the sole investigator and author of this publication.

Bibliography

[1] K. Kainulainen, Phys. Lett. B **244**, 191 (1990).

[2] J. M. Cline, Phys. Rev. Lett. **68**, 3137 (1992).

[3] S. Dodelson and L. M. Widrow, Phys. Rev. Lett. **72**, 17 (1994).

[4] L. Stodolsky, Phys. Rev. D **36**, 2273 (1987).

[5] B. H. J. McKellar and M. J. Thomson, Phys. Rev. D **49**, 2710 (1994).

[6] K. Enqvist, K. Kainulainen, and J. Maalampi, Phys. Lett. B **244**, 186 (1990).

[7] K. Enqvist, K. Kainulainen, and J. Maalampi, Nucl. Phys. B **349**, 754 (1991).

[8] G. Raffelt, G. Sigl, and L. Stodolsky, Phys. Rev. Lett. **70**, 2363 (1993).

[9] G. Sigl and G. Raffelt, Nucl. Phys. **B406**, 423 (1993).

[10] P. Strack and A. Burrows, Phys. Rev. D **71**, 093004 (2005).

[11] D. Boyanovsky and C.-M. Ho, J. High Energy Phys. **2007**, 030 (2007).

[12] A. Vlasenko, G. M. Fuller, and V. Cirigliano, Phys. Rev. D **89**, 105004 (2014).

[13] X. Shi, Phys. Rev. D **54**, 2753 (1996).

[14] R. Foot, M. J. Thomson, and R. R. Volkas, Phys. Rev. D **53**, R5349 (1996).

[15] R. Foot and R. R. Volkas, Phys. Rev. D **55**, 5147 (1997).

[16] N. F. Bell, R. R. Volkas, and Y. Y. Y. Wong, Phys. Rev. D **59**, 113001 (1999).

[17] R. R. Volkas and Y. Y. Y. Wong, Phys. Rev. D **62**, 093024 (2000).

[18] P. Di Bari and R. Foot, Phys. Rev. D **61**, 105012 (2000).

[19] K. S. M. Lee, R. R. Volkas, and Y. Y. Y. Wong, Phys. Rev. D **62**, 093025 (2000).

[20] A. D. Dolgov, S. H. Hansen, S. Pastor, and D. V. Semikoz, Astropart. Phys. **14**, 79 (2000).

[21] A. D. Dolgov, Nucl. Phys. **B610**, 411 (2001).

[22] S. Hannestad, R. S. Hansen, T. Tram, and Y. Y. Wong, J. Cosmol. Astropart. Phys. **2015**, 019 (2015).

[23] S. Hannestad, R. S. Hansen, and T. Tram, Phys. Rev. Lett. **112**, 031802 (2014).

[24] M. Archidiacono, S. Hannestad, R. S. Hansen, and T. Tram, Phys. Rev. D **91**, 065021 (2015).

[25] L. Johns and G. M. Fuller, Phys. Rev. D **100**, 023533 (2019).

[26] A. D. Dolgov, Phys. Rept. **370**, 333 (2002).

[27] X. Shi and G. M. Fuller, Phys. Rev. Lett. **82**, 2832 (1999).

[28] K. Abazajian, G. M. Fuller, and M. Patel, Phys. Rev. D **64**, 023501 (2001).

[29] K. N. Abazajian, Phys. Rev. Lett. **112**, 161303 (2014).

[30] C. T. Kishimoto and G. M. Fuller, Phys. Rev. D **78**, 023524 (2008).

[31] T. Venumadhav, F.-Y. Cyr-Racine, K. N. Abazajian, and C. M. Hirata, Phys. Rev. D **94**, 043515 (2016).

[32] L. Johns, M. Mina, V. Cirigliano, M. W. Paris, and G. M. Fuller, Phys. Rev. D **94**, 083505 (2016).

[33] L. Johns and G. M. Fuller, Phys. Rev. D **97**, 023020 (2018).

[34] K. Abazajian, N. F. Bell, G. M. Fuller, and Y. Y. Y. Wong, Phys. Rev. D **72**, 063004 (2005).

Chapter 7

Self-interacting sterile neutrino dark matter: the heavy-mediator case

7.1 Abstract

For active–sterile mixing to be responsible for the full relic abundance of dark matter additional new physics is needed beyond the keV-scale sterile neutrino itself. The extra ingredient we consider here is the presence of self-interactions among the sterile neutrinos. We examine whether active-to-sterile conversion is amplified enough in this scenario that the observed abundance of dark matter can be obtained with a subconstraint mixing angle. This turns out never to be the case in the region we explore: either self-interactions have too small an impact and cannot escape bounds on the mass and mixing angle, or they have too great an impact and cause dark matter to be overproduced. The sharp transition from marginal to excessive effectiveness occurs because a resonance criterion is met in the effective in-medium mixing angle. Once the system goes resonant the game is as good as over, as nonlinearity in the Boltzmann equation leads to runaway production of sterile neutrinos, beginning at a plasma temperature of a few hundred MeV and typically ending at a few tens of MeV. The scenario is therefore ruled out largely by its

own dynamics. In this study we focus exclusively on mediators heavier than ~ 1 GeV; future work will extend the analysis to lighter mediators, allowing for contact to be made with the kinds of scenarios motivated by issues of small-scale structure.

7.2 Introduction

Dark matter has thus far refused to cooperate with the intense experimental efforts to detect it, inspiring many physicists to broaden the search. A great deal of energy in recent years—sometimes motivated by dark matter, sometimes not—has gone toward sterile neutrinos, toward self-interacting dark sectors, and occasionally toward the overlap. We work here in the spirit of an expansive assessment of dark matter candidates, asking how production is affected when the paradigms of sterile neutrinos and self-interactions intersect.

There is good reason to think nonminimally about sterile neutrino dark matter. The simplest scenario [1], in which sterile neutrinos are the only beyond-Standard-Model (BSM) physics and are populated by their mixing with the active states, is strongly disfavored by observations [2–5]. X-ray and γ-ray experiments, which look for monochromatic photons from sterile-neutrino decay, bound the mixing angle from above [6–13], and a number of structure-related probes, including phase space, subhalo counts, the Lyman-α forest, and reionization history, bound the mass from below [14–24]. The combination of these constraints has made it necessary to look beyond the classic Dodelson–Widrow mechanism if one wants sterile neutrinos to comprise all of the dark matter observed in the universe.

Several alternative ways of producing the sterile neutrinos have been proposed, all sharing in common the fact that they invoke at least one additional piece of new physics aside from the sterile neutrino itself. Some of these scenarios amplify production by methods unrelated to active–sterile mixing, as when sterile neutrinos appear as decay products of another new particle [25–28], when an overabundant population of sterile neutrinos is diluted by new sources

of entropy [29], or when sterile neutrinos undergo thermalization [30] or a SIMP-like freeze-out [31]. Other scenarios alter the mixing itself, as when the vacuum parameters are mediated by an axionlike [32] or scalar [33, 34] field or when a large cosmic lepton number alters the effective in-medium mixing angle [35–40]. The last of these, known as the Shi–Fuller mechanism, has garnered perhaps the most attention among the alternatives, especially in the years following the first detections of an unidentified X-ray line near 3.5 keV in the spectra of various galaxies and galaxy clusters [41, 42]. Whether this line can be attributed to the radiative decay of sterile neutrinos remains contentious, but forthcoming instruments with high energy resolution will put it definitively to the test [43–45].

We consider an alternative to the Dodelson–Widrow scenario in which production is facilitated by interactions in the sterile sector. The effect of self-interactions is twofold: First, the nonzero interaction rate of sterile neutrinos boosts the rate of decoherence, which in turn enhances the transition rate from active to sterile. Second, the nonzero coherent scattering of sterile neutrinos modifies the dispersion relation of neutrinos in the plasma, increasing the effective in-medium mixing angle. The two factors—larger scattering rate and stronger mixing—work in the same direction, suggesting the possibility that, at the expense of introducing self-interactions, the observed abundance of dark matter might be generated with a much smaller vacuum mixing angle than is needed in Dodelson–Widrow. The similarities with Shi–Fuller, moreover, suggest that self-interacting sterile neutrinos might even be consistent with the 3.5 keV line, exchanging the lepton number for a new coupling. The point of this paper is to evaluate these suspicions.

More generally, self-interactions of dark matter are under intensely active investigation because of their possibly ameliorative influence on small-scale structure [46, 47]. While we are interested in making contact with this body of work, we will not be able to do so here because we focus exclusively on the limit in which the new mediator is very heavy, an assumption that simplifies the analysis in a number of ways. Keeping the coupling perturbative, while at the same time staying in the heavy-mediator limit, precludes any consideration of the large cross sections

needed to hold sway over the dynamics of dark matter halos. The tantalizing case of lighter mediators is left for future work. We settle here for making some brief remarks in the conclusion on how that analysis is expected to differ from the present one.

It is also worth noting that self-interactions among sterile neutrinos have been discussed in connection to the persistent anomalies in short-baseline oscillation experiments [48–63]. These are sterile neutrinos of a different variety, being at the eV scale and therefore much too light to be of relevance to dark matter. In fact, the problem facing eV sterile neutrinos is somewhat like the reverse of the problem facing those at the keV scale: because experimental fits indicate a small mass and a large mixing angle, the challenge is to *prevent* eV sterile neutrinos from being populated in the early universe. This, indeed, is the purpose for which self-interactions are invoked. But despite the difference in model-building philosophy, the underlying physics is closely related.

One last tie-in deserves mention. If they exist, sterile neutrinos at the MeV scale and below are not only frozen into the early universe but are also, much later, produced and emitted by core-collapse supernovae. This includes, of course, the keV dark matter contenders, whose creation benefits from the active neutrinos encountering at least one resonance on their way out of the proto-neutron star, as in Refs. [36, 64–66]. Formulating accurate constraints on the basis of sterile neutrino production in supernovae is a challenge, made even more so if the particles are self-interacting. We do not take up the task here, but we refer to Ref. [67] for a recent analysis of the standard scenario, where sterile neutrinos are truly inert except for their mixing.

In the rest of this paper we study whether self-interactions are a viable way to rescue sterile neutrino dark matter from current bounds on the mass and mixing. In the heavy-mediator limit, the answer is a flat no, as the factors poised to abet production ultimately conspire to make self-interactions far too much of a good thing. The central finding is that, for any choice of coupling, the (m_s, θ) parameter space is split into two regions, one where the effect of self-interactions is only marginal and one where it is overwhelming (Figs. 7.1 and 7.2). The difference between

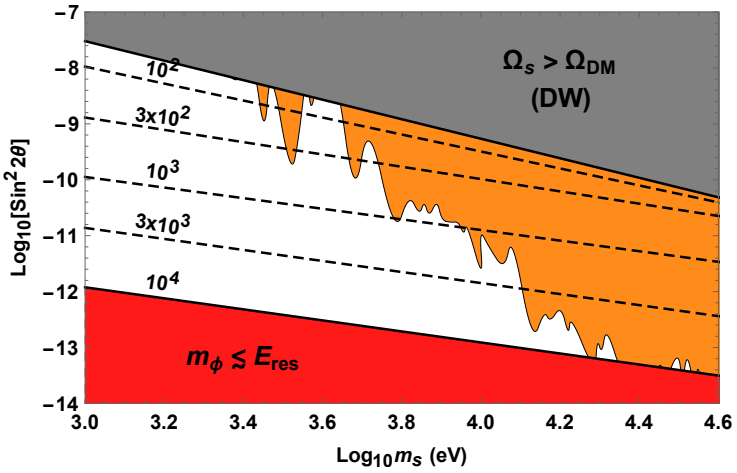

Figure 7.1: Curves indicate the vacuum mixing angles above which sterile neutrinos are overproduced ($\Omega_s > \Omega_{\rm DM}$) for various choices of self-interaction strength G_ϕ (up to $10^4 G_F$, past which either the heavy-ϕ assumption breaks down or the coupling becomes nonperturbative). The Dodelson–Widrow mechanism produces $\Omega_s = \Omega_{\rm DM}$ along the solid line bordering the gray region. X-ray and γ-ray constraints (orange) [8, 11, 13, 17] are plotted to orient the overproduction curves relative to bounds from radiative decay.

these regions is whether the active–sterile mixing ever becomes resonant. As we show below, both numerically and analytically, resonance is guaranteed whenever the rate of self-interactions is large enough to be very impactful—and, because the Boltzmann equation is nonlinear in the density of sterile neutrinos, runaway production inevitably results. Even fine-tuning the parameters is to no avail, since the transition between these regions is a sharp one. In the end, either dark matter is severely underproduced or it is severely overproduced.

In the next section we set up the equations governing sterile-neutrino production, discuss the underlying physics, and introduce the model used in the calculations. In Sec. 7.4 we present the results, showing that self-interacting sterile neutrinos cannot be all of the dark matter if their interactions are mediated by a very heavy particle. In Sec. 7.5 we conclude and reflect on how the analysis changes if the mediator is made lighter. The Appendix contains a few notes on the calculation of the sterile-neutrino scattering rate.

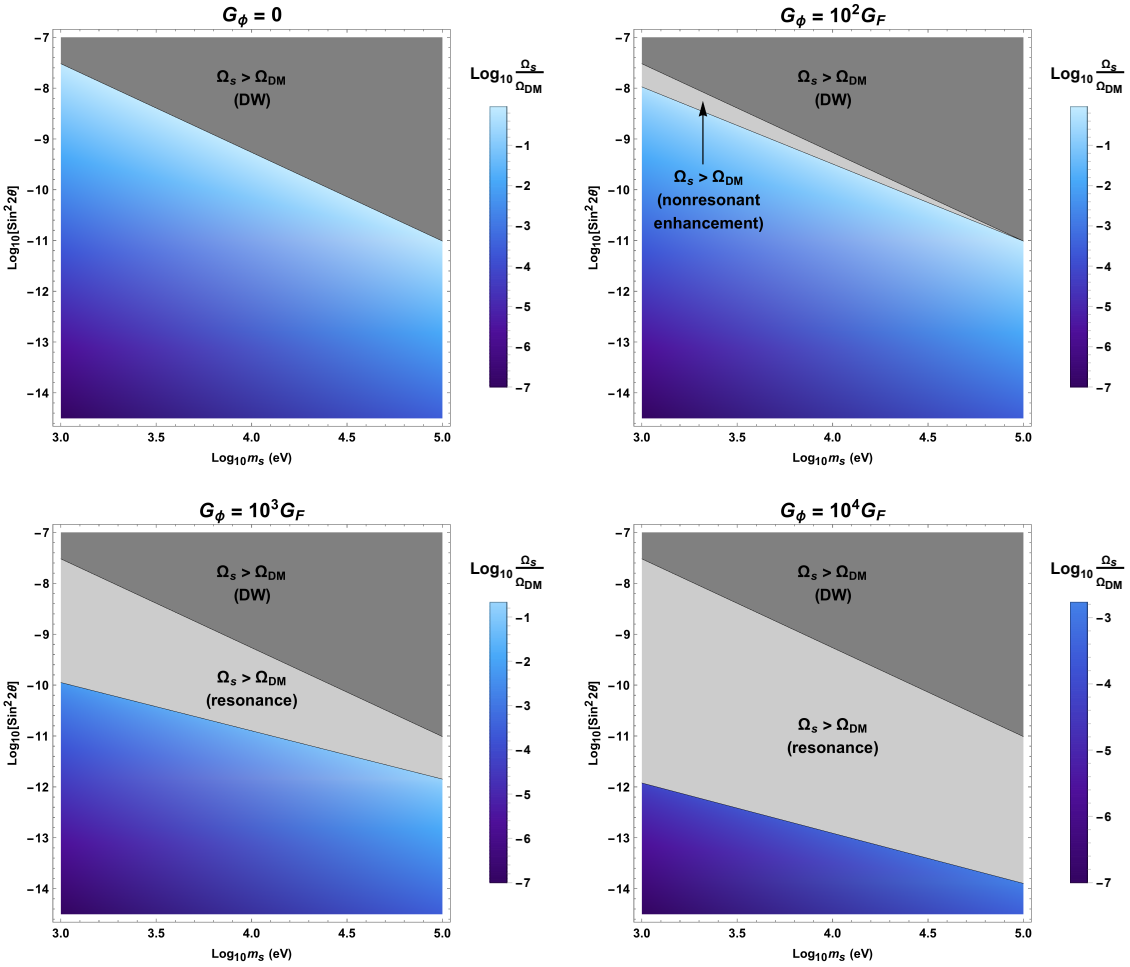

Figure 7.2: Fraction of relic sterile neutrino density Ω_s to observed dark matter density $\Omega_{\rm DM}$. Dark gray indicates overproduction due to the Dodelson–Widrow mechanism, light gray indicates overproduction due to self-interactions. For $G_\phi = 10^2 G_F$, $\Omega_s/\Omega_{\rm DM} = 1$ is achieved at slightly smaller mixing compared to $G_\phi = 0$ because $\Gamma_{\rm tot}$ is slightly larger and θ_m is nonresonantly enhanced. For $G_\phi = 10^3 G_F$ and $G_\phi = 10^4 G_F$, $\Omega_s/\Omega_{\rm DM}$ never reaches unity because resonant enhancement sets in.

7.3 Production mechanism and particle model

If the Standard Model (SM) neutrinos mix with a sterile state, then the propagating modes in the cosmic plasma are active–sterile mixtures, with lifetimes that are finite due to interactions in the medium. Decay of these quasiparticles—or, in other words, flavor decoherence of the propagating modes—is what sources the sterile neutrinos that accumulate in the early universe. In the Dodelson–Widrow scenario, only SM couplings contribute to the in-medium active–sterile mixing and decoherence rate. In a scenario with self-interacting sterile neutrinos, the new coupling contributes as well. As is typical, we assume that no sterile neutrinos inhabit the universe prior to their creation through this mechanism.

Letting $\Gamma_{\text{tot}} = \Gamma_a + \Gamma_s$ be the sum of the interaction rates of active and sterile neutrinos, the Boltzmann equation for the sterile neutrino distribution function $f_s(p,t)$ is then

$$\frac{\partial f_s}{\partial t} - Hp\frac{\partial f_s}{\partial p} = \frac{\Gamma_{\text{tot}}}{2}\frac{\sin^2 2\theta_m}{1+\left(\frac{\Gamma_{\text{tot}}}{2\omega_m}\right)^2}(f_a - f_s) + \mathcal{C}_s, \tag{7.1}$$

where all variables tacitly depend on neutrino momentum p and time t. The functional $\mathcal{C}_s$, which depends on f_s of all momenta, denotes the collision integrals for all-sterile scattering processes; H is the Hubble parameter; and the subscript m indicates that in-medium values are used for the mixing angle and oscillation frequency. In terms of the vacuum mixing angle θ and the vacuum oscillation frequency $\omega = \delta m^2/2p$, the defining formulae are

$$\omega_m^2 = \omega^2 \sin^2 2\theta + (\omega\cos 2\theta - \mathcal{V})^2 \tag{7.2}$$

and

$$\omega_m^2 \sin^2 2\theta_m = \omega^2 \sin^2 2\theta. \tag{7.3}$$

The potential $\mathcal{V}$, also a function of p, is generated by forward scattering of neutrinos on particles in the medium. To be consistent with previous studies [36, 38, 40], we take ν_a to be a muon neutrino. Muons are then the relevant charged-lepton population, with total (μ^+ and μ^-) energy density ρ_μ. The potential $\mathcal{V} = \mathcal{V}_\mu + \mathcal{V}_a + \mathcal{V}_s$ is then composed of

$$\mathcal{V}_\mu = -\frac{8\sqrt{2}G_F}{3m_W^2}\rho_\mu p \tag{7.4}$$

from ν_a scattering on $\mu^\pm$,

$$\mathcal{V}_a = -\frac{8\sqrt{2}G_F}{3m_Z^2}\rho_a p \tag{7.5}$$

from ν_a scattering on ν_a, and a contribution $\mathcal{V}_s$ from ν_s scattering on ν_s. The exact form of this last piece depends on the properties of the mediator of ν_s scattering. For the model that we study, it is

$$\mathcal{V}_s = +\frac{G_\phi}{3m_\phi^2}\rho_s p, \tag{7.6}$$

valid only when m_ϕ is much larger than the typical neutrino energy. The analogue of the Fermi coupling constant is defined as $G_\phi = (g_\phi/m_\phi)^2$, where g_ϕ is the sterile-sector coupling and m_ϕ is the mediator mass.

One-loop self-energy diagrams also generate a potential proportional to the difference of the neutrino and antineutrino number densities. Although any asymmetry in the active sector does get partially transferred to the sterile sector, we have confirmed that this potential is always unimportant if the lepton number is comparable to the baryon asymmetry, which we assume to be true. If the lepton number is much larger, then the physics explored here will interact in complicated ways with the Shi–Fuller mechanism and with flavor evolution in the active sector [68–75].

The scattering rate of muon neutrinos can be written in the form

$$\Gamma_a = c(p,T)G_F^2 T^4 p, \tag{7.7}$$

where $c(p,T)$ is a momentum- and temperature-dependent coefficient. In our calculations we use the results of Venumadhav et al. [40], who computed $c(p,T)$ over the range of temperatures relevant to sterile-neutrino production, accounting for the changing degrees of freedom through the quark-hadron transition. We also employ their tabulated data for the relativistic degrees of freedom g_* and g_{*S}, which appear in H and in the relation between time and temperature.

For the calculations that follow, we adopt a simple model in which the sterile neutrino ψ_s couples to a heavy real scalar ϕ:

$$\begin{aligned}\mathcal{L}_s =& \frac{1}{2}\bar{\psi}_s\left(i\partial\!\!\!/ - m_s\right)\psi_s + \frac{1}{2}(\partial_\mu\phi)^2 \\ &- \frac{1}{2}m_\phi^2\phi^2 - \frac{g_\phi}{2}\bar{\psi}_s\psi_s\phi. \end{aligned} \tag{7.8}$$

As we see in the next section, self-interactions facilitate active–sterile conversion through a series of resonances beginning at a temperature $T_{\rm res}$. For ϕ to qualify as heavy, it must have a mass $m_\phi \gg E_{\rm res}$, where $E_{\rm res} \sim 3T_{\rm res}$, to ensure that Eq. (7.6) is valid at the onset of resonance. In practice this means that m_ϕ must be at least ~ 1 GeV.

The ν_s scattering rate Γ_s is

$$\Gamma_s \approx 3\times 10^{-2}\alpha G_\phi^2 T^4 p. \tag{7.9}$$

where α is a normalization constant appearing in the ansatz $f_s(p) \simeq \alpha f_{\rm FD}(p)$, $f_{\rm FD}$ being the thermal Fermi–Dirac spectrum. Taking f_s to have this form is a reasonable approximation that makes it possible to parametrize Γ_s in a form similar to Γ_a. The other approximations implicit in Eq. (7.9) are noted in the Appendix. We assume that Γ_s never becomes so large that the deviations of f_a from equilibrium are important. This assumption has the potential to break down near resonance, since the factor of $\sin^2 2\theta_m$ in Eq. (7.1) fails to significantly suppress the f_a depletion rate. We will find in the next section that the approximation is justified nonetheless. The fractional

change in f_a that occurs over a weak-interaction time scale is always small in the parameter space that we explore.

In addition to enhancing active-to-sterile conversion, self-interactions also modify the thermodynamics of the sterile population. The 2-to-2 process $\nu_s\nu_s \to \nu_s\nu_s$ kinetically equilibrates the sterile neutrinos provided that $\Gamma_s \gtrsim H$. If self-interactions occur rapidly enough to have a substantial impact on production (that is, if $\Gamma_s \gtrsim \Gamma_a$), then they are guaranteed to be rapid enough to cause kinetic equilibration, by the fact that $\Gamma_a \gg H$ at the temperatures that concern us.

Less obvious is whether the higher-order 2-to-4 and 4-to-2 processes are fast enough to cause chemical equilibration. Dimensionally, one expects $\Gamma_{2\to4} \sim G_\phi^2 T^4 \Gamma_s$. Using the assumption $\Gamma_s \gtrsim \Gamma_a$ and the approximation $H \sim T^2/m_{Pl}$, the condition $\Gamma_{2\to4} \gtrsim H$ at $T \sim 100$ MeV translates to $G_\phi \gtrsim O(10^4) G_F$, which is the upper limit of what we study in this paper. Since sterile-neutrino equilibration does not feed back into production in any considerable way, and since number-changing processes are only expected to be important in a region of parameter space that we find to be ruled out regardless of their presence, we ignore these effects in the results that follow (*i.e.*, $\mathcal{C}_s = 0$ in Eq. (7.1)). We have checked our results against those obtained when approximate expressions are used for the rates of number-changing interactions, finding that our conclusions are unaltered. Number densities are enhanced by chemical equilibration at large G_ϕ, but the only cases in which this effect changes the subsequent course of production are those in which the dark matter abundance is overproduced regardless.

7.4 The relic density

By numerically solving the Boltzmann equation, we find that self-interactions facilitated by a heavy mediator are unable to rescue sterile neutrino dark matter from constraints. Either self-interactions have too small an impact and are unable to move production out of the observationally excluded region, or they have too great an impact and elicit excessive production. The reason is

that for any choice of G_ϕ, m_ϕ, and m_s, there is some critical vacuum mixing angle θ_c above which a resonance criterion is satisfied. Whether the mixing angle is above or below θ_c makes a radical difference in the dynamics and outcome of production.

The curves in Fig. 7.1 represent the mixing angles above which $\Omega_s > \Omega_{\rm DM}$, for various choices of G_ϕ (fixing $g_\phi = 0.5$). The curves move progressively downward until G_ϕ tops out at $\sim 10^4 G_F$, past which the heavy-ϕ assumption begins to be violated. (Alternatively, g_ϕ must become nonperturbative if ϕ is to remain heavy beyond $\sim 10^4 G_F$.) The orange region marks the part of parameter space excluded by X-ray and γ-ray observations assuming that sterile neutrinos are all of the dark matter [8, 11, 13, 17], and the gray region marks the part excluded by overproduction of sterile neutrinos solely through the Dodelson–Widrow mechanism. To be clear, the points within these regions are not excluded a priori in the self-interacting model; they are only necessarily excluded if G_ϕ is chosen such that the produced density of sterile neutrinos matches or exceeds the observed density of dark matter.

Other constraints could be drawn on the plot, including upper bounds on m_s from Milky Way satellite counts or Lyman-α observations, which in the Dodelson–Widrow scenario severely limit the open window in Fig. 7.1 [14–24]. But the final spectrum—on which these constraints depend—is parameter-dependent in the self-interacting model and generally differs from either a Dodelson–Widrow spectrum or a thermal one. If self-interactions were enabling the production of the observed dark-matter density well below the Dodelson–Widrow curve (solid black in Fig. 7.1, bordering the gray region), then a careful analysis of the resulting spectrum and its effects on structure would be warranted. This is especially true since number-changing processes might come into play at stronger couplings, thereby causing sterile neutrinos to proliferate and cool and causing structure-related constraints to weaken. Based on our results, however, such an analysis does not appear to be necessary, and the main role of pre-existing bounds on m_s is only to disfavor the smallest values of G_ϕ, namely those for which θ_c lies above the mixing angle required by Dodelson–Widrow. At these couplings ($G_\phi \lesssim 10^2 G_F$), we expect the constraints to

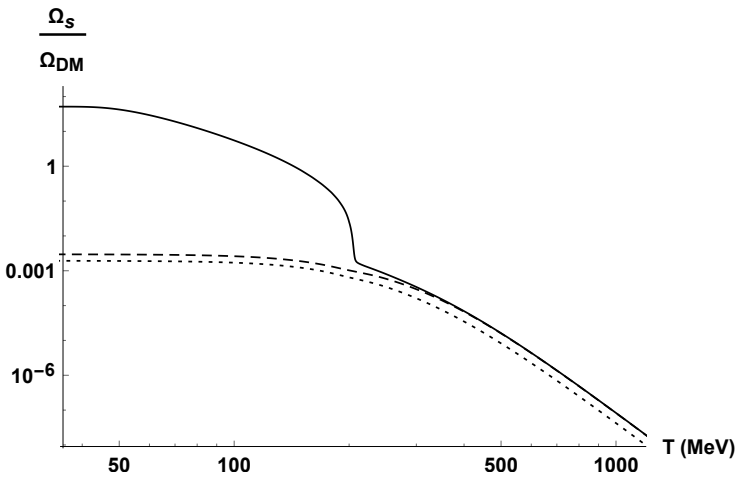

Figure 7.3: $\Omega_s/\Omega_{\rm DM}$ as a function of temperature. The solid curve corresponds to the test case described in the text (and plotted in Figs. 7.4 through 7.6 as well): $m_s = 10$ keV, $G_\phi = 3 \times 10^3 G_F$, $\sin^2 2\theta = 2 \times 10^{-12}$. The dashed curve has the same parameters but with $G_\phi = 0$. The dotted curve has the same parameters as the solid curve (including $G_\phi = 3 \times 10^3 G_F$) but with $\sin^2 2\theta = 1 \times 10^{-12}$, which lies below the critical mixing angle required for resonant production.

apply approximately as they do in the absence of self-interactions.

While Fig. 7.1 locates the overproduction curves relative to radiative-decay constraints, Fig. 7.2 shows that their deeper significance depends on the self-interaction strength. At large couplings, the curves signal sharp transitions from a production regime in which the sterile-neutrino density Ω_s is much less than the observed dark-matter density $\Omega_{\rm DM}$, to one in which it is much greater. This is true of $G_\phi = 10^3 G_F$ and $G_\phi = 10^4 G_F$, for which the fraction $\Omega_s/\Omega_{\rm DM}$ only reaches about 10^{-1} and 10^{-3}, respectively, before the resonance threshold is crossed. The $G_\phi = 0$ (Dodelson–Widrow) panel, in contrast, depicts the fraction smoothly passing through unity. Only in the vicinity of $G_\phi = 10^2 G_F$ do self-interactions allow for $\Omega_s/\Omega_{\rm DM} = 1$ to be achieved with a mixing angle smaller than in the Dodelson–Widrow scenario, and even then the effect is likely too small to evade constraints. Although not shown in the figure, $\sin^2 2\theta_c$ in this case nearly coincides with the Dodelson–Widrow curve: low enough to have a visible impact, but high enough not to induce a resonance before all of the observed abundance is made. The message, ultimately, is that there is very little leeway for self-interactions to assist in production without overdoing it.

To zero in on how production changes once θ_c is surpassed, we shine the spotlight in

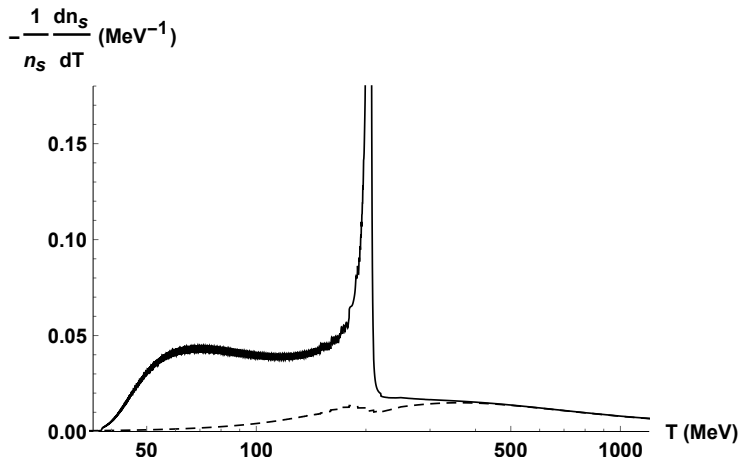

Figure 7.4: Logarithmic growth rate in sterile neutrino number density n_s. The dashed curve has the same mixing parameters as the test case (solid curve) but with $G_\phi = 0$. The solid curve peaks at a value of ~ 0.5—well off the plot—right when resonant production first sets in, and remains elevated while the resonance sweeps down, and then back up, the neutrino spectrum.

Figs. 7.3 through 7.6 on a single test case: a 10 keV sterile neutrino with $G_\phi = 3 \times 10^3 G_F$ and $\sin^2 2\theta = 2 \times 10^{-12}$. This mixing angle lies just above θ_c, and as Fig. 7.3 shows, the conversion of active neutrinos into sterile ones departs dramatically from what it looks like with the same θ but $G_\phi = 0$ (dashed curve in the figure) or with the same G_ϕ but $\theta < \theta_c$ (dotted curve). At very high temperatures the effect of self-interactions on the abundance is fairly slight, but once the universe cools to $T \sim 200$ MeV, production in the resonant regime (solid curve) suddenly shoots up. After this short-lived period of precipitous fractional growth, $\Omega_s/\Omega_{\rm DM}$ steadily climbs another four orders of magnitude before being shut off by Hubble expansion. Nonresonant production over the same temperature span is negligible by comparison. Indeed, the similarity in the shapes of the dashed and dotted curves attests to the fact that production in the nonresonant regime is essentially Dodelson–Widrow-like, the normalizations being different only because θ is.

Like the preceding plot, Fig. 7.4 shows how the sterile-neutrino abundance develops, now presented as a fractional rate of growth. Evident again is the peak right around 200 MeV, which reaches its maximum off the plot. Following the peak, the growth rate oscillates about a track that remains fairly steady, compared to the monotonic decline of the $G_\phi = 0$ curve, down to ~ 60

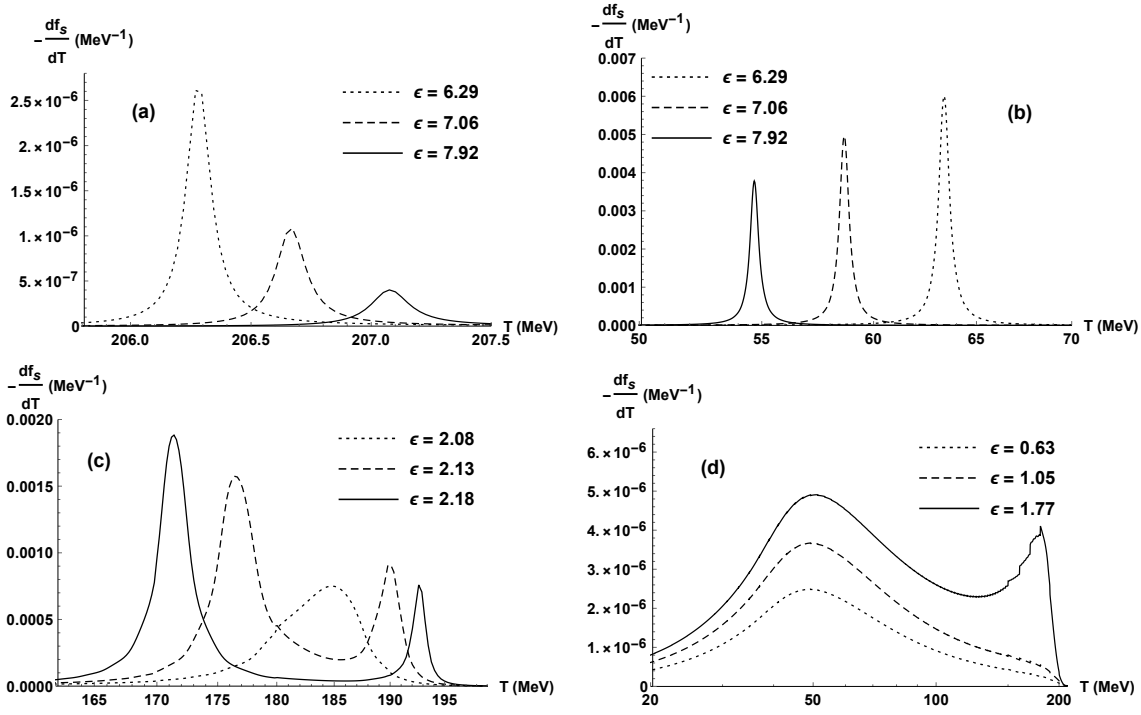

Figure 7.5: Growth rate of the sterile neutrino distribution functions due to active–sterile conversion. (a) Neutrinos with energies above the cutoff $\varepsilon_{\rm res}$ go through resonance in quick succession, from high to low energy, leading to a sharp spike in production beginning just above 200 MeV. (b) These neutrinos then pass back through resonance at much lower temperatures, from low to high energy. (c) Neutrinos with energies below $\varepsilon_{\rm burst}$ but above a lower threshold $\varepsilon_{\rm res}$ are pushed through resonance by the burst in production at energies above $\varepsilon_{\rm burst}$. Some of these neutrinos subsequently pass through resonance multiple times; the peaks shown in the panel correspond to these lower-temperature traversals. (d) Neutrinos with energies below $\varepsilon_{\rm res}$ never pass through resonance.

MeV. At ~ 40 MeV most of the final abundance has frozen in, but by that point sterile neutrinos already exceed the dark matter density by a factor of ~ 50. All of these features—the spike in the growth rate, the subsequent phase during which it remains elevated, and its oscillations—reflect the fact that sterile neutrinos are feeding back into their own production.

With the help of Fig. 7.5—which shows the growth rates of $f_s(p,T)$ for various neutrino energies and temperature ranges—we can begin to understand the dynamics of the resonant regime. Panel (a) highlights the origin of the peak in Fig. 7.4: all neutrinos with comoving energies above a cutoff $\varepsilon_{\rm res}$ pass through resonance, one after another, beginning at a temperature just above 200 MeV. Having a sizable fraction of the spectrum go through resonance causes all subsequent evolution of the abundance to differ markedly from Dodelson–Widrow production.

Why resonances are traversed by neutrinos with $\varepsilon \gtrsim \varepsilon_{\rm res}$ can be understood as follows. A resonance occurs for neutrinos of a given energy if there is some temperature at which the potential $\mathcal{V}_s$ equals (in magnitude) the SM part of the Hamiltonian. Since $\omega \propto 1/\varepsilon$, this criterion is most easily met by high-energy neutrinos, for which the contribution to the Hamiltonian of $\omega\cos 2\theta$ is small. Taking that term to be negligible, the resonance criterion is $|\mathcal{V}_s| \approx |\mathcal{V}_\mu + \mathcal{V}_a|$, or equivalently

$$\rho_s \approx 8\sqrt{2}\frac{G_F}{G_\phi}\left(\frac{m_\phi^2}{m_W^2}\rho_\mu + \frac{m_\phi^2}{m_Z^2}\rho_a\right). \tag{7.10}$$

We have seen already that the production of sterile neutrinos prior to the resonance is only marginally enhanced by self-interactions. Put another way, $\rho_s \approx \rho_s^{\rm DW}$ at these temperatures, where the latter quantity is the energy density of sterile neutrinos generated when G_ϕ is set to zero. If this substitution is made on the left-hand side, then Eq. (7.10) depends only on self-interaction parameters through their explicit appearance on the right, and the equation becomes a statement about how large θ must be for the highest-energy neutrinos to have reached resonance at a given temperature. Solving the Boltzmann equation with $G_\phi \neq 0$ is unnecessary for establishing whether a resonance occurs in the system, because the appearance of a resonance depends only (in this approximation) on whether the seed population generated by Dodelson–Widrow production is

large enough.

Eq. (7.10) is independent of ε, meaning that it applies to the neutrino population as a whole. The smallest θ that satisfies the inequality at any temperature is the critical value θ_c: at and above this mixing angle the system is guaranteed to hit a resonance. The same equation tells us, for $\theta \geq \theta_c$, the temperature $T_{\rm res}$ at which resonance is first broached. It does not tell us, however, *which* neutrino energies are involved. The value of $\varepsilon_{\rm res}$ cannot be so easily estimated as θ_c or $T_{\rm res}$, because as the resonance sweeps downward in energy, $\mathcal{V}_s$ rapidly diverges from the track it follows in the Dodelson–Widrow scenario. In other words, $\varepsilon_{\rm res}$ is set by the nonlinear dynamics of production. We can be sure, however, that resonance will not pass through the *entire* spectrum. Since $\omega \cos 2\theta \to \infty$ as $\varepsilon \to 0$, there must be some finite cutoff below which $\mathcal{V}_s$ never exceeds (again, in magnitude) the vacuum part of the Hamiltonian.

As the temperature drops, $\omega \cos 2\theta$ begins to dominate over $\mathcal{V}_\mu + \mathcal{V}_a$ even for neutrinos at the high end of the spectrum. But even though $\mathcal{V}_s$ likewise dilutes with five powers of the scale factor, the rapid creation of sterile neutrinos delays the crossing of $\omega \cos 2\theta$ and $\mathcal{V}_s$ till lower temperature. When the crossing does finally occur, neutrinos pass back through resonance, leading to the spikes in production shown in panel (b) of Fig. 7.5. This time higher-energy neutrinos pass through later than lower-energy ones, as dictated by the scaling of ω and $\mathcal{V}_s$. In the end, the sweep of resonance across the spectrum is stretched out over a protracted period from ~ 200 MeV down to ~ 40 MeV. If all energies were instead to pass through resonance in unison, total production would be much more limited. As it is, each resonance takes advantage of the one that preceded it, amplifying the feedback between scattering (Γ_s) and dispersion (θ_m) and explaining why the magnitudes of production are so much larger in panel (b) than they are in panel (a). Resonant production is self-reinforcing in this way: the growth of ρ_s due to resonant conversion competes against the decline of $\mathcal{V}_s$ due to Hubble expansion, prolonging the sweep from low back up to high energies. And while the growth of ρ_s also *shortens* the initial downward sweep, it compensates by spreading the resonance to more of the spectrum than one would expect

without feedback on $\mathcal{V}_s$.

Panel (c) illustrates the dynamics of neutrinos near $\varepsilon_{\rm res} \simeq 2.1$. As ε descends on the cutoff, the two resonance peaks move closer together (solid and dashed curves) until finally merging into one. Just below $\varepsilon_{\rm res}$ (dotted), production remains enhanced by a large θ_m but never reaches unity. The growth of the resonant peaks as temperature decreases is a reflection of the feedback alluded to in the previous paragraph. Much later the trend reverses, as seen in panel (b), due to the resonance reaching the sparsely populated upper parts of the spectrum.

As shown in panel (d), neutrinos of energies $\varepsilon < \varepsilon_{\rm res}$ do not go through resonance at all. Neutrinos in this energy range make a modest contribution to the sterile-neutrino abundance, their production primarily reflecting the scattering rate. The gentle peak near 50 MeV, for example, marks the point at which active–sterile conversion can no longer overcome the redshifting of Γ_s. Higher-energy neutrinos in this range do see another peak before this one, indicative of the minor enhancement of θ_m that occurs when sterile neutrinos above $\varepsilon_{\rm res}$ pass through resonance for the first time, but it is pronounced only for energies close to the resonant threshold.

Fig. 7.6 shows the relic spectrum left over after active–sterile conversion has shut off, juxtaposing the test case (solid) with the Dodelson–Widrow (dashed) and nondegenerate Fermi–Dirac (dotted) spectra. The resonantly produced spectrum is the "hottest" of the three, with a negligibly small fraction of number density below $\varepsilon_{\rm res}$. (The small spike right at the cutoff is due to $\varepsilon_{\rm res}$ lingering near resonance while the sweep reverses its direction.) As noted earlier, alterations to the spectrum from sterile-sector scattering—which tend to push it toward an equilibrium distribution—are not included in the calculation.

We have addressed in this section why a series of resonances occurs (in those cases where it does) and what its consequences are. We have not addressed, however, why it is not possible to have Γ_s significantly boost production while at the same time avoiding resonance. The explanation is straightforward: whenever Γ_s is significant, so is $\mathcal{V}_s$, as shown by the following short argument. If $\Gamma_s \gtrsim \Gamma_a$ at some temperature, then $\alpha \gtrsim (G_F/G_\phi)^2$ at the same temperature,

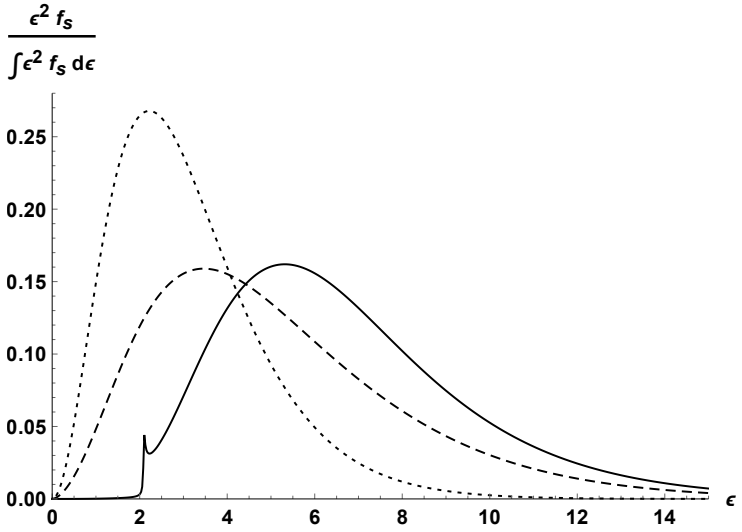

Figure 7.6: Normalized relic spectra, comparing the test case (solid) to Dodelson–Widrow (dashed) and nondegenerate Fermi–Dirac (dotted). The solid curve cuts off sharply at $\varepsilon_{\rm res}$.

assuming the numerical coefficients in Eqs. (7.7) and (7.9) to be comparable. But since

$$\left|\frac{\mathcal{V}_s}{\mathcal{V}_a}\right| = 8\sqrt{2}\alpha\frac{G_\phi}{G_F}\left(\frac{m_Z}{m_\phi}\right)^2, \tag{7.11}$$

the lower bound on α, along with perturbativity of g_ϕ, implies that $|\mathcal{V}_s| \gtrsim |\mathcal{V}_a|$.

7.5 Discussion

We have studied active–sterile conversion in a model with sterile neutrinos coupled to a new heavy mediator, finding that self-interactions either have very limited impact or cause gross overproduction of dark matter. The essential point, we have seen, is that if self-interactions are strong enough to have a significant effect on the decoherence rate, they are also strong enough to trigger a cascade of resonances in the active–sterile mixing.

For $G_\phi \lesssim O(10^2)G_F$, parameters can be found for which the observed abundance of dark matter is reproduced at a mixing angle smaller than the one required by the Dodelson–Widrow mechanism, but the mixing angle is still not small enough—nor the relic spectrum cold

enough—to evade constraints. In the range $O(10^2)G_F \lesssim G_\phi \lesssim O(10^4)G_F$, resonant production prevents the observed abundance from being reproduced at all. And for $G_\phi \gtrsim O(10^4)G_F$, the heavy-mediator approximation, which we have used throughout the study, becomes illegitimate. We have observed some hints in our calculations that above $\sim 10^4 G_F$ the correct relic abundance might plausibly be generated for the right choices of parameters. Resonant production still amplifies the active–sterile conversion, just not to excess. But given that the heavy-ϕ assumption is dubious in these cases, and given that we are not tracking the effects of number-changing processes, we have chosen, conservatively, to let the $10^4 G_F$ cutoff be a strict one.

Our focus, for the sake of simplicity, has been on a scalar mediator, but the results are expected to be similar for other spins so long as the mass is heavier than the energy scale at which production first becomes appreciable. The differences will be numerical, not qualitative, ones, stemming from the different coefficients in $\mathcal{V}_s$ and Γ_s. (Compare, for instance, to the formulae in the supplemental materials to Ref. [48].)

We have also assumed throughout this paper that the coupling g_ϕ is not much smaller than 1. At fixed four-fermion coupling G_ϕ, smaller g_ϕ means smaller m_ϕ, which in turn means that the system enters resonance more readily ($\mathcal{V}_s \propto 1/m_\phi^2$). We do not find varying g_ϕ independently of G_ϕ to be of any help in matching the dark matter abundance inferred in the universe.

In theories with keV sterile neutrinos, the primordial plasma is not their only place of origin: supernovae also create them. It is an intriguing question how the constraints apply if self-interactions are involved. Should a large enough seed population of sterile neutrinos be present, the particles may trap themselves and, as in the early universe, trigger a resonance. (Precedents for some of the relevant dynamics can be found in Refs. [76] and [77], in the context of neutrino–Majoron couplings.) This line of inquiry will be made especially salient if regimes other than the one studied here are discovered to give rise to the full relic abundance without defying cosmological bounds.

If the goal is to have self-interacting sterile neutrinos make up all of the dark matter, the

most promising simple extension of the model studied here is one with a lighter mediator. Masses below ~ 1 GeV are small enough that the sterile-sector scattering rates and the oscillation potential are sensitive to the mediator momentum and the presence of an ambient on-shell population. The effect on the potential may be especially important for lighter masses, since $\mathcal{V}_s$ changes sign in passing from $T \gg m_\phi$ to $T \ll m_\phi$.

Aside from having dynamics potentially quite different from the heavy-mediator scenario, models with lighter mediators are also compelling from the standpoint of small-scale structure, which has motivated much of the work on self-interactions. Because even the largest cross sections attainable in the perturbative heavy-mediator limit are still several orders of magnitude too weak to affect halo structure, we cannot yet comment definitively on whether viable regions of parameter space can be found in which halo observations are relevant. Scaling arguments suggest that models with $m_\phi \sim 10^{-3} m_s$—a condition which establishes a velocity-dependence of the cross section that is consistent with observations from dwarf- up to cluster-sized halos [46]—may be inefficient at converting active neutrinos into sterile ones due to suppression of θ_m, much like what happens to eV sterile neutrinos in Refs. [48, 49] and elsewhere. Of course, self-interactions need not alleviate tension at small scales for them to play a decisive part in generating sterile neutrino dark matter. Indeed, halos can just as well be regarded as offering constraints rather than asking for a cure. More work is needed before a comprehensive assessment can be made of sterile-sector interactions on the neutrino portal.

7.6 Acknowledgments

We thank Baha Balantekin, Susan Gardner, Evan Grohs, Jung-Tsung Li, Amol Patwardhan, and Sebastien Tawa for helpful conversations. This work was supported by NSF Grant No. PHY-1614864 and by the NSF N3AS Hub Grant No. PHY-1630782 and Heising-Simons Foundation Grant No. 2017-228.

This chapter is a reprint of L. Johns and G. M. Fuller, Phys. Rev. D 100, 023533 (2019). I was the primary investigator and author of this publication.

7.A Calculation of Γ_s

For the process $\nu_s\nu_s \to \nu_s\nu_s$, the spin-summed square of the amplitude is

$$\sum |\mathcal{M}|^2_{2\to 2} = 24\left(\frac{g_\phi}{m_\phi}\right)^4 \Big[(p_1\cdot p_2)^2 + (p_1\cdot p_3)^2 + (p_1\cdot p_4)^2\Big], \tag{7.12}$$

where p_1 and p_2 label the ingoing momenta, p_3 and p_4 the outgoing. (Unlike in the main text, here we are using p to denote four-momentum, E to denote energy.) Neglecting Pauli blocking, the 2-to-2 scattering rate for a sterile neutrino of momentum p_1 is

$$\Gamma_s = \frac{1}{8E_1}\int d\Pi_2 d\Pi_3 d\Pi_4 (2\pi)^4\delta^4(p_1+p_2-p_3-p_4)\sum |\mathcal{M}|^2_{2\to 2} f_2, \tag{7.13}$$

where f_2 is the distribution function of the sterile neutrino with momentum p_2 and $d\Pi_i$ is the Lorentz-invariant phase-space volume $d\vec{p}_i{}^3/(2\pi)^3 2E_i$. Since the $(p_i\cdot p_3)^2$ and $(p_i\cdot p_4)^2$ parts become equal once integrated over, only two phase-space integrals need to be computed. We assume that the distribution function of the scatterer is

$$f_2 = \frac{\alpha}{\exp\left(\frac{E_2}{T}\right)+1}. \tag{7.14}$$

The first of the phase-space integrals then evaluates to

$$\begin{aligned} L_1 &= \int d\Pi_2 d\Pi_3 d\Pi_4 (2\pi)^4 \delta^4(p_1+p_2-p_3-p_4) \\ &\qquad \times (p_1\cdot p_2)^2 f_2 \\ &= \frac{7\pi}{2880}\alpha E_1^2 T^4. \end{aligned} \tag{7.15}$$

The second integral can also be done analytically, but the result is a lengthy expression containing polylogarithms of various orders. We coerce it into a form comparable to L_1 by setting $E_1 = \langle E_1 \rangle \approx 3.15T$ and then factoring out two powers of energy:

$$\begin{aligned} L_2 &= \int d\Pi_2 d\Pi_3 d\Pi_4 (2\pi)^4 \delta^4(p_1+p_2-p_3-p_4)(p_1\cdot p_3)^2 f_2 \\ &\approx 4\times 10^{-4}\ \alpha E_1^2 T^4. \end{aligned} \tag{7.16}$$

Combining these,

$$\Gamma_s \approx 0.03\alpha G_\phi^2 T^4 E_1, \tag{7.17}$$

where $G_\phi = (g_\phi/m_\phi)^2$.

Bibliography

[1] S. Dodelson and L. M. Widrow, Phys. Rev. Lett. **72**, 17 (1994).

[2] A. Kusenko, Phys. Rept. **481**, 1 (2009).

[3] R. Adhikari, M. Agostini, N. A. Ky, T. Araki, M. Archidiacono, M. Bahr, J. Baur, J. Behrens, F. Bezrukov, P. B. Dev, D. Borah, A. Boyarsky, A. de Gouvea, C. de S. Pires, H. de Vega, A. Dias, P. D. Bari, Z. Djurcic, K. Dolde, H. Dorrer, M. Durero, O. Dragoun, M. Drewes, G. Drexlin, C. DÃŒllmann, K. Eberhardt, S. Eliseev, C. Enss, N. Evans, A. Faessler, P. Filianin, V. Fischer, A. Fleischmann, J. Formaggio, J. Franse, F. Fraenkle, C. Frenk, G. Fuller, L. Gastaldo, A. Garzilli, C. Giunti, F. GlÃŒck, M. Goodman, M. Gonzalez-Garcia, D. Gorbunov, J. Hamann, V. Hannen, S. Hannestad, S. Hansen, C. Hassel, J. Heeck, F. Hofmann, T. Houdy, A. Huber, D. Iakubovskyi, A. Ianni, A. Ibarra, R. Jacobsson,

T. Jeltema, J. Jochum, S. Kempf, T. Kieck, M. Korzeczek, V. Kornoukhov, T. Lachenmaier, M. Laine, P. Langacker, T. Lasserre, J. Lesgourgues, D. Lhuillier, Y. Li, W. Liao, A. Long, M. Maltoni, G. Mangano, N. Mavromatos, N. Menci, A. Merle, S. Mertens, A. Mirizzi, B. Monreal, A. Nozik, A. Neronov, V. Niro, Y. Novikov, L. Oberauer, E. Otten, N. Palanque-Delabrouille, M. Pallavicini, V. Pantuev, E. Papastergis, S. Parke, S. Pascoli, S. Pastor, A. Patwardhan, A. Pilaftsis, D. Radford, P.-O. Ranitzsch, O. Rest, D. Robinson, P. R. da Silva, O. Ruchayskiy, N. Sanchez, M. Sasaki, N. Saviano, A. Schneider, F. Schneider, T. Schwetz, S. SchÃnert, S. Scholl, F. Shankar, R. Shrock, N. Steinbrink, L. Strigari, F. Suekane, B. Suerfu, R. Takahashi, N. T. H. Van, I. Tkachev, M. Totzauer, Y. Tsai, C. Tully, K. Valerius, J. Valle, D. Venos, M. Viel, M. Vivier, M. Wang, C. Weinheimer, K. Wendt, L. Winslow, J. Wolf, M. Wurm, Z. Xing, S. Zhou, and K. Zuber, J. Cosmol. Astropart. Phys. **2017**, 025 (2017).

[4] K. N. Abazajian, Phys. Rept. **711-712**, 1 (2017).

[5] A. Boyarsky, M. Drewes, T. Lasserre, S. Mertens, and O. Ruchayskiy, Prog. Part. Nucl. Phys. **104**, 1 (2019).

[6] K. Abazajian, G. M. Fuller, and W. H. Tucker, Astrophys. J. **562**, 593 (2001).

[7] H. Yüksel, J. F. Beacom, and C. R. Watson, Phys. Rev. Lett. **101**, 121301 (2008).

[8] A. Boyarsky, D. Malyshev, A. Neronov, and O. Ruchayskiy, Mon. Not. R. Astron. Soc. **387**, 1345 (2008).

[9] C. R. Watson, Z. Li, and N. K. Polley, J. Cosmol. Astropart. Phys. **2012**, 018 (2012).

[10] K. C. Y. Ng, S. Horiuchi, J. M. Gaskins, M. Smith, and R. Preece, Phys. Rev. D **92**, 043503 (2015).

[11] K. Perez, K. C. Y. Ng, J. F. Beacom, C. Hersh, S. Horiuchi, and R. Krivonos, Phys. Rev. D **95**, 123002 (2017).

[12] C. Dessert, N. L. Rodd, and B. R. Safdi, arXiv:1812.06976 (2018).

[13] K. C. Ng, B. M. Roach, K. Perez, J. F. Beacom, S. Horiuchi, R. Krivonos, and D. R. Wik, arXiv:1901.01262 (2019).

[14] A. Boyarsky, O. Ruchayskiy, and D. Iakubovskyi, J. Cosmol. Astropart. Phys. **2009**, 005 (2009).

[15] A. Boyarsky, J. Lesgourgues, O. Ruchayskiy, and M. Viel, J. Cosmol. Astropart. Phys. **2009**, 012 (2009).

[16] E. Polisensky and M. Ricotti, Phys. Rev. D **83**, 043506 (2011).

[17] S. Horiuchi, P. J. Humphrey, J. Oñorbe, K. N. Abazajian, M. Kaplinghat, and S. Garrison-Kimmel, Phys. Rev. D **89**, 025017 (2014).

[18] S. Horiuchi, B. Bozek, K. N. Abazajian, M. Boylan-Kolchin, J. S. Bullock, S. Garrison-Kimmel, and J. Onorbe, Mon. Not. R. Astron. Soc. **456**, 4346 (2016).

[19] A. Schneider, J. Cosmol. Astropart. Phys. **2016**, 059 (2016).

[20] A. Rudakovskyi and D. Iakubovskyi, J. Cosmol. Astropart. Phys. **2016**, 017 (2016).

[21] J. F. Cherry and S. Horiuchi, Phys. Rev. D **95**, 083015 (2017).

[22] J. Baur, N. Palanque-Delabrouille, C. Yèche, A. Boyarsky, O. Ruchayskiy, É. Armengaud, and J. Lesgourgues, J. Cosmol. Astropart. Phys. **2017**, 013 (2017).

[23] A. Schneider, Phys. Rev. D **98**, 063021 (2018).

[24] S. Vegetti, G. Despali, M. R. Lovell, and W. Enzi, Mon. Not. R. Astron. Soc. **481**, 3661 (2018).

[25] M. Shaposhnikov and I. Tkachev, Phys. Lett. B **639**, 414 (2006).

[26] K. Petraki and A. Kusenko, Phys. Rev. D **77**, 065014 (2008).

[27] A. Merle, V. Niro, and D. Schmidt, J. Cosmol. Astropart. Phys. **2014**, 028 (2014).

[28] B. Shuve and I. Yavin, Phys. Rev. D **89**, 113004 (2014).

[29] A. V. Patwardhan, G. M. Fuller, C. T. Kishimoto, and A. Kusenko, Phys. Rev. D **92**, 103509 (2015).

[30] R. S. L. Hansen and S. Vogl, Phys. Rev. Lett. **119**, 251305 (2017).

[31] J. Herms, A. Ibarra, and T. Toma, J. Cosmol. Astropart. Phys. **2018**, 036 (2018).

[32] A. Berlin and D. Hooper, Phys. Rev. D **95**, 075017 (2017).

[33] F. Bezrukov, A. Chudaykin, and D. Gorbunov, J. Cosmol. Astropart. Phys. **2017**, 051 (2017).

[34] F. Bezrukov, A. Chudaykin, and D. Gorbunov, arXiv:1809.09123 (2018).

[35] X. Shi and G. M. Fuller, Phys. Rev. Lett. **82**, 2832 (1999).

[36] K. Abazajian, G. M. Fuller, and M. Patel, Phys. Rev. D **64**, 023501 (2001).

[37] C. T. Kishimoto, G. M. Fuller, and C. J. Smith, Phys. Rev. Lett. **97**, 141301 (2006).

[38] C. T. Kishimoto and G. M. Fuller, Phys. Rev. D **78**, 023524 (2008).

[39] J. Ghiglieri and M. Laine, J. High Energy Phys. **2015**, 171 (2015).

[40] T. Venumadhav, F.-Y. Cyr-Racine, K. N. Abazajian, and C. M. Hirata, Phys. Rev. D **94**, 043515 (2016).

[41] E. Bulbul, M. Markevitch, A. Foster, R. K. Smith, M. Loewenstein, and S. W. Randall, Astrophys. J. **789**, 13 (2014).

[42] A. Boyarsky, O. Ruchayskiy, D. Iakubovskyi, and J. Franse, Phys. Rev. Lett. **113**, 251301 (2014).

[43] M. Tashiro, H. Maejima, K. Toda, R. Kelley, L. Reichenthal, J. Lobell, R. Petre, M. Guainazzi, E. Costantini, M. Edison, R. Fujimoto, M. Grim, K. Hayashida, J.-W. den Herder, Y. Ishisaki, S. Paltani, K. Matsushita, K. Mori, G. Sneiderman, Y. Takei, Y. Terada, H. Tomida, H. Akamatsu, L. Angelini, Y. Arai, H. Awaki, L. Babyk, A. Bamba, P. Barfknecht, K. Barnstable, T. Bialas, B. Blagojevic, J. Bonafede, C. Brambora, L. Brenneman, G. Brown, K. Brown, L. Burns, E. Canavan, T. Carnahan, M. Chiao, B. Comber, L. Corrales, C. de Vries, J. Dercksen, M. Diaz-Trigo, T. Dillard, M. DiPirro, C. Done, T. Dotani, K. Ebisawa, M. Eckart, T. Enoto, Y. Ezoe, C. Ferrigno, Y. Fukazawa, Y. Fujita, A. Furuzawa, L. Gallo, S. Graham, L. Gu, K. Hagino, K. Hamaguchi, I. Hatsukade, D. Hawes, T. Hayashi, C. Hegarty, N. Hell, J. Hiraga, E. Hodges-Kluck, M. Holland, A. Hornschemeier, A. Hoshino, Y. Ichinohe, R. Iizuka, K. Ishibashi, M. Ishida, K. Ishikawa, K. Ishimura, B. James, T. Kallman, E. Kara, S. Katsuda, S. Kenyon, C. Kilbourne, M. Kimball, T. Kitaguti, S. Kitamoto, S. Kobayashi, T. Kohmura, S. Koyama, A. Kubota, M. Leutenegger, T. Lockard, M. Loewenstein, Y. Maeda, L. Marbley, M. Markevitch, H. Matsumoto, K. Matsuzaki, D. McCammon, B. McNamara, J. Miko, E. Miller, J. Miller, K. Minesugi, I. Mitsuishi, T. Mizuno, H. Mori, K. Mukai, H. Murakami, R. Mushotzky, H. Nakajima, H. Nakamura, S. Nakashima, K. Nakazawa, C. Natsukari, K. Nigo, Y. Nishioka, K. Nobukawa, M. Nobukawa, H. Noda, H. Odaka, M. Ogawa, T. Ohashi, M. Ohno, M. Ohta, T. Okajima, A. Okamoto, M. Onizuka, N. Ota, M. Ozaki, P. Plucinsky, F. S. Porter, K. Pottschmidt, K. Sato, R. Sato, M. Sawada, H. Seta, K. Shelton, Y. Shibano, M. Shida, M. Shidatsu, P. Shirron, A. Simionescu, R. Smith, K. Someya, Y. Soong, Y. Suagawara, A. Szymkowiak, H. Takahashi, T. Tamagawa, T. Tamura, T. Tanaka, Y. Terashima, Y. Tsuboi, M. Tsujimoto, H. Tsunemi, T. Tsuru, H. Uchida, H. Uchiyama, Y. Ueda, S. Uno, T. Walsh, S. Watanabe, B. Williams, R. Wolfs, M. Wright, S. Yamada, H. Yamaguchi, K. Yamaoka, N. Yamasaki, S. Yamauchi, M. Yamauchi, K. Yanagase, T. Yaqoob, S. Yasuda, N. Yoshioka, J. Zabala, and Z. Irina, Proc. SPIE **10699**, 520 (2018).

[44] X. Barcons, K. Nandra, D. Barret, J.-W. den Herder, A. C. Fabian, L. Piro, and M. G. W. and, J. Phys. Conf. Ser. **610**, 012008 (2015).

[45] A. Neronov and D. Malyshev, Phys. Rev. D **93**, 063518 (2016).

[46] S. Tulin and H.-B. Yu, Phys. Rept. **730**, 1 (2018).

[47] C. Argüelles, N. Mavromatos, J. Rueda, and R. Ruffini, J. Cosmol. Astropart. Phys. **2016**, 038 (2016).

[48] B. Dasgupta and J. Kopp, Phys. Rev. Lett. **112**, 031803 (2014).

[49] S. Hannestad, R. S. Hansen, and T. Tram, Phys. Rev. Lett. **112**, 031802 (2014).

[50] T. Bringmann, J. Hasenkamp, and J. Kersten, J. Cosmol. Astropart. Phys. **2014**, 042 (2014).

[51] P. Ko and Y. Tang, Phys. Lett. B **739**, 62 (2014).

[52] X. Chu, B. Dasgupta, and J. Kopp, J. Cosmol. Astropart. Phys. **2015**, 011 (2015).

[53] M. Archidiacono, S. Hannestad, R. S. Hansen, and T. Tram, Phys. Rev. D **91**, 065021 (2015).

[54] A. Mirizzi, G. Mangano, O. Pisanti, and N. Saviano, Phys. Rev. D **91**, 025019 (2015).

[55] Y. Tang, Phys. Lett. B **750**, 201 (2015).

[56] M. Archidiacono, S. Hannestad, R. S. Hansen, and T. Tram, Phys. Rev. D **93**, 045004 (2016).

[57] M. Archidiacono, S. Gariazzo, C. Giunti, S. Hannestad, R. Hansen, M. Laveder, and T. Tram, J. Cosmol. Astropart. Phys. **2016**, 067 (2016).

[58] J. F. Cherry, A. Friedland, and I. M. Shoemaker, arXiv:1605.06506 (2016).

[59] F. Forastieri, M. Lattanzi, G. Mangano, A. Mirizzi, P. Natoli, and N. Saviano, J. Cosmol. Astropart. Phys. **2017**, 038 (2017).

[60] P. Bakhti and Y. Farzan, Phys. Rev. D **95**, 095008 (2017).

[61] N. Song, M. Gonzalez-Garcia, and J. Salvado, J. Cosmol. Astropart. Phys. **2018**, 055 (2018).

[62] Y. S. Jeong, S. Palomares-Ruiz, M. H. Reno, and I. Sarcevic, J. Cosmol. Astropart. Phys. **2018**, 019 (2018).

[63] X. Chu, B. Dasgupta, M. Dentler, J. Kopp, and N. Saviano, J. Cosmol. Astropart. Phys. **2018**, 049 (2018).

[64] J. Hidaka and G. M. Fuller, Phys. Rev. D **74**, 125015 (2006).

[65] J. Hidaka and G. M. Fuller, Phys. Rev. D **76**, 083516 (2007).

[66] M. L. Warren, G. J. Mathews, M. Meixner, J. Hidaka, and T. Kajino, Int. J. Mod. Phys. A **31**, 1650137 (2016).

[67] C. A. Argüelles, V. Brdar, and J. Kopp, Phys. Rev. D **99**, 043012 (2019).

[68] A. D. Dolgov, S. H. Hansen, S. Pastor, S. T. Petcov, G. G. Raffelt, and D. V. Semikoz, Nucl. Phys. **B632**, 363 (2002).

[69] K. N. Abazajian, J. F. Beacom, and N. F. Bell, Phys. Rev. D **66**, 013008 (2002).

[70] Y. Y. Y. Wong, Phys. Rev. D **66**, 025015 (2002).

[71] G. Mangano, G. Miele, S. Pastor, T. Pinto, O. Pisanti, and P. D. Serpico, Nucl. Phys. **B729**, 221 (2005).

[72] S. Pastor, T. Pinto, and G. G. Raffelt, Phys. Rev. Lett. **102**, 241302 (2009).

[73] L. Johns, M. Mina, V. Cirigliano, M. W. Paris, and G. M. Fuller, Phys. Rev. D **94**, 083505 (2016).

[74] E. Grohs, G. M. Fuller, C. T. Kishimoto, and M. W. Paris, Phys. Rev. D **95**, 063503 (2017).

[75] L. Johns and G. M. Fuller, Phys. Rev. D **97**, 023020 (2018).

[76] G. Fuller, R. Mayle, and J. Wilson, Astrophys. J. **332**, 826 (1988).

[77] R. V. Konoplich and M. Y. Khlopov, Sov. J. Nucl. Phys. **47**, 565 (1988).